UNIVERSITA' DEGLI STUDI DI MILANO

FACOLTA' DI SCIENZE E TECONOLOGIE

Ph.D. in Chemistry, XXXIV Cycle

CHALLENGES AND OPPORTUNITIES OF MAYTANSINOL, CANNABIDIOL AND CALLYSPONGIOLIDE IN NATURAL PRODUCT CHEMISTRY

Tutor: Prof. Daniele PASSARELLA

Co-Tutor: Prof. Stefano PIERACCINI

Ph.D. Candidate

Paola MARZULLO

R12394

Academic Year 2020-2021

A mia mamma,

la mia roccia e la mia luce che mi ha
insegnato a lottare e a non arrendermi
di fronte agli imprevisti della vita

Contents

List of Abbreviations

ACN	Acetonitrile
AcOH	Acetic acid
ADC	Antibody-Drug Conjugate
AIDS	Acquired Immune Deficency Syndrome
CAN	Ceric Ammonium Nitrate
CB1	Cannabinoid Receptor type 1
CB2	Cannabinoid Receptor type 2
CBD	Cannabidiol
CBS	Corey-Bakshi-Shibata catalyst
CuAAC	Copper (I)-catalysed Azide-Alkyne Cycloaddition
DABCO	1,4-diazabicyclo[2,2,2]octane
DCC	N,N′-Dicyclohexylcarbodiimide
DCM	Dichloromethane
DCU	Dicyclohexyl urea
DEAD	Diethyl Azodicarboxylate
DIAD	Diisopropyl Azodicarboxylate
DIPEA	N, N-Diisopropylethylamine
DMAP	4-Dimethylaminopyridine
DMF	Dimethylformamide
DMG	Direct Metalation Group
DMP	Dess-Martin Periodinane
DMPU	*N*,*N*′-Dimethylpropyleneurea
DMSO	Dimethyl Sulfoxide
DPTS	4-(Dimethylamino)pyridinium 4-toluenesulfonate
EAE	Experimental Autoimmune Encephalitis
EDC	1-Ethyl-3-(3-dimethylaminopropyl)carbodiimide
EDG	Electron Donating Group
EDTA	Ethylenediaminetetraacetic Acid
EGTA	Glycol Ether Diamine Tetraacetic Acid
EWG	Electron Withdrawing Group
FDA	Food and Drug Administration
GDP	Guanosine Diphosphate
GTP	Guanosine Triphosphate
HATU	Hexafluorophosphate Azabenzotriazole Tetramethyl Uronium
HMDS	Hexamethyldisilazide
HMPA	Hexamethylphosphoramide
HOAt	1-Hydroxy-7-azabenzotriazole
KHMDS	Potassium Hexamethyldisilazide
LDA	Lithium Diisopropylamide
MAP	Microtubule-Associated Protein
MARK	Microtubule Affinity Regulating Protein Kinase
MDA	Microtubule Destabilising Agent
MOM	Methoxymethyl

MSA	Microtubule Stabilising Agent
MT	Microtubule
MTDA	Methyl Trimethylsilyl Dimethylketene Acetal
MTOC	Microtubule-Organizing Centre
MTT	3-(4,5-Dimethylthiazol-2-yl) -2,5-diphenyltetrazolium bromide
NaPi	Sodium Phosphate
NP	Natural Product
NT	Neurotubule
Piv	Pivaloyl
PPTS	Pyridinium *p*-Toluenesulfonate
PPy	4-Pyrrolidinopyridine
PTSA	p-Toluensulfonic acid
Py	Pyridine
RCM	Ring-closing Metathesis
SAR	Structure-Activity Relationship
TBSOTf	*tert*-Butyldimethylsilyl Trifluoromethanesulfonate
T-DM1	Trastuzumab-emtansine
TEA	Triethylamine
TEBA	Tri Ethyl Benzyl Ammonium
TESOTf	Triethylsilyl Triflate
TFA	Trifluoroacetic Acid
THC	Tetrahydrocannabidiol
THF	Tetrahydrofuran
TMEDA	N,N,N',N'-Tetramethyl Ethylenediamine
TMS	Trimethylsilane
TMS-Cl	Trimethylsilyl Chloride
γ-TuRC	γ-Tubulin Ring Complex

Chapter I General Background

The development of new drugs has long been inspired by Nature as the main source of the biologically active compounds. Many Natural Products (NPs), commonly referred to as "secondary metabolites" (the end-products of gene-expression), have been isolated from bio-diverse plants, animals, fungi, and microorganisms such as bacteria, which exist in a great variety on Earth. An extract from any one of these sources typically contains novel, structurally diverse chemical compounds. This practice has motivated total synthesis and diversity-oriented synthesis in the drug discovery and drug design process as it allows an exploration of chemical biology through molecular design.

Until now, NPs are the most consistent success source of drug leads and provide greater structural diversity than standard combinatorial chemistry. They offer great opportunities to find new low molecular weight structures active against a wide range of assay targets. The pharmaceutical industry is in agreement with this fundamental concept, in fact 34% of current drugs are inspired or derived from NPs, over 60% of the anticancer drugs available are directly developed on the basis of NPs, 66% of NPs in the form of semisynthetic drugs are the basis of current drugs on the market, and almost 65% of the world's population has incorporated them into their primary modality of health care.[1]

1 Natural Products

A NP is a chemical compound or substance produced by a living organism-found in Nature that exhibits a pharmacological or biological activity useful in the health care. NPs are characterised by huge structural diversity and complexity. Compared to libraries of synthetic compounds, they typically have a higher molecular mass, a greater number of oxygen and sp^3 carbon atoms, but fewer nitrogen and halogen atoms, larger numbers of H-bond acceptors and donors, higher hydrophilicity, greater molecular rigidity, which may be useful in drug discovery that address protein–protein interactions.[2ab] The NPs are structurally optimised by the boost of evolutionary adaptation to ensure the performance of particular biological functions,[2] including the regulation of endogenous defence mechanisms and interaction with other organisms, which explains the high relevance in the treatment of infectious diseases and cancer.

Present in medicinal plants, NPs represent a suitable source for the discovery of new and potential drugs for the whole of humanity. For thousands of years, NPs have played an important role around the world in the treatment and prevention of human disease, especially for cancer, infectious,[2ac] cardiovascular diseases, and multiple sclerosis.[3] The value of NPs can be appreciated using three criteria: *a*) the extent of chemical and structural diversity introduced, including the use as templates for semisynthetic and total synthetic modification; *b*) the number of diseases treated or prevented by these substances; and *c*) the frequency of use in the treatment of diseases.[4]

---

1 a] N. R. Farnsworth, O. Akerele, et al., *Bull. World Health Organ.* **1985**, *63*, 965–81; b] G. M. Cragg, D. J. Newman, *Biochim. Biophys. Acta - Gen. Subj.* **2013**, *1830*, 3670–3695.

2 **a]** A. G. Atanasov, B. Waltenberger, et al., *Biotechnol. Adv.* **2015**, *33*, 1582–1614; **b]** M. Feher, J. M. Schmidt, *J. Chem. Inf. Comput. Sci.* **2003**, *43*, 218–227; **c]** A. L. Harvey, R. Edrada-Ebel, R. J. Quinn, *Nat. Rev. Drug Discov.* **2015**, *14*, 111–129.

3 **a]** D. J. Newman, G. M. Cragg, *J. Nat. Prod.* **2016**, *79*, 629–661; **b]** B. Waltenberger, A. Mocan, et al., *Molecules* **2016**, *21*, 807; **c]** M. Tintore, A. Vidal-Jordana, J. Sastre-Garriga, *Nat. Rev. Neurol.* **2019**, *15*, 53–58.

4 Y.-W. Chin, M. J. Balunas, et al., *AAPS J.* **2006**, *8*, E239–E253.

The use of plants as a source of therapeutic agents has helped to introduce single chemical entities into modern medicine. Historically, plants have always been the most used for early drug discovery in medicine, because their wide and unique elements of molecular diversity and biological functionality are indispensable for drug discovery. Using plants as sources of therapeutic agents allows to: *a*) isolate biologically active compounds for direct use as drugs; *b*) produce biologically active compounds with higher activity and/or lower toxicity through a semi-synthetic pathway, by exploiting new or known structures as lead compounds; *c*) use them as pharmacological tools; and *d*) use the whole plant or part of it as an herbal remedy.[5] In addition, the known characteristic of NPs of possessing numerous stereogenicenters compared to synthetic products offers stereo-specificity and chemotypes useful in drug design. Overall, the NP pool is rich in bioactive compounds that cover a much larger area of chemical space than typical small molecule synthetic libraries.[6]

Research for the discovery of new plant-derived drugs requires a multidisciplinary research team of botanists, chemists, pharmacologists, and biologists. The biological activity of new compounds is studied in detail to determine structure-activity relationships (SARs) and to evaluate their potential as active agents in various biology and chemistry laboratories. The exploration of synthetic pathways to obtain the various biologically active NPs and the rational design of new analogues based on NPs are also planned. The results related to the screening of both NPs and analogues allow the subsequent design of improved second-generation analogues.

Drug discovery involves many steps, including several types of research.[7] First, it is necessary find a "lead", namely the product that shows good biological activity in an *in vitro* assay, by examining numerous compounds selected from existing NPs or synthesised in the laboratory. After the lead compound has been identified, it is essential to analytically determine which compounds are responsible for the observed effect. In the case of NPs, this step requires an elaborate process of isolation and purification of the compounds present in natural extracts, as plants contain many active principles. Isolation involves many complicated processes and often their structural elucidation is difficult. Subsequently, *in vivo* clinical trials on animals begin to determine the toxicity of the compound and its efficacy against the disease, and if the drug is safe, it is then tested in human clinical studies. Finally, if the tests are successful and provide good results, the drug is approved and it can be produced for marketing. For this last step, it is necessary to develop an industrial-scale chemical process that promises the purity required by the standards.

Creating/discovering and evaluating drugs for the treatment of human disease requires long time and it is cost dependent. However, the development of strategies for providing drug leads from NPs, the creation of structural chemical databases consisting of a wide variety of chemotypes, and the simultaneous availability of databases on target genes and proteins have eliminated the main limitations of chemical screening. Indeed, the complete process simplifies the creation of new compounds through computational molecular modelling for pharmacological evaluation.[8] Drug discovery starts with attempts to find a molecule that causes a specific biological response, but the trend in drug discovery points toward rapid, high-throughput screening of large compound libraries. Furthermore, the sequencing of the human genome and numerous pathogen genomes offers the opportunity to discover new pharmacologic targets. Chemogenomics turns out to be a new and valid technology to discover targets using active compounds as probes, and NPs are ideal for this purpose.[9]

The evolution of the drug discovery will result from a combination of research on NPs and synthetic approaches. The development of new drugs from plants today is expensive and time-consuming, even though the world of therapeutic plants has been thoroughly investigated. The biologically active substance isolated from plants are for the most part known; however, many species are still to be studied in forecast of a rational use. This means that many plant constituents with potentially suitable biological properties remain unknown. The trend at nowadays, mainly in an industrial field, is to look for biologically active compounds from plants that can serve as lead compounds for synthetic or semisynthetic development. To remain competitive, drug discovery from NP must

5 M. Lahlou, *Expert Opin. Drug Discov.* **2007**, *2*, 697–706.

6 H. Lachance, S. Wetzel, et al., *J. Med. Chem.* **2012**, *55*, 5989–6001.

7 J. Shrager, *Des. Sci.* **2001**, *11*, 325–348.

8 L. J. Nisbet, M. Moore, *Curr. Opin. Biotechnol.* **1997**, *8*, 708–712.

9 B. Patwardhan, A. D. B. Vaidya, M. Chorghade, *Curr. Sci.* **2004**, *86*, 789–798.

continuously improve the speed of screening, isolation and elucidation processes, as well as facing the problems related to large-scale manufacturing. Drug discovery is inevitably a teamwork based on experimental results, planning, and synergies between different scientific fields.

2 Natural Products in Drug Discovery[10]

NPs continued to play a very significant role in the drug discovery and development process. That Nature has in one way or another continued to influence the design of small molecules is demonstrated by the numerous drugs that have entered the market based on NPs over the past four decades, a time period in which the development system has been perfected. The shift from large combinatorial libraries to small focused collections that contain much of the "structural aspects" of NPs has continued with emphasis over time. Very recently, an extension of methodologies has shown how libraries of compounds with privileged structures can lead to compounds identified as useful as probes.[11] However, the development skill of combinatorial chemistry in structural optimisation works very well when an active skeleton is identified. To this purpose, NPs provide a broad and solid basis for investigations. Based on the results, it is possible to plan their use as they are (both pure N and in complex botanical mixtures NB), as derivatives following semi-synthetic modifications ND, as inspiration to create synthetic isosteric structures obtaining completely different compounds that may have little similarity to the original S, or the active pharmacophore can be included in a synthetic molecule S*.

Despite the greatly reduced level of NPs-based drug discovery programs in major pharmaceutical companies, NPs retain an important role. The data shown (**Figure 2.1**) underline how NPs from all sources are influent in the development of medical therapies, also taking into account the relative structures derived and the exploitation of the pharmacophore.

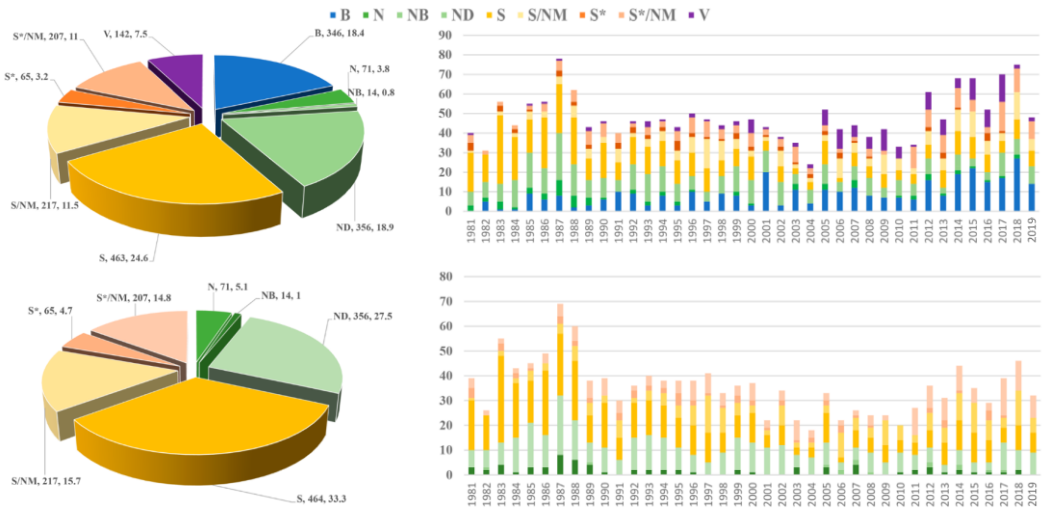

Figure 2.1 All approved drugs by source/year 1981-2019.[10] Biological (**B**), large peptide or protein isolated from an organism; Natural product (**N**); Natural product Botanical (**NB**); Derived (**ND**) from a natural product after semi-synthetic modification; Totally Synthetic drug found by random screening/modification of an existing agent (**S**), or by keeping the pharmacophore of a NP (**S***); Natural product mimic (/**NM**), modifications of NP by combinatorial methods; Vaccine (**V**).

A substantial difference is evident starting from the 90s, in which purely synthetic products have left more and more space for compounds of natural origin. By removing biological products and vaccines, the graphs show that natural and derived small-molecules are 40-45% for most of the 1989-2000 period, dropping to 18-26% from 2001 to 2012, with the exception of 2002 and the 2005, when the figures rose above 30%, and from 2011 to 2019

10 D. J. Newman, G. M. Cragg, *J. Nat. Prod.* **2020**, *83*, 770–803.

11 R. F. Dantas, T. C. S. Evangelista, et al., *Expert Opin. Drug Discov.* **2019**, *14*, 1269–1282.

the range is 27-46%. Over 39 years, the average of the values is 32%, but including the classifications inspired by NPs (S*, S*, /NM, and S/NM) to evaluate the overall influence of NPs on pharmaceutical development would increase this value to the 67%. In the discovery of small-molecule drugs, these data highlight the constant influence of compounds other than totally synthetic ones, which lead to new drugs not based on natural pharmacophores.

Figure 2.2 shows the classes of drugs with the highest number of compounds developed and approved to treat the associated diseases. Antibacterial and anticancer are particularly prominent from the point of view of NPs and derivatives.

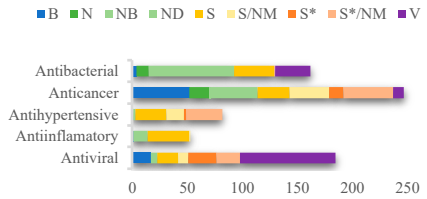

Figure 2.2 Diseases of interest in drug discovery with the highest number of drugs approved 1981-2019.

Antibacterial – 36 of the 162 agents approved over the time frame of this review were biologics B (4) and vaccines V (32). Of the remaining, 78 (48%) fall into the N and ND categories, and 36 (22%) are totally synthetic.

In the period from 2017 to 2019, a derivative of the aminoglycoside **sisomycin** was approved to produce **plazomycin**. Following aminoglycoside changes, three tetracycline agents, **omadacycline**, **eravacycline** and **sarecycline**, were also approved at the end of 2018, followed by **lefamulin**, which is a derivative of the product natural fungal pleuromutilin. There are also mixtures of agents, such as Recarbrio (imipenem/cilastine + **relebactam**), or Vabomere (meropenem/**vaborbactam**). In 2019 **cefiderocol** was approved, developed as a combination of cephalosporin and siderophore.

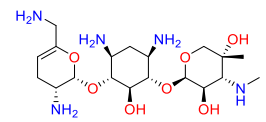

R = NH_2: **Sisomycin**
R = $NHCH_2CH_2OH$: **Plazomycin**

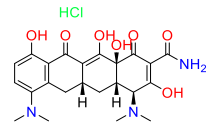

Omadacycline

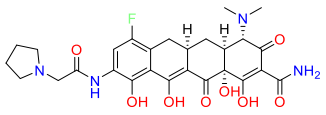

Eravacycline

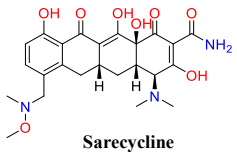

Sarecycline

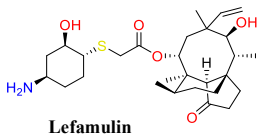

Lefamulin

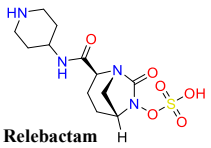

Relebactam

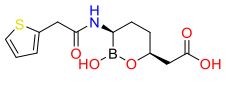

Vaborbactam

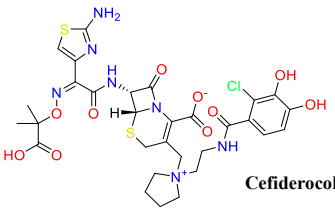

Cefiderocol

Anticancer – It is the most widely studied area, because there are many types of cancer, depending on the affected cells, the affected organ, the origin of the tumour, and how it progresses. To date, medicine has made great progress with the aim of having a targeted cure for each tumour, due to the different response of the tumour on each affected patient. In recent years, the rapid progress of scientific research, signal transduction, cell cycle regulation, induction of apoptosis, angiogenesis and other basic processes in cancer cells have been progressively elucidated[12] by identifying new cellular targets for anticancer therapies.[13] New antineoplastic drugs are approved every year, particularly those with high efficacy/low toxicity ratios designed to act on specific targets. These

12 S. Whittaker, R. Marais, A. X. Zhu, *Oncogene* **2010**, *29*, 4989–5005.

13 E. Agarwal, M. G. Brattain, S. Chowdhury, *Cell. Signal.* **2013**, *25*, 1711–1719.

drugs can be divided into ten classes based on target:[14] tyrosine kinase inhibitors (TK), mitogen-activated protein kinases inhibitors (MAPK), cyclin-dependent kinases inhibitors (CDK), poly (ADP-ribose) polymerase inhibitors (PARP), phosphatidylinositol 3-hydroxy kinase inhibitors (PI3K), smoothened receptor antagonists (SMO), androgen receptor antagonists (AR), somatostatin receptor inhibitors (SSTR), isocitrate dehydrogenase inhibitors (IDH), and others.

In the time period 1981-2019, 247 drugs were developed for the treatment of cancer. Of these 185 (75%) are small molecules, divided into 18 N (10%), 1 NB (0.5%), 43 ND (23%), 29 S (16%), 36 S/NM (19.5%), 13 S* (7%), 45 S*/NM (24%). On the basis of these data it is evident that the influence of NPs is significant in this category, in fact 84% of the compounds are obtained as inspiration from natural sources. In addition to the already known compound, in the period 2015-2019 there have been significant approvals of nature-inspired drugs. The unmodified marine NP **aplidine**, which differs from **didemnin B** (the first marine NP to enter antitumor clinical studies) in the oxidation of the lactyl group in the side chain. In the ND category, there are five approved agents including **midostaurin**, **forodesin**, two antibody-drug conjugates (ADCs) **inotuzumab ozogamicin**, derivative of calicheamicin, and **polatuzumab vedotin**. Although no S* molecules have been approved within this period, 21 S*/NM have been approved as kinase inhibitors, among them **dacomitinib**, **lenvatinib**, **tivozanib**, **palbociclib**. Six are the approved S including **cobimetinib**, **rucaparib**, **selinexor**, while 17 are the small molecules of the S/NM category; **alectinib**, **niraparib**, **alpelisib**, **darolutamide**, and **ixazomib** are just some examples.

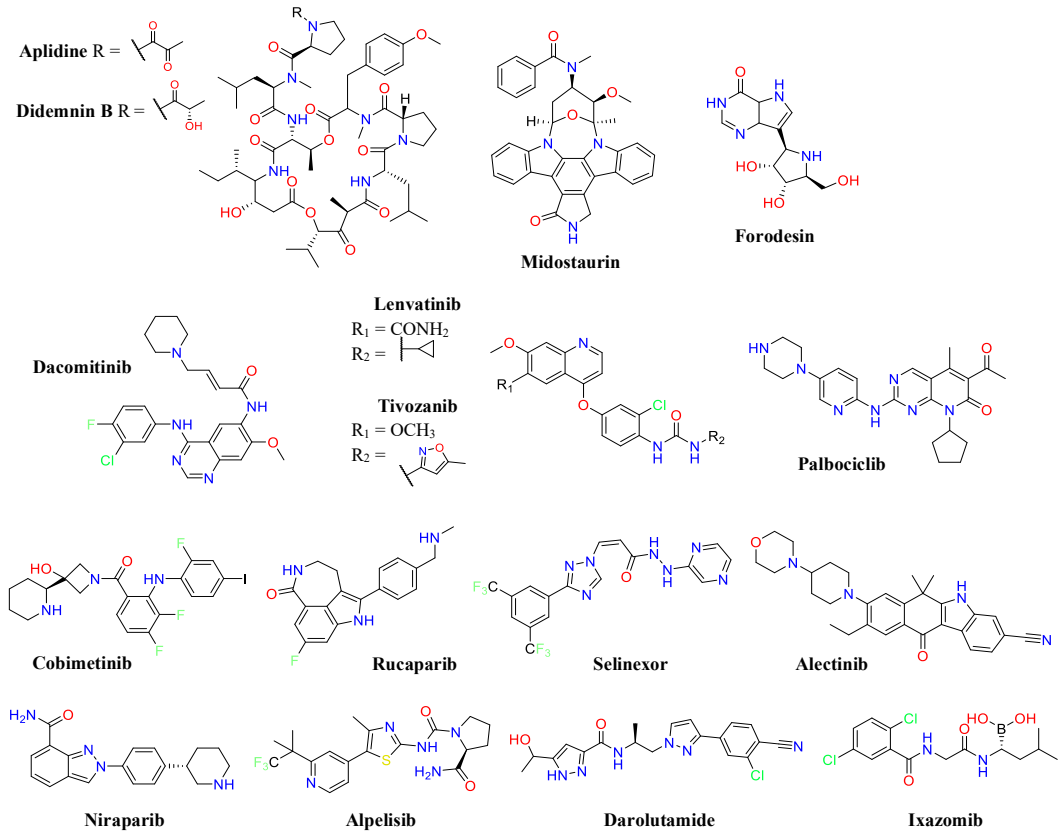

Antiviral – 47% of approved agents are Vs, created against various influenza serotypes. These include the ND **tenofovir disoproxil orotate**, two S agents for HIV, one for CMV and one for HSV1. Recently, **doravirine**, engineered by **MK-1107** to be active against HIV reverse transcriptase. Epclusa (sofosbuvir/**velpatasvir**) have been approved for the treatment of HCV, in the S*/NM category are Maviret (glecaprevir/pibrentasvir),

14 X. Liang, P. Wu, et al., *Eur. J. Med. Chem.* **2021**, *220*, 113473.

narlaprevir, and **danoprevir**, and in the S/NM are grazoprevir, elbasvir, **baloxavir**, and **tecovirimat**.

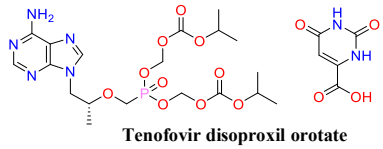

Tenofovir disoproxil orotate

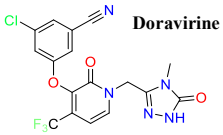

Doravirine

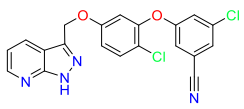

MK-1107

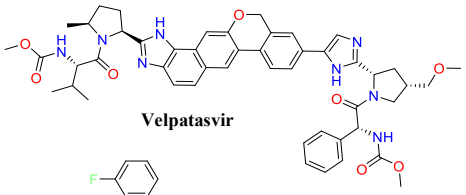

Velpatasvir

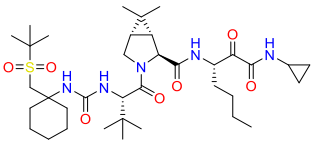

Narlaprevir

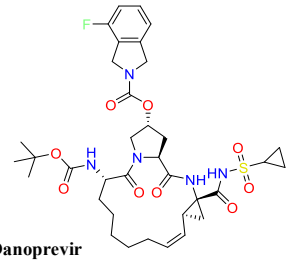

Danoprevir

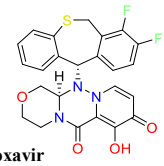

Baloxavir

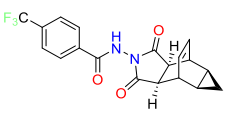

Tecovirimat

Chapter II Synthesis of Maytansinol-based Conjugates as Microtubule Modulators

Microtubule-associated proteins (MAPs) regulate the microtubule (MT) polymerisation dynamics by an unclarified conformational recognition of tubulins. Targeting tubulin founds new application in neurodegenerative diseases to stabilize MT, because in some of these pathologies τ-MAP becomes defective and no longer stabilizes MTs properly.[15] Furthermore, binding drug causes small conformational change of tubulin, which can propagate at long distances in the MT preventing the appropriate recognition by the MAPs. The result is an abnormal function of MT dynamics related to various side effects.

1 Introduction

MTs are polymers of α/β tubulin heterodimers and constitute the cell cytoskeleton, together with microfilaments and intermediate filaments. They are important in a number of cellular processes: they are involved in the maintenance of the cellular structure, guarantee the correct neuronal function, and provide platforms for intracellular transport. MTs are responsible for the movement of secretory vesicles, organelles and intracellular macromolecular complexes and actively participate in cell division through the formation of mitotic spindles, used to separate eukaryotic chromosomes.[17]

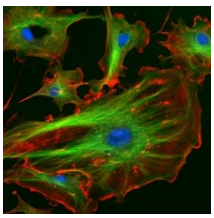

Figure 1.1 Components of the eukaryotic cytoskeleton: actin filaments (red), MTs (green), and nuclei (blue).[16]

MTs can provide structure and shape to eukaryotic cells, because of the formation of intracellular structures. In most mammalian cells *in vivo*, MTs originate a 25 nm diameter cylinder made up of 13 protofilaments. Instead, *in vitro* it is possible to assemble MTs from 9 to 16 protofilaments with varying diameters as a consequence.[18]

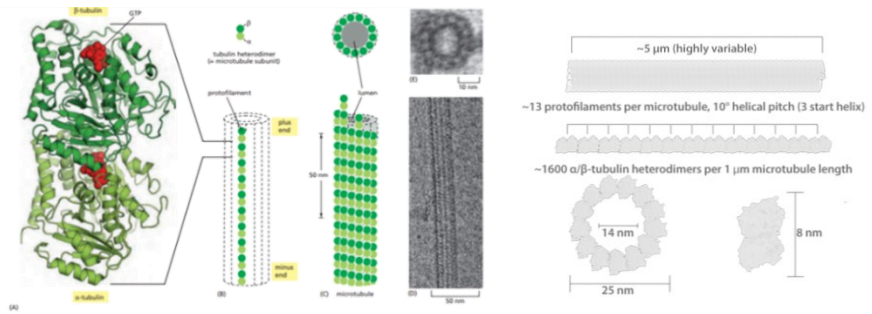

Figure 1.2 Structure of a microtubule and its subunits.[19]

Tubulins are made by the association of an α and a β globular proteins (formed by a sequence of 445-450 amino

15 **a]** E. I. Pchitskaya, V. A. Zhemkov, I. B. Bezprozvanny, *Biochem.* **2018**, *83*, 1068–1074; **b]** M. Salama, A. Shalash, et al., *PLoS One* **2018**, *13*, 1–11.

16 "FluorescentCells.jpg," can be found under https://imagej.nih.gov/ij/images/, **n.d.**

17 R. D. Vale, *Cell* **2003**, *112*, 467–480.

18 L. A. Amos, D. Schlieper, *Adv. Protein Chem.* **2005**, *71*, 257–298.

19 B. Alberts, A. Johnson, *Molecular Biology of the Cell*, Garland Science, **2014**.

acids) in protofilament that can associate to form a hollow tube, the MT. The β-subunit of a dimer non-covalently interacts with the α-subunit of another dimer in a head-to-tail assembly process to form a linear protofilament. Several protofilaments cluster longitudinally to form a sheet that folds into the characteristic hollow cylindrical shape of the MT.[20]

1.1 MT Polymerisation

The interactions exploit polar-type properties: the minus end exposes the α-tubulins and is the least dynamic end, while the plus end is composed by β-tubulins and expresses properties that are more dynamic. MTs are subject to dynamic polymerisation; they undergo growth and shrinkage cycles due to the association and dissociation of tubulins at the extremities.

MT dynamics are managed by the hydrolysis of guanosine triphosphate (GTP) to guanosine diphosphate (GDP) when a tubulin dimer adds to a MT.[22] There are two different binding sites for GTP on the tubulin dimer structure. The first one is located on the α-tubulin at the interphase with the β-subunit, it is called N-site. In this position, GTP is tightly bound between the subunits; therefore, it is neither exchangeable nor hydrolysable.[19] The second site is placed on the top of the β-subunit, and it is named E-site because it is exchangeable. During the polymerisation step, a GTP-containing tubulin dimer at both the N- and E-sites is added to a growing MT. At this point, the GTP hydrolyses into GDP, releasing inorganic phosphate (P_i). Therefore, the depolymerisation process implicates the ejection of GDP-containing subunits and the cycle can starts again.[23]

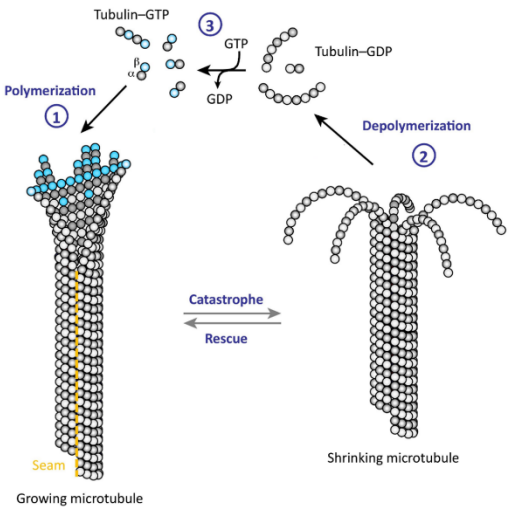

Figure 1.3 MT dynamic instability. (1) Tubulin-GTP dimers (b-tubulin shown in blue) add to growing MT plus-end that are stabilized by the GTP-cap. (2) Once the GTP-cap is lost, MT ends rapidly depolymerise into tubulin-GDP dimers (b-tubulin shown in white). (3) The tubulin dynamic cycle is completed by exchanging the GDP nucleotide with GTP.[21]

Both growth and shrinkage processes occur mainly at the plus end, at the interface of the β-subunit. The transition from polymerisation to depolymerisation is called “catastrophe”, while the opposite event is called “rescue”. In 1984, Mitchison and Kirschner observed these phenomena and described them as a whole using the term "dynamic instability".[24] This dynamic behaviour involves MT growth/shrinkage rate, and rescue/catastrophe frequencies as variables.

Nucleation

The polymerisation dynamics of MTs are considered to be different from most polymers. Polymerization begins with the nucleation process that is the slow formation of a short "nucleus" of MT. α- and β-tubulins are the main building blocks of MTs and they are capable to nucleate spontaneously when present in high concentration. Into the cell, nucleation and organisation begins with the formation of MT from tubulin dimers linked to a microtubule-organising centre (MTOC). This organelle is a centrosome, a non-membranous structure located near the nucleus of the cell and surrounded by an amorphous mass of protein responsible for the formation, demolition, and organisation of the MT. The boundaries of the centrosome are indistinguishable; however, the position is

20 J. Zhou, P. Giannakakou, *Curr. Med. Chem. - Anti-Cancer Agents* **2005**, *5*, 65–71.

21 M. O. Steinmetz, A. E. Prota, *Trends Cell Biol.* **2018**, *28*, 776–792.

22 M. A. Jordan, L. Wilson, *Nat. Rev. Cancer* **2004**, *4*, 253–265.

23 A. Desai, T. J. Mitchison, *Annu. Rev. Cell Dev. Biol.* **1997**, *13*, 83–117.

24 T. Mitchison, M. Kirschner, *Nature* **1984**, *312*, 237–242.

identify by the presence of centrioles, a pair of cylindrical structures of MTs contained within.

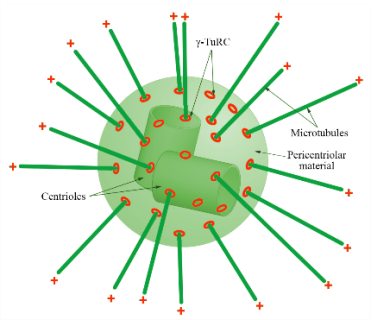

Figure 1.4 MTs nucleation in a centrosome.

MTOC contains the proteins responsible for the MT nucleation, including the microtubule-associated proteins (MAPs), a pair of centrioles, and the γ-tubulin,[25] which is another type of tubulin and it is different from the α- and β-subunits. The γ-tubulin combines with several other associated proteins to form a washer-like structure known as a "γ-Tubulin Ring Complex" (γ-TuRC). This complex serves as a template for α/β-tubulin dimers to induce polymerisation. It acts as a cap at the minus end, so the MT can grow reversibly by the addition of new tubulin dimers in the plus direction consequently away from the MTOC.[23]

Polymerisation

After the nucleation event, tubulin monomers must be added to the growing MT. The monomer addition/removal process depends on the concentration of the α/β-tubulin dimers versus the critical concentration, which is the concentration of dimers at which there is no longer any net assembly or disassembly at the plus end of the MT. If the dimer concentration is greater than the critical concentration, the MT will polymerises and grows, whereas if the concentration is below the critical concentration, the MT length will decreases.

1.2 Microtubule dynamics

Dynamic instability

The reversibility of the polymerisation and depolymerisation phenomenon can be explained through the "cap model". Dynamic instability refers to the assembly and disassembly processes at the ends of a MT. In this region, the MT can dynamically switch between growth and shrinkage phases.[26]

As mentioned, tubulin dimers bind two GTP molecules, one of which is subsequently hydrolysed because of assembly. GTP bound to the N-site of the α/β-tubulin interphase has a structural function and is responsible for strong lateral interactions leading to a high stability of the MT, while GTP bound to the E-site of the β-tubulin can be hydrolysed to GDP. The assembly properties of GTP-tubulin differ from those of GDP-tubulin, which causes weaker interactions promoting the depolymerisation.[27] Based on this MT structure, the main effect of hydrolysis on lateral interactions is restricted to the β-subunit. A GDP-bound tubulin subunit at the tip of a MT will tend to fall out, but a GDP-bound tubulin in the middle cannot spontaneously escape from the polymer. Accordingly, the stability of a MT end is determined by the lateral interactions of the last monomer.

When a new tubulin dimer adds to the plus end of MT, hydrolysis of the GTP in the E-site of the second last dimer occurs. Therefore, the last tubulin subunit at the tip exposes the GTP until a new dimer adds.[27a] Thus, it is assumed that a cap of GTP-bound tubulin exists at the tip of the MT, preventing disassembly. When the hydrolysis reaches the tip, the rapid catastrophe process begins, involving depolymerisation through a weak lateral interactions between the tubulins of neighbouring protofilaments. Then, the GTP-bound tubulin can begin adding to the tip again, generating a new cap and giving rise to the rescue phase.[24]

Studies have shown that MT only grow at the plus end in the exclusive presence of GTP. When GTP and GDP are simultaneously present, MTs grow at the minus end, suggesting that GDP-induced growth inhibition at the

25 M. A. Jordan, *Curr. Med. Chem. - Anti-Cancer Agents* **2002**, *2*, 1–17.

26 G. Karp, in *Cell Mol. Biol. Concepts Exp.*, **2005**, p. 355.

27 **a]** E. Nogales, *Annu. Rev. Biophys. Biomol. Struct.* **2001**, *30*, 397–420; **b]** R. C. Weisenberg, W. J. Deery, P. J. Dickinson, *Biochemistry* **1976**, *15*, 4248–4254.

plus end reverses the growth polarity of MTs.[28] At the minus end, contact is made between the E-site of the new incoming dimer and the last α-tubulin subunit exposed. Therefore, there is no GTP cap at the minus end, but the last lateral contact always consists of an α-subunit independent of the phosphorylation state. In fact, the α-tubulin always contains a non-hydrolysable GTP in the N-site and therefore the minus end is stable enough for lateral interactions due to the strong contacts between α-tubulins.[29]

Treadmilling

A second consequence of assembly-driven GTP hydrolysis is the "treadmilling" phenomenon. The net growth at one end of the MTs is balanced by the net shortening at the opposite end in a dynamic behaviour.[30] It involves the flow of tubulin subunits from the plus end to the minus end without changing the length of the MT and is regulated by the differences in critical concentrations of the subunits at the extremities. Treadmilling was observed through a radiolabelled ^{3}H-GTP placed at the plus end. The marked dimer remained within the MT for a certain time before being expelled at the minus end.[31]

Dynamic instability and treadmilling are compatible with each other and MTs can exhibit only one behaviour or a combination of both.

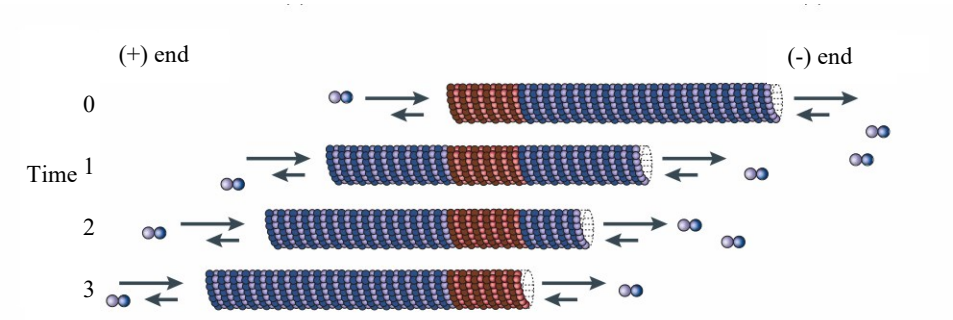

Figure 1.5 Treadmilling microtubules.[22] Tubulin heterodimers are added to the plus end of the MT at time 0, displace through the MT, and are lost from the minus end at time 3. The length of the MT is unchanged. Treadmilling is determined by the different critical concentrations of tubulin at opposite ends.

1.3 The role of MTs in mitosis

MTs are involved in many fundamental processes. They take part in the formation of the mitotic spindle during the cell division metaphase; therefore, they participate in the vital mechanism of cellular reproduction. The cell cycle consists of an ordered sequence of events to duplicate the genetic material present in the cell nucleus. The result is the division of the parent cell into two identical daughter cells.

The cell cycle is divided into four phases: G1, S, G2, M. In the *S phase*, DNA synthesis takes place with chromosomal duplication. Subsequently, in the *M phase*, cell division occurs. This step includes nuclear division, called mitosis, and cytoplasmic division, called cytokinesis. G1 and G2 are the *gap phases*: periods that allow the cell to make the generation of new proteins and organelles, and to grow adequately before division.

At the end of the S phase, the DNA molecules in each pair of duplicated chromosomes are held together by specialised proteins. Following the G2 transition, in a stage called *prophase* of mitosis, the two DNA molecules are gradually separated and condensed into pairs of linked sister chromatids. Outside the nucleus, the two replicated centrosomes set the basis for the formation of the mitotic spindle. Through the nucleation, the MTs

28 Y. Tanaka-Takiguchi, T. J. Itoh, H. Hotani, *J. Mol. Biol.* **1998**, *280*, 365–373.

29 E. Nogales, M. Whittaker, et al., *Cell* **1999**, *96*, 79–88.

30 R. L. Margolis, L. Wilson, *Bioessays* **1998**, *20*, 830–6.

31 R. L. Margolis, L. Wilson, *Nature* **1981**, *293*, 705–711.

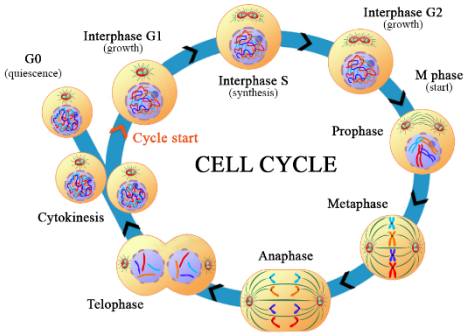

Figure 1.6 Mitosis in the Eukaryotic Cell Cycle. Mitosis is the multi-phase process in which the nucleus of a cell divides.

can growth generating the spindle. When the nuclear envelope disassembles in the next *prophase*, the chromatid pairs attach to the mitotic spindle and are aligned at the equator in a stage called the *metaphase*. The destruction of the cohesion between chromatids begins during the *anaphase* and separates the chromatids, which are attracted to opposite poles of the spindle. The spindle is then disassembled and the segregated chromosomes are packed into separate nuclei during *telophase*. *Cytokinesis* then splits the cell into two daughter cells, which inherit one of the two nuclei.

Dynamic instability and treadmilling are crucial for the MTs to perform many of their cellular function, such as reorienting the MT network when cells undergo migration or morphological changes and the rearrangement of MTs at the beginning of mitosis. During the metaphase, the duplicated chromosomes bind plus end of MTs *via* kinetochores, which are protein structures of the centromere. There are usually two kinetochores for each centromere, one for each chromatid. The role of kinetochores is to engage the MTs of the mitotic spindle during metaphase. In this way, the chromosomes are correctly aligned at the equator of the spindle and subsequently the pairs are separated and dragged to opposite poles of the cell. The chromatids movement is promoted by the dynamic properties of instability and treadmilling of the MTs: tubulin is added to the MTs at the kinetochores in the metaphase, while during the anaphase the kinetochores pass into a state of depolymerisation/polymerisation at the plus end. Simultaneously, depolymerisation occurs at the minus end due to the treadmilling. The net result is a traction of the chromatids exerted by the MTs in plus-to-end direction towards the centriole until the completion of the segregation of the chromatids.[32]

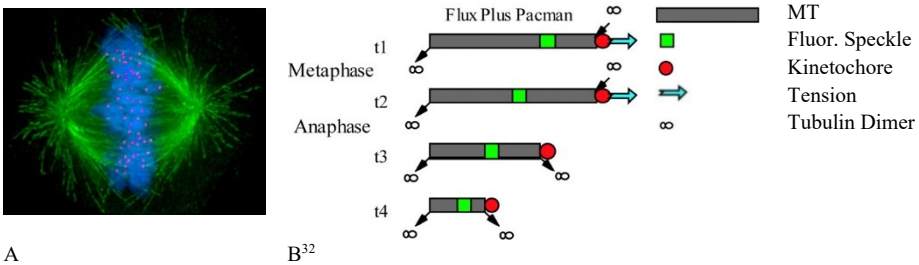

A B[32]

Figure 1.7 a) Fluorescent image of a human cell during metaphase: MTs in green, chromosomes in blue, and kinetochores in pink; b) Models of kinetochore motility and microtubule flux. A single microtubule is shown with the minus end at the left and the plus end attached to the kinetochore on the right. Arrows indicate sites of polymerisation or depolymerisation.

1.4 Microtubule-associated proteins

MTs develop interactions with a large number of microtubule-associated proteins (MAPs). These proteins are capable of binding polymerized or depolymerized tubulin subunits to regulate the stability of MT. MAPs carry out a wide range of functions such as stabilizing and destabilizing MTs, guiding MTs towards specific cellular locations, regulating neuronal development, cross-linking MTs and mediating the interactions of MTs with other

32 P. Maddox, A. Straight, et al., *J. Cell Biol.* **2003**, *162*, 377–382.

proteins in the cell. Based on their mode of action, MAPs can be classified into a) motile MAPs, motor proteins that generate forces and movement; b) enzymes that break or depolymerise MT; c) MT nucleators; d) end-binding proteins that specifically associate with plus- or minus-ends of MT; and e) the so-called structural MAPs.[33]

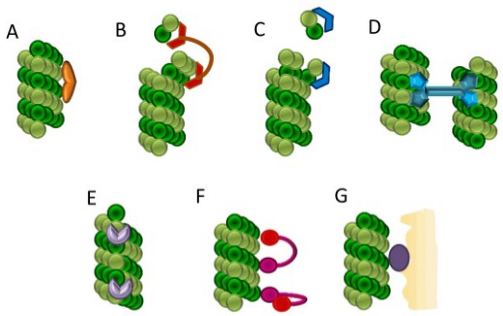

Figure 1.8 Some example of MAPs function on MT: a) stabilizing protofilament; b) promoting polymerisation of tubulin dimer; c) sequestering tubulin and bending protofilament; d) forming MT bundle; e) zipping and tracking the plus end of MT; f) walking along MT; g) linking MT to Golgi network.[34]

Structural MAPs are generally made up of repetitive domains[18] and consequently can bind more than one tubulin dimer. The binding between structural MAPs and specific tubulin domains is responsible for the stabilization/de-stabilization of MT. Changes in the tubulin structure interfere with the correct recognition by the MAPs, thus disturbing the interaction process.

MAP-microtubule binding is regulated through the phosphorylation of MAPs within the cell. This is achieved through the function of the microtubule-affinity-regulating-kinase (MARK) protein. Phosphorylation regulates stabilization as it causes the detachment of the MAP from any MT to which it is bound.[35] This detachment is usually associated with a destabilization of the MT that causes disaggregation.

1.5 The role of MTs in neurons

MTs present in neurons of nerve tissues are called neurotubules (NTs). NTs along with neurofilaments help maintain neuron shape, give mechanical support, and attend the transport of organelles and vesicles containing neurotransmitters, m-RNA and other intracellular molecules within a neuron.[36] Despite having similar mechanical properties, NTs have some differences from MTs. Most NTs are not hooked to the MTOC and therefore they polymerise into the dendrites (the signal receiver) and axons (the signal transmitter) after nucleation in the centrosome with the aid of MAPs.[37] Consequently, both ends of the NTs terminate in the cytoplasm. Neurons have a polarised NT network:[38] plus end of NTs points towards the axon terminal and minus end is oriented towards the soma, while dendrites contain undirected NTs. As in MTs, the two ends differ in growth rate: the plus end grows much faster than the minus end,[39] and they are subject to dynamic instability and treadmilling. The net polymerisation of tubulin determines the

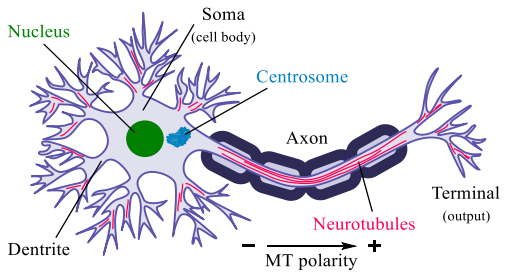

Figure 1.9 Neuron structure.

33 S. Bodakuntla, A. S. Jijumon, et al., *Trends Cell Biol.* **2019**, *29*, 804–819.

34 "protein_kind," can be found under http://systbio.cau.edu.cn/mappred/images/protein_kind.gif, **n.d.**

35 G. Drewes, A. Ebneth, E. M. Mandelkow, *Trends Biochem. Sci.* **1998**, *23*, 307–311.

36 C. Janke, M. Kneussel, *Trends Neurosci.* **2010**, *33*, 362–372.

37 M. Wilsch-bräuninger, C. C. Hoogenraad, et al., **2010**, 704–708.

38 A. C. Kwan, D. A. Dombeck, W. W. Webb, *Proc. Natl. Acad. Sci. U. S. A.* **2008**, *105*, 11370–11375.

39 R. King, *Microscopic Anatomy: Normal Structure*, Elsevier B.V., **2013**.

length of the NTs and the dynamics allow the transport of load signals to synapses over long distances. Kinesin and dynein are defined motor MAPs and perform the transport function. The kinesin moves along the NT filaments from the minus to the plus end according to an *anterograde* transport; instead, the dynein is involved in *retrograde* transport in the opposite direction. NTs serve as subcellular pathways for motor proteins carrying multiple organelles and macromolecules.[40]

Neurodegeneration

The rates of polymerisation, depolymerisation and catastrophe of NTs vary according to the MAPs present throughout the filament.[41] Their role is to control assembly and some of them can bind more than one tubulin dimer. MAP-tubulin binding is responsible for the stabilization and destabilization of NT, and structural changes in tubulin interfere with the correct recognition of MAPs, thus disturbing the stabilization process. Consequently, the onset of neurodegenerative diseases is possible, due to the interruption of the correct dynamics of recognition.

Neurodegeneration is the progressive loss of structure and activity of neurons. NTs participate in neurodegeneration due to their role in the long-distance transport of material, furthermore the alterations of their dynamics contribute to the establishment of polarity errors of the NTs, and the maintenance of neuronal morphology and synaptic transmission are compromised. Disorganisation of NTs polarity can result in an incorrect localisation of cargo.

MAPs identified in brain tissue can be classified into two types based on their molecular weight. The class that includes MAPs with a molecular weight less than 55-62 kDa are called τ-proteins and promote nucleation, prevent disassembly, induce the formation of parallel arrays of MTs,[42] and assists motor transport creating space around NTs.[43] Furthermore, they stabilize MTs in axons[15ab,18,44] and are associated to some neurodegenerative diseases called *tauopathy,* such as Parkinson and Alzheimer.[15ab,44,45]

When τ-MAP is overexpressed, it accumulates on the surface of the NTs disrupting the transport of motor proteins and causing disease.[15a] Tauopathy involves the aggregation of τ-protein into neurofibrillary or gliofibrillary tangles in the human brain. Tangles are formed by hyperphosphorylation of the τ-protein, causing dissociation of the protein from MTs and the formation of insoluble aggregates.[46] The mechanism of tangle formation is not well understood, but it appears to be linked to the cause of Alzheimer's disease.

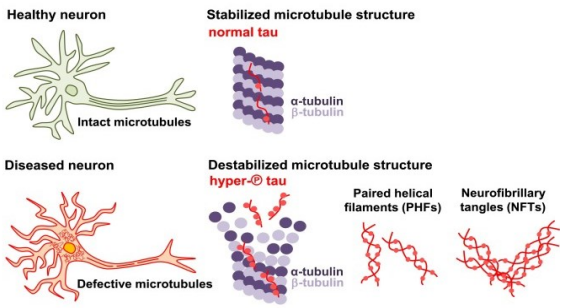

Figure 1.10 Tauopathy of neuron.

1.6 Tubulin-binding drugs and chemical effects

The multiple functions in which MTs are involved make them an interesting pharmacological target. Their relevance as a target in anticancer treatment is a consequence of their role in the cell cycle. The aim is to act against the rapid cell replication typical of cancer cells, therefore a wide variety of discovered drugs can bind tubulin and modify its assembly properties.

These compounds are called MT targeting agents (MTAs) and are divided in stabilizer (MSAs) and destabilizer

40 Y. P. Wairkar, C. D. Link, et al., *Front. Cell. Neurosci.* | *www.frontiersin.org* **2015**, *9*, 343.

41 E. L. F. Holzbaur, D. Ph, S. S. Scherer, *North* **2012**, 2011–2013.

42 E. Mandelkow, E. M. Mandelkow, *Curr. Opin. Cell Biol.* **1995**, *7*, 72–81.

43 J. S. Kresge, C. T., Leonowicz, M. E., Roth, W. J., Vartuli, J. C., Beck, *Nature* **1992**, *359*, 710–713.

44 G. T. Bramblett, M. Goedert, et al., *Neuron* **1993**, *10*, 1089–1099.

45 P. Lei, S. Ayton, et al., *Int. J. Biochem. Cell Biol.* **2010**, *42*, 1775–1778.

46 M. Goedert, M. G. Spillantini, *Mol. Brain* **2017**, *10*, 18.

(MDAs) based on the effect induced. Both can manage MT dynamics by acting on the polymerisation process. The suppression of MTs treadmilling and dynamic instability by use of antimitotic drugs appears to block the advancement of the cell cycle at the anaphase stage. If the mitotic process is stopped, the cell dies by apoptosis.[25] Cancer cells are rapidly proliferating cells characterised by an enhanced cell cycle, so antimitotic drugs have greater effects on cancer cells than healthy ones. In general, the dynamics are normally suppressed by low sub-toxic concentrations of drugs, which also inhibit cell migration and angiogenesis.

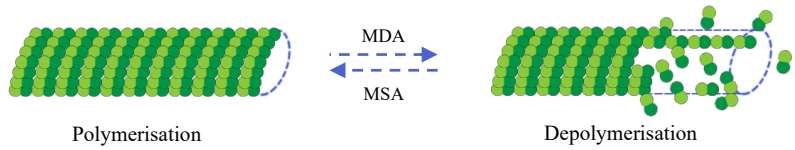

Figure 1.11 Effect of drugs on MT dynamic. MSA promotes polymerisation and MDA promotes depolymerisation (MSA = MT Stabilizing Agent; MDA = MT Stabilizing Agent).

Today it is known that many natural molecules are able to interact with the soluble tubulin and/or with part of it present in the MT, causing interference in the dynamic functions of the MTs and consequently producing a cytotoxic effect.[21]

Several binding sites for MTAs have been characterised on the surface β-tubulin.[21] The vinca domain is located near the GTP exchangeable site at the positive end. It hosts the vinca alkaloids, the first compounds developed targeting MTs. These molecules, such as vincristine and vinblastine, are anticancer agents extracted from the leaves of *Catharantus roseus* - commonly known as Madagascar periwinkle - that have been used in traditional medicine since the 17th century. Vincristine and vinblastine were mainly used as hypoglycaemic drugs, but their anti-leukemic properties were later discovered. Therefore, they have been widely and successfully used for the treatment of haematological neoplasms, their success has been such that they are considered "wonder drugs". The study of the mechanism of action of these alkaloids has laid the foundation for the development of new semisynthetic derivatives (vinorelbine, vindesine) which are still used against leukaemia or other solid tumors, both as single agents and in cocktails. Their action is strongly dependent on the concentration of the drug: at high concentrations, they cause the arrest of mitosis due to the disassembly of the MTs. On the contrary, at low concentrations these alkaloids modify the MT dynamics without changing the length of the spindle: they remain in a state of pause. In both situations, the antitumor effect is due to the interruption of the mitotic process and therefore to the induced apoptosis.

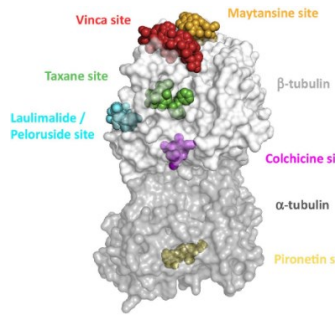

Figure 1.12 Tubulin binding sites on β-tubulin.[47]

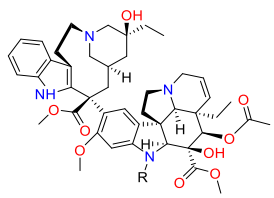

R = CHO: **Vincristine**
R = CH_3: **Vinblastine**

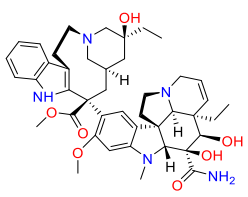

Vindesine

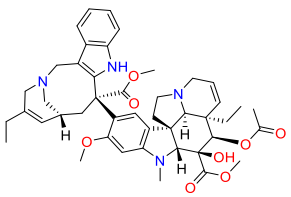

Vinorelbine

Other natural compounds such as halichondrins, eribulin, and dolastatins bind the vinca domain and are currently under study for the clinical development in cancer treatment.[21,48] Eribulin binds plus end and trigging apoptosis of tumor cells following a prolonged and irreversible mitotic block.

47 A. E. Prota, K. Bargsten, et al., *Proc. Natl. Acad. Sci.* **2014**, *111*, 13817–13821.

48 A. ML, J. J, et al., *Ann. Oncol. Off. J. Eur. Soc. Med. Oncol.* **2003**, *14*, 1607–1615.

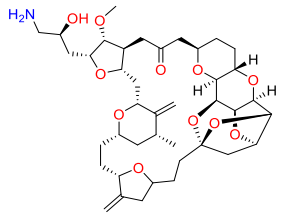

Eribulin

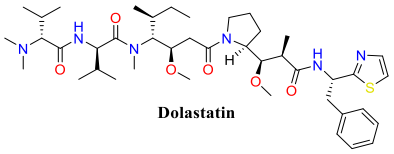

Dolastatin

Colchicine is an alkaloid isolated from *Colchicum autumnale*, commonly known as meadow saffron. Colchicine has a specific site located on the β-tubulin at the interface between α and β monomers.[49] Like the vinca alkaloids, colchicine preferentially binds the single heterodimer and block the polymerisation of MT. The use of colchicine for the clinical treatment of cancer was soon suppressed due to the high toxicity expressed towards healthy tissues. However, the in-depth study of mechanism of interaction with tubulins has allowed the development of new drugs that bind to the same site and with the same inhibiting effect of MT dynamics, such as cambretastatins and nocodazole, a family of NPs that show an interesting antitumor activity.[20,50]

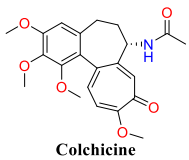

Colchicine

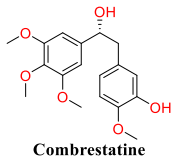

Combrestatine

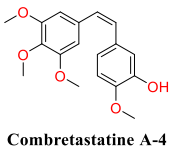

Combretastatine A-4

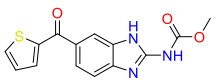

Nocodazole

Taxol - or paclitaxel - is a complex diterpene isolated from the bark of *Taxus Brevifolia*, is used in the treatment of breast and lung cancers. The interest in this plant arose from the observation of the high antiproliferative effect of the bark extract during a screening promoted in 1962 for the exploration of new anticancer agents.[49] Taxol was then approved by the FDA in 1992 for the treatment of ovarian cancer. The peculiarity of this molecule is the mechanism of action never observed before, which blocks dynamic instability by stabilizing GDP-bound tubulin on the inner surface of the MT. Therefore, even when hydrolysis of GTP reaches the tip of the MT, there is no depolymerisation and the MT does not shrink, causing the arrest of the cell cycle and thus apoptosis.[51] This characteristic made taxol the precursor of a new generation class of anticancer drugs. After paclitaxel, its semisynthetic analogue docetaxel was registered and today they are used both alone and in combination with *cis*-platin in mammary and gynaecological neoplasms, squamous cell carcinomas (head and neck cancers, some lung cancers) and Kaposi's sarcoma.[49]

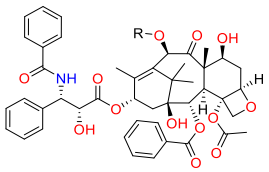

R = $COCH_3$, **Paclitaxel (Taxol)**
R = H, **Docetaxel**

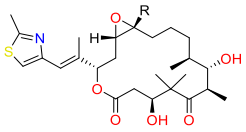

R = H, **Epothilone A**
R = CH_3, **Epothilone B**

The study of the SAR of taxane class of terpenes has made it possible to discover other NPs that bind the same tubulin site. These include epothilone A and B (isolated from the myxobacterium *Sorangium cellulosum*), discodermolide (extracted from the sea sponge *Discodermia dissolute*) and sarcodictyins (from the coral *Sarcodictyon roseum*).

49 K.-H. Altmann, J. Gertsch, K.-H. Altmann Jürg Gertsch, *Nat. Prod. Rep* **2006**, *24*, 327–357.

50 Y. Y. Chao, C. R. Jan, et al., *Drug Dev. Res.* **2002**, *55*, 91–96.

51 E. A. Perez, *Mol. Cancer Ther.* **2009**, *8*, 2086–2095.

The MTs are also being studied for their involvement in neurodegenerative diseases. Understanding the relationships between MT dynamics and dendritic spines could be offered by studies using MT-targeted drugs. Furthermore, using MSAs to normalise the dynamics of MTs may be useful in the treatment of neurodegenerative diseases that cause loss of MT stability and synaptic connectivity.[15ab]

EpoD,[52] CNDR-51657,[52] and Dictyostatin[53] show neuroprotective effects in mouse models of Alzheimer's and tauopathies.

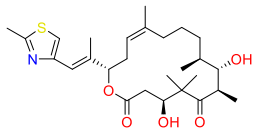

Epothilone D

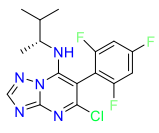

CNDR-51657

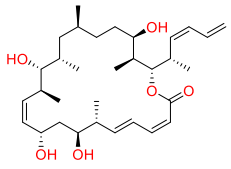

Dictyostatin

However, the use of MSAs in cancer therapy has shown that they have a number of negative side effects[54] that may limit their application in the treatment of Alzheimer's disease. Both stabilization and destabilization of MTs have detrimental effects on dendritic spines. Therefore, an effective Alzheimer's disease drug targeting MT should be neuronspecific (to reduce side effects) and have a mild effect on MT dynamics without severe tubulin cytoskeleton disturbances.

1.7 Focus on maytansinoids, microtubule destabilizing agents

In addition to these classes of MT-targeted compounds, the plant-derived maytansinoids and their microbial counterparts, the ansamitocins, have been noted for their ability to inhibit tubulin polymerisation and induce apoptosis.[55] Due to this characteristic, they are used as extremely potent anticancer agents *in vitro* and in tumor-bearing animals, as they block the assembly of tubulin in functional microtubules. Kupchan *et al*. reported the structure of maytansine, which is the first isolated compound from the East African shrubs *Maytenus ovata* in 1972.[56] Maytansinoids and ansamitocins are members of the ansamycin group of NPs[57] and are characterised by 19-membered ansamacrolide structures linked to a chlorinated benzene ring.

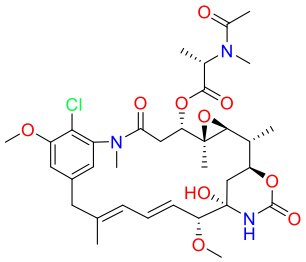

Maytansine

Figure 1.13 A general aspect of Maytenus plant and structure of maytansine isolated.

Despite their high antimitotic activity,[56] maytansinoids show lack of specificity towards cancer cells, and this has led to many failures during clinical trials due to high neurotoxicity and side effects were encountered.[58]

52 J. Kovalevich, A.-S. Cornec, et al., *J. Pharmacol. Exp. Ther.* **2016**, *357*, 432.

53 V. Makani, B. Zhang, et al., *Acta Neuropathol. Commun. 2016 41* **2016**, *4*, 1–12.

54 K. Lou, Y. Yao, et al., *J. Med. Chem.* **2014**, *57*, 6116–6127.

55 M. Lopus, E. Oroudjev, et al., *Mol. Cancer Ther.* **2010**, *9*, 2689–2699.

56 S. M. Kupchan, Y. Komoda, et al., *J. Am. Chem. Soc.* **1972**, *94*, 1354–1356.

57 K. L. Rinehart, L. S. Shield, in *Fortschr. Chem. Org. Naturst.*, Fortschr Chem Org Naturst, **1976**, pp. 231–307.

58 B. F. Issell, S. T. Crooke, *Cancer Treat. Rev.* **1978**, *5*, 199–207.

However, antibody-drug conjugates (ADCs) of maytansinoids have been created to increase selectivity in order to take advantage of the high cytotoxicity.

ADCs are complex molecules made up of a monoclonal antibody bound to a drug. The advantage of this type of compounds comes from the targeting abilities of monoclonal antibodies with the cancer-killing ability of cytotoxic drugs. The antibody portion specifically targets an antigen ideally expressed only by cancer cells. The antibodies attach the target antigens on the cell surface, and the biochemical reaction between the antibody and the protein triggers the antibody uptake signal along with the linked cytotoxin. After the ADC has been internalised, the cytotoxin works by attacking the cancer. Therefore, the specificity of the drug is enhanced against cancer cells while preserving healthy cells due to the lack of expression of this antigen. In this way, the systemic toxicity of the drug is significantly reduced.[59] In 2013, the US Food and Drug Administration (FDA) approved trastuzumab-emtansine (T-DM1, the ADC of maytansine) for the treatment of HER2 positive breast cancer. This therapy has also given positive results against tumors resistant to other treatments and in case of relapse. The drug is made up by a natural maytansine derivative associated to the antibody Trastuzumab through a non-reducible thioether linker (4-[*N*-maleimidomethyl]cyclohexane-1-carboxylate, MCC). The linker binds Maytansine with an ester and Trastuzumab *via* the many lysine residues present on the surface of the antibody.[60] T-DM1 binds HER2 receptors exploiting the Trastuzumab portion and releases the drug into the cell through a receptor-mediated endocytosis.[59] In this way, drug targets preferentially the cancer cells that expose HER2 antigen and inhibits the cancer proliferation by stopping the cell mitosis step.[61]

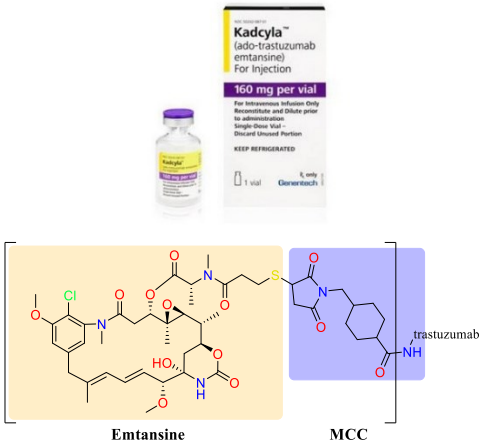

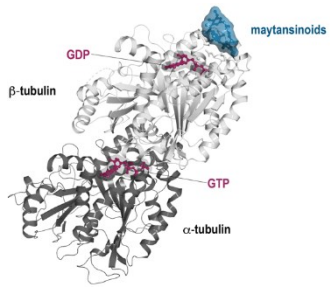

Figure 1.14 Overall view on the interaction between maytansinoids (blue) and tubulin (grey) in relation to the bound nucleotides (purple).

The maytansine binding site on tubulin is shared with rhizoxine and is located adjacent to the vinca site on top of β-tubulins and in the proximity to the exchangeable site of GTP (**Figure 1.14**).[62] Thus, binding of maytansine inhibits vinblastine binding and prevents association of GTP with tubulin. The effect produced is similar to that of the vinca alkaloids, but 100 times stronger[55] and with a different mechanism of action. In the absence of ligands, α/β-tubulins undergo a curve-to-straight conformational transition when assembling to form MT (**Figure 1.15** - 1). Vinca ligands destabilize MT by introducing a wedge at the interface between two tubulin dimers, inhibiting the curve-to-straight conformational transition required to build MT (**Figure 1.15** - 2). The ligands of maytansine-site bind β-tubulin hindering the formation of longitudinal contacts between the dimers of MT. At low concentrations, they inhibit the addition of tubulin subunits as they are bound to the plus ends of the growing MT (**Figure 1.15** - 3a); at high concentrations, they directly prevent the assembly of single tubulin subunits because they are already bound to the dimers (**Figure 1.15** - 3b).

X-ray crystallography can well elucidate the accommodation of maytansine into the binding site of tubulin. Examination of the binding of tubulin to maytansine revealed three points of interaction within the active site: hydrogen bonds between the oxazinanone carbonyl group and the residues Asn102 and Lys105, hydrogen bonds between the carbonyl oxygen of the amide and the Val181, and hydrophobic interactions between the methyl

59 P. Khongorzul, C. J. Ling, et al., *Mol. Cancer Res.* **2020**, *18*, 3–19.

60 J. F. Ponte, X. Sun, et al., *Bioconjug. Chem.* **2016**, *27*, 1588–1598.

61 E. Oroudjev, M. Lopus, et al., *Mol. Cancer Ther.* **2010**, *9*, 2700–2713.

62 M. Takahashi, S. Iwasaki, et al., *Biochim. Biophys. Acta - Gen. Subj.* **1987**, *926*, 215–223.

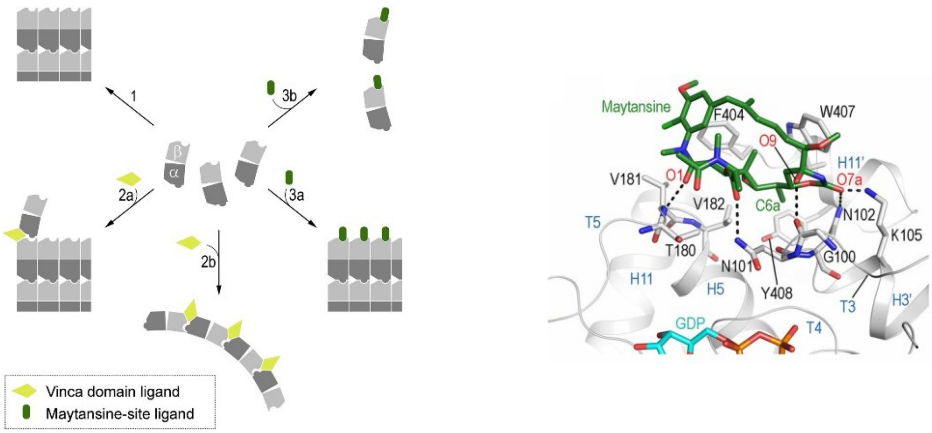

Figure 1.15 Mechanism of inhibition of vinca domain ligands and of maytansine-site and structure of tubulin-maytansine complex.[47]

placed near the epoxide and a pocket formed by the residues Asn101, Asn102, Val182, Phe404 and Tyr408. In addition, it was demonstrated that the presence of hydroxyl oxazinanone and the epoxide is essential for the antiproliferative activity.[56] The N-methyl alanine group of maytansine is exposed to the solvent and does not take part in the interactions of the complex. This evidence suggests that bulky substituents on the adjacent hydroxide should not interfere with binding to the protein.

2 Aim of the project

MTs constitute a heterogeneous and dynamic filament network with great chemical and functional complexity. Their dynamics play a key role in the cell cycle to maintain the cell vitality and in neuron activity; therefore MTs represent suitable targets for anticancer therapy as well as for neurodegenerative diseases treatment. Due to their frequent use in cancer treatment, tubulin-targeted therapy has provided extensive information on the systemic effects of modulating MT dynamics in living organism.

Changes in MT stability are associated with many neurodegenerative diseases. Tauopathies show abnormal presence of τ-MAP aggregates in the somatodendritic compartment of affected neurons.[15a] The use of low doses of MSA has been proposed to stabilize MT in axons to compensate the loss of τ-MAP in this compartment[63] hopping that such treatment can restore the physiological dynamism of MT and effective axonal transport preventing neuronal death. However, there are two drawbacks that need to be considered; first, many MSAs do not cross the blood brain barrier, and second, MSA treatments are known to cause peripheral neurotoxicity, suggesting that modulation of MTs in peripheral neurons is toxic.[64] In the case of MDAs, which affect the integrity of MTs, the reason for the neuropathy can be easily understood, since a perturbed MT disturbs axonal transport. However, in the case of paclitaxel, which is widely used as a MSA, the biochemical effect is the stabilization of MTs, so the reason why it causes toxicity of postmitotic neurons is not immediately evident. This problem must be solved to ensure the use of MSAs in the treatment of neurodegenerative diseases.

The most plausible hypothesis is that the perturbations in neuronal function come from anomalous structural alterations of the MT and from changes in interaction with the MAPs involved. The interactions are based on small chemical differences between the tubulin subunits, which allow the MAPs to recognise the different portions of the MTs.

X-ray analysis and electron microscopy studies indicate that paclitaxel binding induces structural changes in

63 C. Ballatore, A. B. Smith, et al., *Top. Med. Chem.* **2016**, *24*, 159–179.

64 P. SB, L. CS, et al., *Muscle Nerve* **2011**, *43*, 367–374.

MTs, both in the lateral and longitudinal direction.[65] Therefore, it can be assumed that these alterations sufficiently change the structure of the MT to disrupt the structural signals necessary for the functioning of MAPs and motor proteins (kinesin and dynein, responsible for microtubule-dependent vesicular transport). The presence of 1 μM of paclitaxel has been shown to reduce the binding of τ-MAP in axons by more than 15%.[66] Since these recognitions are extremely dependent on the geometric parameters of the MT, it is interesting to investigate how the binding with MSA and MDA influences the dynamics and functionality.

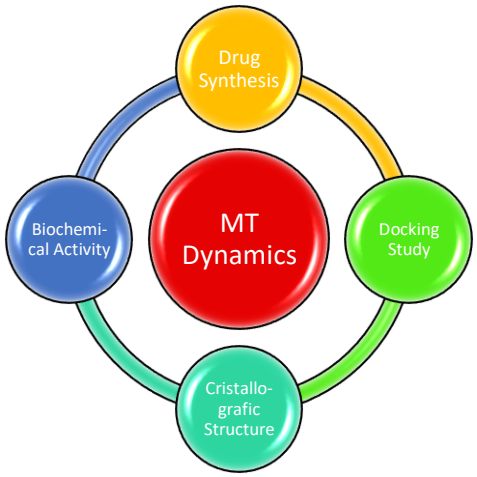

The development of the project stimulates an interdisciplinary approach; therefore, other groups belonging to different chemical areas have joined to create productive collaborations with the aim of identifying the principles that can guide the development of MTs modulators with minimal neuronal toxicity. To understand the structural changes that occur during the binding of the drug with the active site, it is necessary to perform high-resolution structural determinations of the MTs in the presence of different ligands. In addition, molecular biology, protein chemistry, cell biology, and cell imaging studies are needed to understand how these structural changes affect the interactions of MAPs, motor proteins, and how the whole the factors are reflected in neurotoxicity. The contribution of the chemical-organic approach is the synthesis of the various ligands necessary for studies by functionalising NPs, which already have known stabilization and destabilization effects. Knowing the relationship between the structural variation and the biological effect induced on the basis of the chemical interactions with the drug, could allow to reduce and regulate the changes in the MT to obtain the desired structural effects and consequently the desired biological effect.

Maytansine is a well-known ligand of β-tubulin[67] and performs a high destabilizing effect causing cytotoxicity. Since maytansinoids can influence MT dynamics, they are suitable substrates for the development of new molecules to begin to deepen the understanding of dynamics by preliminary studies. In addition to the various natural maytansinoids, wide semisynthetic analogues can be prepared to help establish SAR using maytansinol as starting building block. Kupchan *et al.* first obtained maytansinol by isolation from *Putterlickia verrucose* and chemical removal of the acyl group from the hydroxyl at C_3 position.[68] It exhibits lower polymerisation inhibitory activity than maytansine, which means that the ester moiety at the C_3 position plays a significant role in biological activity.[69] Therefore, maytansinol is a valuable precursor as the esterification of the hydroxyl at C_3 position allows to access to a series of natural and new semisynthetic maytansinoids exploiting the structural variability of the side chain.[70]

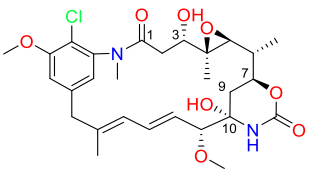

Maytansinol

The maytansinol acylation reaction is a crucial step in the preparation of maytansinoid antibody-drug conjugates or maytansinoid nanoparticles, which constitute a revolutionary class in anticancer therapies.[71] Some attempts

65 A. JM, B. J, et al., *J. Mol. Biol.* **1992**, *226*, 169–184; E. H. Kellogg, N. M. A. Hejab, et al., *J. Mol. Biol.* **2017**, *429*, 633–646.

66 W. C, R. HJ, et al., *Traffic* **2009**, *10*, 1655–1668.

67 T.-W. Yu, L. Bai, et al., *Proc. Natl. Acad. Sci.* **2002**, *99*, 7968–7973.

68 S. M. Kupchan, Y. Komoda, et al., *J. Org. Chem.* **1977**, *42*, 2349–2357.

69 S. Ikeyama, M. Takeuchi, *Biochem. Pharmacol.* **1981**, *30*, 2421–2425; T. W. Yu, H. G. Floss, in *Anticancer Agents from Nat. Prod.*, CRC Press, **2011**, pp. 423–444.

70 **a]** A. Kawai, H. Akimoto, *Chem. Pharm. Bull.* **1984**, *32*, 3441–3451; **b]** W. C. Widdison, S. D. Wilhelm, et al., *J. Med. Chem.* **2006**, *49*, 4392–4408.

71 T. Nittoli, M. P. Kelly, et al., *Bioorg. Med. Chem.* **2018**, *26*, 2271–2279; W. C. Widdison, J. F. Ponte, et al., *Bioconjug. Chem.* **2015**, *26*, 2261–2278; J. A. Costoplus, K. H. Veale, et al., *ACS Med. Chem. Lett.* **2019**, *10*, 1393–1399; P. Zhao, Y. Zhang, et al., *Acta Pharm. Sin. B* **2020**, *10*, 1589–1600; S. J. M. Hale, R. D. Perrins, et al., *Bioconjug. Chem.* **2019**, *30*, 703–713; J. Porter, Y. Ding, et al., *Bioorg. Med. Chem. Lett.* **2020**, *30*, 127634.

have also been made recently to conjugate maytansinoids prepared in this way with peptides.[72] Furthermore, maytansinol acylation may serve to build molecular probes useful for a better understanding the SARs of maytansinoids or for identifying new ligands of the maytansine site, which is the most recently identified and least explored site.[47,73]

Docking studies revealed a proximity of the exchangeable binding site of GDP and the vinca domain, where eribulin binds, to the maytansine pocket on β-tubulin. This characteristic inspired the idea of obtaining maytansinoid hybrids by synthesis.

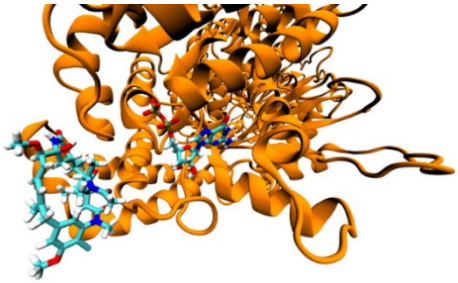

Figure 2.1 Illustration of docking study showing the location of maytansinol and GDP placed into their corresponding binding site.

Therefore, the aim of the chemical part of the project is the synthesis of new drugs and bifunctional drugs based on maytansinol and supported by docking studies to correlate the structural variation induced in MTs by drugs and the evaluation of biological effects. In this way, the results can shed light and more explain the MT dynamics. The length of the linker is of primary importance for the synthesis of conjugated compounds, in fact a too short chain would prevent the correct interaction with the binding pockets, while a too longer linker would increase too much the size of the molecule and the degrees of freedom.

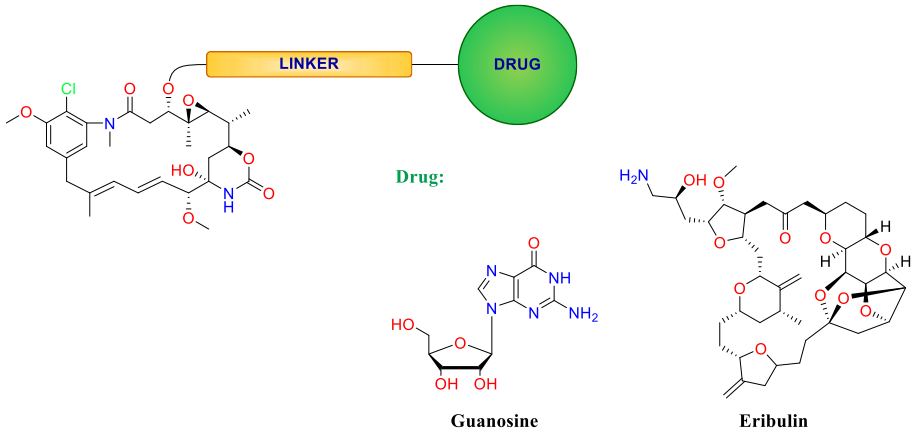

Figure 2.2 Maytansinoid hybrids representation.

The decision to start from the synthesis of hybrid compounds contending guanosine is determined by the high cost-effectiveness, by the simple commercial availability, and by a lower chemical complexity of the nucleotide base compared to eribulin. Computational suggests an optimal linker length of 12-14 carbon atoms to create maytansinoid-guanosine hybrid molecules. The subsequent crystallographic and X-Ray electron microscopy techniques carried out on MT bound to these compounds can determine the structural parameters with atomic resolution, allowing the synthesis of further tubulin-targeted drugs to optimise the structural changes.

72 Y. Liang, S. Li, et al., *Theranostics* **2017**, *7*, 3306–3318; B. H. White, K. Whalen, et al., *J. Med. Chem.* **2019**, *62*, 2708–2719.

73 G. Menchon, A. E. Prota, et al., *Nat. Commun.* **2018**, *9*, 2106.

3 Results and discussion

3.1 Chemical

3.1.1 Retrosynthetic approach

Maytansinol can be linked to the second drug molecule with carbon chain or pseudo-peptidic linker of length of 12-14 atoms. The hybrid can be obtained from a click reaction between an alkyne and an azide generating the corresponding triazole through catalysed 1,4-cycloaddition. The first fragment **A** derives from an acylation of maytansinol at the hydroxyl group, and the second fragment **B** derives from an enzymatic reaction of an activated ester on hydroxyl group of guanosine or from a coupling with a carboxylic acid.

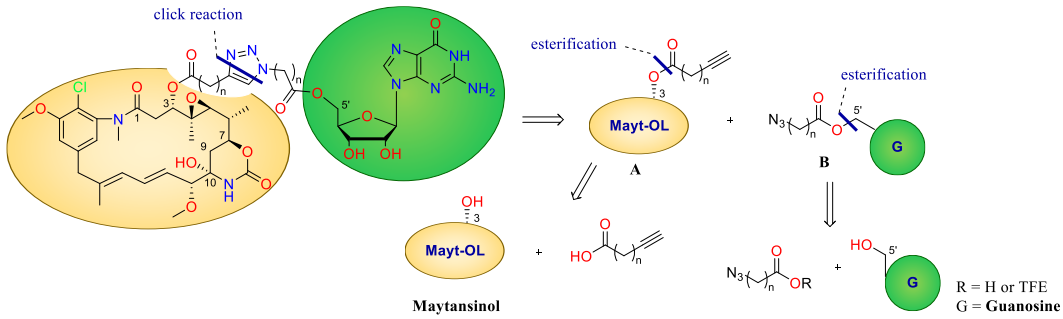

Scheme 3.1 General retrosynthetic analysis.

The synthesis of compounds structured in the same way but having the azide and alkyne groups inverted is also considered.

3.1.2 Synthesis of fragments type A: maytansinol esterification

Analysing the structure of maytansinol, its complexity is evident; therefore, it is reasonable to assume that reactions carried out under hard conditions are not compatible with the substrate. In fact, the carbinolamide part (the N-carbonyl derivative of a hemiaminal R_2-C(OH)-NH-CO-R') of the oxazinanone could be cleavage, the epoxide could be open, and some epimerisations may occur.

Before planning the click reaction to connect type A and B fragments, the creation of a pseudopeptide linker was tried based on some information reported. The literature is very poor regarding maytansinol derivatisation reactions, and the suggested procedures with DIPEA/Na_2SO_4/$Zn(OTf)_2$/Aln-NCA[74] or PhCOOH/DCC/$ZnCl_2$[75] appear to have no effect on this NP (**Scheme 3.2** and **Scheme 3.3**). These reactions were tried on a substrate tester to verify their reactivity: the first did not provide any product, but the second worked.

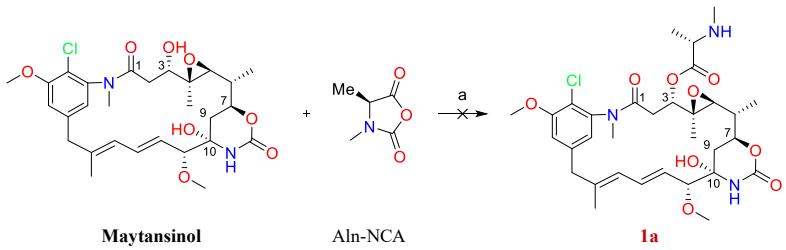

Scheme 3.2 *Reaction condition*: a) Aln-NCA 7.5 eq, DIPEA 5 eq, Na_2SO_4 1.4 eq, $Zn(OTf)_2$ 7 eq, DMF/THF 75:25, 10 d, rt.

74 T. H. Pillow, J. Tien, et al., *J. Med. Chem.* **2014**, *57*, 7890–7899.

75 W. C. Widdison, S. D. Wilhelm, et al., *J. Med. Chem.* **2006**, *49*, 4392–4408.

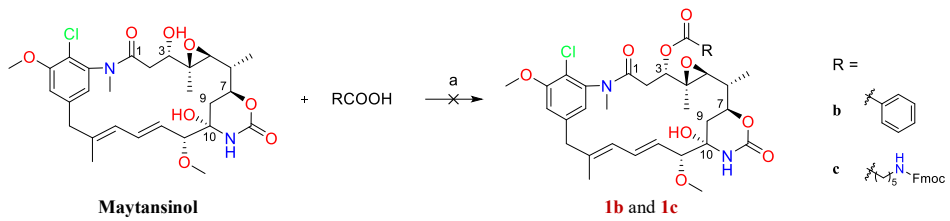

Scheme 3.3 *Reaction condition*: a) RCOOH 6 eq, DCC 6 eq, $ZnCl_2$ 1.2 eq, DCM/Et_2O, 2h, rt.

Reactions similar to those listed above are also described in other articles/patents. However, they should be performed on a large amount of maytansinol (approximately 5 g), but the reported yields are very low or non-specific, and the reaction time is very long (approximately 5-7 days). The limited availability of the starting material, due to the high price and the lack of suppliers, made these procedures too expensive to perform and therefore they were abandoned.

An attempt has been done using succinic anhydride/DMAP, but no results were achieved.

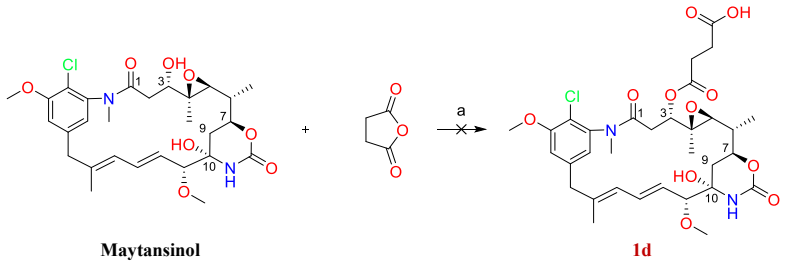

Scheme 3.4 *Reaction condition*: a) succinic anhydride 20 eq, DMAP 1.1 eq, dioxane, 3d, 50°C.

In addition, classic mild methods, such as coupling of carboxylic acid with HATU/HOAt/DMAP or DCC/DMAP, did not seem to affect the molecule in any case.

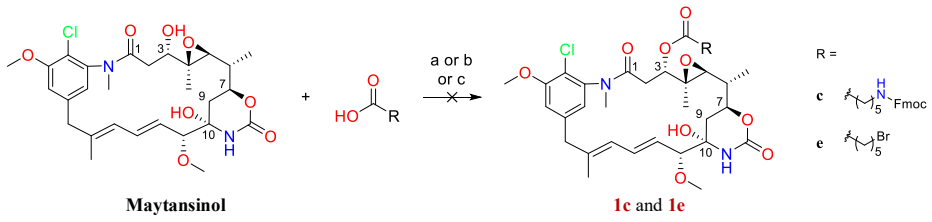

Scheme 3.5 *Reaction condition*: a) 6-Fmoc-aminoexenoic acid 2.6 eq, HATU 2.6 eq, HOAt 2.6 eq, DMAP 0.5 eq, DIPEA 2 eq, DCM, 2 d, rt; b) 5-bromoexenoic acid 1.3 eq, DCC 2 eq, DMAP 0.8 eq, DCM, 1 d, rt; c) 6-Fmoc-aminoexenoic acid 2 eq, DCC 6 eq, DMAP 6 eq, DCM, 1 d, rt.

Maytansinol was then subjected to an alkylation reaction, using propargyl bromide under basic deprotonation conditions. The reaction was performed in ACN/DMF using Cs_2CO_3 as base, KI to generate alkyl iodide by substitution of the bromide, and TEBA as the phase transfer catalyst (**Scheme 3.6**). The result was the formation of an unexpected new product: 4-hydroxy 2-oxazinanone of maytansinol was cleaved to give the unsaturated ketone **2** with 35% of yield. Interestingly, repeating the same reaction in the absence of the alkylating agent did not lead to the formation of any product. Hence, it is reasonable to assume that elimination can only occur following nitrogen alkylation of oxazinanone that induces the formal release of carbon dioxide and water through a concerted mechanism. The hydrolysis of imine thus produced leads to the elimination of propargyl amine yielding the αβ-unsaturated ketone.

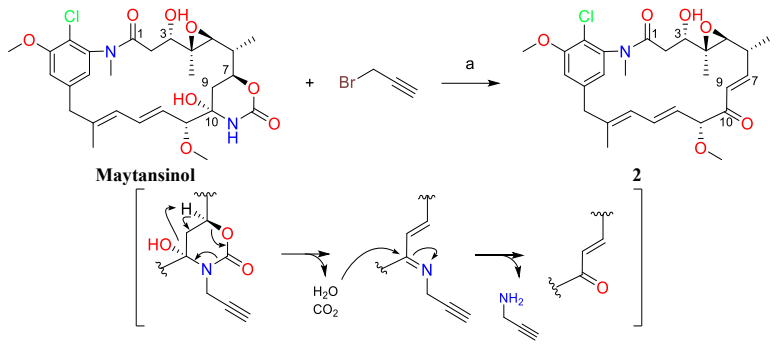

Scheme 3.6 *Reaction condition*: a) Cs_2CO_3 2.5 eq, TEBA cat, propargylbromide 2 eq, KI 2 eq, ACN + DMF 14%, 2 h, rt, 35%.

These experiments highlight the poor reactivity of the secondary alcohol, due to the steric hindrance. Therefore, another synthetic strategy was the use of more reactive acyl chlorides. Altmann *et al.* first described this type of procedure performed directly on maytansinol (**Scheme 3.7**).[73]

The research group coordinated by Prof. Altmann spent a lot of time studying this reaction and was able to perform this functionalisation only after much effort. In order to carry out the acylation reaction with aliphatic acyl chloride, some time was spent at ETH Zurich University to improve the knowledge about this reaction condition. In 7 days, the reaction required the addition of 6-heptinoic chloride in large excess, TEA to quench the HCl formed as the conversion proceeds, and 4-pyrrolidinopyridine (PPy) as acyl transfer. The purification step was vital, preparative RP-LC technique is necessary to separate properly the wide by-products. Thereby, a little amount (12 mg) of the interested product **1f** was gained with 16% of yield.

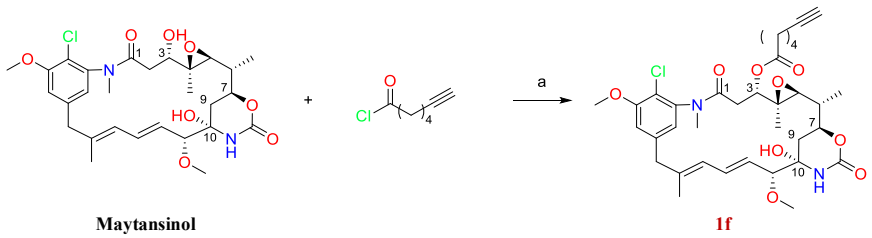

Scheme 3.7 *Reaction condition*: a) 6-heptynoic chloride 8 eq, TEA 20 eq, PPy 1 eq, DCM, 7 d, rt, 16% with RP purif.

The same reaction was performed using benzoyl chloride and half-molar ratio of reagents (**Scheme 3.8**). Surprisingly, the starting material was converted rapidly and completely in two new products **3b** and **4b**. 2D-NMR experiments and HRMS confirmed and elucidated the structures. Attention should be paid on the hydroxyl group of the hemiaminal, which dehydrated allowing the formation of a new double bond in 9-10 position. Compounds with dehydration and polyalcylation were also observed using 6-heptynoic chloride, but their formation was strongly in the minority. It was possible to shift the percentage in favour of these by-products by increasing the temperature at 50°C.

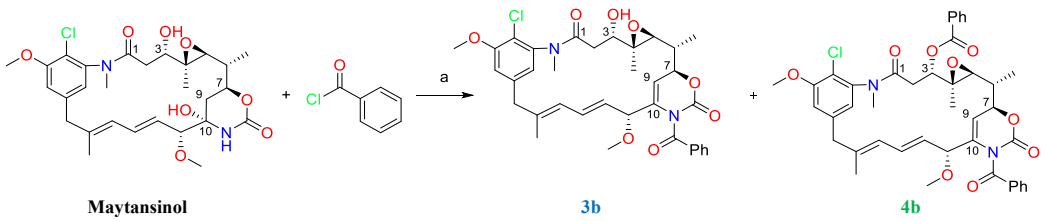

Scheme 3.8 *Reaction condition*: a) benzoyl chloride 4 eq, TEA 10 eq, PPy 0.5 eq, DCM, 4 h, rt, **3b** 33% and **4** 67%.

This behaviour suggests that maytansinol has a particularly strong affinity for benzoyl; therefore, it was interested studying the reaction in more details, considering also the influence of EWG (Electron Withdrawing Group) and EDG (Electron Donating Group) as substituents on benzyl.

Halving the molar ratio of benzoyl chloride (2 eq) resulted in a mixture of compounds with the further formation of a new product **5b** in 31% of yield (**Scheme 3.9**).

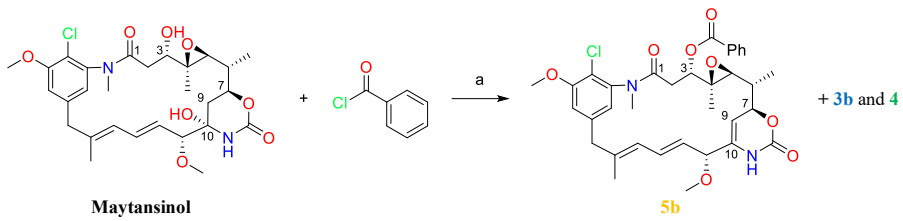

Scheme 3.9 *Reaction condition*: a) benzoyl chloride 2 eq, TEA 4 eq, PPy 0.5 eq, DCM, 20 h, 0°C to rt, **3b** 10%, **4b** 42%, and **5b** 31%.

The second modification was decreasing the molar ratio of benzoyl chloride up to one. In this way, the output was completely different: the formation of two new products **1b** and **6** were observed with a low yield (**Scheme 3.10**) and the polyacylated product **4b** was detected in small traces as expected (**Scheme 3.10**).

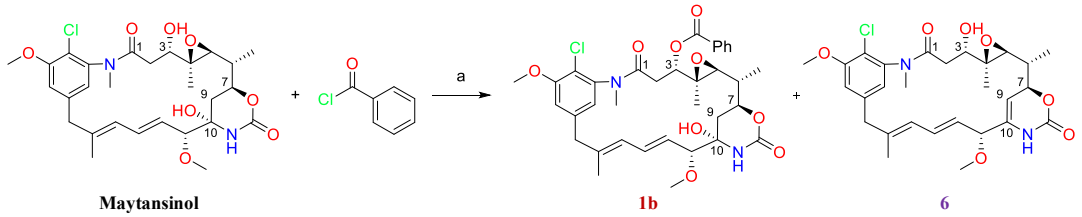

Scheme 3.10 *Reaction condition*: a) benzoyl chloride 1 eq, TEA 2 eq, PPy 0.5 eq, DCM, 6 h, 0°C to rt, **1b** 11% and **6** 11%.

The goal was to find conditions such as to make the reaction selective, since it was not possible to discriminate completely **1b** and **6** products with flash chromatographic purification. It has been deduced that **6** is the kinetic product by studying the reaction progression through qualitative evaluations of TLCs. Subsequently, **1b** is formed and **5b**, **3b**, and later **4b** can be observed allowing the reaction to continue further, with reduction of the amount of **1b** and **6**. Therefore, the reaction was repeated under the same conditions, but at low temperature (-20°C) and stirring for two hours. The yields shifted more towards product **6** with 15% at the expense of **1b**, which was 2%, and **4b** was not detected. Then, the amount of benzoyl chloride was further reduced to 0.5 eq providing **6** almost selectively with 10% of yield. The result became selective with lower yield (5%) by reducing of the reaction time to 0.5 h, and lower temperatures caused a decrease in yields.

Table 3.1 Studying the influence of benzoyl chloride on maytansinol acylation reaction.

benzoyl chloride [eq]	T [°C]	time [h]	4b	3b	5b	1b	6	M
4	rt	4	67	33	-	-	-	-
2	rt	20	42	10	31	-	-	-
1	rt	6	traces	traces	-	11	11	75
1	-20	2	-	-	-	2	15	80
1	-40	2	-	-	-	-	traces	94
0.5	-20	2	-	-	-	2	10	73
0.5	-20	0.5	-	-	-	-	5	82

In order to obtain **1b**, a reaction performed in pyridine as solvent gave the desired product with 25% of yield (**Scheme 3.11**). Increasing the amount of benzoyl chloride did not provided to any other derivative.

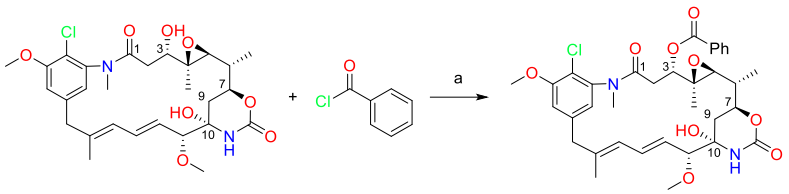

Maytansinol **1b**

Scheme 3.11 *Reaction condition*: a) benzoyl chloride 6 eq, Py, 5 h, rt, **1b** 25%.

The attempt to obtain **5a** selectively starting from **6** failed, due to the instability of starting material (**Scheme 3.12**). This behaviour was highlighted by NMR analysis, which displayed many new unknown signals.

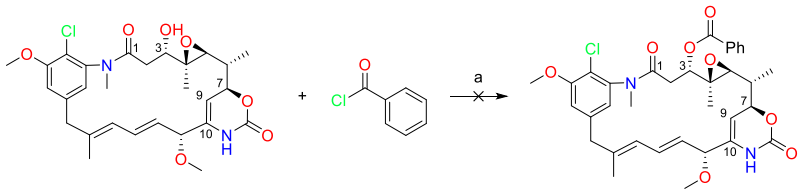

6 **5b**

Scheme 3.12 *Reaction condition*: a) benzoyl chloride 6 eq, Py, 1 d, rt.

The reactions performed with acetyl chloride (from 1 eq up to 7 eq) gained **1g** as only product with the best yield of 46% (**Scheme 3.13**).

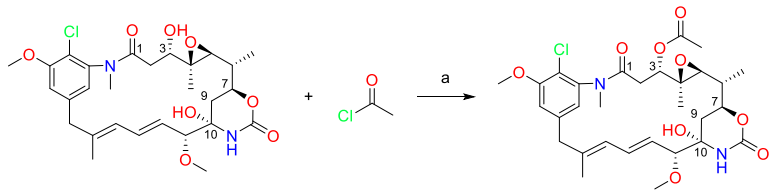

Maytansinol **1g**

Scheme 3.13 *Reaction condition*: a) acyl chloride 2 eq, TEA 4 eq, PPy 0.5 eq, DCM, 6 h, 0°C to rt, **1g** 46%.

Rationalising the results, the use of aliphatic acyl chlorides predominantly produces the acylated derivative, showing a weak tendency to form the corresponding dehydrated compounds unlike the use of benzoyl chloride. A certain reactivity has been observed using acyl chlorides, but their preparation is difficult and often they were found in not negligible traces together with the products after purification.

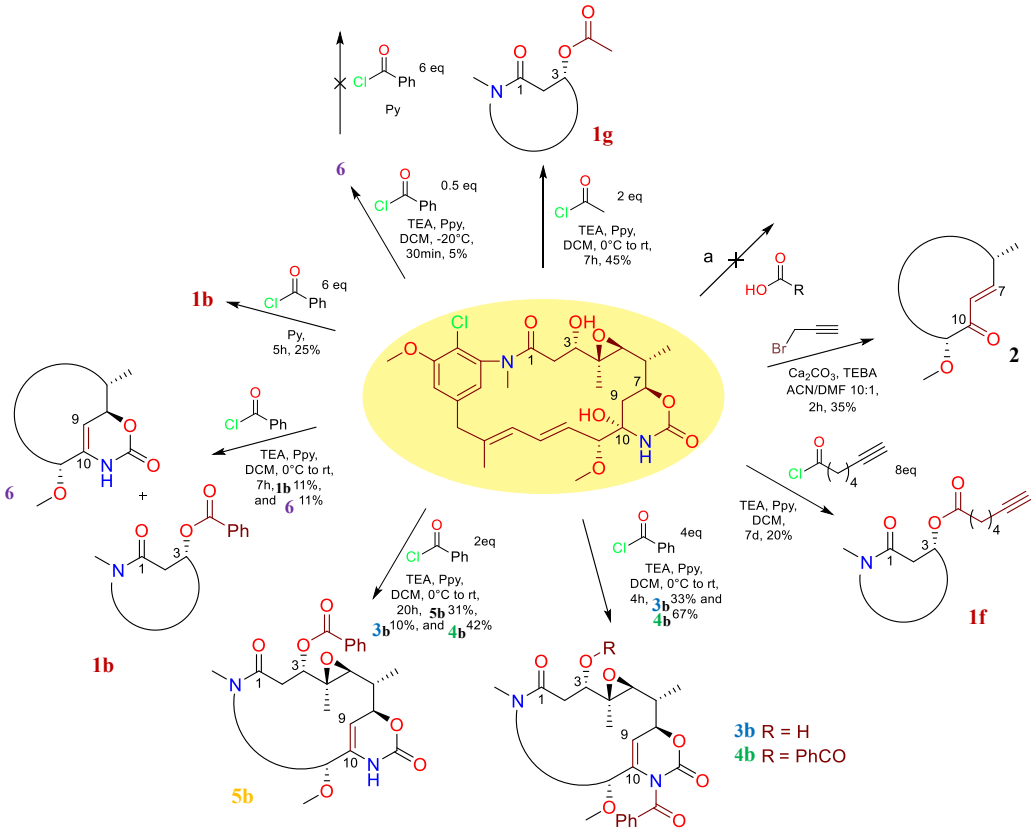

Scheme 3.14 Summary of reaction on maytansinol. *Reaction condition*: a) HATU/HOAt/DMAP or DCC/DMAP or DCC/$ZnCl_2$ or DIPEA/Na_2SO_4/$Zn(OTf)_2$.

Therefore, both the purity and the stability of the obtained compounds were adversely affected. It was possible to observe a change in the aspect of the products: they turned into intense yellow/orange oils over short time. In addition, the dehydrated compounds showed particular instability at temperatures above -20°C and against acid solvents usually used in NMR. In fact, the dissolution of the compounds in *d-chloroform* generates a yellow solution that rapidly turns into a more intense yellow in which isomerisations or/and degradations occur. Therefore, *acetone-d6* has been selected as a suitable solvent from which products can be easily and better recovered. *DMSO-d6* was another suitable NMR solvent for the analysis.

Although an appreciable amount of maytansinol could be recovered in almost any reaction, for all the problems encountered in the maytansinol acylation reaction, it was still necessary to find a better reaction to provide the compounds concerned with satisfactory degrees of purity, yield, reaction times and reproducibility. As mentioned classic mild methods, such as esterification of carboxylic acid with HATU/HOAt/DMAP or DCC/DMAP, did not seem to affect the molecule. Instead of solid DCC addition to the reaction mixture as in the previous attempts, dropping large excess DCC solution into the reaction similarly containing large excesses of all reactants (RCOOH and DMAP) resulted in the corresponding C_3 acylated compounds.

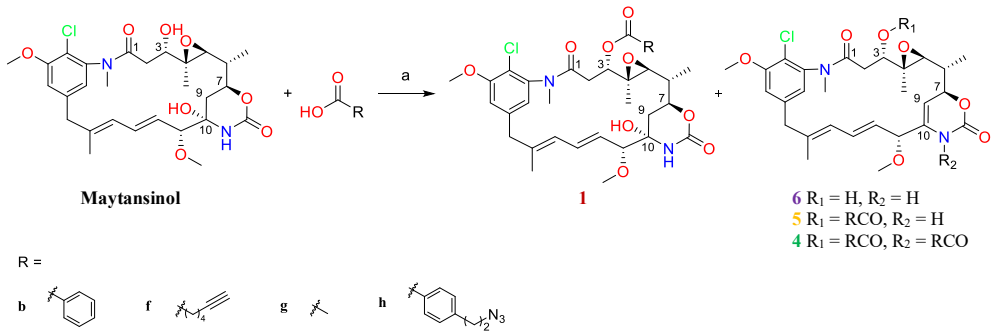

Scheme 3.15 *Reaction condition*: a) RCOOH 3 eq, DMAP 3 eq, DCC 3.3 eq in DCM (or EDC-HCl 3.3 eq, TEA 3.3 eq), DCM, time, rt, RP purif.

Table 3.2 Yield of maytansinol derivatives obtained with Steglich esterification.

R			Time [h]	M	6	1	5	4
b		DCC (6 eq)	48	-	-	-	15	31
		DCC	8	4	5	35	26	18
		EDC	24	21	8	39	12	7
		EDC	48	-	-	15	47	20
f		DCC	3	7	9	37	30	6
		EDC	18	17	4	36	15	6
g		DCC	4	-	-	42	43	-
h	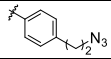	DCC	3	20	-	29	11	2
		EDC	24	22	8	38	11	8

The reaction works well regardless of the use of aromatic or aliphatic acids, unlike the reactivity found by reactions with acyl chlorides. In addition, the improvement of the purification using BIOTAGE instrument with a reversed phase cartridge installed allowed perfectly separation the compounds formed and presenting in the crude.

The use of excess DCC affects the purity of the obtained products due to the impossible complete removal of the DCU by-product, even after chromatographic purification. Therefore, the replacement of the DCC with the coupling agent EDC solved this problem, although it requires a longer reaction time of 18-24 h as the satisfactory yields represent a good compromise. Furthermore, the condensations with EDC have a lower tendency to form dehydrated products **5** and **4**, unlike reactions carried out with DCC.

In these reactions, maytansinol is almost completely converted into the products. However, letting the reactions run with longer reaction times to obtain a greater conversion of maytansinol does not increase the yields because the conversion of compound **6** and **1** takes place in favour of the formation of products **5** and **4**, which are not interesting from the point of view of cellular activity according to preliminary biological tests. Considering the poor reactivity of maytansinol, the yields and reaction times are more satisfactory with the new method developed compared to the results obtained using acyl chlorides.

An HPLC method was refined in order to follow easily the conversion and to determine the composition percentage of the reaction mixture. **Figure 3.1** displays an example of the retention times of the main products that can be obtained using benzoyl. The analysis was performed on a ZORBAX SB C8 column (3.5 µm × 4.6 × 150 mm). The pressure was about 85 bar with a constant flow rate of 1 mL/min. UV spectra were recorded at 254 nm and 210 nm with DAD detection. The mobile phase consisted of a mixture of H_2O/ACN and the gradient was programmed using the following method: isocratic for 1 min at 50% ACN, then gradient for 10 min to 90% ACN. The system was washed keeping this condition for another 1 min and then bringing back to the beginning condition. The retention times were maytansinol, 3.10 min; **6**, 4.08 min; **1b**, 5.20 min; **5b**, 6.90 min; **3b**, 7.20 min; **4b**, 9.40 min. The method allowed an excellent separation of maytansinol from the derivatives, and it was

possible to perfectly recognise each peaks, although **5b** and **3b** were quite close.

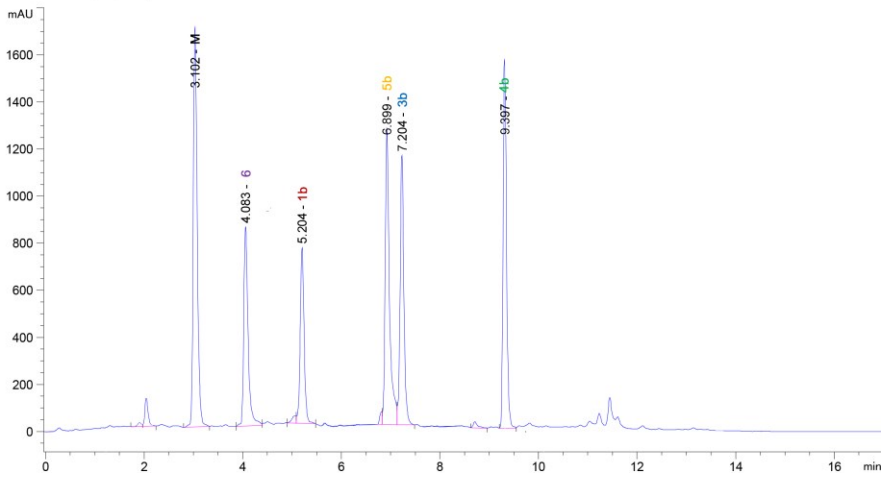

Figure 3.1 Representative HPLC chromatogram of a mixture of maytansinoid.

Having available a stable and reproducible synthesis reaction with a valid HPLC method suitable for easily monitoring, the reaction conditions were modified to try to shift the composition percentages in favour of type **1** products, identified as target molecules. It is known that coupling reaction strongly depends on the solvent, pK_a of the carboxylic acid, and pH of the mixture.[76] To deeply discuss the esterification promoted by coupling agent and to identify the critical steps that can obstruct the desired path, the general reaction mechanism is reported below.

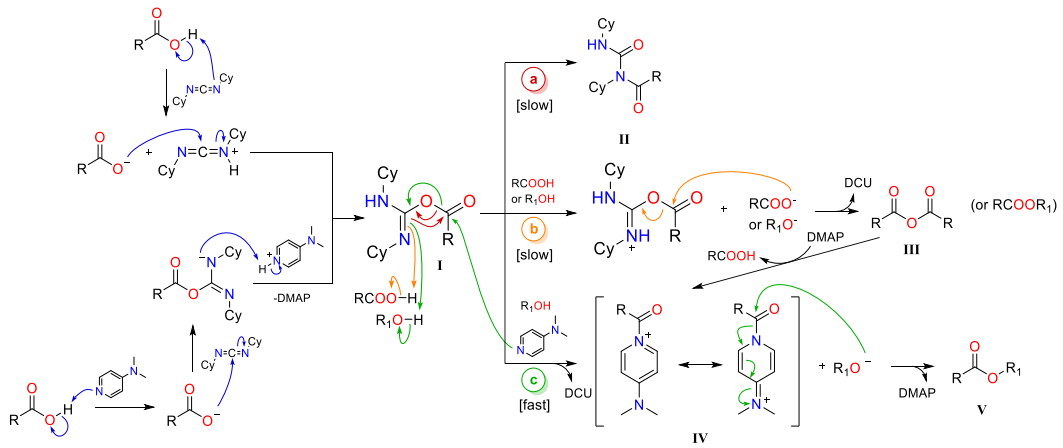

Scheme 3.16 Reaction pathways in carbodiimide assisted condensation of a carboxylic acid and alcohol.

The mechanism of carbodiimide condensation (**Scheme 3.16**) involves the deprotonation of the acid by N atom of DCC followed by the nucleophilic attack of the carboxylate to provide an *O*-acylisourea intermediate **I**, which offers similar reactivity to the corresponding carboxylic acid anhydride. In the presence of DMAP, the carboxylic acid can be activated more quickly by removal of an H^+ due to the easy protonation of the basic pyridine nitrogen, providing the highly reactive nucleophilic carboxylate. The subsequent nucleophilic attack on the carbodiimide favours the formation of the *O*-acylisourea intermediate **I**.

76 M. Mikolajczyk, P. Kielbasinski, *Tetrahedron* **1981**, *37*, 233–284.

Many reactions can evolve from this intermediate. The formation of *N*-acylurea **II** occurs by intramolecular transfer of an acyl group from an oxygen atom to a nitrogen atom (path **a**). This *N*-acylurea is inactive and prevents the formation of condensation products, but its formation is slow.

The bimolecular reaction with a second carboxylic acid (or an alcohol) and *O*-acylisourea leads to the formation of urea and anhydride **III** or ester (path **b**). Acylation of anhydride assisted by DMAP provides an active *N*-acylpyridinium intermediate **IV**, which can also be obtained more rapidly through a reaction between the *O*-acylisourea intermediate and the stronger nucleophile DMAP, with the formation of urea (path **c**). Finally, the *N*-acylpyridinium intermediate **IV** reacts with an alcohol regenerating the catalyst and forming the ester bond **V**. The role of DMAP is to limit the formation of *N*-acylurea **II** by reacting with the intermediate *O*-acylisourea **I** before rearrangement can occur.

Firstly, it was investigated the impact of benzoic acid substituent: an EWG promotes the reaction by lowering the pK_a and making the carboxyl more susceptible to nucleophilic attack, while an EDG completely inhibits the reactivity and neither the *O*-acylated nor dehydrated products were observed. The use of p-nitrobenzoic acid provided **1l** as only product by HPLC estimation with a good conversion of maytansinol.

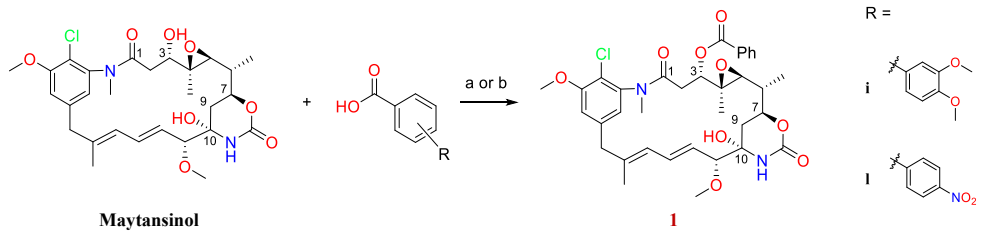

Scheme 3.17 *Reaction condition*: a) 3,4-dimetoxybenzoic acid 3 eq, DMAP 3 eq, EDC-HCl 3.3 eq, TEA 3.3 eq, DCM, 120 h, rt, **1i** nr; b) p-nitrobenzoic acid 3 eq, DMAP 3 eq, EDC-HCl 3.3 eq, TEA 3.3 eq, DCM, 48 h, rt, **1l** 60% (estimated by HPLC).

According to the literature, the addition of PTSA (p-toluensulfonic acid) should further prevent the formation of *N*-acylurea **II**: the positive charge generated on the imine nitrogen of one of the tautomeric forms of the *O*-acylisourea **I** decreases the nucleophilicity of the nitrogen atom and suppresses the rearrangement to *N*-acylurea.[77] Another role of PTSA is to lower the pH of the reaction, which again results in the suppression of *N*-acylurea formation.

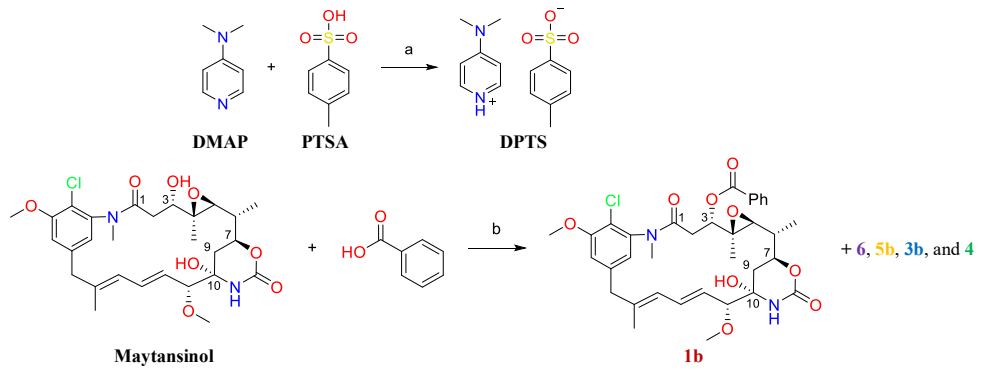

Scheme 3.18 *Reaction condition*: a) DMAP 1 eq, p-toluensulfonic acid 1 eq, THF, 40 min, rt, 60%; b) benzoic acid 1 eq, DPTS 0.5 eq, DCC 2.6 eq in DCM, DCM, 120 h, rt, **1b** 18%, **6** 4%, **5b** 14%, **3b** 5%, **4** 4% (estimated by HPLC).

Therefore, DPTS (4-(Dimethylamino)pyridinium 4-toluenesulfonate) salt was easily prepared by acid-base reaction between DMAP and PTSA in THF and added in catalytic amount to reaction mixture. Performing the esterification using a stoichiometric amount of DCC with DPTS as acyl transfer agent instead of DMAP did not

77 B. Vanhaecht, M. N. Teerenstra, et al., *J. Macromol. Sci. - Pure Appl. Chem.* **2000**, *37 A*, 633–643.

improve the selectivity and also the kinetic was too slow to consider the result interesting.

Looking at chromatograms, it is evident that the main compound generate after 48h is **5b** with 21% of area versus only 6% of **1b**. As the conversion of maytansinol proceeds, compound **1b** becomes the main product at 120 h with 18% of area versus 14% of **5b**. At the same time, it is possible to observe the beginning of the formation of the other derivatives.

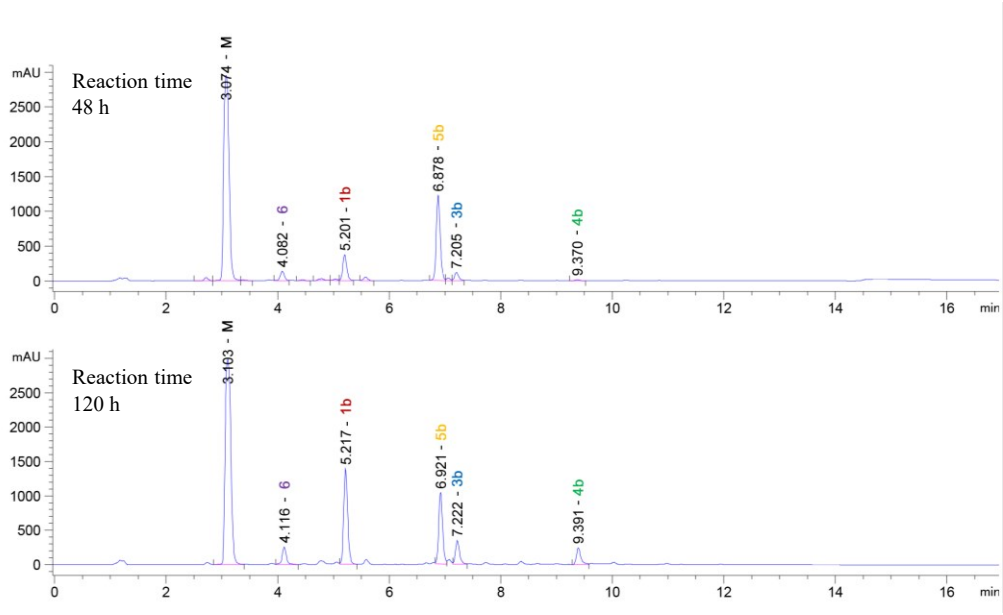

Figure 3.2 HPLC chromatogram of the proceeding of the reaction performed with DCC/DPTS.

Alcohols do not react with DCC in the absence of a catalyst, hence the reaction should require very drastic conditions (*i.e.* high pressure and temperature). Protonation of the N atom in carbodiimide increases considerably the electrophilicity of the central C atom. The result is an increase in the reactivity because C atom becomes more susceptible to a nucleophilic attack. In the similar way, adding copper or zinc salt as catalyst generates a coordinative complex on the N atom, which contributes to a significant increase of electrophilicity of the central C atom.[77] *O*-alkylisourea is very reactive with alcohol *via* alkoxy attack, mercaptans, and carboxylic acid *via* acid anion attack on alkyl group leading to the ether, thioether, and ester, respectively (**Scheme 3.19**).

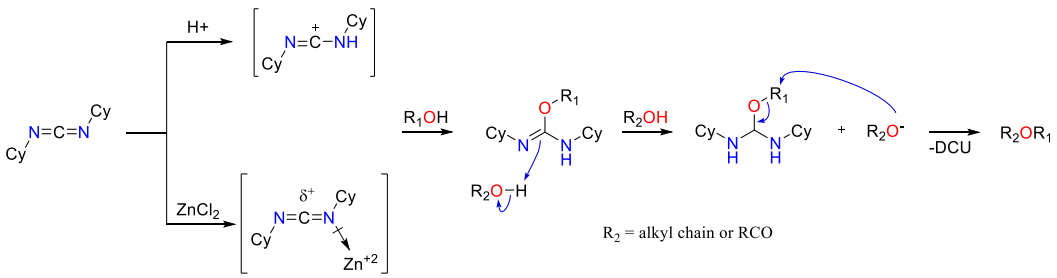

Scheme 3.19 Reaction mechanism of the catalysed carbodiimide-assisted condensation of a carboxylic acid and alcohol.

Since this stage does not require the formation of a tetrahedral transition intermediate at the carbonyl carbon atom, it is possible to use this method for esterification of the sterically hindered acids or maybe for alcohol with low reactivity like maytansinol. Considering also that maytansinol has a low reactivity, it is reasonable excluding the formation of a dimer ether. Taking advantage of these concepts, it could be possible to add carboxylate obtained by deprotonation with DMAP from the corresponding acid to the *O*-alkylisourea intermediate.

Adding an excess of $ZnCl_2$ yielded the reaction much more selective for the preferential formation of the compound **1b**, even if the reaction time increased. Let running the reaction for more than 48h did not provide to a significant increasing of the percentage area of **1b**; on the contrary, it led to an increase in undesired derivatives.

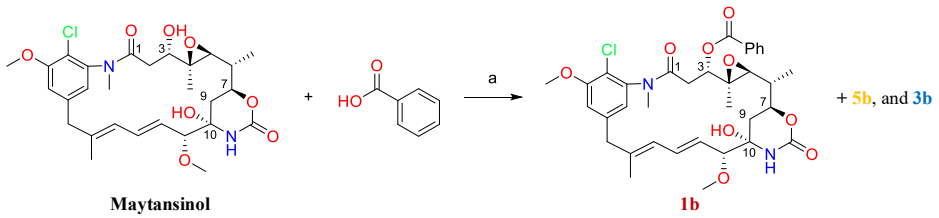

Scheme 3.20 *Reaction condition*: a) benzoic acid 3 eq, DMAP 3 eq, $ZnCl_2$ 3 eq, DCC 3.3 eq in DCM, DCM + 10% DMF, 120 h, rt, **1b** 63%, **5b** 9%, **3b** 3% (estimated by HPLC).

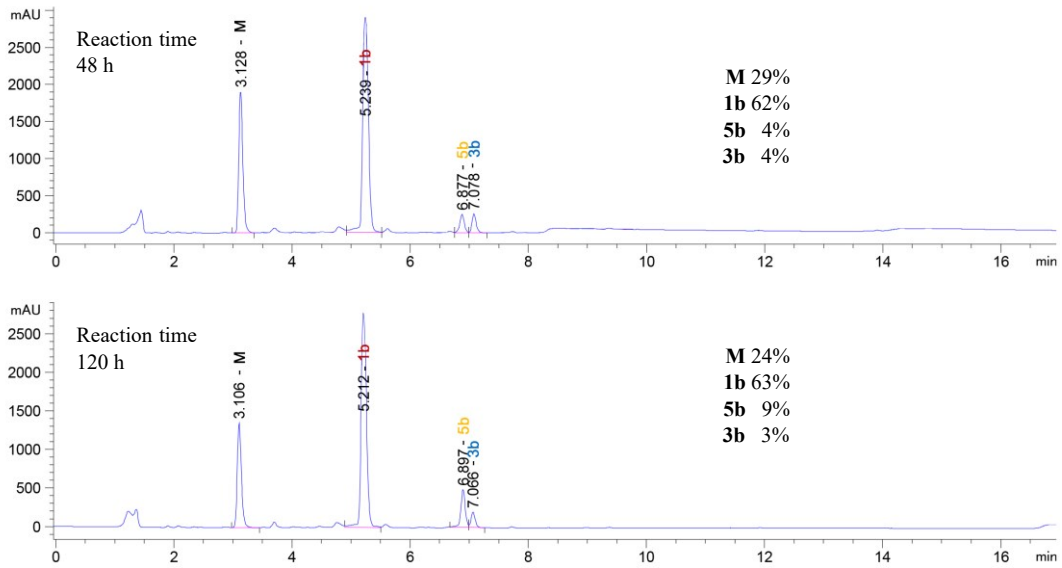

Figure 3.3 HPLC chromatogram of the proceeding of the reaction performed with $ZnCl_2$/DCC/DMAP.

Based on this result, it would be interesting to work in the future on several factors that could affect the kinetics to improve the outcome. Specifically, EDC can be used as a carbodiimide source, the influence of the amount of $ZnCl_2$ added can be considered, and the molar ratios of all the reagents can be modified to evaluate their incidence on the reaction.

Furthermore, it would be advisable to check whether:

a) the reaction proceeds according to the mechanism explained in the **Scheme 3.19** providing such a different and promising selectivity;

b) the reaction occurs as Steglich esterification, in which the carboxylate generated by deprotonation with DMAP attacks the zinc activated carbodiimide generating *O*-acylisourea which subsequently reacts with maytansinol;

c) zinc plays a dual role as activator of carbodiimide and inhibitor of dehydration by coordinating the electron-rich heteroatoms of maytansinol.

3.1.3 Synthesis of fragments type B: guanosine esterification

Guanosine is a purine nucleoside comprising guanine attached to a ribose ring via a β-N9-glycosidic bond. The 5'-*O*-esterification might seem like an easy challenge, but the poor solubility of the substrate in most organic solvents complicates the reactivity and the handling. However, guanosine exhibits good solubility in DMSO and acetic acid, and is slightly soluble in water.

The first attempt was to connect selectively a linker to the hydroxyl group of interest by enzymatic reaction. For this purpose, an activated acid was required to allow proper enzymatic function. Starting from 6-Br-hexanoic acid, the acid moiety was subjected to coupling reaction with trifluoroethanol, and subsequently the corresponding azide was obtained through S_N2 reaction using NaN_3 as nucleophile (**Scheme 3.21**). The substrate was placed in the presence of the enzyme, but the choice of solvent was a problem. The enzyme worked well in water, but the guanosine was insoluble. Acidification could have been a solution, but the work up of the reaction was an obstacle that made the procedure impossible. DMSO was a suitable solvent for guanosine, but definitely not for the enzyme. Therefore, it was not possible to get **10** in this way.

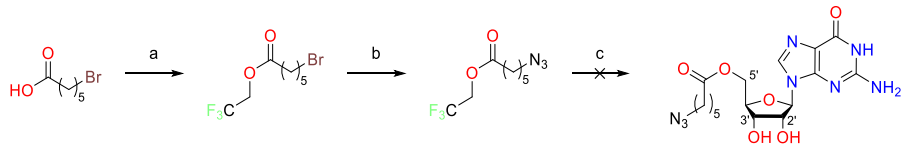

Scheme 3.21 *Reaction condition*: a) F_3CCH_2OH 1.5 eq, DCC 2 eq, DMAP 0.8 eq, DCM, 0°C to rt, overnight, 66%; b) NaN_3 1.1 eq, DMSO, rt, 18h, 95%; c) guanosine, enzyme, solvent.

Hence, the solvation problem in the guanosine acylation reaction was faced through a chemical pathway. To improve the solubility of guanosine, 2',3'-diol or free amine protections are well discussed strategies in the literature.[78] The protection of the diol was considered as first attempt since it would involve an increase in selectivity for the subsequent 5'-*O* esterification reaction. Several protecting groups exist, but the formation of isopropylidene ketal was explored due to easy formation and removal in acid condition. Guanosine was treated with perchloric acid providing **11** quantitatively.

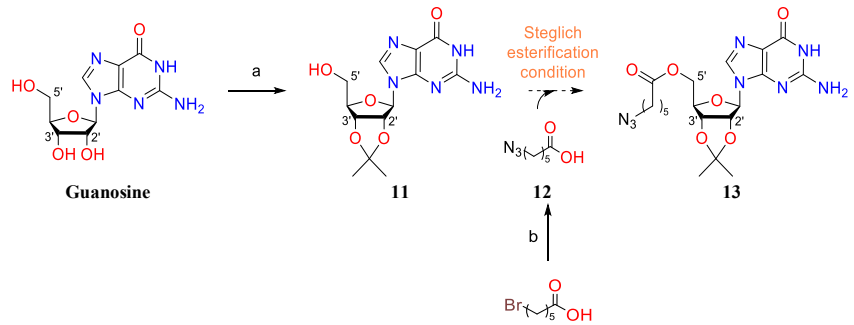

Scheme 3.22 *Reaction condition*: a) $HClO_4$ 60%, acetone, rt, o.n., >98%; b) NaN_3 1.1 eq, DMSO, rt, 18 h, 91%.

The literature reports various reaction conditions useful for performing acylation of 2',3'-isopropylidene guanosine at the 5' position, which involve the use of acyl halides, anhydrides, and acids under coupling conditions.[78ac,79] Considering the experience acquired with acyl chloride in the synthesis of maytansinoids, the first

78 **a]** S. Vertuani, A. Baldisserotto, et al., *Eur. J. Med. Chem.* **2012**, *54*, 202–209; **b]** Y. Pavan Kumar, P. Saha, et al., *ChemBioChem* **2016**, *17*, 388–393; **c]** J. Camacho-García, C. Montoro-García, et al., *Org. Biomol. Chem.* **2015**, *13*, 4506–4513; **d]** Y. Xu, H. Jin, et al., *Tetrahedron* **2009**, *65*, 5228–5239; **e]** B. Zhang, Z. Cui, L. Sun, *Org. Lett.* **2001**, *3*, 275–278; **f]** R. Shah, A. Strom, et al., *ACS Med. Chem. Lett.* **2016**, *7*, 780–784; **g]** S. Vincent, S. Grenier, et al., *J. Org. Chem.* **1998**, *63*, 7244–7257.

79 Y. Xiong, J. Lu, et al., *ACS Med. Chem. Lett.* **2017**, *8*, 61–66.

approach was set up for the use of acid commercially available. Therefore, **12** was prepared by nucleophilic substitution of bromide with azide starting from 6-Br-hexanoic acid and it was used in a coupling reaction carried out with DCC/DMAP. The purposed solvents were DMF or DCM, thus the reaction was performed in DMF, but it was highlighted solubility problem of **11** and no reaction occurred (**Scheme 3.23**, a).

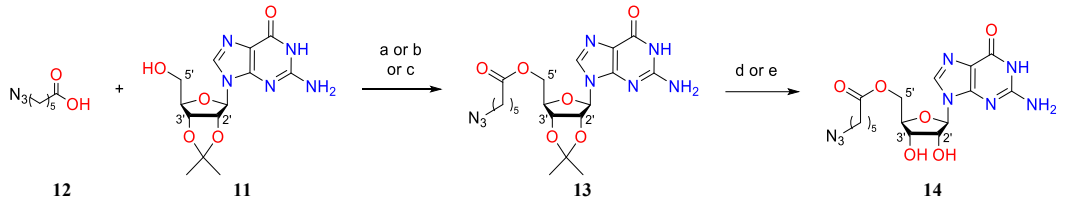

Scheme 3.23 *Reaction condition*: a) DCC 1.2 eq, DMAP 0.4 eq, DMF, rt, o.n., n.r; b) DCC 1.8 eq, DMAP 0.4 eq, DCM, rt, o.n., 47%; c) EDC-HCl 1.8 eq, TEA 2.2 eq, DMAP 0.6 eq, DCM, rt, o.n., 71% with RP purif; d) **13**, TFA 50% aq, rt, 4 h, 47%; e) **13**, TFA 80% aq, rt, 30 min, 81% with RP purif;

Therefore, the reaction was repeated by changing the solvent to DCM and the substrate was dissolved after some minutes of stirring. Also in this case, the development of emulsions and suspensions related to the problem of the solubility of DCU and isopropylidene guanosine made the work up difficult, however the product was isolated with a moderate yield of 47% (**Scheme 3.23**, b). Finally, in the last developed procedure, DCC was replaced with EDC solving the main problems and providing **13** with a better yield equal to 71% (**Scheme 3.23**, c).

Considering that deprotection in acidic condition could affect the maytansinol fragment in the final conjugate compound, the cleavage of isopropylidene was carried out in this step, before the click cycloaddition. Therefore, compound **13** was treated with TFA 50% in water[78a] giving the product with 47% of yield. To improve the result, a higher concentration of TFA (80%)[78df,79] was used, obtaining **14** with 81%.

The same procedures of EDC condensation with 6-heptynoic acid and ketal removal with TFA 80% were successfully applied for the synthesis of guanosine derivative **16**. BIOTAGE purification with reversed phase cartridge allowed the separation and isolation of all compounds with high level of purity (gradient elution W/ACN from 5% ACN to 40% ACN) better than a flash chromatography purification performed on silica.

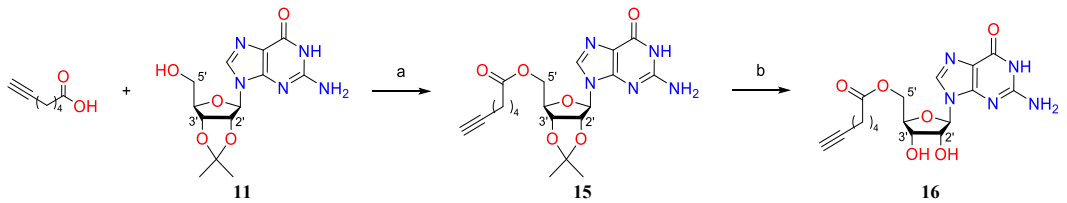

Scheme 3.24 *Reaction condition*: a) EDC-HCl 1.8 eq, TEA 2.2 eq, DMAP 0.6 eq, DCM, rt, o.n., 78%; b) **15**, TFA 80% aq, rt, 30 min, >98%.

3.1.4 Click chemistry and troubleshooting

The last step of the synthesis involves the union of type **A** fragments with those of type **B** by click chemistry. This concept refers to the possibility of synthesising complex substances quickly and easily by joining smaller molecules. This type of reactivity is inspired by nature, which operating mostly in an aqueous environment produces an enormous variety of complex molecules starting from a few basic molecules.

The Huisgen azide-alkyne cycloaddition is a 1,3-dipolar cycloaddition between an azide and a terminal or internal alkyne to form a 1,2,3-triazole. The copper (I) catalysed variant described in 2002 by Morten Meldal, Valery Fokin and Barry Sharpless embraces this philosophy. Although it leads to the formation of a 1,2,3-triazole from a terminal alkyne and an azide, formally it is not a 1,3-dipolar cycloaddition. For this reason it should not be called Huisgen cycloaddition, but Copper (I)-catalysed Azide-Alkyne Cycloaddition (CuAAC).

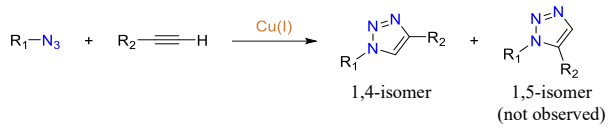

Scheme 3.25 Copper (I)-catalysed azide-alkyne cycloaddition reaction.

The Cu (I) species forms a π-complex with the triple bond of the terminal alkyne by coordination and in the presence of a base the terminal hydrogen is eliminated to generate a Cu-alkyne intermediate. However, the coordination of copper lowers the p*K*a of the C-H bond of the alkyne by 9.8 units.[80] Consequently, under appropriate conditions the reaction can proceed even in the absence of bases. L ligands possess labile and poorly coordinating bonds with copper, therefore azide easily exchanges with one of them forming a four-membered copper-azide-acetylide complex. One copper atom is bonded to alkyne, while another copper atom activates azide by coordination. At this point cyclisation occurs, followed by protonation. The source of hydrogen is the base that had initially acquired the proton of the terminal alkyne. Finally, the product dissociates and the catalyst is ready for another reaction cycle.

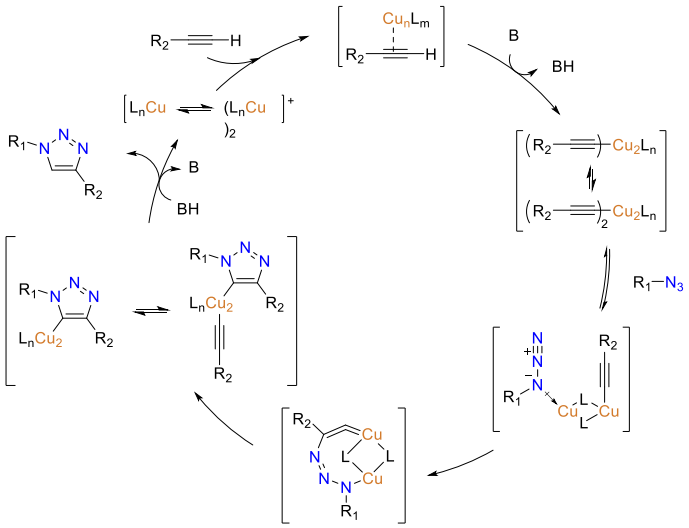

Scheme 3.26 Reaction mechanism of CuAAC.

The reaction rate of CuAAC depends upon the copper (I) source, solvent, ligand used, and the type of azide used. The reaction can be conducted using commercial copper (I) sources such as bromide or copper (I) iodide, but the reaction works much better using a mixture of a copper (II) compound (e.g. copper sulfate) and a reducing agent (e.g. sodium ascorbate) to produce Cu (I) *in situ*. Water is the preferred solvent mainly because it is able to support the reactive state of the copper (I) acetylide. Furthermore, the ability of copper (I) to engage the terminal alkynes and the rapid exchange of these and other ligands in its coordination sphere is enhanced.[80,81] Since Cu (I) is unstable in aqueous solvents, stabilizing binders are used to improve the reaction yield. The reaction can be carried out in several solvents and mixtures of water and other partially miscible organic solvents such as alcohols, DMSO, DMF, tBuOH and acetone. Acetonitrile should be avoided as a solvent, because nitriles coordinate Cu (I) very effectively. It is not essential that the starting reagents are completely soluble for the reaction to work.

Investigations on the CuAAC mechanism suggest that the delay in protonation of triazole cuprate constitute an obstacle to the formation of triazoles.[82] Facilitating this step increases the speed of the reaction and minimises the formation of side products. As reported, the combination of 1,4-diazabicyclo[2,2,2]octane/acetic acid (DABCO/AcOH) dramatically decreases the reaction time from hours to minutes. AcOH is an excellent proton source and accelerates both cycloaddition and protonation of triazole cuprate, whereas DABCO prevents the formation of the unreactive polynuclear copper (I) acetylide and facilitates the coordination of azide to copper during the ligand exchange step.

For these reasons, $CuSO_4$/Na-ascorbate/DABCO/AcOH conditions in 1:4 mixture of water/t-BuOH have been

80 F. Himo, T. Lovell, et al., *J. Am. Chem. Soc.* **2005**, *127*, 210–216.

81 J. E. Hein, V. V. Fokin, *Chem. Soc. Rev.* **2010**, *39*, 1302–1315.

82 P. B. Sarode, S. P. Bahekar, H. S. Chandak, *Synlett* **2016**, *27*, 2681–2684.

applied to rapidly join the fragments **A** and **B**, but no product formation was observed.

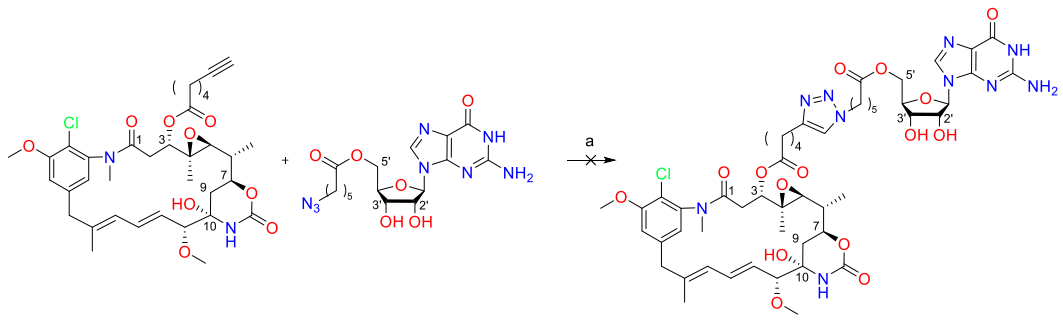

1f **14** **17**

Scheme 3.27 *Reaction condition*: a) **1f** 1 eq, **14** 1.5 eq, $CuSO_4$-$5H_2O$ 0.06 eq, DABCO 0.16 eq, AcOH 0.16 eq, Na-ascorbate 0.24 eq, H_2O/t-BuOH 1:4, rt, o.n.

Still assuming problems attributable to guanosine, some reactions were carried out between the guanosine derivative **16** and the test substrate **18** instead of the maytansinol derivative. In short, increasing the amount of all reactants from catalytic to stoichiometric and shifting the solvent to a higher percentage of water did not provide good results; therefore, DMSO was selected as organic solvent to be mixed with water. As expected, the solvation property of DMSO made it possible to overcome the problems encountered and it was possible to detect the formation of the desired product after 2 hours of reaction. The molar ratio of reagents and the percentage of DMSO were increased to push the reaction faster and as a consequence the yield achieved was satisfactory after 8 hours. This process made possible to select water/DMSO 1:2 as a suitable solvent.

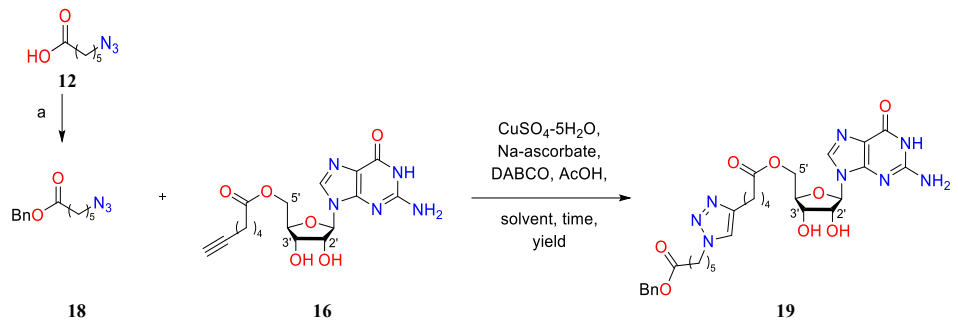

18 **16** **19**

Scheme 3.28 *Reaction condition*: a) $PhCH_2OH$ 1.5 eq, DCC 2 eq, DMAP 0.6 eq, DCM, 18 h, rt, 66%.

Table 3.3 Reaction conditions in CuAAC with RP purification.

$CuSO_4$ [eq]	Na-ascorbate [eq]	DABCO [eq]	AcOH [eq]	Solvent	Time [h]	Yield [%]
0.2	0.8	0.4	0.4	H_2O/t-BuOH 1:1	7	-
0.4	1.6	0.8	0.8	H_2O/t-BuOH 2:1	7	-
0.8	3.2	1.6	1.6	H_2O/t-BuOH 3:1	7	-
1	4	2	2	H_2O/t-BuOH 4:1	18	10
0.2	0.8	0.4	0.4	H_2O/DMSO 1:1	2	43
0.6	2.4	1.2	1.2	H_2O/DMSO 2:1	8	70
0.6	2.4	1.2	1.2	H_2O/DMSO 1:2	7	90

The applied conditions were used to perform other clicks between the two available pairs of maytansinoid and guanosine fragments (**1f**/**14** and **1h**/**16**), but no triazole ring was obtained neither by increasing the reagents considerably. Hence, the reaction was stopped and the substrates were recovered.

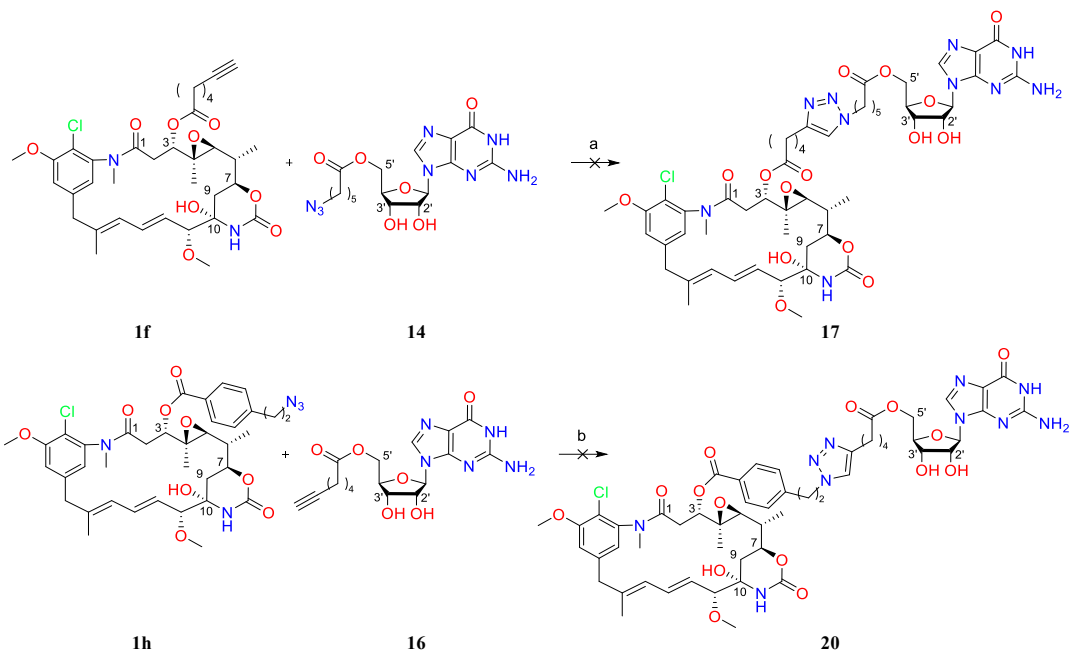

Scheme 3.29 *Reaction condition*: a) **1f** 1 eq, **14** 1.5 eq, $CuSO_4$-$5H_2O$ 0.8 eq, DABCO 1.6 eq, AcOH 1.6 eq, Na-ascorbate 3.2 eq, H_2O/DMSO 1:2, rt, o.n; b) **1h** 1 eq, **16** 1.5 eq, $CuSO_4$-$5H_2O$ 1.6 eq, DABCO 3.2 eq, AcOH 3.2 eq, Na-ascorbate 6.4 eq, H_2O/DMSO 1:2, rt, 48 h.

In order to improve the reactivity of guanosine and thus to better support the solubility and the reaction, an alternative strategy to carry out the CuAAC was considered. The new route involves making the click using the guanosine intermediate with isopropylidene protection and subsequently performing the cleavage of the ketal in the final adduct. Therefore, it was necessary to find the experimental conditions for the removal of the protecting group without altering the integrity of the sensitive structure of maytansinol.

Literature reports several reaction conditions for deprotection of isopropylidene:[83]

1. 1 *N* HCl, THF (1:1), 20°C;
2. 60–80% AcOH, rt, 2 h, 92% yield;
3. HCOOH/ether 2:3, 4 h, 60%;
4. $NaHSO_3$·SiO_2, DCM, rt, 82–100% yield;
5. TFA, DCM, rt, 2–11 h, 77–92% yield;
6. TFA, THF, H_2O, 83% yield;
7. 40% aqueous HF, ACN, >56% yield;
8. Phosphomolybdic acid (PMA) supported on silica gel, ACN, rt, 4–7 min, 89–95% yield;
9. EtSH, TsOH, $CHCl_3$, >76% yield;
10. BCl_3, 25°C, 2 min, 100% yield;
11. $PdCl_2(CH_3CN)_2$, ACN, H_2O, rt;
12. $(Bu_2SnNCS)_2O$, diglyme, H_2O, 100°C, 82% yield;
13. $FeCl_3$·SiO_2, $CHCl_3$, 74% yield;
14. $CuCl_2$-$2H_2O$, ACN, -5°C, 4 h, 96%;
15. $CeCl_3$·$7H_2O$, oxalic acid, ACN, rt, 64–98% yield;
16. Ce(IV) ammonium nitrate (CAN), ACN, water, 75–90% yield;
17. $Zn(NO_2)_2$·$6H_2O$, ACN, 6–8 h, 82–88% yield;
18. $BiCl_3$, ACN or DCM, 10–30 min, 79–93% yield;
19. $SnCl_2$, CH_3NO_2, H_2O, >80% yield;
20. Me_2BBr, DCM, -78°C, ~50%;
21. SO_2, H_2O, 40°C, >67% yield.

From this short list, some entries have been discarded and those considered potentially compatible with the needs were tested on mixtures of maytansinol and **13** on a small scale (2 mg + 2 mg). In **Table 3.4** are summarised the results of the screening.

83 P. G. M. Wuts, in *Greene's Prot. Groups Org. Synth.*, **2014**, pp. 400–410.

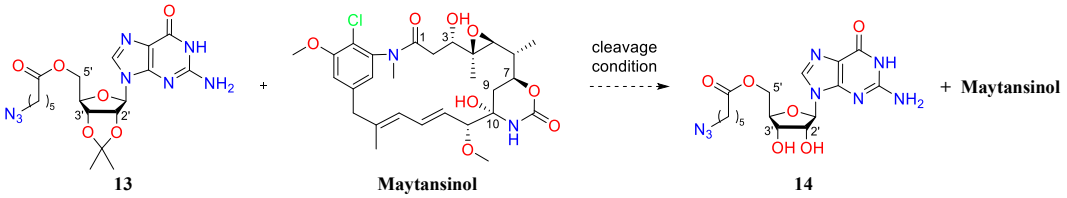

13 **Maytansinol** **14**

Scheme 3.30 Reaction for selective deprotection of isopropylidene guanosine.

Table 3.4 Cleavage conditions of ketal on guanosine.

Cleavage Conditions monitored by TLC	**Result**
80% AcOH, 25°C, 48 h	×
80% AcOH, 65°C, 18 h	×
$PdCl_2(CH_3CN)_2$, 60°C, ACN, H_2O, 24 h	×
CAN, ACN, rt, 48 h	×
PPTS, ACN, rt, 48 h	×
$CuCl_2$-$2H_2O$, ACN, 0°C 4h then rt 48 h	×
HCOOH 50% aq, rt, 48 h[84]	×
HCOOH 70% aq, rt, 48 h	×
HCOOH 70% aq, 40°C, 2 h	✓

All conditions except the use of $PdCl_2$ did not affect maytansinol, but at the same time they failed in the cleaving of ketal. Although the use of formic acid with the conditions reported in the literature for the specific removal of acetonide from guanosine did not produce any results, increasing the acid concentration and heating slightly to 40°C successfully led to the goal. ^{1}H-NMR analysis confirmed maytansinol integrity and guanosine deprotection.

At this point, the CuAAC reactions were performed again by treating the protected 5'-*O*-acylguanosine with an excess of $CuSO_4$ and Na-ascorbate in 1:2 H_2O/DMSO. The combination DABCO/AcOH to accelerate the reaction was not considered because it was preferred to simply opt for an increase of the active species Cu (I). As expected, the protecting group improved the solubility of guanosine allowing to obtain excellent results: the triazole ring was formed in few hours with a yield of 89% for compound **21** and with a yield of 85% for **22**.

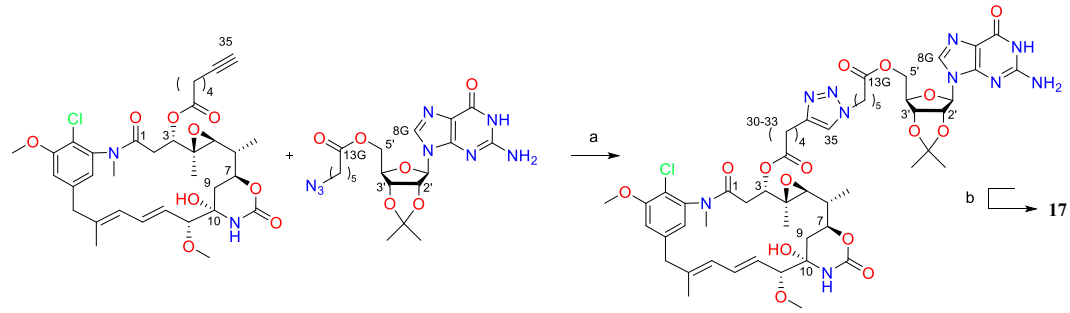

1f **13** **21**

Scheme 3.31 *Reaction condition*: a)) **1f** 1 eq, **13** 1.5 eq, $CuSO_4$-$5H_2O$ 1.6 eq, Na-ascorbate 6.4 eq, H_2O/DMSO 1:2, rt, 3 h, 89% with RP purif; b) HCOOH 70% aq, 40°C, 4 h, 62% with RP purif.

84 B. Zhang, Z. Cui, L. Sun, *Org. Lett.* **2001**, *3*, 275–278.

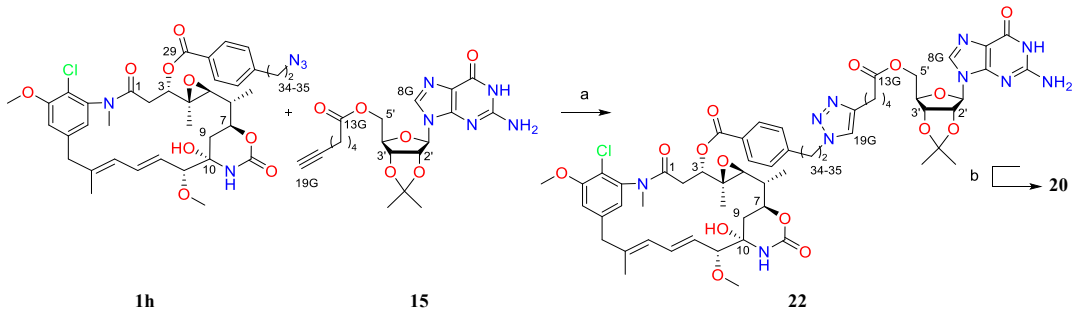

Scheme 3.32 *Reaction condition*: a) **1h** 1 eq, **15** 1.5 eq, $CuSO_4$-$5H_2O$ 1.6 eq, Na-ascorbate 6.4 eq, H_2O/DMSO 1:2, rt, 3 h, 85% with RP purif; b) HCOOH 70% aq, 40°C, 4 h, 77% with RP purif.

The high resolution mass found the corresponding masses of the products:

21 HRMS (ESI) m/z $[M+Na]^+$ 1157.4691 (calcd for $C_{54}H_{71}ClN_{10}O_{15}Na$ 1157.4687);

22 HRMS (ESI) m/z $[M+Na]^+$ 1191.4546 (calcd for $C_{57}H_{69}ClN_{10}O_{15}Na$ 1191.4530).

In addition, the NMR elucidations were completed to confirm the structures and the shifting of the diagnostic signals demonstrated the formation of triazole on **21** and **22**:

Table 3.5 Diagnostic ^{1}H NMR spectroscopic data of **21** and **22** in *DMSO-d6.*

Atom		^{1}H-NMR[a,b]		^{13}C-NMR[a,c]	
		from	to	from	to
21	33	2.28[e]	2.65	18.04[e]	28.82
	34	-	-	84.20[e]	146.89
	35	1.95[e]	7.85	69.0[e]	122.13
	18G	3.29	4.25	51.59	49.38
22	35	3.70[d]	4.64	52.48[d]	50.23
	17G	2.14	2.53	18.50	25.07
	18G	-	-	85.28	146.84
	19G	2.74	7.78	72.40	121.96

[a] Chemical shifts (in ppm) were determined with reference to TMS; [b] Spectra determined at 400 MHz; [c] Spectra determined at 101 MHz; [d] Solvent is *acetone-d6*; [e] Solvent is *chloroform-d.*

Both products were treated with formic acid 70% aq at 40°C providing the final products **17** and **20** after 4 hours with yields of 62% and 77% respectively. The MS and NMR analyses confirmed the isopropylidene deprotection.

3.2 Comparison of NMR assessments

All compounds discussed were fully characterised in detail by NMR experiments with different solvents and the complete ^{1}H and ^{13}C NMR assignments have been determined based on 1D and 2D NMR spectra (^{1}H and ^{13}C NMR, COSY, HSQC, and HMBC). The separation of the ^{1}H signals is well appreciable in *acetone-d6* and allows recognising easily the characteristic peaks by chemical shift and shape. To explain the differences in the assessment of the structures, the diagnostic signals indispensable to understand quickly the modifications of maytansinol are compared in **Table 3.6**.

The evaluation of the main differences between **M** and the O-acylated derivatives **1b**, **5b**, and **4b** shows an evident shift of H-3 signal from 3.34 to about 5 ppm, as a consequence of the successfully esterification at the OH-3. Simultaneously, the shift of the H-2 signals from 2.36 and 1.91 ppm to about 2.9 and 2.2 ppm is observed. The corresponding signals of the compounds **2**, **6** and **3b** do not undergo significant changes excluding an involvement of the hydroxyl group.

The dehydration of **M** present in **6**, **5b**, **3b**, and **4b** at C_8-C_9 is marked by the merge of the two diasterotopic

protons H-8 towards 5 ppm, a typical area of the double bonds, and the non-detection of 9-OH supports the same interpretation. Furthermore, the characteristic H-7 signal disappears leading to the presence of a new signal at more deshielded fields changing the multiplicity to a dd. Similarly, can be noted a new revealing of the H-10 over 4.15 ppm. It is possible to observe a similar behaviour for the protons H-7, H-8, and H-10 involved in the modification of compound **2**; however, the shift of H-7 and H-8 are much more accentuated than that observed for the other derivatives due to the formation of the α,β-unsaturated ketone. The olefinic protons signals H-11, H-12, and H-13 are all shifted slightly to higher fields, except compound **2**. Finally, the disappearance of the NH signal indicates an acylation of oxazinanone as regard the compounds **3b** and **4b**, and the cleavage for the compound **2**.

Table 3.6 Diagnostic ^{1}H NMR spectroscopic data of maytansinoid compounds in ppm.

Atom	M[a]	2[a]	6[c]	1b[b]	5b[b]	3b[c]	4b[b]
2	2.36, 2.13	2.34 – 2.24 2.03	2.32 2.14	2.88 – 2.79 2.26	2.91, 2.22	2.37, 2.12	2.99 – 2.87, 2.27
3	3.55	3.38	3.59	5.04 – 4.85[e]	5.02	3.61	5.04
7	4.25	6.87 – 6.68[d]	4.78	4.31 – 4.14	4.56	4.86	4.92 – 4.76[f]
8	1.91, 1.41	6.42	5.02 – 4.96	1.59, 1.54 – 1.39	4.43	5.43 – 5.33	4.92 – 4.76[f]
10	3.64	4.60	4.20 – 4.12	3.50	4.15	4.42	4.35
11	5.52	5.31	5.54	5.04 – 4.85[e]	4.88	5.54	4.92 – 4.76[f]
12	6.70	6.87 – 6.68[d]	6.46	6.61	6.54	6.48	6.64
13	6.20	6.12	6.16	6.04	6.13	6.15	6.12
OH-3	4.50	-	-	-	-	-	-
9-OH	4.80	-	-	4.47	-	-	-
NH	6.42	-	7.08	6.33	8.03	-	-

Chemical shifts (in ppm) were determined with reference to TMS; Spectra determined at 400 MHz; [a] Solvent is *methanol-d4*; [b] Solvent is *acetone-d6*; [c] Solvent is *chloroform-d*; [d-f] Chemical shifts bearing the same symbol overlap.

The recorded spectra show the distinctive structure of maytansinol for all derivatives. The NMR data are reported below highlighting in blue the key protons that undergo the evident changes and that provide fundamental indications to deduce the type of derivative obtained, as explained in **Table 3.6**.

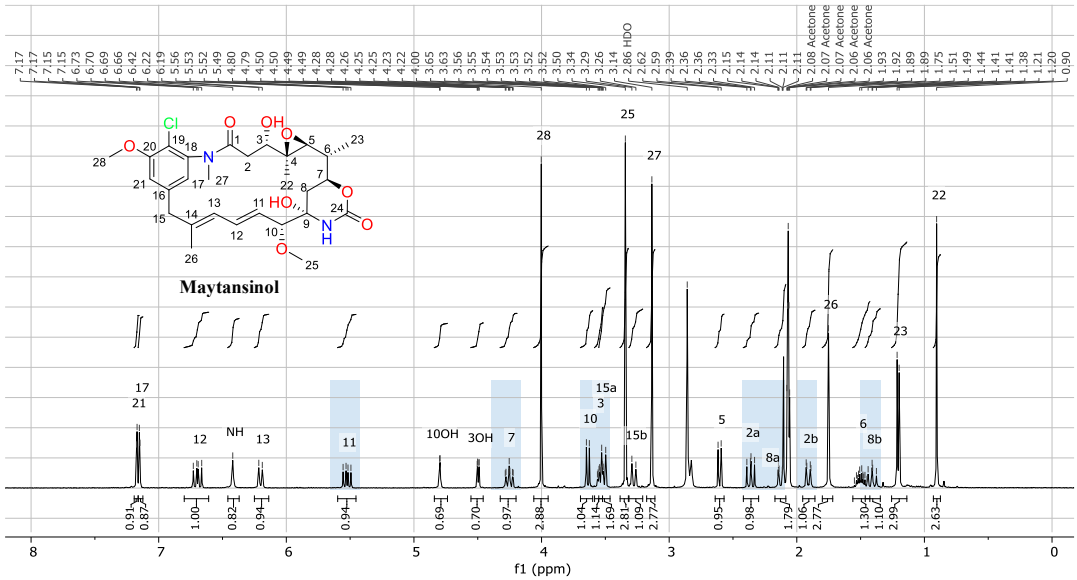

Figure 3.4 ^{1}H NMR Spectrum (400 MHz, *acetone-d6*) of **maytansinol**.

Table 3.7 ^{1}H- and ^{13}C-NMR assignments for maytansinol.

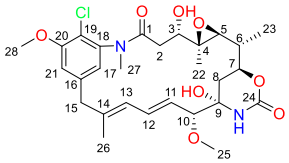

Maytansinol

Atom	^{1}H-NMR[a,b] *chloroform-d*	^{1}H-NMR[a,b] *acetone-d6*	^{1}H-NMR[a,b] *methanol-d4*	^{13}C-NMR[a,c] *methanol-d4*
1				172.41
2	2.28 (dd, *J* = 13.3, 11.0 Hz, 1H) 2.12 (dd, *J* = 13.0, 1.8 Hz, 1H)	2.36 (dd, *J* = 13.0, 11.1 Hz, 1H) 2.13 (dt, *J* = 12.3, 1.3 Hz, 1H)	2.35 (dd, *J* = 12.9, 11.3 Hz, 1H) 1.95 (dd, *J* = 12.8, 2.3 Hz, 1H)	34.94[f]
3	3.54 – 3.44 (m, 3H)[d]	3.55 (dd, *J* = 5.0, 2.0 Hz, 1H)	3.41 – 3.38 (m, 4H)[e]	75.25
4				63.20
5	2.59 (d, *J* = 9.8 Hz, 1H)	2.60 (d, *J* = 9.8 Hz, 1H)	2.50 (d, *J* = 9.7 Hz, 1H)	66.86
6	1.62 – 1.48 (m, 1H)	1.56 – 1.43 (m, 1H)	1.67 – 1.52 (m, 1H)	37.59
7	4.37 (ddd, *J* = 12.3, 10.4, 1.8 Hz, 1H)	4.25 (ddd, *J* = 12.4, 10.3, 2.2 Hz, 1H)	4.30 (ddd, *J* = 12.4, 10.5, 1.9 Hz, 1H)	75.40
8	2.21 (dt, *J* = 13.9, 1.7 Hz, 1H) 1.28 – 1.23 (m, 1H)	1.91 (dd, *J* = 12.9, 2.0 Hz, 1H) 1.41 (dd, *J* = 13.9, 12.2 Hz, 1H)	2.07 (dd, *J* = 14.1, 2.0 Hz, 1H) 1.47 (dd, *J* = 14.1, 12.2 Hz, 1H)	34.88
9				80.75
10	3.54 – 3.44 (m, 3H)[d]	3.64 (d, *J* = 9.2 Hz, 1H)	3.65 – 3.58 (m, 1H)	88.21
11	5.53 (dd, *J* = 15.2, 9.2 Hz, 1H)	5.52 (dd, *J* = 15.3, 9.2 Hz, 1H)	5.58 – 5.46 (m, 1H)	126.90
12	6.44 (dd, *J* = 15.3, 10.9 Hz, 1H)	6.70 (dd, *J* = 15.3, 11.0 Hz, 1H)	6.66 – 6.53 (m, 1H)	133.45
13	6.15 (d, *J* = 10.9 Hz, 1H)	6.20 (d, *J* = 11.0 Hz, 1H)	6.18 (d, *J* = 10.9 Hz, 1H)	125.00
14				138.60
15	3.54 – 3.44 (m, 3H)[d] 3.12 (d, *J* = 12.7 Hz, 1H)	3.51 (d, *J* = 12.6 Hz, 1H) 3.28 (d, *J* = 12.6 Hz, 1H)	3.50 (d, *J* = 12.6 Hz, 1H) 3.24 (d, *J* = 12.6 Hz, 1H)	46.19
16				140.75
17	6.81 (d, *J* = 1.9 Hz, 1H)	7.15 (d, *J* = 1.9 Hz, 1H)	7.12 (d, *J* = 1.8 Hz, 1H)	123.53
18				141.83
19				117.89
20				155.63
21	7.04 (d, *J* = 1.8 Hz, 1H)	7.17 (d, *J* = 1.9 Hz, 1H)	7.08 (d, *J* = 1.9 Hz, 1H)	113.05
22	0.84 (s, 3H)	0.90 (s, 3H)	0.85 (s, 3H)	9.96
23	1.31 (d, *J* = 6.4 Hz, 3H)	1.21 (d, *J* = 6.4 Hz, 3H)	1.26 (s, 2H)	13.25
24				153.94
25	3.36 (s, 3H)	3.34 (s, 3H)	3.38 (m, 4H)[e]	55.44
26	1.69 (d, *J* = 1.3 Hz, 3H)	1.75 (s, 3H)	1.73 (d, *J* = 1.3 Hz, 3H)	14.44
27	3.21 (s, 3H)	3.14 (s, 3H)	3.19 (s, 3H)	34.94[f]
28	3.99 (s, 3H)	4.00 (s, 3H)	3.98 (s, 3H)	55.72
3-OH	-	4.50 (dd, *J* = 5.0, 1.1 Hz, 1H)	-	
9-OH	-	4.80 (d, *J* = 1.8 Hz, 1H)	-	
NH	6.35 (d, *J* = 1.4 Hz, 1H)	6.42 (s, 1H)	-	

[a] Chemical shifts (in ppm) were determined with reference to TMS; [b] Spectra determined at 400 MHz; [c] Spectra determined at 101 MHz; [d-f] Chemical shifts bearing the same symbol overlap.

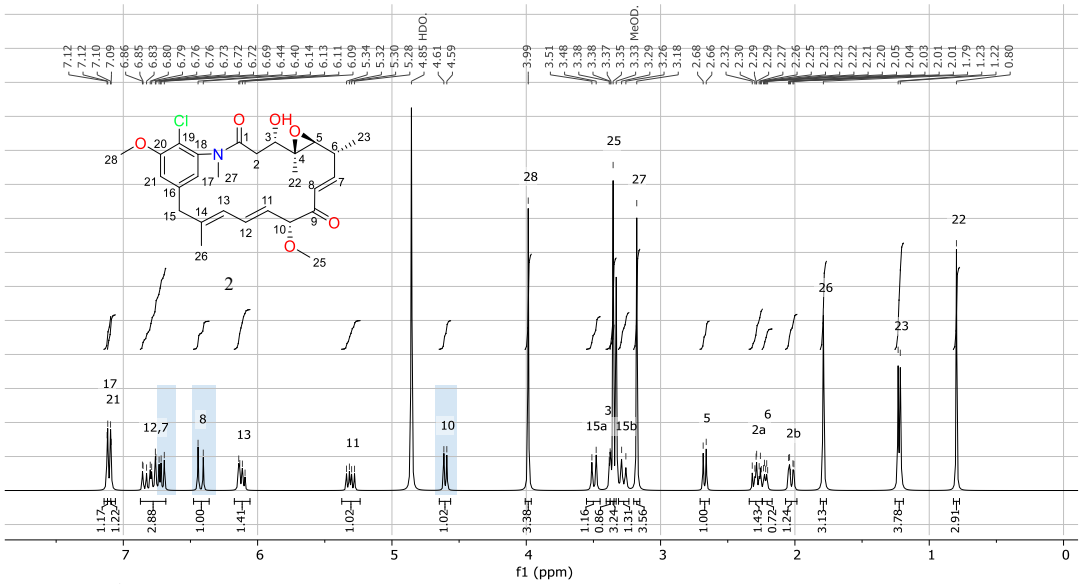

Figure 3.5 ^{1}H NMR Spectrum (400 MHz, *methanol-d4*) of **2**.

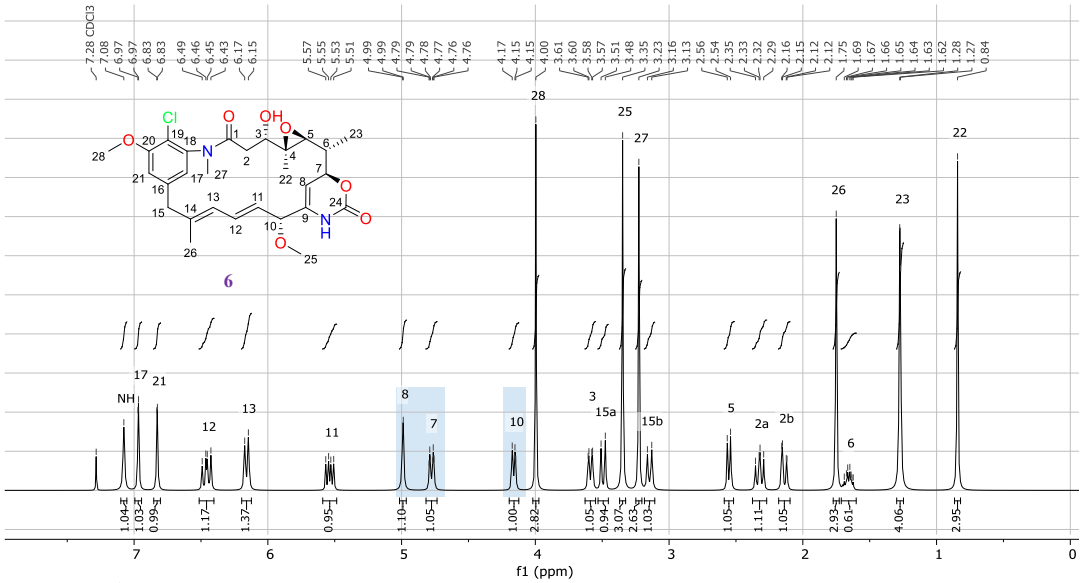

Figure 3.6 ^{1}H NMR Spectrum (400 MHz, *chloroform-d*) of **6**.

Table 3.8 ^{1}H- and ^{13}C-NMR assignments for **2** in *methanol-d4* and for **6** in *chloroform-d.*

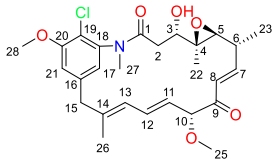

2

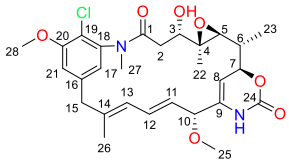

6

Atom	^{1}H-NMR[a,b] *methanol-d4*	^{13}C-NMR[a,c] *methanol-d4*	^{1}H-NMR[a,b] *chloroform-d*	^{13}C-NMR[a,c] *chloroform-d*
1		172.20		171.60
2	2.34 – 2.24 (m, 1H) 2.03 (dd, *J* = 13.0, 2.9 Hz, 1H)	34.99	2.32 (dd, *J* = 13.6, 10.8 Hz, 1H) 2.14 (dd, *J* = 13.7, 2.3 Hz, 1H)	35.69
3	3.38 (t, *J* = 2.7 Hz, 1H)	73.49	3.59 (dd, *J* = 10.9, 2.4 Hz, 1H)	75.85
4		62.37		62.39
5	2.67 (d, *J* = 9.1 Hz, 1H)	66.21	2.55 (d, *J* = 9.7 Hz, 1H)	66.17
6	2.24 – 2.17 (m, 1H)	37.33	1.66 (td, *J* = 10.1, 6.4 Hz, 1H)	39.02
7	6.87 – 6.68 (m, 2H)[d]	146.34	4.78 (dt, *J* = 10.5, 2.3 Hz, 1H)	80.09
8	6.42 (d, *J* = 15.6 Hz, 1H)	127.27	5.02 – 4.96 (m, 1H)	99.08
9		196.02		136.09
10	4.60 (d, *J* = 8.8 Hz, 1H)	87.53	4.20 – 4.12 (m, 1H)	80.00
11	5.31 (dd, *J* = 15.2, 8.7 Hz, 1H)	126.04	5.54 (dd, *J* = 15.2, 8.5 Hz, 1H)	126.85
12	6.87 – 6.68 (m, 2H)[d]	133.34	6.46 (dd, *J* = 15.2, 10.8 Hz, 1H)	133.50
13	6.12 (dd, *J* = 13.3, 5.5 Hz, 1H)	125.14	6.16 (d, *J* = 11.1 Hz, 1H)	124.74
14		139.64		140.32
15	3.50 (d, *J* = 12.8 Hz, 1H) 3.27 (d, *J* = 12.8 Hz, 1H)	45.94	3.49 (d, *J* = 12.8 Hz, 1H) 3.15 (d, *J* = 12.9 Hz, 1H)	46.82
16		140.61		140.40
17	7.12 (d, *J* = 1.9 Hz, 1H)	123.34	6.97 (d, *J* = 1.9 Hz, 1H)	123.26
18		141.96		143.01
19		118.01		118.98
20		155.77		156.14
21	7.09 (d, *J* = 2.0 Hz, 1H)	113.02	6.83 (d, *J* = 1.9 Hz, 1H)	112.50
22	0.80 (s, 3H)	9.96	0.84 (s, 3H)	11.23
23	1.22 (d, *J* = 6.6 Hz, 3H)	14.76	1.27 (d, *J* = 2.3 Hz, 3H)	14.55
24	-	-		151.53
25	3.35 (s, 3H)	55.38	3.35 (s, 3H)	56.61
26	1.79 (s, 3H)	16.11	1.75 (s, 3H)	16.41
27	3.18 (s, 3H)	34.77	3.23 (s, 3H)	35.96
28	3.99 (s, 3H)	55.73	4.00 (s, 3H)	56.70
3-OH			-	
9-OH			-	
NH			7.08 (s, 1H)	

[a] Chemical shifts (in ppm) were determined with reference to TMS; [b] Spectra determined at 400 MHz; [c] Spectra determined at 101 MHz;
[d] Chemical shifts bearing the same symbol overlap.

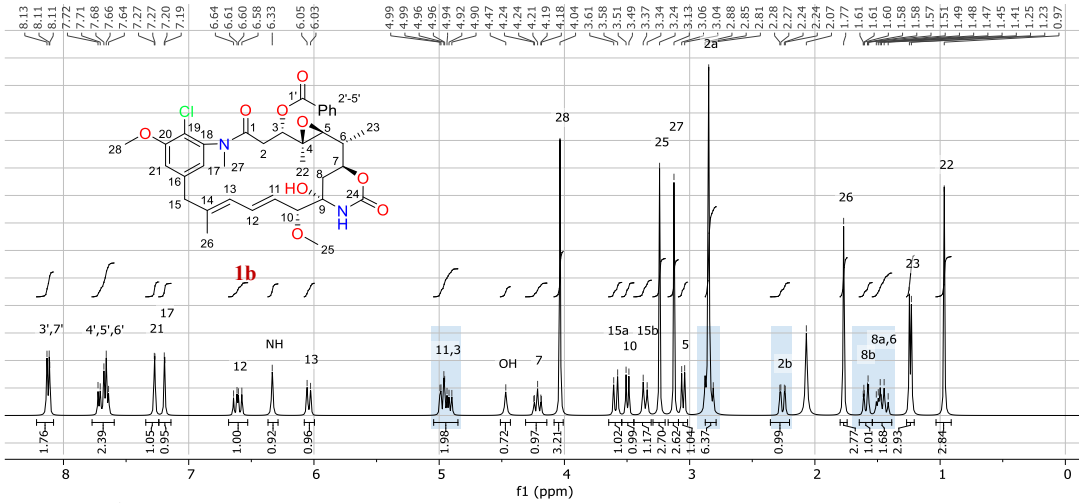

Figure 3.7 ^{1}H NMR Spectrum (400 MHz, *acetone-d6*) of **1b**.

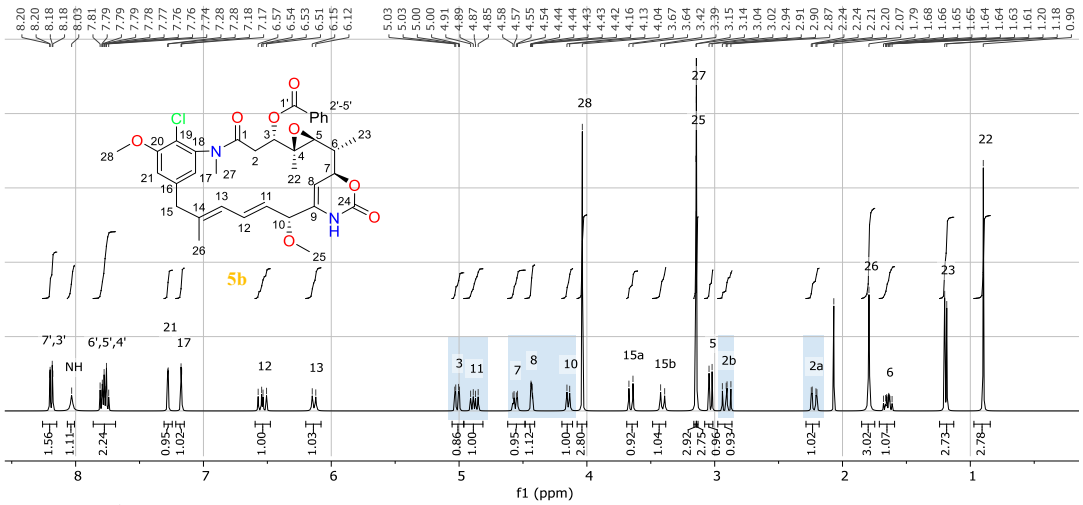

Figure 3.8 ^{1}H NMR Spectrum (400 MHz, *acetone-d6*) of **5b**.

Table 3.9 ^{1}H- and ^{13}C-NMR assignments for **1b** and **5b** in *acetone-d6*.

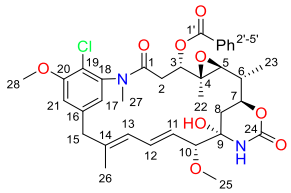

1b

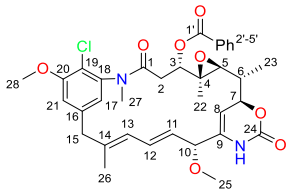

5b

Atom	^{1}H-NMR[a,b] *acetone-d6*	^{13}C-NMR[a,c] *acetone-d6*	^{1}H-NMR[a,b] *acetone-d6*	^{13}C-NMR[a,c] *acetone-d6*
1		168.04		167.98
2	2.88 – 2.79 (m, 1H) 2.26 (dd, *J* = 14.4, 3.1 Hz, 1H)	32.69	2.91 (dd, *J* = 14.6, 12.0 Hz, 1H) 2.22 (dd, *J* = 14.6, 3.0 Hz, 1H)	32.24
3	5.04 – 4.85 (m, 2H)[d]	77.45	5.02 (dd, *J* = 11.9, 3.0 Hz, 1H)	77.91
4		60.50		60.16
5	3.05 (d, *J* = 9.5 Hz, 1H)	66.35	3.03 (d, *J* = 9.6 Hz, 1H)	67.02
6	1.54 – 1.39 (m, 2H, 6)[e]	38.68	1.65 (ddd, *J* = 10.6, 9.7, 6.5 Hz, 1H)	39.45
7	4.31 – 4.14 (m, 1H)	73.79	4.56 (dd, *J* = 10.8, 3.4 Hz, 1H)	78.23
8	1.59 (dt, *J* = 13.6, 1.9 Hz, 1H) 1.54 – 1.39 (m, 2H, 6)[e]	36.17	4.43 (dt, *J* = 3.2, 1.5 Hz, 1H)	97.96
9		80.53		137.00
10	3.50 (d, *J* = 9.1 Hz, 1H)	88.87	4.15 (d, *J* = 8.5 Hz, 1H)	79.51
11	5.04 – 4.85 (m, 2H)[d]	128.58	4.88 (dd, *J* = 15.3, 8.4 Hz, 1H)	126.73
12	6.61 (dd, *J* = 15.5, 11.1 Hz, 1H)	132.39	6.54 (dd, *J* = 15.3, 10.9 Hz, 1H)	133.01
13	6.04 (d, *J* = 11.0 Hz, 1H)	124.71	6.13 (d, *J* = 11.0 Hz, 1H)	124.05
14		139.57		140.71
15	3.59 (d, *J* = 12.6 Hz, 1H) 3.36 (d, *J* = 12.7 Hz, 1H)	46.25	3.66 (d, *J* = 12.7 Hz, 1H) 3.41 (d, *J* = 12.6 Hz, 1H)	46.18
16		141.32		141.16
17	7.19 (d, *J* = 1.8 Hz, 1H, 17)	122.12	7.17 (d, *J* = 1.8 Hz, 1H)	122.18
18		142.40		142.34
19		118.66		118.67
20		156.19		156.22
21	7.27 (d, *J* = 1.9 Hz, 1H)	113.51	7.28 (d, *J* = 1.8 Hz, 1H)	113.37
22	0.97 (s, 3H)	12.12	0.90 (s, 3H)	11.65
23	1.24 (d, *J* = 6.4 Hz, 3H)	14.01	1.19 (d, *J* = 6.5 Hz, 3H)	13.50
24		151.08		149.86
25	3.24 (s, 3H)	55.79	3.15 (s, 3H)	55.39
26	1.77 (s, 3H)	14.88	1.79 (s, 3H)	15.10
27	3.13 (s, 3H)	34.57	3.14 (s, 3H)	34.66
28	4.04 (s, 3H)	56.17	4.04 (s, 3H)	56.15
3-OH	4.47 (s, 1H)			
9-OH	6.33 (s, 1H)		8.03 (s, 1H)	
NH				

[a] Chemical shifts (in ppm) were determined with reference to TMS; [b] Spectra determined at 400 MHz; [c] Spectra determined at 101 MHz; [d-e] Chemical shifts bearing the same symbol overlap.

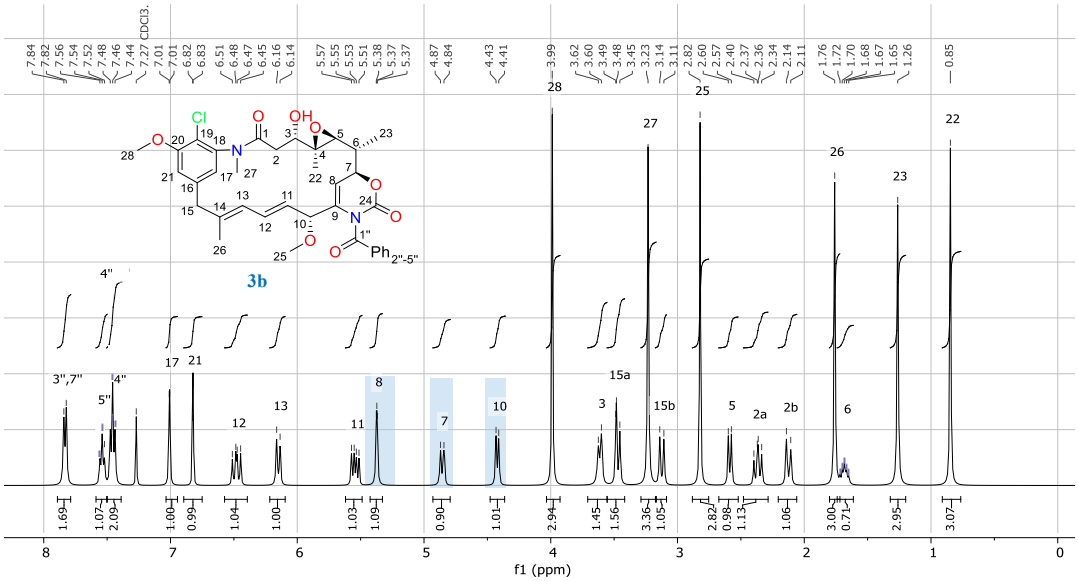

Figure 3.9 ^{1}H NMR Spectrum (400 MHz, *chloroform-d*) of **3b**.

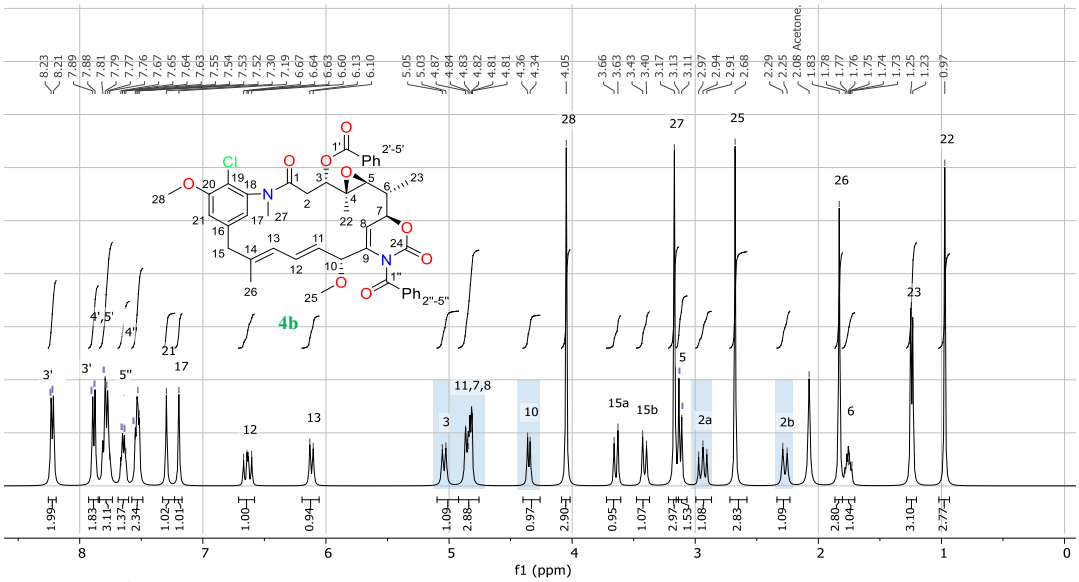

Figure 3.10 ^{1}H NMR Spectrum (400 MHz, *acetone-d6*) of **4b**.

Table 3.10 ^{1}H- and ^{13}C-NMR assignments for **3b** in *chloroform-d* and **4b** in *acetone-d6*.

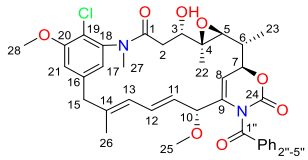

3b

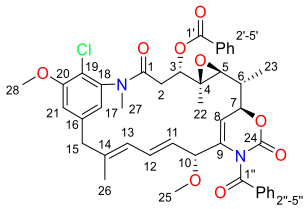

4b

Atom	^{1}H-NMR[a,b] *chloroform-d*	^{13}C-NMR[a,c] *chloroform-d*	^{1}H-NMR[a,b] *acetone-d6*	^{13}C-NMR[a,c] *acetone-d6*
1		172.18		168.04
2	2.37 (dd, J = 13.7, 10.9 Hz, 1H) 2.12 (d, J = 13.6 Hz, 1H)	36.36	2.99 – 2.87 (m, 1H) 2.27 (d, J = 14.2 Hz, 1H)	32.31
3	3.61 (d, J = 9.7 Hz, 1H)	76.46	5.04 (d, J = 11.6 Hz, 1H)	78.16
4		63.59		60.23
5	2.59 (d, J = 9.6 Hz, 1H)	67.06	3.12 (d, J = 9.2 Hz, 1H)	66.94
6	1.68 (q, J = 4.9, 4.5 Hz, 1H)	40.59	1.75 (dq, J = 8.3, 5.0, 4.5 Hz, 1H)	40.36
7	4.86 (d, J = 10.8 Hz, 1H)	80.38	4.92 – 4.76 (m, 3H)[d]	78.39
8	5.43 – 5.33 (m, 1H)	103.13	4.92 – 4.76 (m, 3H)[d]	102.06
9		137.55		137.25
10	4.42 (d, J = 8.4 Hz, 1H)	78.51	4.35 (d, J = 8.2 Hz, 1H)	77.63
11	5.54 (dd, J = 15.2, 8.4 Hz, 1H)	127.12	4.92 – 4.76 (m, 3H)[d]	125.75
12	6.48 (dd, J = 15.2, 10.8 Hz, 1H)	134.41	6.64 (dd, J = 15.3, 11.1 Hz, 1H)	134.46
13	6.15 (d, J = 10.8 Hz, 1H)	125.38	6.12 (d, J = 11.0 Hz, 1H)	123.81
14		140.67		141.59
15	3.56 – 3.42 (m, 1H) 3.12 (d, J = 13.0 Hz, 1H)	47.27	3.64 (d, J = 12.5 Hz, 1H) 3.41 (d, J = 12.6 Hz, 1H)	46.21
16		140.99		141.08
17	7.01 (d, J = 1.8 Hz, 1H)	123.87	7.19 (s, 1H)	122.23
18		142.95		142.31
19		119.35		118.67
20		156.49		156.25
21	6.82 (d, J = 1.8 Hz, 1H)	112.93	7.30 (s, 1H)	113.36
22	0.85 (s, 3H)	11.64	0.97 (s, 3H)	11.62
23	1.26 (m, 3H)	14.92	1.24 (d, J = 6.4 Hz, 3H)	13.46
24		149.66		148.29
25	2.82 (s, 3H)	56.22	2.68 (s, 3H)	54.59
26	1.76 (s, 3H)	16.86	1.83 (s, 3H)	15.18
27	3.23 (s, 3H)	36.56	3.17 (s, 3H)	34.73
28	3.99 (s, 3H)	57.21	4.05 (s, 3H)	56.18
3-OH	-			

[a] Chemical shifts (in ppm) were determined with reference to TMS; [b] Spectra determined at 400 MHz; [c] Spectra determined at 101 MHz; [d] Chemical shifts bearing the same symbol overlap.

3.3 Docking

Studies of the binding sites of the tubulin were preliminary performed through docking study to develop the conjugate compound. Prof. S. Pieraccini's group at department of chemistry in University of Milan suggested a proximity between maytansine binding site into the vinca domain and guanosine pocket (**Figure 3.11** A).

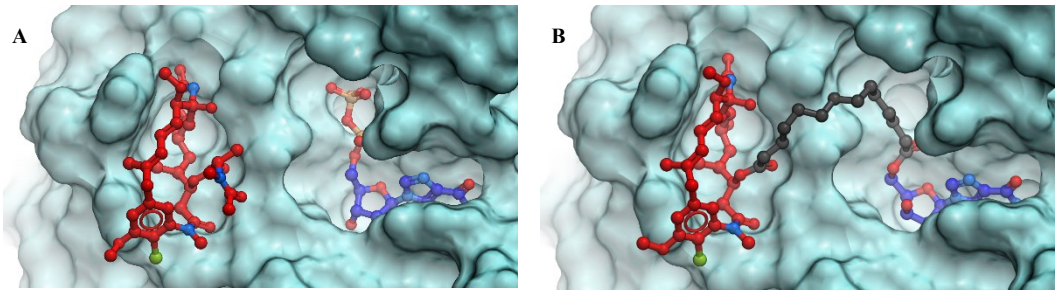

Figure 3.11 (**A**) Maytansine and GDP located in their binding site; (**B**) Maytansinol linked to guanosine via ester carbon chain of length of 14 atoms.

The crystallographic structure of the maytansine bounds to β-tubulin was placed into the site as a control measure to test the accuracy of the docking engine AutoDock Vina3. Subsequently, the geometry assigned by AutoDock Vina3 for maytansine was superimposed on the crystallographic orientation. Since the docking was able to reproduce the crystallographic results, the simulation data obtained by AutoDock Vina3 was found to be reliable.

Therefore, the distance between the two functionalisable hydroxyl groups of maytansinol and guanosine placed in the respective sites was calculated. Computational proposed a linker of 14 atoms of length (**Figure 3.11** B) and admitted the presence of triazole ring in the middle of carbon chain.

In addition, docking studies were used to predict the spatial coordinates acquired by the obtained maytansinoids in the binding mode within the maytansine site (**Figure 3.12**, **Figure 3.13**) and by the final compounds with simultaneous binding in the guanosine active site (**Figure 3.14**). To validate the results of the computational modelling experiments, the best conformer of each maytansinoid was superimposed on its corresponding crystal structure. In all cases, the orientation of the maytansinol ring remained in the same spatial arrangement, acquiring a similar binding mode to the parent compound. The introduction of bulky substituents in the O-3 position does not alter the expected three-dimensional arrangement. Therefore, the binding of maytansinoids to β-tubulin appears to be very tolerant to changes in the hydroxyl group and it is reasonable to assume that the binding mode of the studied molecules resembles the parent compound.

Table 3.11 Protein-ligand binding free energies of the best docking geometries by AutoDock Vina3 calculations on β-tubulin 4TV81.

Maytansinoid	**6**	**1b**	**1f**	**1g**	**5b**	**5f**	**5g**
ΔG^0 (kcal/mol)	-7.5	-7.4	-6.7	-8.2	-6.8	-7.4	-7.5

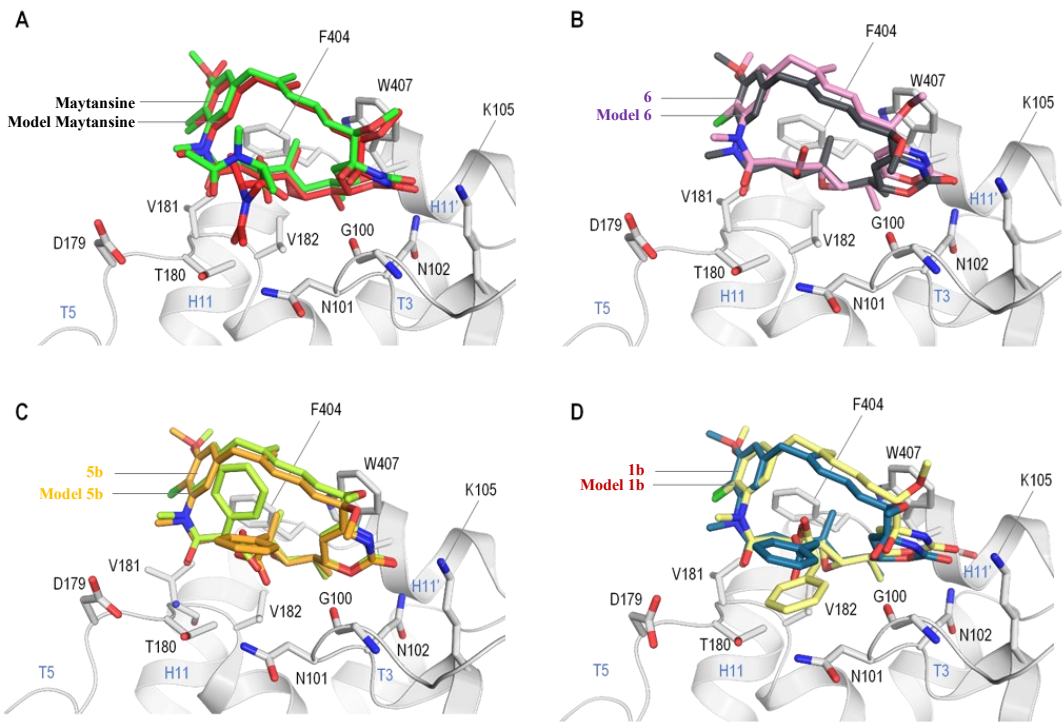

Figure 3.12 Docking of synthesised maytansinoids bound to β-tubulin active site overlapped with the corresponding crystallographic structure.

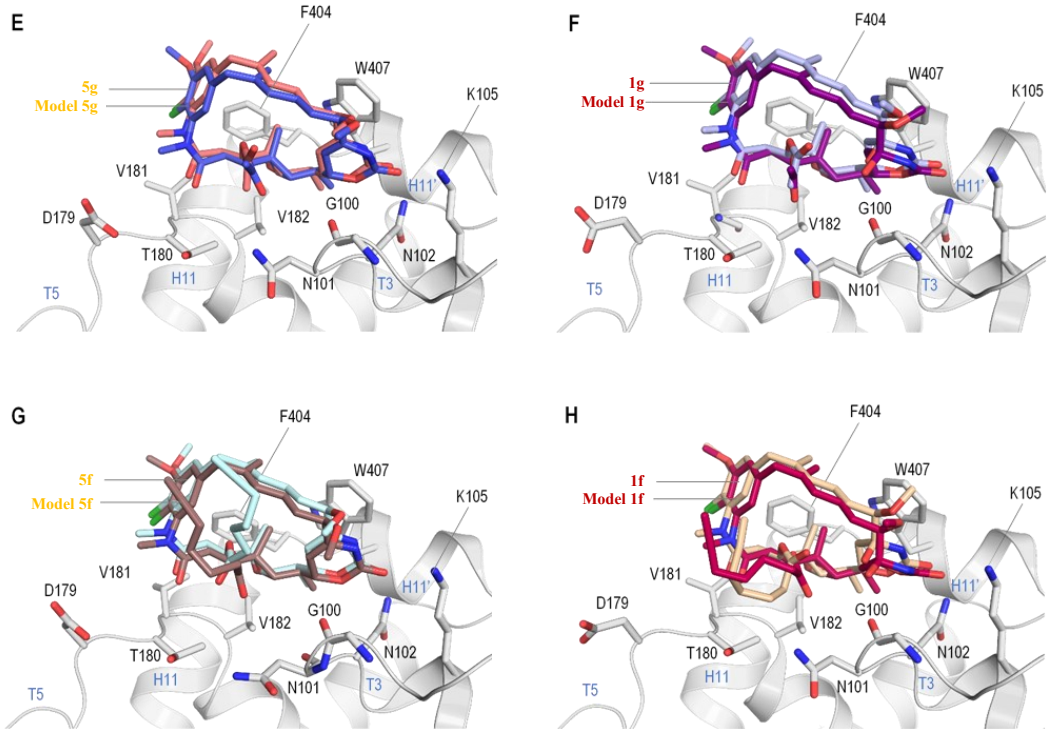

Figure 3.13 Docking of synthesised maytansinoids bound to β-tubulin active site overlapped with the corresponding crystallographic structure.

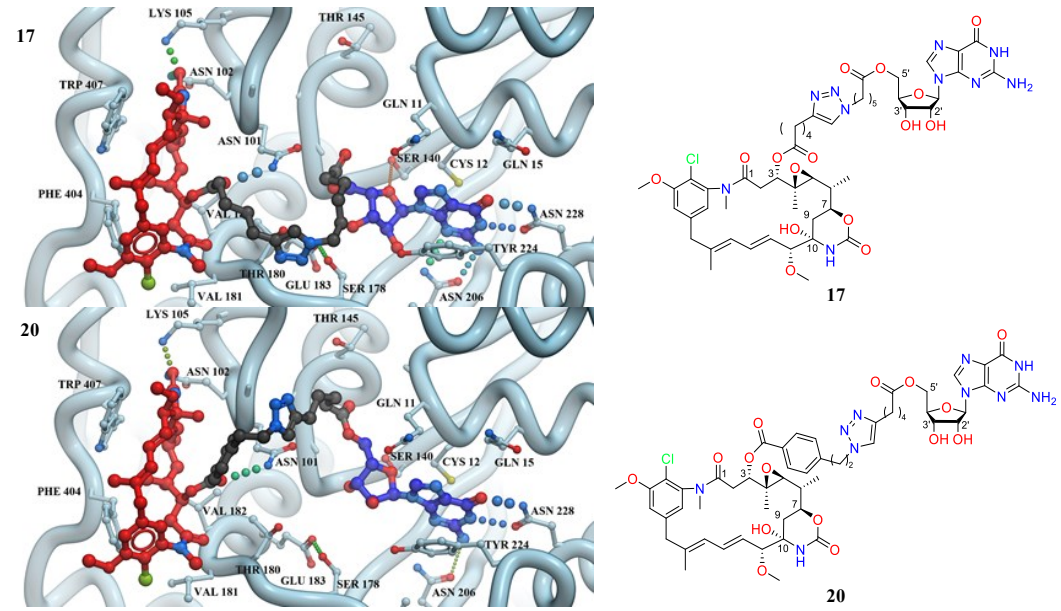

Figure 3.14 Docking of **17** and **20** bound to β-tubulin active site.

3.4 Biological evaluation

To evaluate the activity of compounds **2**, **6**, **1b**, **1f**, **1g**, **1h**, **5b**, **5f**, **5g**, **5h**, **3b**, **4b**, **17**, and **20** on tubulin and MTs, the effect on MT assembly dynamics was explored and subsequently the binding affinities with tubulin dimers and cell toxicity were determined. J. F. Diaz's group at Margarita Salas Biological Research Centre Higher Council for Scientific Research in Madrid performed the assessments.

Inhibition of tubulin assembly

A convenient method for studying tubulin polymerisation is to monitor the increase in turbidity of a tubulin solution under specific conditions. As the dimers assemble, increasing the size of the MT changes the physical properties of the solution.[85] The increase in turbidity of the solution can be monitored through spectrophotometric measurements, and therefore the polymerisation process can be correlated to the absorbance of a tubulin solution at a specified wavelength. The effect of a MSA favours the formation of MT by causing a more evident increase in turbidity, consequently a reduction in absorbance is associated. Opposite is the effect of a MDA.

The applied method consists in polymerising a 27.5 µM solution of tubulin in GAB buffer (10 mM NaPi pH 6.8, 30% glycerol, 1 mM EGTA, 0.1 mM GTP) at 37°C in the presence of different compounds at 27.5 µM in DMSO. Subsequently, the concentrations of the tested compounds were decreased to evaluate the affinity. Polymerisation was monitored by measuring the absorbance at 350 nm for 1.5 h. The ability to inhibit tubulin assembly of compounds were tested on A549 cell line (non-small lung cell carcinoma) using DMSO as negative control, and maytansine, which completely blocks tubulin polymerisation, and maytansinol, which has an evident effect at stoichiometric concentrations, as positive controls.

All the compounds analysed in stoichiometric ratios inhibited the assembly of tubulin to MTs with different potencies. Compounds **1b**, **1f**, **1g**, **1h**, **5g**, **3b**, **17**, and **20** were found to be strong MDAs as they were able to completely block the assembly of MTs with a similar effect of maytansine. In contrast, compounds **6**, **5f**, and **4b** showed mild inhibition, while compounds **2**, **5b** and **5h** had a very weak action.

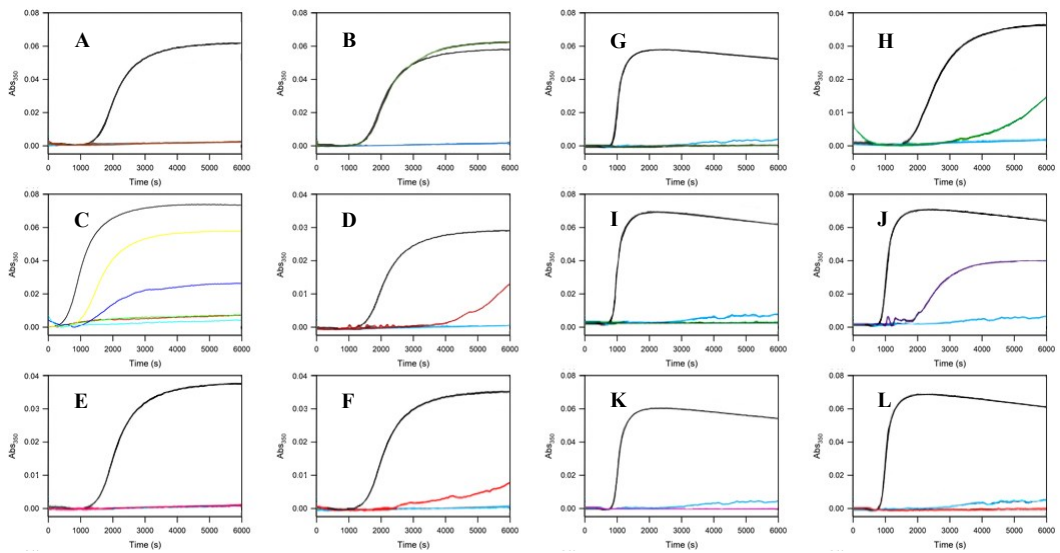

Figure 3.15 Docking inhibition of tubulin assembly activity. All experiments were performed in triplicate. Time course of assembly of 25 µM Tubulin in GAB in the presence of DMSO (vehicle, black), 27.5 µM Maytansine (cyan), 27.5 µM compounds; (**A**) **1b** (brown); (**B**) 5**b** (green); (**C**) Maytansine (red), Maytansinol (green), **2** (yellow), 3**b** (cyan), and 4**b** (blue); (**D**) 6 (red); (**E**) **1g** (pink); (**F**) 5**g** (red); (**G**) **1f** (green); (**H**) 5**f** (green); (**I**) **1h** (green); (**J**) 5**h** (violet); (**K**) **17** (pink); (**L**) **20** (red).

85 M. Mirigian, K. Mukherjee, et al., *Methods Cell Biol.* **2013**, *115*, 215–229.

Dose-response

The best candidates in polymerisation study (**1b**, **1f**, **1g**, **1h**, **17**, and **20**) were subjected to dose-response assay with a fixed concentration of ligand.

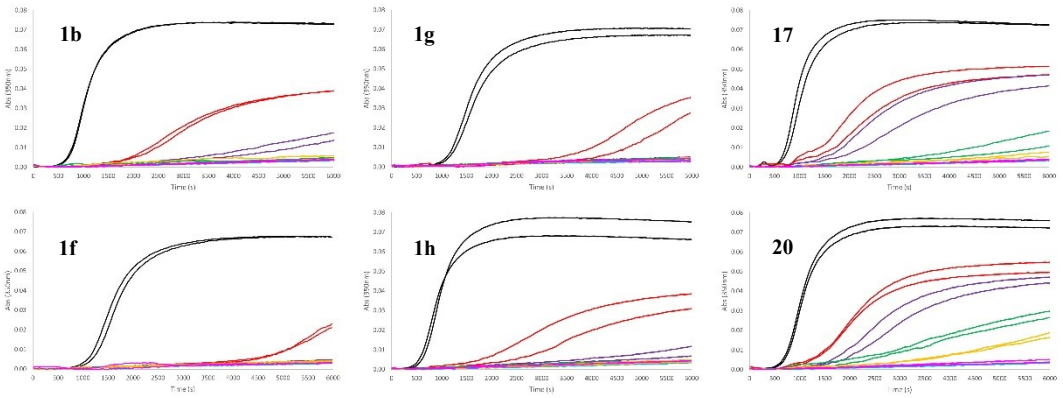

Figure 3.16 Dose-response of tubulin assembly activity by selected compounds. Time course of assembly of 25 µM Tubulin in GAB in the presence of DMSO (vehicle, black), 27.5 µM Maytansine (cyan), 27.5 µM (pink) 20 µM (yellow) 15 µM (green) 10 µM (violet) 5 µM (red) selected compounds.

1f and **1g** display similar polymerisation dynamics to that of maytansine at 10µM. However, the effect of conjugated compound **17** having a similar structure in maytansinol moiety appears to be worse than the previous ones. Similarly, comparing **1b**, **1h** and **20** it is observed that the precursors have an effect on dynamics at 15µM as maytansine, while tubulin is able to polymerise with the same concentration of **20**. In conclusion, it appears that nucleotide conjugated compounds are worse MDAs. The best compounds in this test are **1f** and **1g**, while **1b** and **1h** exert a slightly less effect on tubulin polymerization dynamics.

Binding affinities

In order to correlate the inhibition of tubulin assembly with the binding affinities of the compounds for the maytansine site, the binding constants were determined by competition against Fc Maytansine.[73]

A mix of 10 nM tubulin in PEDTA buffer (10 mM NaPi, 1 mM EDTA, 0.1 mM GTP and 1.5 mM $MgCl_2$) with 10 nM Fc Maytansine was incubated at 25ºC with increasing amounts of the different compounds. Up 2.5 µM of Maytansine was used as a control, whereas we employed a range of concentrations up to 10 µM for **1b**, **1g**, **1f** and **1h**, while the range was increased up to 15 µM for **17** and **20**.

Contrary to other microtubule-targeting agents, potency does not correlate well with determined binding affinities. The reason for this is that all tested compounds have at least the affinity of the order of µM. Furthermore, the inhibition of tubulin assembly depends on the binding affinity of the compound for the site, which must be significant at the concentrations of the inhibition assay. Since the concentrations of tubulin and the drugs used in the assay were an order of magnitude higher than the weakest dissociation constant measured for **3b** (3 mM), all ligands should have been bound to the protein. Therefore, binding affinity should not affect the *in vitro* assembly inhibition activity as has been observed.

The best compounds in this series are **1g**, **1f** and **1h** due to their Kb value similar to that of maytansine, indicating that both small and bigger substituents can easily replace the N-acetyl-N-methyl-L-alanine. These values correlate with dose-response dosage because these compounds are the best in that experiment. Compound **1b** with a phenolic ester at position C_3 was a slightly weaker binder, but at dose-response this compound has a similar dynamics to **1g**, **1f** and **1h**. The series of hydroxyl-free compounds at the C_9 position (**2**, **6**, **5b**, **5g**, and **5f**) showed a binding affinity in the range of 1 µM, suggesting that the C_9 hydroxyl acts as a point of critical anchoring to allow the establishment of a strong interaction with the site. The remaining compounds devoid of hydroxyl in

the C_9 position and with modifications to C_3 and/or nitrogen of oxazinanone (**3b** and **4b**) showed affinity in the sub mM range. Finally, the conjugated compounds **17** and **20** have worse Kb values than those detected for the precursors.

Table 3.12 Binding affinities of maytansinoid compounds.

Compound	Kb [M^{-1}] × 10^5	Kd [nM]
Maytansine	903±117	14±2
Maytansinol	13.0±0.6	780±40
2	14.2±0.8	720±50
6	12.0±0.3	830±20
1b	200±10	51±3
1g	900±100	11±1
1f	540±50	20±2
1h	130±26	92±17
5b	9.2±0.3	1090±40
5g	11.7±0.4	860±30
5f	5.6±0.4	1800±120
3b	6±2	3000±100
4b	5.0±0.5	2000±200
17	124±16	88±11
20	125±12	83±8

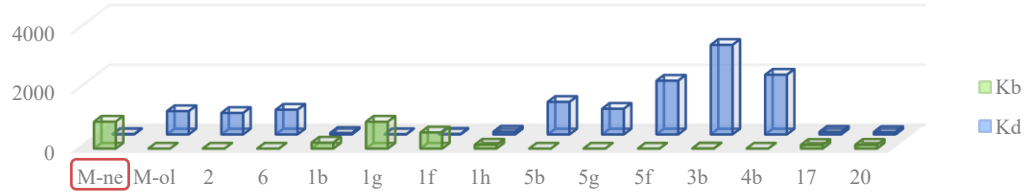

Figure 3.17 Comparison of Kb and Kd of maytansine, maytansinol, and maytansinoids synthesised.

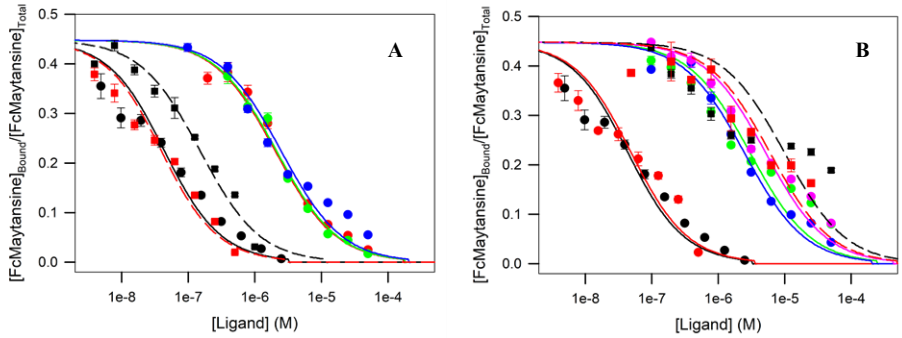

Figure 3.18 Determination of the binding constant of the ligands. Displacement of Fc-maytansine assays for the ligands. (**A**) Maytansine (black circles and lines), Maytansinol (red circles and lines), **2** (green circles and lines), **6** (blue circles and lines), **1b** (black squares and dashed lines), **1g** (red squares and dashed lines); (**B**) Maytansine (black circles and lines), **1f** (red circles and lines), **5b** (green circles and lines), **5g** (blue circles and lines), **5f** (pink circles and lines), **3b** (black squares and dashed lines), **4b** (red squares and dashed lines). The data are from three independent experiments and represent mean ± SEM. The solid lines represent fits to the data.

Cytotoxicity

Cytotoxicity requires effective binding of the ligand to tubulin at concentrations that are approximately one order magnitude lower than the dissociation constants of the corresponding ligand.[86] To correlate the binding potency with toxicity and to investigate the ability of compounds to overcome multidrug resistance mediated by membrane pumps, the cytotoxicity of the compounds was tested in A549 (small cell lung cancer), in A2780 (ovarian cell carcinoma), and in its resistant counterpart (A2780AD, ovarian cell carcinoma that overexpress pGp).

MTT was performed to determine IC_{50}. It is a colorimetric test based on the reduction of the MTT cell viability marker (3-(4,5-dimethylthiazol-2-yl) -2,5-diphenyltetrazolium bromide) by the mitochondrial reductase of living cells. MTT is a water-soluble, yellow-coloured tetrazole. Its reduction leads to the formation of Formazan, which precipitates in the aqueous phase. The compound is solubilised in a convenient solvent producing a purple solution, the absorbance of which is measured. The determination of the concentration of Formazan produced is directly proportional to the number of living cells with which IC_{50} is calculated.

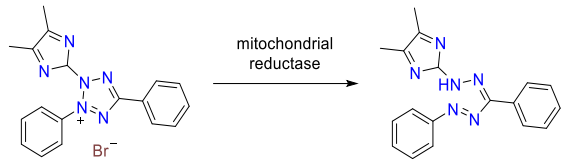

MTT **Formazan**

The method consists of culturing the cells for 24 hours and then adding the tested compounds at different concentrations. The MTT is added after 48 hours of incubation of the cells with the compounds, after 2 hours the reaction is stopped, and the concentration of Formazan is determined by spectrophotometry.

Table 3.13 IC_{50} of maytansinoid compounds in A549, A2780, and A2780AD cell lines.

Compound	A549 IC_{50} [nM]	A2780 IC_{50} [nM]	A2780AD IC_{50} [nM]
Maytansine	0.28±0.04	0.31±0.02	19±1
Maytansinol	60±3	23.78±1.65	1460±148
2	15±2	9.64±0.97	981±200
6	28±2	74±4	>19706
1b	0.24±0.03	0.11±0.01	11±1
1g	1.2±0.3	0.25±0.01	20±1
1f	0.070±0.008	0.033±0.003	4.7±0.6
1h	1.1±0.2	0.14±0.01	17±2
5b	>570	338±5	2626±187
5g	190±40	130±20	>6156
5f	320±40	225±15	>7956
5h	40±5	10.6±0.8	>5263±17
3b	>1030	2088±99	13477±623
4b	47±6	241±32	3496±320
17	>1246±97	-	-
20	>336±19	-	-

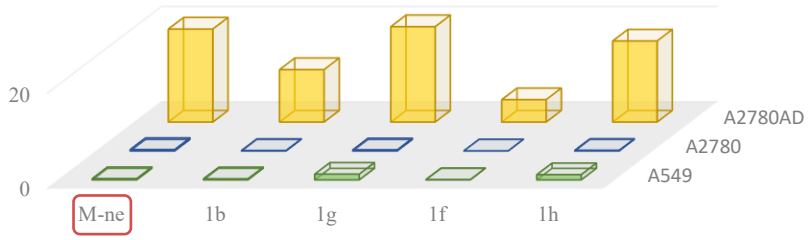

Figure 3.19 Comparison of IC_{50} of the main active compounds.

86 R. Matesanz, I. Barasoain, et al., *Chem. Biol.* **2008**, *15*, 573–585.

The cytotoxicities determined in this study are well correlated with the binding affinities: the high affinity of compounds **1b**, **1f**, **1g**, and **1h** exhibit behaviour almost like maytansine, showing nano- to subnanomolar cytotoxicity, while compounds with micro- and submicromolar affinity are less cytotoxic. In contrast, the conjugated compounds **17** and **20** have the worst IC_{50} values of this series. Furthermore, the data also highlights that the active compounds are better substrates in pGp than maytansine, showing higher resistance rates than the parent compound, but all compounds are worse than the values obtained in A2780, which means that none of them can overcome the resistance of the A2780AD cell line.

Effects on tubulin cytoskeleton

In order to complete the biological characterisation of the synthesised maytansinoids, the effect of the compound **1b** on cellular MT was further investigated. For this purpose, a fluorescence microscopy was performed on A549 by incubating the cells with increasing concentrations of the ligand for 48 h and comparing the effects with those obtained with the reference ligands maytansine, maytansinol and the vehicle.

At the interphase in the control cell (**Figure 3.20** A), the MT network covers the whole cytoplasm, while in the cells dividing during the metaphase there are regular bipolar spindles which allow the correct positioning and segregation of the chromosomes in the subsequent phases of division (**Figure 3.20** B, C). Effects of 5nM maytansine can be appreciated at the interphase and in mitosis (**Figure 3.20** D, E). At the interphase, a disorganised MT network is observed with incipient signs of depolymerisation in an irregular binucleate cell. Furthermore, there are multipolar anomalous spindles in mitosis with the DNA starting to condense. Maytansinol requires concentrations of 100 nM in interphase cells and 50 nM in mitotic cells to observe the same destabilizing effect observed with maytansine (**Figure 3.20** F, G). With **1b**, concentrations of 10 nM in interphase cells and 5nM in mitotic cells are sufficient to observe effects similar to those observed with maytansine (**Figure 3.20** H, I).

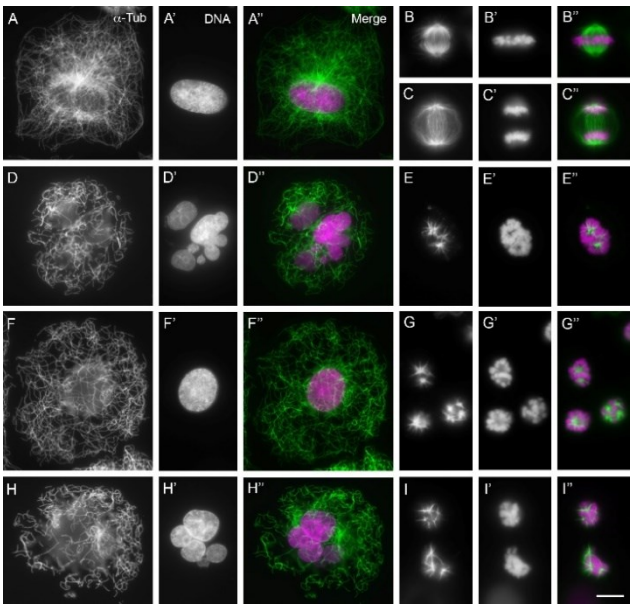

Figure 3.20 Effects of maytansinoids on A549 tumor cells in interphase and mitosis by fluorescence microscopy. Cells were treated for 24 h with the different compounds: control-DMSO 0.5% (A-C''), Maytansine 5 nM (D-E''), Maytansinol 100 nM (F-G'') and **1b** 5 nM (H-I''). Cells were immunostained for α-tubulin (A-I), stained for DNA (A'-I') and images obtained were merged (tubulin in green and DNA in magenta) (A''-I''). (A-A'') Interphase cells treated with drug vehicle (DMSO) have a regular MT network uniformly distributed in the cytoplasm. (B-B'') Control metaphase cell with a normally distributed bipolar mitotic spindle in which all chromosomes are positioned in the metaphase plate. (C-C'') Control late anaphase cell in which sister chromatids are observed segregating to the daughter poles through a bipolar anaphase spindle; no anaphases are observed in treated cells. (D-D'', F-F'', H-H'') Interphase cells showing a less dense MT networks range and MT mass reduction compared to A-A''. (E-E'', G-G'', I-I'') Mitotic cells blocked with condensed chromosomes showing a smaller microtubular mass organised in shape of star or comet. Scale bar is 10 μm.

3.5 Crystallography

To validate the computational analysis and complete the biological assays, the crystal structures of the respective tubulin-maytansinoid complexes were determined by Dr. A.E. Prota in Laboratory of Biomolecular Research at Paul Scherrer Institute of Villigen. For this purpose the compounds **6**, **1b**, **1g**, and **1f** were tested. In addition, **5b**, **5g**, and **5f** analogues were also tested to evaluate the impact of the C_8-C_9 double bond on the interaction. Crystals of the T_2R-TTL protein complex (containing two α dimers, β-tubulin, the stathmin RB_3 protein and the tubulin tyrosine ligase TTL) were cultured as described by Prota *et al*.[87] The compounds were impregnated in the crystals over 6 h, which allowed to resolve the T_2R-TTL-maytansinoid structures at high resolution, between 2.25 and 2.7 Å. All tested ligands were bound to the maytansine site of β-tubulin in the T_2R-TTL complex because the electron density difference observed for all tested derivatives indicated that the ligands were bound.

The overall T_2R-TTL-maytansinoid structures overlap very well with the protein structure obtained in the absence of a ligand, suggesting that maytansinoid binding has no effect on the overall conformation of tubulin. The binding position of all maytansinoids within the maytansine site is very similar to that described for the parent compound,[47] and all major interactions are conserved. In short, all compounds form hydrogen bonds between the C_1-O and the nitrogen atom of the main chain of Val181 and between the C_{24}-O and the side chains of Lys105 and Asn102. Furthermore, the 9-OH group of compounds **1b**, **1g**, and **1f** establishes a hydrogen bond with the carbonyl of the Gly100 main chain. **Figure 3.21** shows the position of **1b**, the best-resolved maytansinoid, compared with the orientation of maytansine and **5b**.

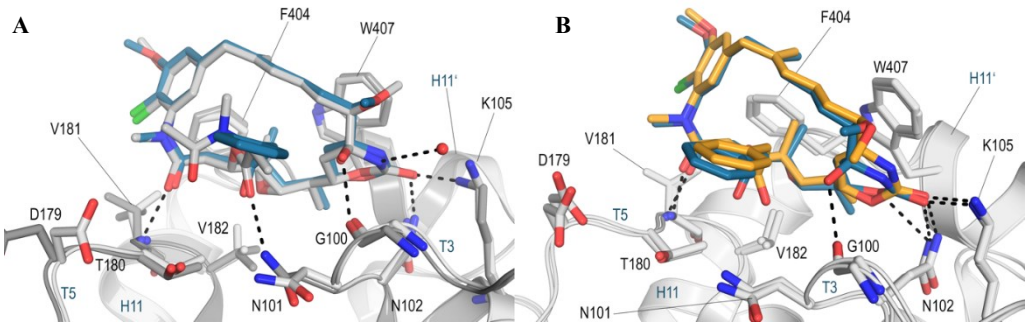

Figure 3.21 X-ray analysis of the T_2R-TTL-maytansinoid complexes. (**A**) Superposition of the T_2R-TTL-maytansine (grey) and the **1b**-T_2R-TTL (blue) structures. (**B**) Superposition of the T_2R-TTL-**1b** (blue) and the T_2R-TTL-**5b** (orange) structures. Although the heterocycle moiety is flattened by the double bond in **5b**, the position of the ring is anchored at its position by coordination to Asn102 and Lys105.

All modifications introduced in the C_3 position point towards the solvent and do not disturb the environment near the maytansine site. For the larger C_3 substituents, such as the phenyl ring, a slight reorientation of the C_3 carbonyl group is observed, which increases the distance from the Asn101 carbonyl group thus weakening this interaction. However, biological assays have shown that this small change in ligand coordination does not affect the efficacy and binding constants. For **1b**, **1g**, and **1f** the determined values are close to those of maytansine, therefore the introduction of larger groups in position C_3 has no apparent impact on the position, affinity or efficacy of the binding.

The structural analysis of maytansinoids **6**, **5b**, **5g**, and **5f** also reveals that the elimination of the hydroxyl group at C_9 does not affect the binding mode of the ligands. As shown in **Figure 3.21** B, the heterocycle is anchored by two hydrogen bonds established between the C_{24}-O and the side chains of Asn102 and Lys105, which highlights that the interaction is not affected by the introduction of the double bond. However, the loss of a hydrogen bond between the 9-OH group and the Gly100 main chain carbonyl cannot fully explain the observed lower affinity and efficacy of these maytansinoids compared to their hydroxylated analogues. This suggests the presence of other factors, such as compound solubility or reduced stability.

87 **a]** A. E. Prota, M. M. Magiera, et al., *J. Cell Biol.* **2013**, *200*, 259–270; **b]** A. E. Prota, K. Bargsten, et al., *Science (80-.).* **2013**, *339*, 587–590.

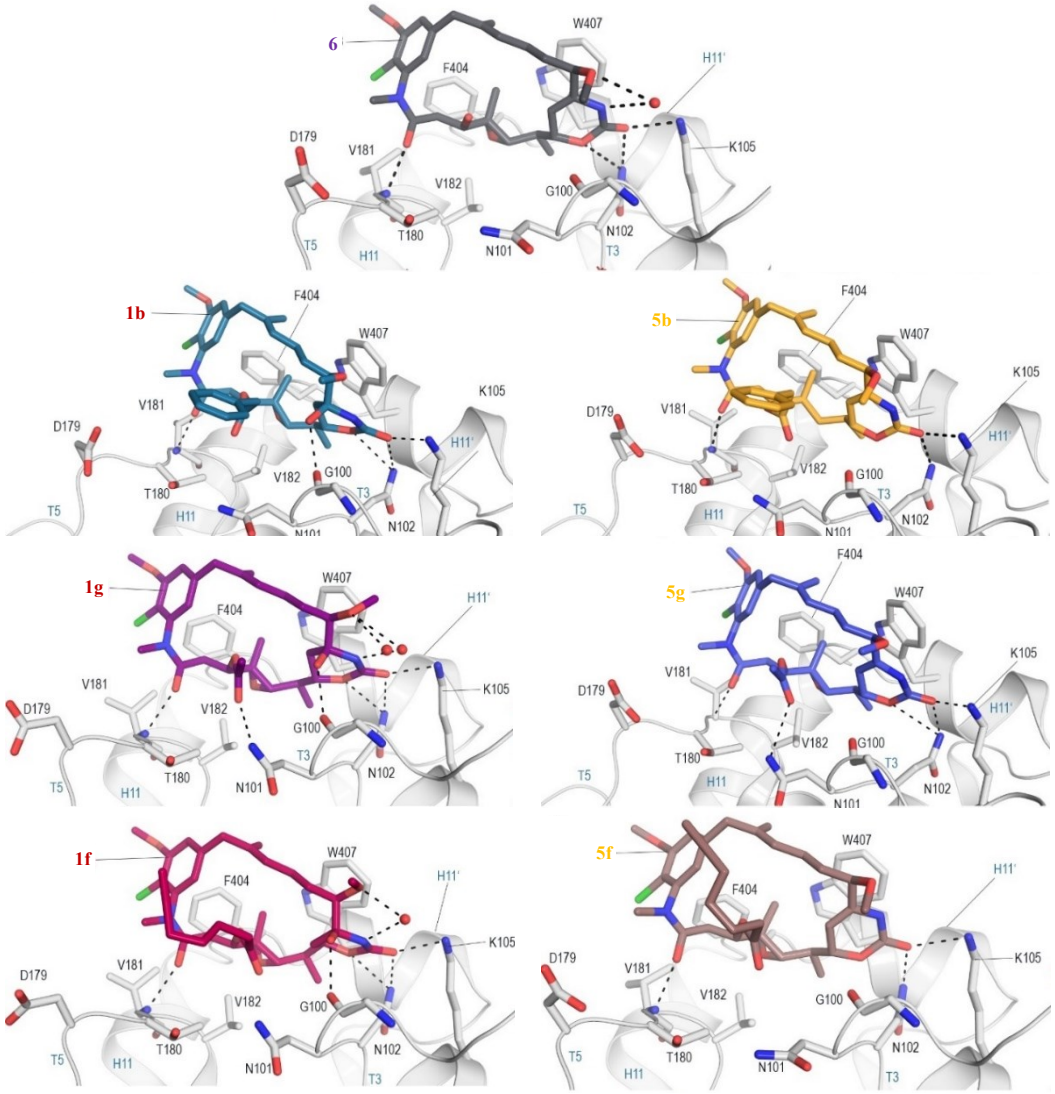

Figure 3.22 X-ray analysis of the T_2R-TTL-maytansinoid complexes.

To validate the docking results, the crystal structures obtained for each maytansinoid were superimposed with the corresponding best conformer resulting from the docking studies. For all molecules, the docking results match the patterns determined by X-ray crystallography, confirming the reliability of the protocols used.

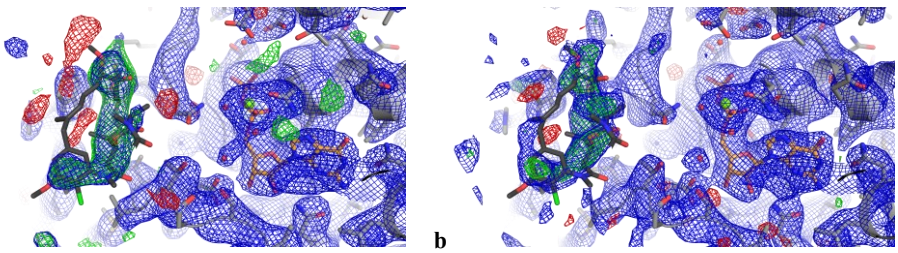

Figure 3.23 Direct electron density map (blue) contoured at 1.0 σ, mFo-Fc map (green/red) contoured at ± 3.0 σ of β-tubulin (grey).The structure of maytansine (black) has been super imposed to **17** (a) and **20** (b) as reference and the structure of the bound GDP (orange) in the site is displayed.

Concerning compounds **17** and **20**, the maytansinol-based fractions bind into the maytansine site. However, in the crystal structures obtained there is no difference density for the linker part connected to guanosine, indicating that the soaking experiments were unsuccessful in replacing the GDP already present into the target site (**Figure 3.23**). Therefore, nucleotide exchange in an already preformed crystal seems improbable. Experiments aimed at promoting the exchange by incubating the compound with tubulin in solution or obtaining GDP-free β-tubulin have not led to any success.

4 Conclusion

In conclusion, a series of maytansinoids containing novel modifications of the scaffold obtained through an extensive investigation of the maytansinol acylation reaction were synthesised. The synthesis of maytansinol-guanosine conjugates was completed by exploiting the CuAAC. The related final products **17** and **20** were obtained with a total yield of 13% and 18% respectively.

The synthesis of fragment A was challenging due to the complex structure of the macrocycle that has many functions. This substrate has not been studied much before, so the literature reports few information about its reactivity.

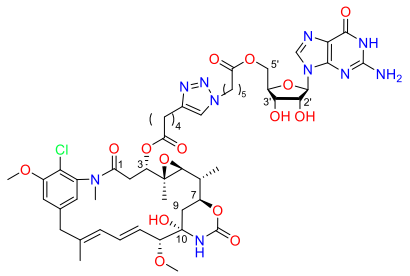

17

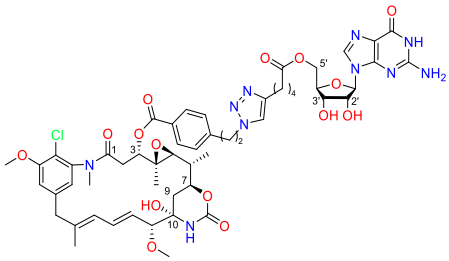

20

However, maytansinol acylation was achieved with interesting results by exploiting the EDC/DMAP combination. Furthermore, the possibility of selectively directing the path of the reaction towards the *O*-acylated product **1** was obtained by adding $ZnCl_2$. Further studies will be carried out in order to find the suitable conditions for a more performing and highly selective esterification. Finally, the slight changes between the maytansinoid structures were carefully analysed and fully characterised using NMR spectroscopy.

All of the biologically tested compounds showed distinctive effects on tubulin assembly *in vitro*. The binding affinity of the molecules to tubulin dimers was evaluated by the displacement of the Fc Maytansine, and some compounds showed similar or superior affinities to maytansine. In fact, the acylation present in compounds **1** is able to strengthen the biological activity of maytansinoids and these results were well correlated with the powerful cytotoxic properties observed in the A549, A2780, and A2780AD cell lines. Compounds **5** lacking the 9-OH group and the conjugate products **17** and **20** show significantly less influence on cells and tubulin in all tests performed.

The structures of the drug-tubulin complexes were determined by X-ray crystallography to further clarify the biological results. This allowed to evaluate the binding mode of the maytansinoids and to validate the docking data, demonstrating that the changes introduced in the C_3 and C_9 positions do not interfere with tubulin binding. Poor activity could be caused by other factors, such as chemical or metabolic stability, entropy or solubility of the compounds. On the other hand, the situation is different for compounds **17** and **20**, in which the guanosine portion is not able to exchange position with the GDP already present in the β-tubulin and for this reason it is not able to bind integrally. This unexpected behaviour necessitates the development of different conjugated maytansinoids.

5 Experimental procedures

5.1 Chemistry

General Experimental Procedures

Unless otherwise stated, reagents were purchased from general suppliers (Sigma Aldrich and Fluorochem) and used without further purification. All solvents were of reagent grade or HPLC grade. All reactions were carried out in oven-dried glassware and dry solvents, under nitrogen atmosphere and were monitored by glasses or aluminium TLC on silica gel (Merck precoated 60F254 plates), with detection by UV light (254 nm) or by TLC stains as permanganate.

Analytical HPLC was performed on Agilent 1100 Series System RP column ZORBAX SB-C8 (3.5µm x 4.6 x 150 mm). The pressure was about 85 bar, with a constant flow rate of 1 mL/min. UV spectra were recorded at 254 nm and 210 nm with DAD detection. The mobile phase consisted of a mixture of H_2O/ACN and the gradient was programmed using the following method: isocratic for 1 min at 50% ACN, then gradient for 10 min to 90% ACN. The system was washed keeping this condition for another 1 min and then bringing back to the beginning condition.

Products were purified by flash column chromatography, using silica gel Merk 60 (230-400 mesh) as stationary phase or by flash purification using Biotage Isolera™ One System and Biotage® Sfär C18 6 g D Duo 30 µm as cartridges (BIOTAGE). The products were eluted from the column with a mixture of H_2O/ACN, running with a gradient from 10% ACN to 95% ACN in 25CV (unless otherwise specified).

^{1}H-NMR spectra were recorded on a Bruker Avance Spectrometer 300 and 400 MHz and ^{13}C-NMR spectra were recorded on the same instrument 101 MHz, using commercially available deuterated (chloroform-d, methanol-d4, acetone-d6) solvent at room temperature. Chemical shifts are reported in parts per million (ppm), compared to TMS as an internal standard. Multiplicities in 1H-NMR are reported as follow: s – singlet, d – doublet, t – triplet, m – multiplet, br s= broad. Data for ^{13}C NMR are reported in terms of chemical shift (δ/ppm).

High resolution mass spectra (HR-MS) were recorded on a Water QToF Premier high resolution UPLC ES MS/MS.

Synthesis of 4-(2-azidoethyl)benzoic acid

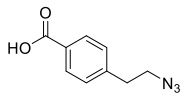

To a solution of 4-(2-bromoethyl)benzoic acid (80 mg, 0.35 mmol) in DMSO (1.4 ml), was added NaN_3 (24.2 mg, 0.38 mmol). The mixture was stirred at room temperature for 20 hours. Then, water (2.8 mL) was added, and the solution was extracted with EtOAc (4 × 6 mL). The organic layer was washed with brine and the combined organic layers were dried over Na_2SO_4 and concentrated under reduced pressure. The crude product was not purified to provide the product (57.5 mg, 0.30 mmol, 86% yield) as white solid.

^{1}H NMR (400 MHz, chloroform-*d*) δ 8.0 (d, J = 8.2 Hz, 2H, 3, 7), 7.3 (d, J = 8.1 Hz, 2H, 4, 6), 3.5 (t, J = 7.1 Hz, 2H, 9), 2.9 (t, J = 7.1 Hz, 2H, 8).

^{13}C NMR (101 MHz, chloroform-*d*) δ 170.35 (1), 144.30 (5), 131.00 (3, 7), 130.76 (2), 129.46 (4, 6), 52.63 (9), 36.00 (8).

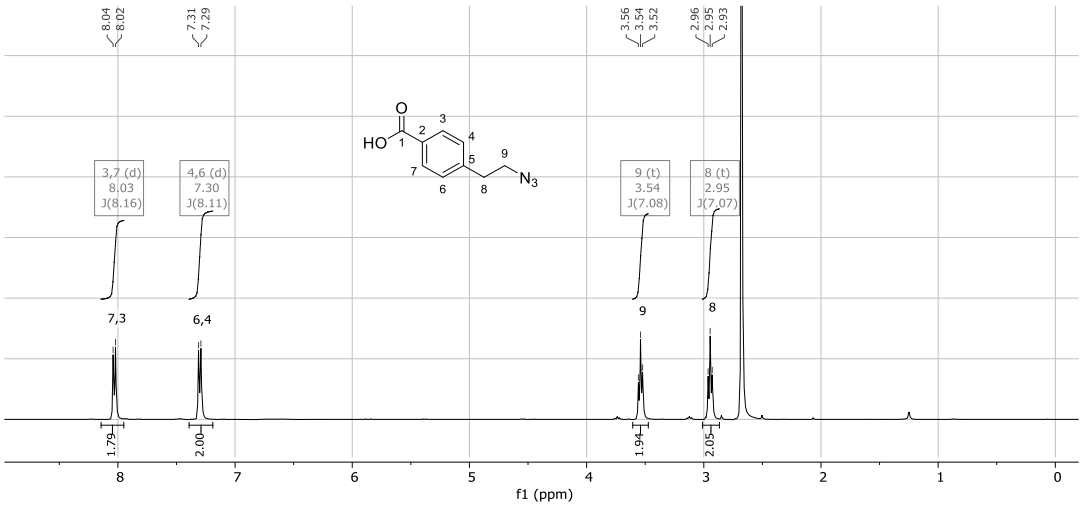
8.04
8.02
7.31
7.29
3.56
3.54
3.52
2.96
2.95
2.93
3,7 (d)
8.03
J(8.16)
4,6 (d)
7.30
J(8.11)
9 (t)
3.54
J(7.08)
8 (t)
2.95
J(7.07)
7,3
6,4
9
8
1.79
2.00
1.94
2.05
f1 (ppm)

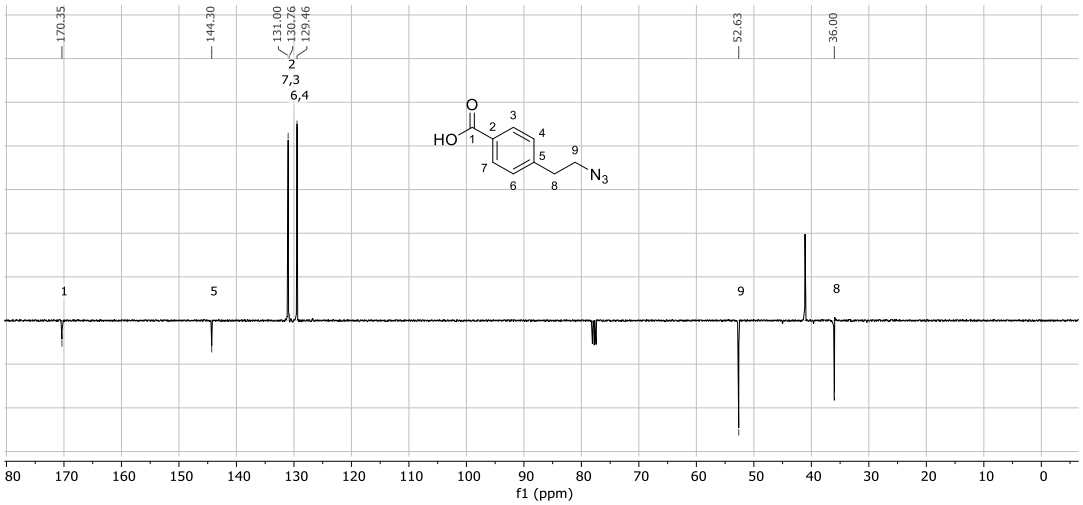
170.35
144.30
131.00
130.76
129.46
52.63
36.00
2
7,3
6,4
1
5
9
8
f1 (ppm)

Synthesis of 2

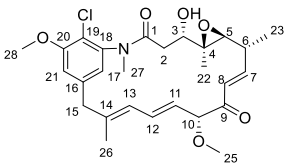

2

To a solution of maytansinol (25 mg, 0.044 mmol) in MeCN/DMF 10:1 (290 µL) was added Cs_2CO_3 (36 mg, 0.111 mmol), TEBA (0.2 mg, 0.001 mmol), KI (14.7 mg, 0.088 mmol), and then was dropped propargyl bromide (8 µL, 0.088 mmol, 80% in Tol). The reaction was stirred for 2.5 h before to quench with a saturated aqueous solution of NH_4Cl and to extract with EtOAc (× 3). The combined organic layers were washed with a saturated aqueous solution of NaCl, dried over Na_2SO_4, and concentrated under reduced pressure. Column chromatography of the residue on silica gel (elution: CH_2Cl_2/MeOH 97:3) provided 8.5 mg (35%) of the product.

HRMS (ESI) *m/z* $[M+Na]^+$ 526.1974 (calcd for $C_{12}H_{16}O_2Na$, 526.1972);

^{1}H NMR (400 MHz, methanol-d_4) δ 7.12 (d, *J* = 1.9 Hz, 1H, 17), 7.09 (d, *J* = 2.0 Hz, 1H, 21), 6.87 – 6.68 (m, 2H, 7, 12), 6.42 (d, *J* = 15.6 Hz, 1H, 8), 6.12 (dd, *J* = 13.3, 5.5 Hz, 1H, 13), 5.31 (dd, *J* = 15.2, 8.7 Hz, 1H, 11), 4.60 (d, *J* = 8.8 Hz, 1H, 10), 3.99 (s, 3H, 27), 3.50 (d, *J* = 12.8 Hz, 1H, 15'), 3.38 (t, *J* = 2.7 Hz, 1H, 3), 3.35 (s, 3H, 24), 3.27 (d, *J* = 12.8 Hz, 1H, 15"), 3.18 (s,34H, 26), 2.67 (d, *J* = 9.1 Hz, 1H, 5), 2.34 – 2.24 (m, 1H, 2'), 2.24 – 2.17 (m, 1H, 6), 2.03 (dd, *J* = 13.0, 2.9 Hz, 1H, 2"), 1.79 (s, 3H, 25), 1.22 (d, *J* = 6.6 Hz, 3H, 23), 0.80 (s, 3H, 22);

^{13}C NMR (101 MHz, methanol-d_4) δ 196.0 (9), 172.2 (1), 155.8 (20), 146.3 (7), 142.0 (18), 140.6 (16), 139.6 (14), 133.3 (12), 127.2 (8), 126.0 (11), 125.1 (13), 123.3 (17), 118.0 (19), 113.0 (21), 87.5 (10), 73.5 (3), 66.2 (5), 62.4 (4), 55.7 (27), 55.4 (24), 45.9 (15), 37.3 (6), 35.0 (2), 34.8 (26), 16.1 (25), 14.8 (23), 10.0 (22).

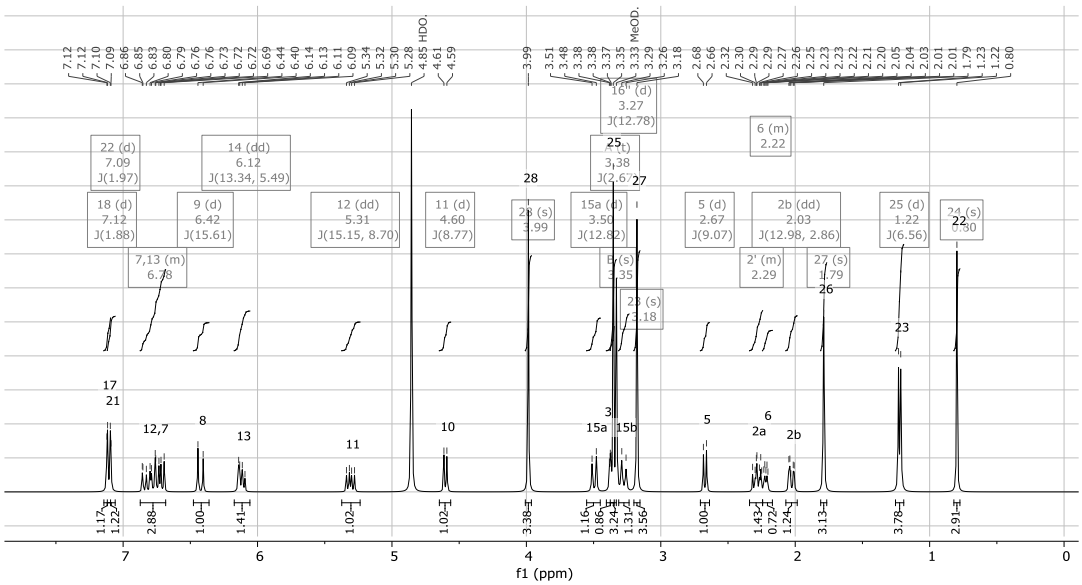

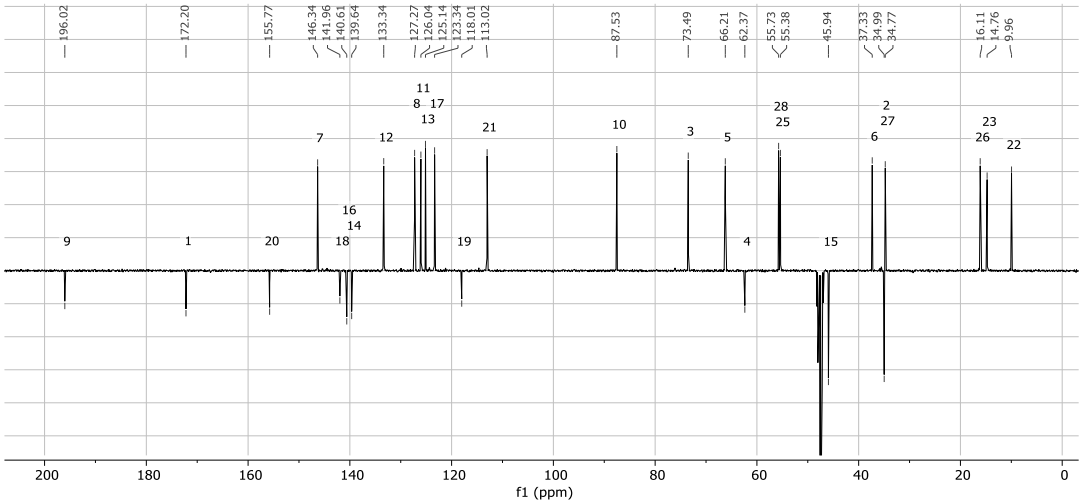

General maytansinol acylation procedures with acyl chloride (see Table 5.1 for more details)

To a solution of maytansinol (50 mg, 0.088 mmol, 1 eq) in CH_2Cl_2 (880 µL) were added trimethylamine freshly distilled and 4-(1-pyrrolidinyl)pyridine under an atmosphere of nitrogen. The reaction was cooled at 0°C and the acyl chloride was dropwise. The mixture was wormed at room temperature and stirred for a specific time. Where specified, trimethylamine, 4-(1-pyrrolidinyl)pyridine, and acyl chloride was added again and the reaction was stirred for a specific time. The mixture was quenched with an excess of diethylamine. $NaHCO_3$ (1 mL) was added and stirred for 5 min. The reaction was extracted with CH_2Cl_2 (3 × 2 mL) and the combined organic layers were dried over Na_2SO_4 and concentrated under reduced pressure. Column chromatography of the residue on silica gel (elution: CH_2Cl_2/MeOH 96:4) provided the products.

General maytansinol acylation procedures with carboxylic acid (see Table 5.1 for more details)

To a solution of maytansinol (50 mg, 0.088 mmol, 1 eq) in dry CH_2Cl_2 (440 µL) were added DMAP and the carboxylic acid at room temperature under a nitrogen atmosphere. Then, a solution 1.3 M of DCC in dry CH_2Cl_2 was slowly added (or was added EDC-HCl followed by dropwise trimethylamine freshly distilled). The mixture was stirred at room temperature for a specific time before filtering off the DCU using cold CH_2Cl_2 (or quenching with an aqueous saturated solution of NH_4Cl, in the case of EDC). The organic phase was washed with H_2O (4 × 1 mL), with brine (1 × 1 mL), then dried over Na_2SO_4, and concentrated under reduced pressure. Column chromatography of the residue on silica gel (elution: CH_2Cl_2/MeOH 96:4), or purification with Biotage Isolera™ One System, provided the products as white powders.

Maytansinol acylation procedures with carboxylic acid and DPTS (see Table 5.1 for more details)

To a solution of DMAP (60 mg, 0.5 mmol) in THF (250 µL) was added a solution of p-TSA (95 mg, 0.5 mmol) in THF (250 µL). The reaction was stirred for 40 minutes at rt before to isolate the precipitate by filtration over a Buchner. The dried product DPTS was used in the next step without further purification. To a solution of maytansinol (50 mg, 0.088 mmol) in dry CH_2Cl_2 (440 µL) was added benzoic acid (11 mg, 0.088 mmol) and DPTS (13 mg, 0.044 mmol) under an atmosphere of nitrogen. Then, a solution 0.5 M of DCC in dry CH_2Cl_2 (24 mg, 0.115 mmol) was added dropwise. The mixture was stirred at room temperature for 5 d. Afterwards, the solution was filtered, dried over Na_2SO_4, concentrated under reduced pressure, and analysed by HPLC. Maytansinol (3.10 min, Area 55%); **6** (4.08 min, Area 4%); **1b** (5.20 min, Area 18%); **5b** (6.90 min, Area 14%); **3b** (7.20 min, Area 5%); **4b** (9.40 min, Area 4%).

Maytansinol acylation procedures with carboxylic acid and $ZnCl_2$ (see Table 5.1 for more details)

To a solution of maytansinol (50 mg, 0.088 mmol) in dry CH_2Cl_2 (440 µL) was added two drops of DMF dry,

DMAP (33 mg, 0.26 mmol), benzoic acid (33 mg, 0.26 mmol), and $ZnCl_2$ (36 mg, 0.27 mmol) under an atmosphere of nitrogen. Then, a solution 1.3 M of DCC in dry CH_2Cl_2 (60 mg, 0.29 mmol) was added dropwise. To promote $ZnCl_2$ dissolution, a minimal quantity of DMF was added. The mixture was stirred at room temperature for 48 h. Afterwards, the solution was filtered, dried over Na_2SO_4, concentrated under reduced pressure, and analysed by HPLC. Maytansinol (3.10 min, Area 29%); **1b** (5.20 min, Area 62%); **5b** (6.90 min, Area 4%); **4b** (7.20 min, Area 4%).

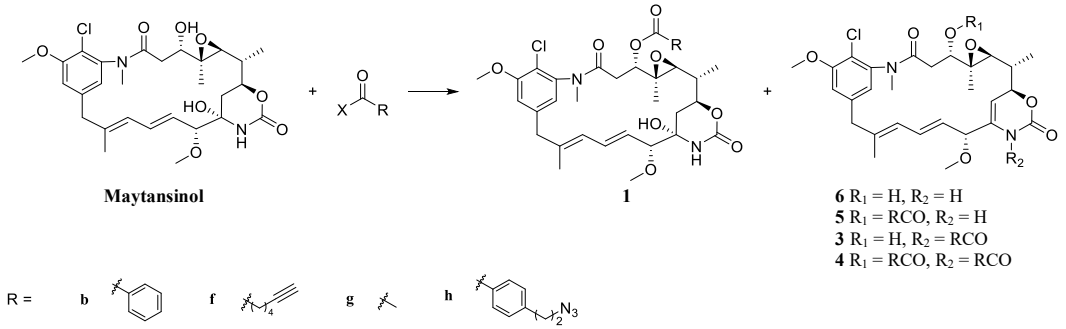

Table 5.1 Condition in the acylation reactions of maytansinol and **y**ield of the product.

R	X	Acyl [eq]	CA [eq]	Conditions [eq]	Time [h]	Yield [%]					
						M	6	1	5	3	4
	Cl	0.5	-	PPy 0.5 TEA 1	0.5	82	5	-	-	-	-
		1	-	PPy 0.5 TEA 2	2	80	15	2	-	-	-
		1	-	PPy 0.5 TEA 2	6	75	11	11	-	-	-
		4	-	PPy 0.5 TEA 10	4	-	-	-	-	33	67
		6	-	Py as solvent	5	51	-	25	-	-	-
b	OH	3	DCC 3.3	DMAP 3	8	4	5	35	26	-	18
		6	DCC 6.6	DMAP 3	48	-	-	-	15	-	31
		1	DCC 1.1	DPTS 0.5	120	55	4	18	14	5	4
		3	DCC 3.3	DMAP 3 $ZnCl_2$ 3	48	29	-	62	4	4	-
		3	EDC 3.3	DMAP 3 TEA 3.7	24	21	8	39	12	-	7
		3	EDC 3.3	DMAP 3 TEA 3.7	48	-	-	15	47	-	20
f	Cl	4+4	-	PPy 0.5+0.5 TEA 10+10	120+48	65	2	16	7	-	-
	OH	3	DCC 3.3	DMAP 3	3	7	9	37	30	-	6
		3	EDC 3.3	DMAP 3 TEA 3.7	18	17	4	36	15	-	6
g	Cl	2	-	PPy 0.5 TEA 4	6	51	-	46	-	-	-
	OH	3	DCC 3.3	DMAP 3	4	-	-	42	43	-	-
h	OH	3	DCC 3.3	DMAP 3	3	20	-	29	11	-	2
		3	EDC 3.3	DMAP 3 TEA 3.7	24	22	8	38	11	-	8

Characterisation of products

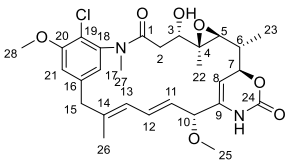

6

HRMS (ESI) *m/z* $[M+Na]^+$ 569.2035 (calcd for $C_{28}H_{35}ClN_2O_7Na$, 569.2030);

^{1}H NMR (400 MHz, chloroform-*d*) δ 7.08 (s, 1H, NH), 6.97 (d, *J* = 1.9 Hz, 1H, 17), 6.83 (d, *J* = 1.9 Hz, 1H, 21), 6.46 (dd, *J* = 15.2, 10.8 Hz, 1H, 12), 6.16 (d, *J* = 11.1 Hz, 1H, 13), 5.54 (dd, *J* = 15.2, 8.5 Hz, 1H, 11), 5.02 – 4.96 (m, 1H, 8), 4.78 (dd, *J* = 10.5, 2.3 Hz, 1H, 7), 4.20 – 4.12 (m, 1H, 10), 4.00 (s, 3H, 28), 3.59 (dd, *J* = 10.9, 2.4 Hz, 1H, 3), 3.49 (d, *J* = 12.8 Hz, 1H, 15'), 3.35 (s, 3H, 25), 3.23 (s, 3H, 27), 3.15 (d, *J* = 12.9 Hz, 1H, 15''), 2.55 (d, *J* = 9.7 Hz, 1H, 5), 2.32 (dd, *J* = 13.6, 10.8 Hz, 1H, 2''), 2.14 (dd, *J* = 13.7, 2.3 Hz, 1H, 2'), 1.75 (s, 3H, 26), 1.66 (td, *J* = 10.1, 6.4 Hz, 1H, 6), 1.27 (d, *J* = 2.3 Hz, 3H, 23), 0.84 (s, 3H, 22);

^{13}C NMR (101 MHz, chloroform-*d*) δ 171.6 (1), 156.1 (20), 151.5 (24), 143.0 (18), 140.4 (16), 140.3 (14), 136.1 (9), 133.5 (12), 126.9 (11), 124.7 (13), 123.3 (17), 119.0 (19), 112.5 (21), 99.1 (8), 80.1 (7), 80.0 (10), 75.9 (3), 66.2 (5), 62.4 (4), 56.7 (28), 56.6 (25), 46.8 (15), 39.0 (6), 36.0 (27), 35.7 (2), 16.4 (26), 14.6 (23), 11.2 (22).

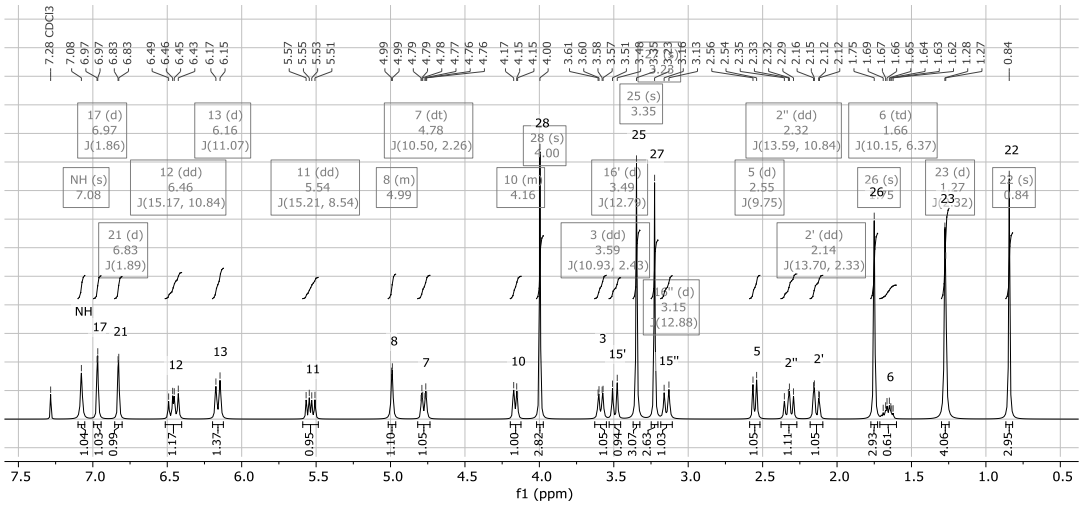

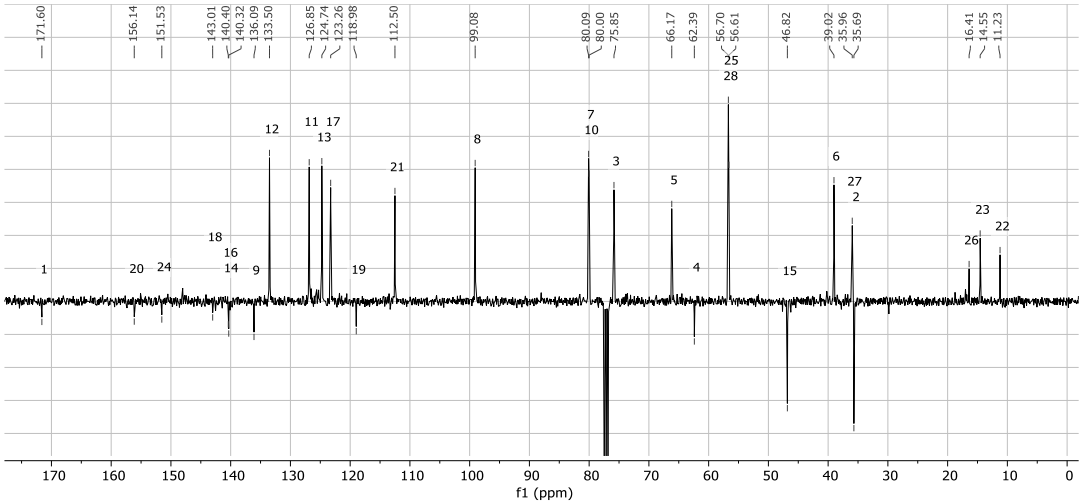

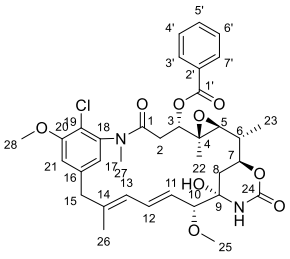

1b

HRMS (ESI) *m/z* $[M+Na]^+$ 691.2396 (calcd for $C_{35}H_{41}ClN_2O_9Na$, 691.2398)

^{1}H NMR (400 MHz, acetone-d_6) δ 8.21 – 8.08 (m, 2H, 3', 7'), 7.77 – 7.59 (m, 3H, 4', 5', 6'), 7.27 (d, *J* = 1.9 Hz, 1H, 21), 7.19 (d, *J* = 1.8 Hz, 1H, 17), 6.61 (dd, *J* = 15.5, 11.1 Hz, 1H, 12), 6.33 (s, 1H, NH), 6.04 (d, *J* = 11.0 Hz, 1H, 13), 5.04 – 4.85 (m, 2H, 3, 11), 4.47 (s, 1H, OH), 4.31 – 4.14 (m, 1H, 7), 4.04 (s, 3H, 28), 3.59 (d, *J* = 12.6 Hz, 1H, 15a), 3.50 (d, *J* = 9.1 Hz, 1H, 10), 3.36 (d, *J* = 12.7 Hz, 1H, 15b), 3.24 (s, 3H, 25), 3.13 (s, 3H, 27), 3.05 (d, *J* = 9.5 Hz, 1H, 5), 2.88 – 2.79 (m, 1H, 2a), 2.26 (dd, *J* = 14.4, 3.1 Hz, 1H, 2b), 1.77 (s, 3H, 26), 1.59 (dt, *J* = 13.6, 1.9 Hz, 1H, 8b), 1.54 – 1.39 (m, 2H, 6, 8a), 1.24 (d, *J* = 6.4 Hz, 3H, 23), 0.97 (s, 3H, 22);

^{13}C NMR (101 MHz, acetone-d_6) δ 168.0 (1), 165.9 (1'), 156.2 (20), 151.1 (24), 142.4 (18), 141.3 (16), 139.6 (14), 133.1 (5'), 132.4 (12), 130.5 (2'), 129.9 (3', 7'), 128.6 (11), 128.2 (4', 6'), 124.7 (13), 122.1 (17), 118.7 (19), 113.5 (21), 88.9 (10), 80.5 (9), 77.5 (3), 73.8 (7), 66.4 (5), 60.5 (4), 56.2 (28), 55.8 (25), 46.3 (15), 38.7 (6), 36.2 (8), 34.6 (27), 32.7 (2), 14.9 (26), 14.0 (23), 12.1 (22).

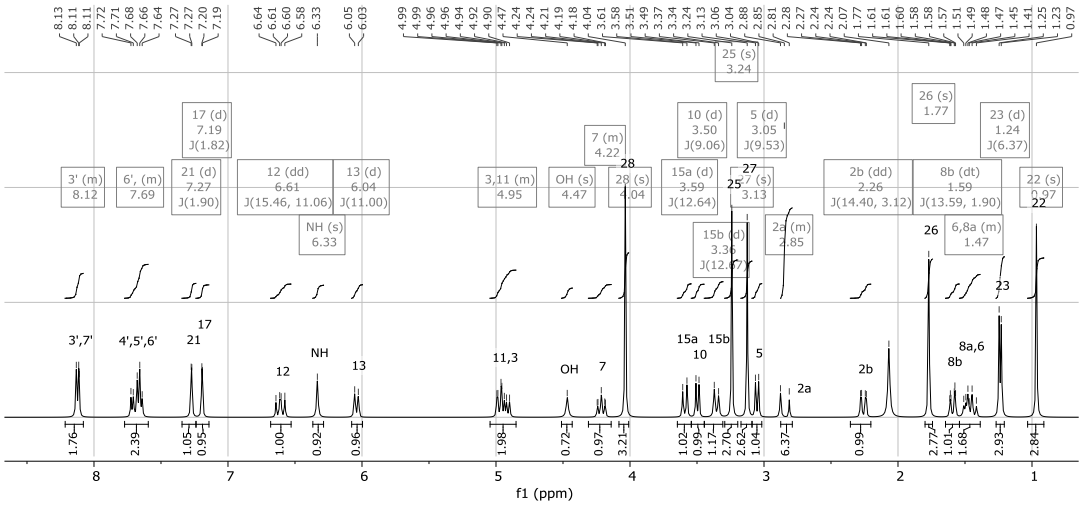

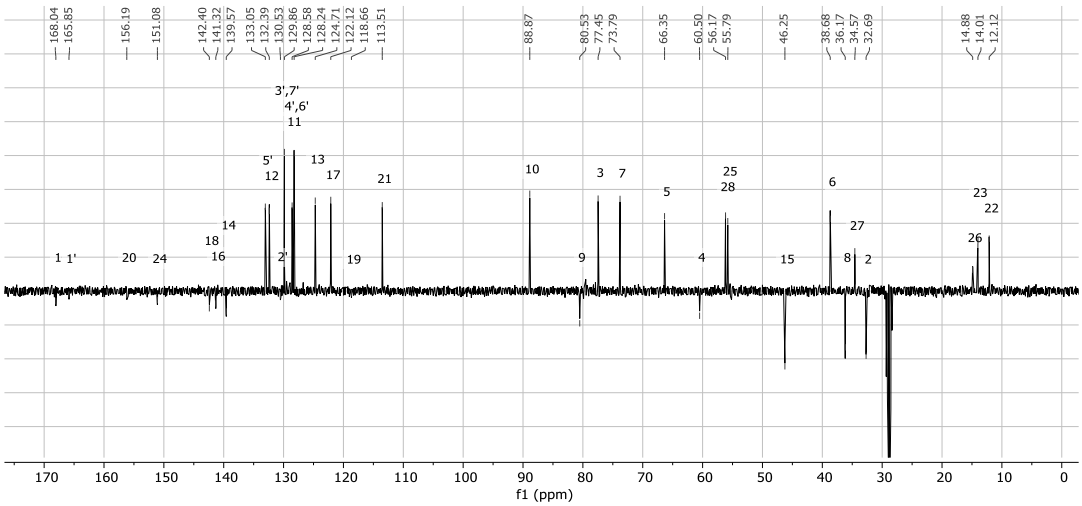

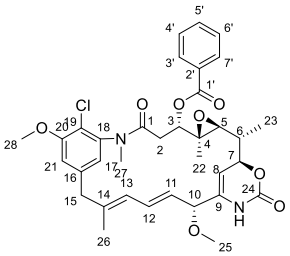

5b

HRMS (ESI) *m/z* $[M+Na]^+$ 673.2295 (calcd for $C_{35}H_{39}ClN_2O_8Na$, 673.2293)

^{1}H NMR (400 MHz, acetone-d_6) δ 8.19 (dd, J = 8.2, 1.6 Hz, 2H, 3', 7'), 8.03 (s, 1H, NH), 7.86 – 7.69 (m, 3H, 4', 5', 6'), 7.28 (d, J = 1.8 Hz, 1H, 21), 7.17 (d, J = 1.8 Hz, 1H, 17), 6.54 (dd, J = 15.3, 10.9 Hz, 1H, 12), 6.13 (d, J = 11.0 Hz, 1H, 13), 5.02 (dd, J = 11.9, 3.0 Hz, 1H, 3), 4.88 (dd, J = 15.3, 8.4 Hz, 1H, 11), 4.56 (dd, J = 10.8, 3.4 Hz, 1H, 7), 4.43 (dt, J = 3.2, 1.5 Hz, 1H, 8), 4.15 (d, J = 8.5 Hz, 1H, 10), 4.04 (s, 3H, 28), 3.66 (d, J = 12.7 Hz, 1H, 15a), 3.41 (d, J = 12.6 Hz, 1H, 15b), 3.15 (s, 3H, 25), 3.14 (s, 3H, 27), 3.03 (d, J = 9.6 Hz, 1H, 5), 2.91 (dd, J = 14.6, 12.0 Hz, 1H, 2b), 2.22 (dd, J = 14.6, 3.0 Hz, 1H, 2a), 1.79 (s, 3H, 26), 1.65 (ddd, J = 10.6, 9.7, 6.5 Hz, 1H, 6), 1.19 (d, J = 6.5 Hz, 3H, 23), 0.90 (s, 3H, 22);

^{13}C NMR (101 MHz, acetone-d_6) ^{13}C NMR (101 MHz,) δ 168.0 (1), 165.7 (1'), 156.2 (20), 149.9 (24), 142.3 (18), 141.2 (16), 140.7 (14), 137.0 (9), 133.7 (5'), 133.0 (12), 130.2 (2'), 129.5 (3', 7'), 128.9 (4', 6'), 126.7 (11), 124.0 (13), 122.2 (17), 118.7 (19), 113.4 (21), 98.0 (8), 79.5 (10), 78.2 (7), 77.9 (3), 67.0 (5), 60.2 (4), 56.2 (28), 55.4 (25), 46.2 (15), 39.5 (6), 34.7 (27), 32.2 (2), 15.1 (26), 13.5 (23), 11.7 (22).

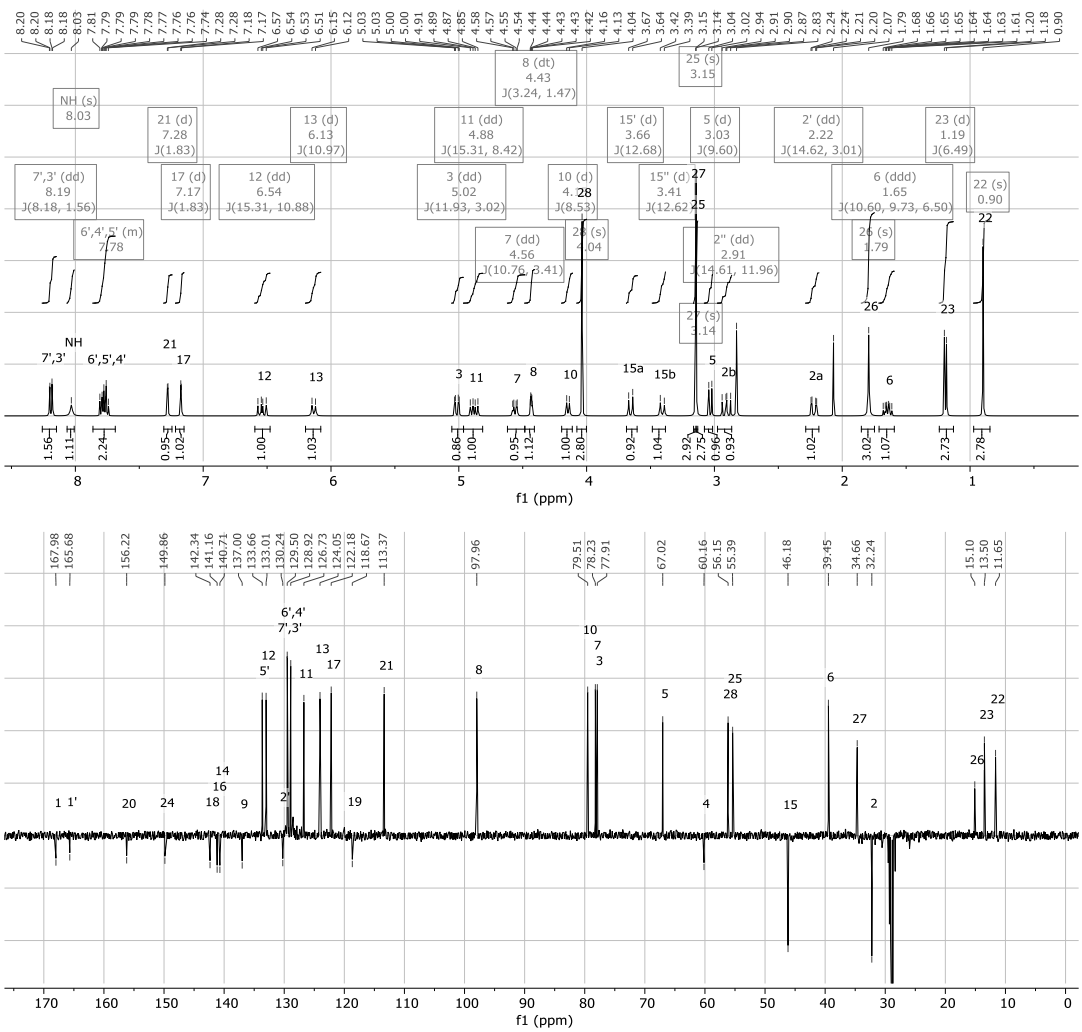

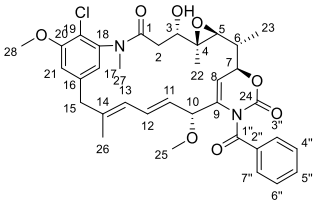

3b

HRMS (ESI) *m/z* $[M+Na]^+$ 673.2296 (calcd for $C_{35}H_{39}ClN_2O_8Na$, 673.2293)

^{1}H NMR (400 MHz, chloroform-*d*) δ 7.83 (d, *J* = 7.6 Hz, 2H, 3", 7"), 7.54 (t, *J* = 7.2 Hz, 1H, 5"), 7.46 (t, *J* = 7.5 Hz, 2H, 4", 6"), 7.01 (d, *J* = 1.8 Hz, 1H, 17), 6.82 (d, *J* = 1.8 Hz, 1H, 21), 6.48 (dd, *J* = 15.2, 10.8 Hz, 1H, 12), 6.15 (d, *J* = 10.8 Hz, 1H, 13), 5.54 (dd, *J* = 15.2, 8.4 Hz, 1H, 11), 5.43 – 5.33 (m, 1H, 8), 4.86 (d, *J* = 10.8 Hz, 1H, 7), 4.42 (d, *J* = 8.4 Hz, 1H, 10), 3.99 (s, 3H, 28), 3.61 (d, *J* = 9.7 Hz, 1H, 3), 3.56 – 3.42 (m, 1H, 15a), 3.23 (s, 3H, 27), 3.12 (d, *J* = 13.0 Hz, 1H, 15b), 2.82 (s, 3H, 25), 2.59 (d, *J* = 9.6 Hz, 1H, 5), 2.37 (dd, *J* = 13.7, 10.9 Hz, 1H, 2a), 2.12 (d, *J* = 13.6 Hz, 1H, 2b), 1.76 (s, 3H, 26), 1.68 (q, *J* = 4.9, 4.5 Hz, 1H, 6), 1.32 – 1.20 (m, 3H, 23), 0.85 (s, 3H, 22);

^{13}C NMR (101 MHz, $CDCl_3$) δ 172.2 (1), 170.2 (1"), 156.5 (20), 149.7 (24), 143.0 (18), 141.0 (16), 140.7 (14), 137.7 (9), 134.8 (2"), 134.4 (12), 132.7 (5"), 129.3 (4", 6"), 128.1 (3", 7"), 127.1 (11), 125.4 (13), 123.9 (17), 119.4 (19), 112.9 (21), 103.1 (8), 80.4 (7), 78.5 (10), 76.5 (3), 67.1 (5), 63.6 (4), 57.2 (28), 56.2 (25), 47.3 (15), 40.6 (6), 36.6 (27), 36.4 (2), 16.9 (26), 14.9 (23), 11.6 (22).

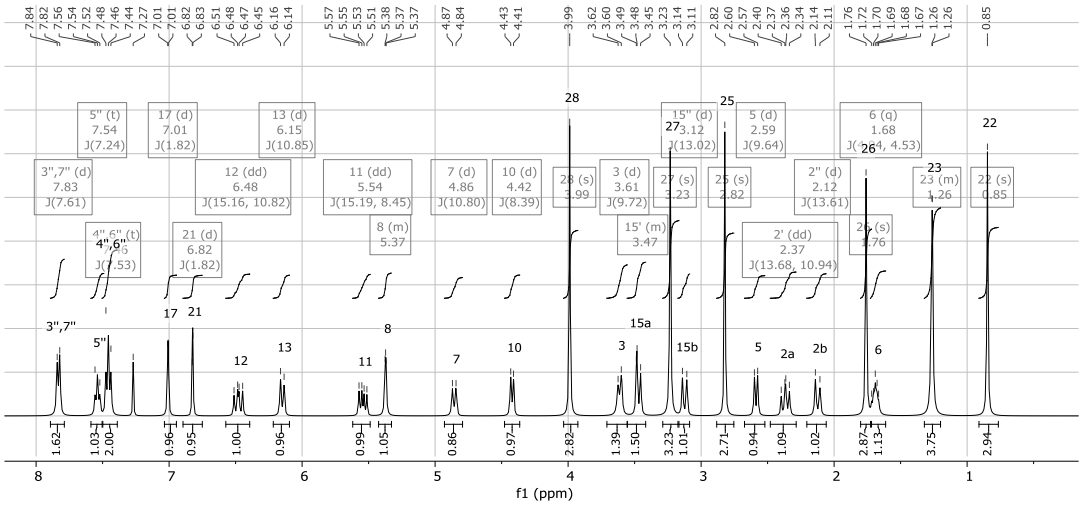

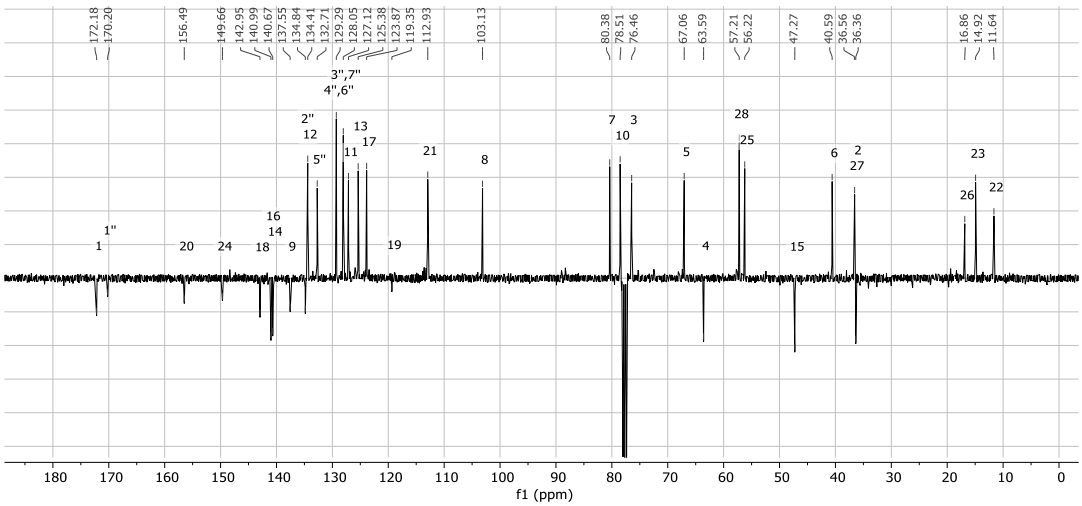

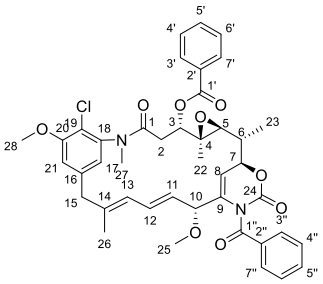

4b

HRMS (ESI) *m/z* $[M+Na]^+$ 777.2559 (calcd for $C_{42}H_{43}ClN_2O_9Na$, 777.2555)

^{1}H NMR (400 MHz, acetone-d_6) δ 8.22 (d, J = 7.4 Hz, 2H, 3', 7'), 7.89 (d, J = 7.7 Hz, 2H, 3", 7"), 7.78 (q, J = 7.4, 6.4 Hz, 3H, 4', 5', 6'), 7.65 (q, J = 5.1 Hz, 1H, 5"), 7.53 (dd, J = 7.9, 4.8 Hz, 2H, 4", 6"), 7.30 (s, 1H, 21), 7.19 (s, 1H, 17), 6.64 (dd, J = 15.3, 11.1 Hz, 1H, 12), 6.12 (d, J = 11.0 Hz, 1H, 13), 5.04 (d, J = 11.6 Hz, 1H, 3), 4.92 – 4.76 (m, 3H, 7, 8, 11), 4.35 (d, J = 8.2 Hz, 1H, 10), 4.05 (s, 3H, 28), 3.64 (d, J = 12.5 Hz, 1H, 15a), 3.41 (d, J = 12.6 Hz, 1H, 15b), 3.17 (s, 3H, 27), 3.12 (d, J = 9.2 Hz, 1H, 5), 2.99 – 2.87 (m, 1H, 2a), 2.68 (s, 3H, 25), 2.27 (d, J = 14.2 Hz, 1H, 2b), 1.83 (s, 3H, 26), 1.75 (dq, J = 8.3, 5.0, 4.5 Hz, 1H, 6), 1.24 (d, J = 6.4 Hz, 3H, 23), 0.97 (s, 3H, 22).

^{13}C NMR (101 MHz, acetone-d_6) δ 168.0 (1), 166.8 (1"), 165.8 (1'), 156.3 (20), 148.3 (24), 142.3 (18), 141.6 (14), 141.1 (16), 137.3 (9), 134.6 (2"), 134.5 (12), 133.8 (5'), 133.3 (5"), 130.2 (2'), 129.7 (3', 7'), 129.5 (3", 7"), 129.0 (4', 6'), 128.4 (4", 6"), 125.8 (11), 123.8 (13), 122.2 (17), 118.7 (19), 113.4 (21), 102.1 (8), 78.4 (7), 78.2 (3), 77.6 (10), 66.9 (5), 60.2 (4), 56.2 (28), 54.6 (25), 46.2 (15), 40.4 (6), 34.7 (27), 32.3 (2), 15.2 (26), 13.5 (23), 11.6 (22).

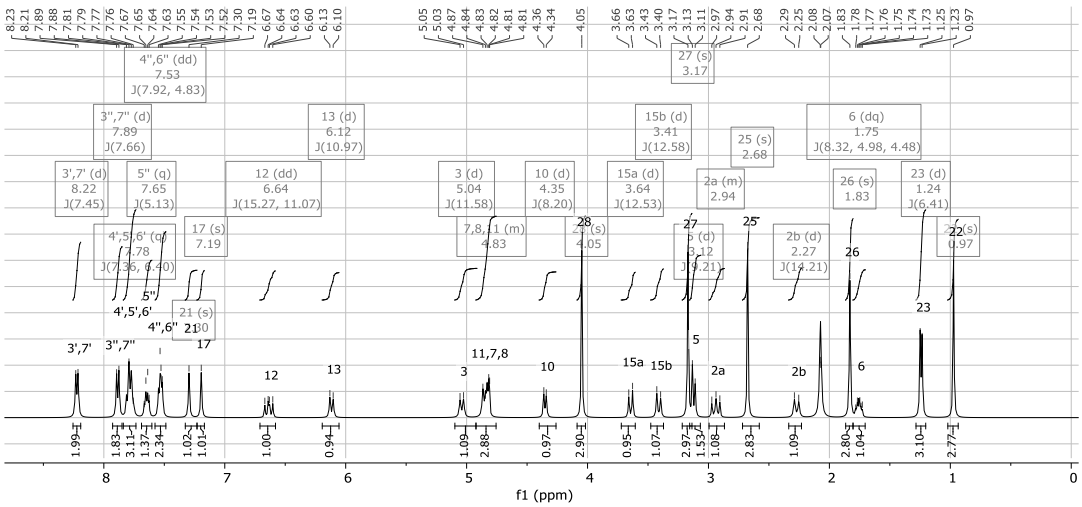

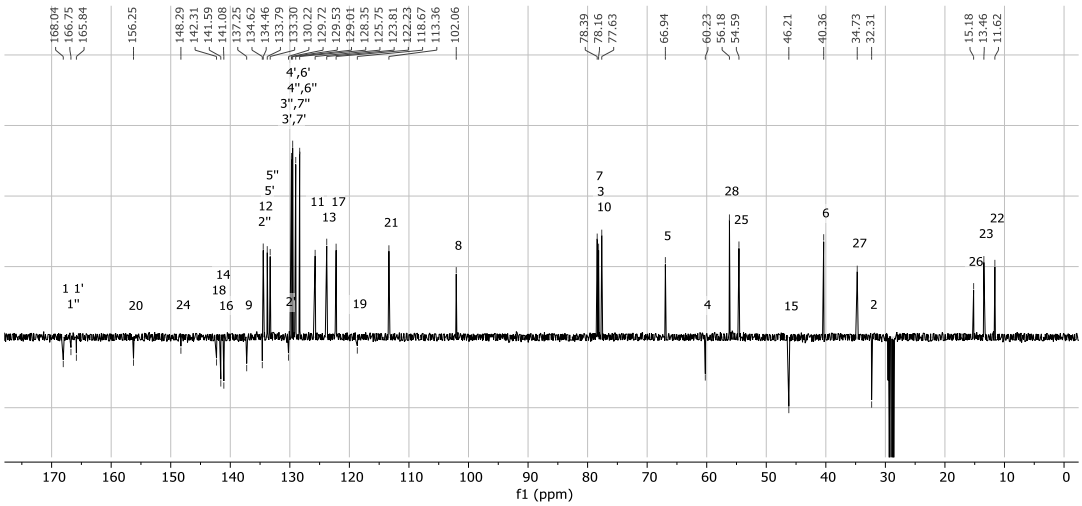

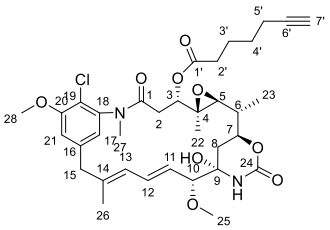

1f

HRMS (ESI) *m/z* $[M+Na]^+$ 695.2710 (calcd for $C_{35}H_{45}ClN_2O_9Na$, 695.2711)

^{1}H NMR (400 MHz, chloroform-*d*) δ 6.83 (d, *J* = 2.0 Hz, 1H, 21), 6.79 (d, *J* = 1.8 Hz, 1H, 17), 6.44 (dd, *J* = 15.5, 11.0 Hz, 1H, 12), 6.31 (s, 1H, NH), 6.16 (d, *J* = 10.9 Hz, 1H, 13), 5.49 (dd, *J* = 15.5, 8.9 Hz, 1H, 11), 4.89 (dd, *J* = 11.9, 3.0 Hz, 1H, 3), 4.25 (ddd, *J* = 12.4, 10.6, 2.0 Hz, 1H, 7), 3.99 (s, 3H, 28), 3.56 – 3.46 (m, 2H, 10, 15a), 3.36 (s, 3H, 25), 3.21 (d, *J* = 13.0 Hz, 1H, 15b), 3.17 (s, 3H, 27), 2.89 (d, *J* = 9.7 Hz, 1H, 5), 2.57 – 2.44 (m, 2H, 2'a, 2b), 2.44 – 2.31 (m, 1H, 2'b), 2.26 (td, *J* = 6.9, 2.7 Hz, 2H, 5'), 2.23 – 2.15 (m, 1H, 2a), 1.95 (t, *J* = 2.6 Hz, 1H, 7'), 1.81 (p, *J* = 7.6 Hz, 2H, 3'), 1.68 (s, 3H, 26), 1.66 – 1.54 (m, 3H, 4', 8b), 1.54 – 1.42 (m, 1H, 6), 1.28 (d, *J* = 6.4 Hz, 3H, 23), 1.26 – 1.18 (m, 1H, 8a), 0.83 (s, 3H, 22).

^{13}C NMR (101 MHz, chloroform-*d*) δ 171.9 (1), 168.8 (1'), 156.2 (20), 152.4 (24), 142.7 (18), 140.2 (16), 140.1 (14), 132.5 (12), 128.2 (11), 124.6 (13), 122.3 (17), 119.6 (19), 113.1 (21), 88.3 (10), 84.2 (6'), 81.1 (9), 77.0 (3), 74.4 (7), 69.0 (7'), 66.5 (5), 60.4 (4), 56.9 (25), 56.7 (28), 47.3 (15), 38.6 (6), 35.9 (8), 35.7 (27), 33.7 (2'), 32.9 (2), 27.9 (4'), 23.9 (3'), 18.4 (5'), 15.9 (26), 14.6 (23), 12.2 (22).

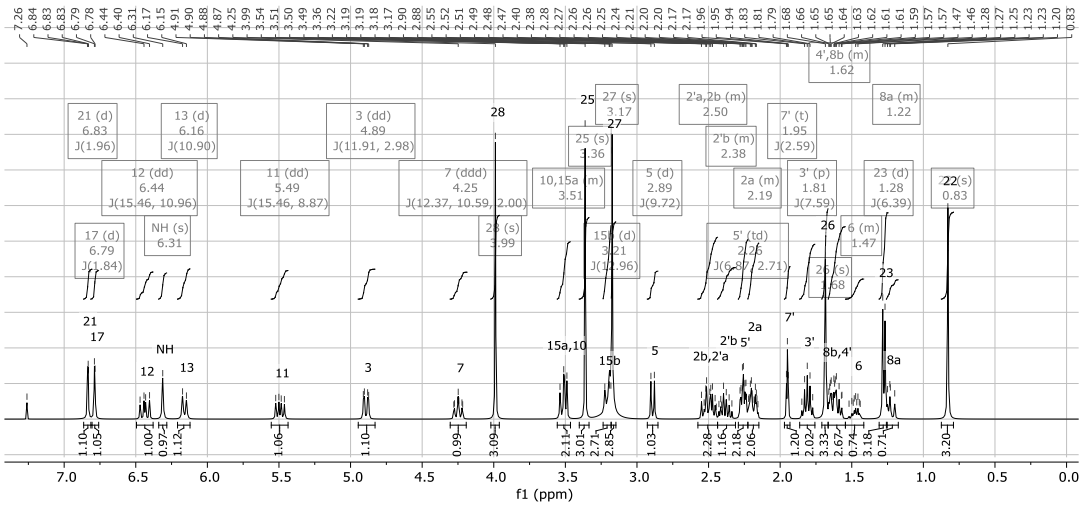

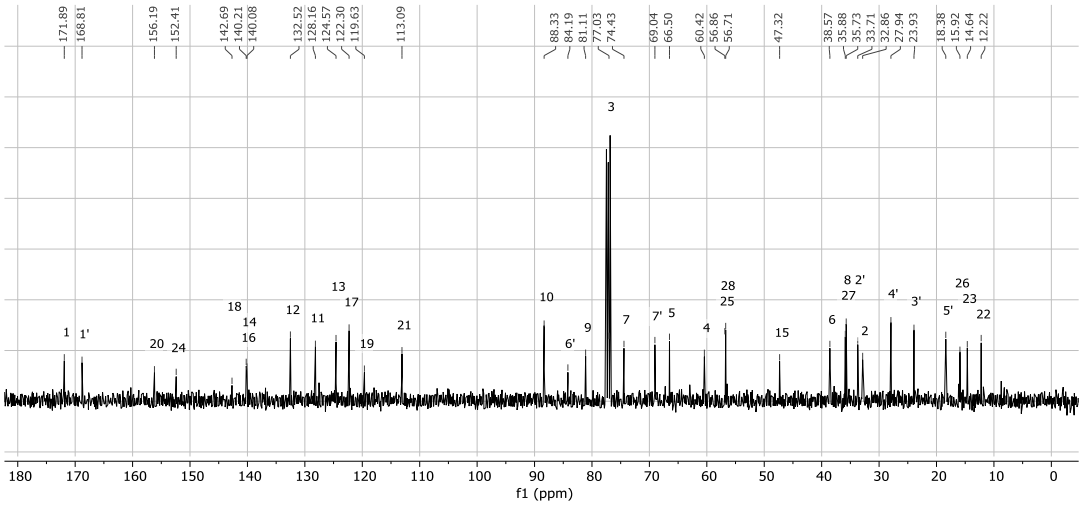

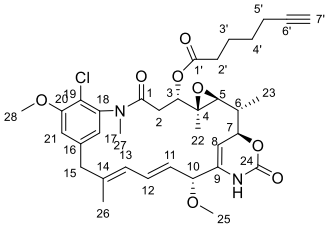

5f

HRMS (ESI) *m/z* $[M+Na]^+$ 677.2601 (calcd for $C_{35}H_{43}ClN_2O_8Na$, 677.2606)

^{1}H NMR (400 MHz, acetone-d_6) δ 8.09 (s, 1H, NH), 7.24 (s, 1H, 21), 7.03 (s, 1H, 17), 6.67 (dd, J = 15.1, 11.1 Hz, 1H, 12), 6.37 (d, J = 11.0 Hz, 1H, 13), 5.63 (dd, J = 15.2, 8.2 Hz, 1H, 11), 4.72 (dd, J = 11.8, 2.2 Hz, 1H, 3), 4.65 – 4.49 (m, 2H, 7, 8), 4.29 (d, J = 8.3 Hz, 1H, 10), 4.02 (s, 3H, 28), 3.63 (d, J = 13.0 Hz, 1H, 15a), 3.38 (d, J = 12.8 Hz, 1H, 15b), 3.31 (s, 3H, 25), 3.15 (s, 3H, 27), 2.84 (d, J = 9.7 Hz, 1H, 5), 2.74 – 2.56 (m, 2H, 2'a, 2a), 2.39 – 2.23 (m, 4H, 2'b, 5', 7'), 2.11 – 1.99 (m, 1H, 2b), 1.81 (q, J = 9.5, 7.8 Hz, 5H, 3', 26), 1.75 – 1.59 (m, 2H, 4'), 1.61 – 1.52 (m, 1H, 6), 1.18 (d, J = 6.5 Hz, 3H, 23), 0.86 (s, 3H, 22).

5c - ^{13}C NMR (101 MHz, acetone-d_6) δ 172.7 (1'), 167.0 (1), 156.6 (20), 150.6 (24), 142.9 (18), 141.6 (16), 141.3 (14), 137.9 (9), 133.8 (12), 127.6 (11), 124.8 (13), 123.3 (17), 119.1 (19), 114.0 (21), 98.4 (8), 84.3 (6'), 80.2 (10), 79.1 (7), 78.3 (3), 70.2 (7'), 67.8 (5), 60.8 (4), 56.8 (28), 56.5 (25), 46.7 (15), 40.0 (6), 35.5 (27), 34.3 (2'), 33.0 (2), 28.4 (4'), 24.9 (3'), 18.4 (5'), 15.8 (26), 14.2 (23), 11.8 (22).

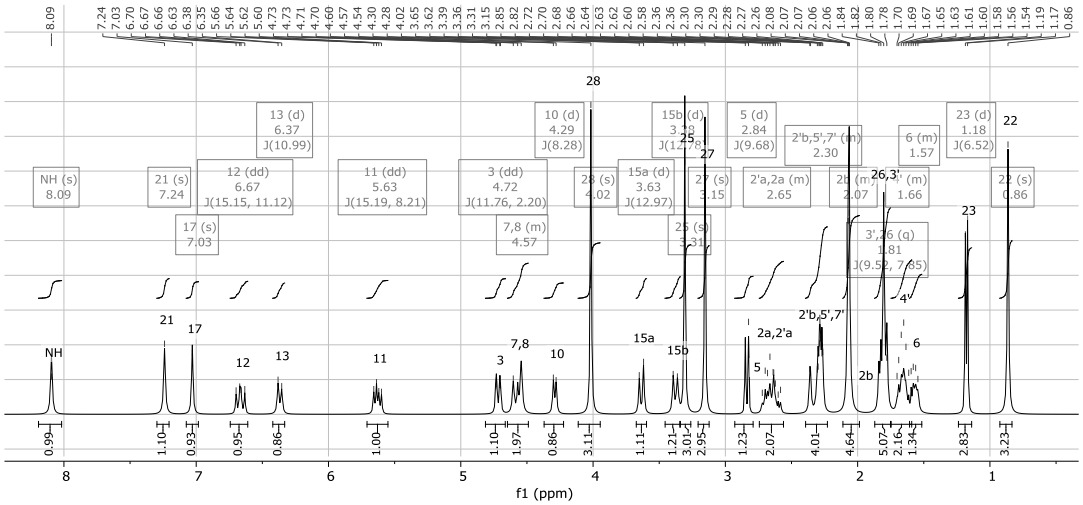

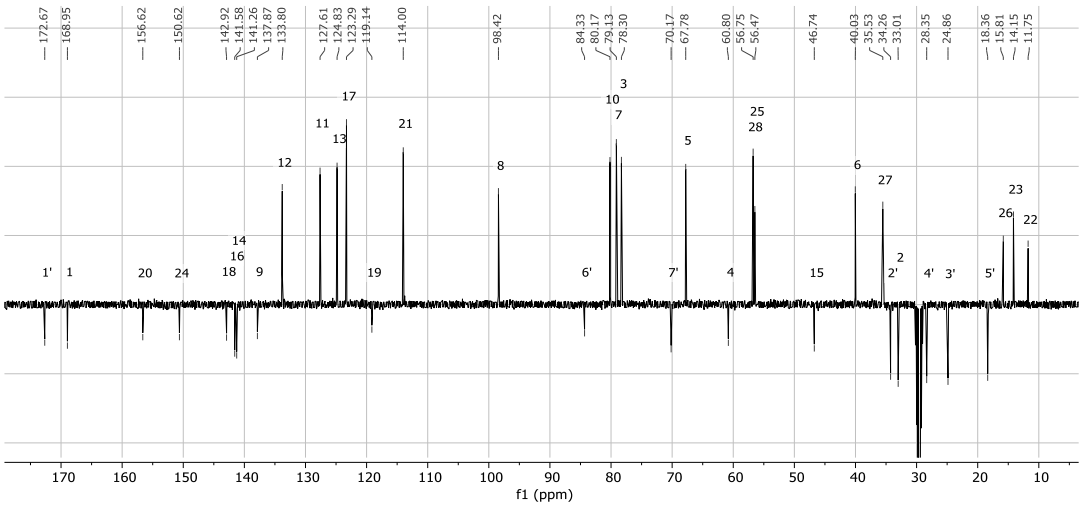

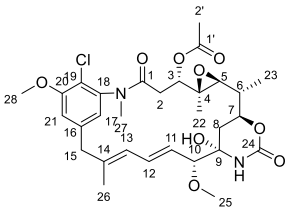

1g

HRMS (ESI) *m/z* $[M+Na]^+$ 629.2244 (calcd for $C_{30}H_{39}ClN_2O_9Na$, 629.2242)

^{1}H NMR (400 MHz, acetone-d_6) δ 7.25 (d, J = 1.9 Hz, 1H, 21), 6.97 (d, J = 1.8 Hz, 1H, 17), 6.75 (dd, J = 15.5, 11.1 Hz, 1H, 12), 6.42 (s, 1H, NH), 6.38 (d, J = 11.1 Hz, 1H, 13), 5.65 (dd, J = 15.4, 9.0 Hz, 1H, 11), 4.99 (s, 1H, OH), 4.83 (dd, J = 11.9, 2.7 Hz, 1H, 3), 4.20 (ddd, J = 12.5, 10.5, 2.3 Hz, 1H, 7), 4.02 (s, 3H, 28), 3.72 – 3.60 (m, 2H, 10, 15a), 3.37 (d, J = 2.3 Hz, 4H, 15b, 25), 3.12 (s, 3H, 27), 2.75 (d, J = 9.8 Hz, 1H, 5), 2.60 (dd, J = 13.8, 11.9 Hz, 1H, 2a), 2.22 (s, 3H, 2'), 2.07 – 1.98 (m, 1H, 2b), 1.77 (s, 3H, 26), 1.72 – 1.62 (m, 1H, 8a), 1.62 – 1.43 (m, 2H, 6, 8b), 1.21 (d, J = 6.3 Hz, 3H, 23), 0.95 (s, 3H, 22).

4b - ^{13}C NMR (101 MHz, acetone-d_6) δ 169.7 (1'), 168.8 (1), 156.6 (20), 151.7 (24), 143.0 (18), 141.8 (16), 140.2 (14), 133.0 (12), 129.5 (11), 125.6 (13), 123.1 (17), 119.2 (19), 114.3 (21), 89.1 (10), 81.5 (9), 77.4 (3), 74.5 (7), 66.8 (5), 61.2 (4), 56.7 (28), 56.5 (25), 46.9 (15), 38.7 (6), 36.7 (8), 35.3 (27), 33.2 (2), 20.9 (2'), 15.5 (26), 14.5, 12.1 (22).

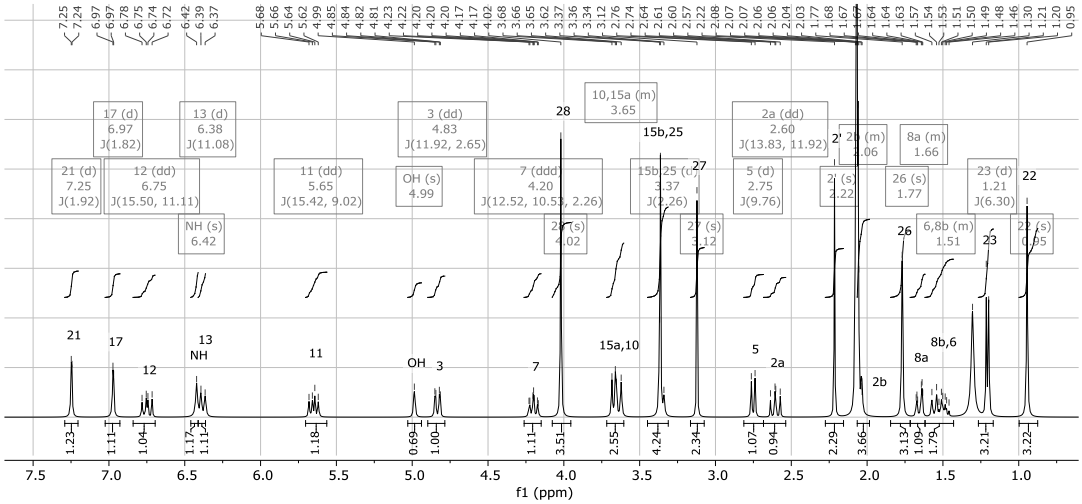

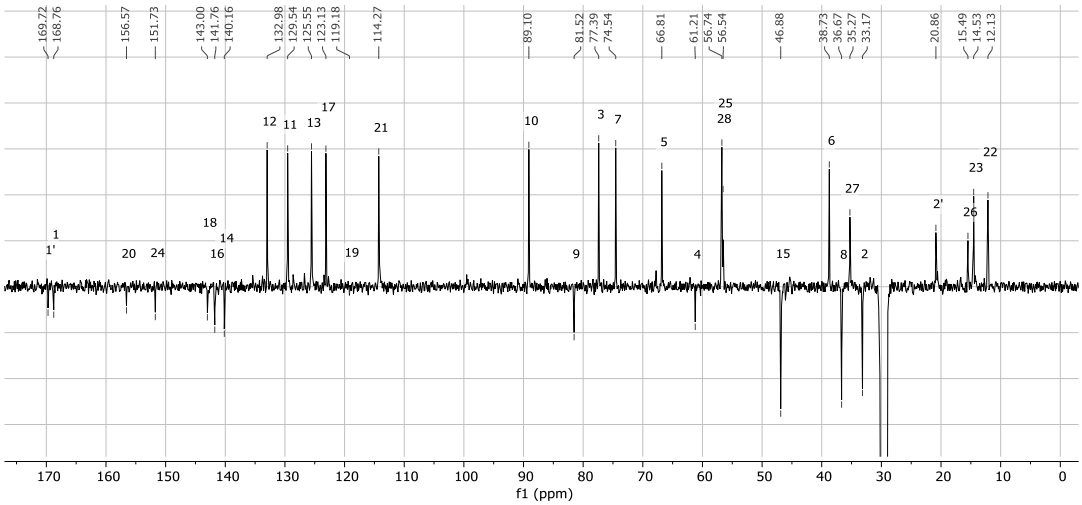

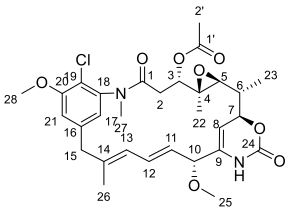

5g

HRMS (ESI) *m/z* $[M+Na]^+$ 611.2141 (calcd for $C_{30}H_{37}ClN_2O_8Na$, 611.2136)

^{1}H NMR (400 MHz, acetone-d_6) δ 8.09 (s, 1H, NH), 7.24 (d, J = 1.8 Hz, 1H, 21), 7.02 (d, J = 1.7 Hz, 1H, 17), 6.67 (dd, J = 15.2, 11.2 Hz, 1H, 12), 6.36 (d, J = 11.1 Hz, 1H, 13), 5.75 – 5.54 (m, 1H, 11), 4.69 (dd, J = 11.8, 2.7 Hz, 1H, 3), 4.64 – 4.49 (m, 2H, 7, 8), 4.29 (d, J = 8.3 Hz, 1H, 10), 4.02 (s, 3H, 28), 3.64 (d, J = 12.7 Hz, 1H, 15a), 3.38 (d, J = 12.7 Hz, 1H, 15b), 3.31 (s, 3H, 25), 3.15 (s, 3H, 27), 2.81 (d, J = 9.7 Hz, 1H, 5), 2.65 (dd, J = 13.9, 11.8 Hz, 1H, 2a), 2.31 (s, 3H, 2'), 2.07 (m, 1H, 2b), 1.80 (s, 3H, 26), 1.69 – 1.53 (m, 2H, 6), 1.17 (d, J = 6.5 Hz, 3H, 23), 0.86 (s, 3H, 22).

5b - ^{13}C NMR (101 MHz, acetone-d_6) ^{13}C NMR (101 MHz, Acetone) δ 169.3 (1'), 168.3 (1), 155.9 (20), 142.3 (18), 140.9 (16), 140.6 (14), 137.3 (24), 133.1 (12), 127.0 (11), 124.1 (13), 122.7 (17), 118.5 (19), 113.4 (21), 97.7 (8), 79.5 (10), 78.5 (7), 77.7 (3), 75.1, 67.1 (5), 60.2 (4), 56.1 (28), 56.1, 55.8 (25), 46.1 (15), 39.4 (6), 34.8 (27), 32.4 (2), 20.5 (2'), 15.1 (26), 13.5 (23), 11.0 (22). Signal of 9 is covered

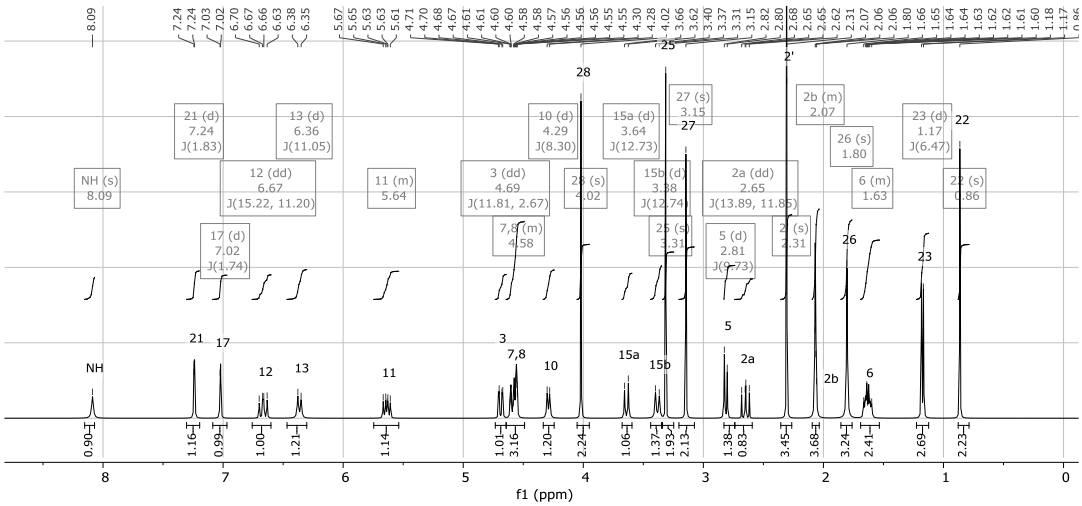

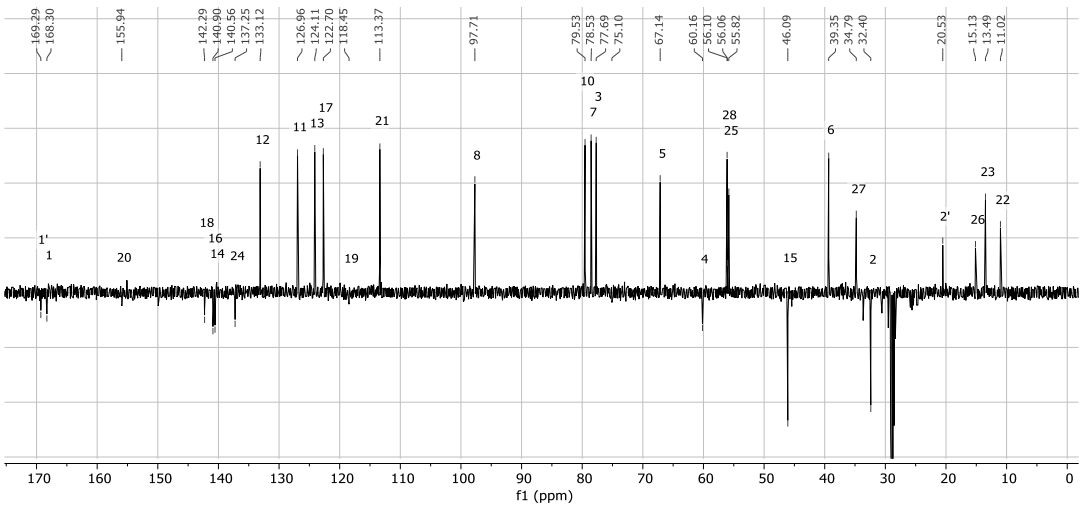

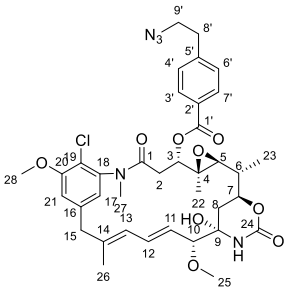

1h

HRMS (ESI) *m/z* $[M+Na]^+$ 760.2732 (calcd for $C_{37}H_{44}ClN_5O_9Na$, 760.2725)

^{1}H NMR (400 MHz, acetone-d_6) δ 8.1 (d, J = 8.2 Hz, 2H, 3', 7'), 7.6 (d, J = 8.0 Hz, 2H, 4', 6'), 7.3 (d, J = 1.9 Hz, 1H, 21), 7.2 (d, J = 1.8 Hz, 1H, 17), 6.6 (dd, J = 15.4, 11.0 Hz, 1H, 12), 6.3 (s, 1H, NH), 6.1 (d, J = 11.0 Hz, 1H, 13), 5.1 – 4.9 (m, 2H, 3, 11), 4.4 (d, J = 2.1 Hz, 1H, OH), 4.2 (ddd, J = 12.5, 10.5, 2.3 Hz, 1H, 7), 4.0 (s, 3H, 28), 3.7 (td, J = 7.0, 2.1 Hz, 2H, 9'), 3.6 (d, J = 12.6 Hz, 1H, 15a), 3.5 (d, J = 9.1 Hz, 1H, 10), 3.4 (d, J = 12.6 Hz, 1H, 15b), 3.2 (s, 3H, 25), 3.1 (s, 3H, 27), 3.1 – 3.0 (m, 3H, 5, 8'), 2.8 (d, J = 14.3 Hz, 1H, 2a), 2.3 (dd, J = 14.4, 3.2 Hz, 1H, 2b), 1.8 (s, 3H, 26), 1.6 (dt, J = 13.5, 2.0 Hz, 1H, 8a), 1.5 – 1.4 (m, 2H, 6, 8b), 1.2 (d, J = 6.4 Hz, 3H, 23), 1.0 (s, 3H, 22).

^{13}C NMR (101 MHz, acetone-d_6) δ 168.68 (1), 166.38 (1'), 156.85 (20), 151.67 (24), 144.97 (5'), 143.08 (18), 141.98 (16), 140.09 (14), 133.00 (12), 130.77 (3', 7'), 129.55 (2'), 129.45 (4', 6'), 129.32 (11), 125.45 (13), 122.79 (17), 119.33 (19), 114.17 (21), 89.49 (10), 81.21 (9), 77.97 (3), 74.44 (7), 66.96 (5), 61.20 (4), 56.82 (28), 56.43 (25), 52.48 (9'), 46.91 (15), 39.36 (6), 36.79 (8), 35.57 (8'), 35.23 (27), 33.35 (2), 15.53 (26), 14.67 (23), 12.78 (22).

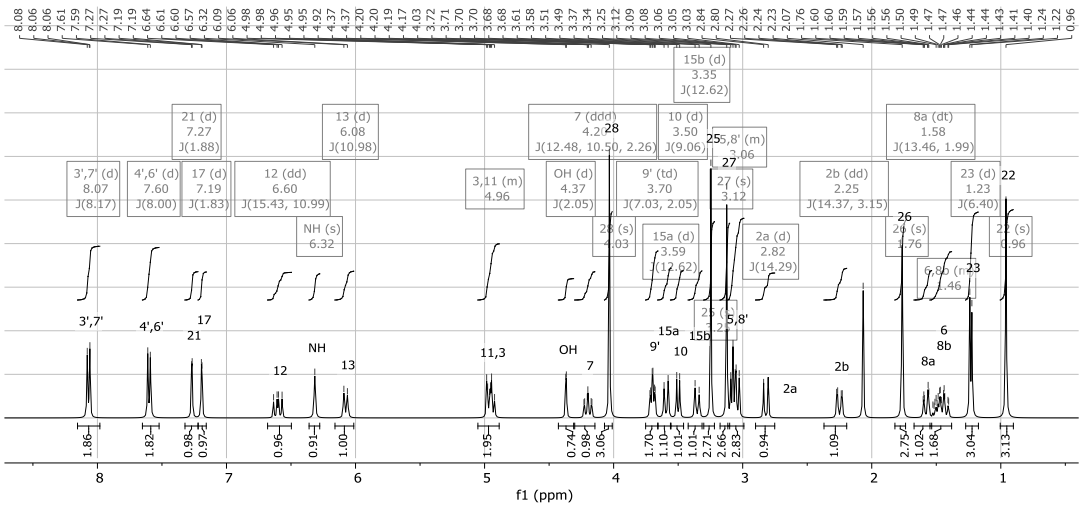

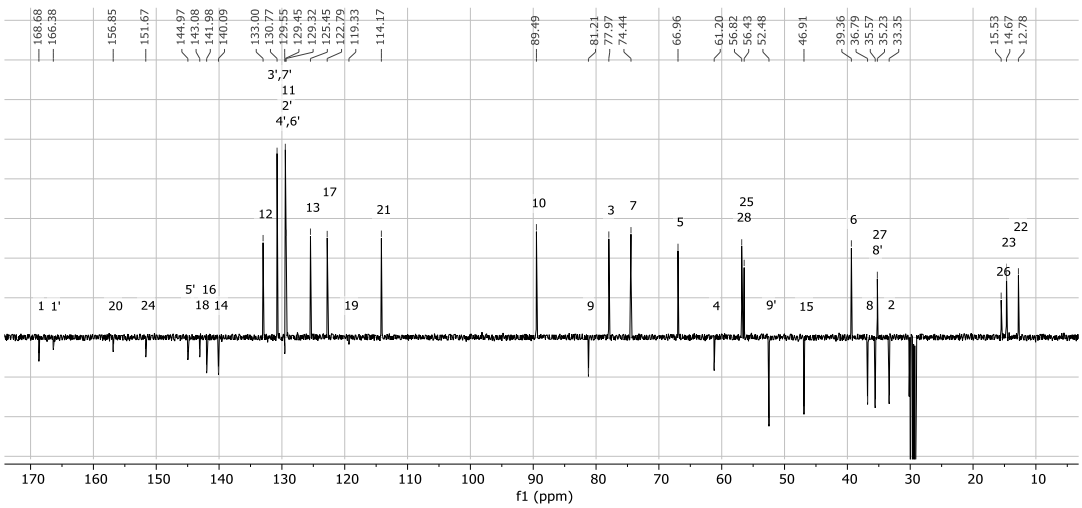

Synthesis of 6-azidohexanoic acid (12)

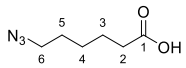

12

To a solution of 4-(2-bromoethyl)benzoic acid (195 mg, 1 mmol) in DMSO (4 ml), was added NaN_3 (69 mg, 1.1 mmol). The mixture was stirred at room temperature for 20 hours. Then, water (4 mL) was added, and the solution was extracted with EtOAc (4 × 8 mL). The organic layer was washed with brine and the combined organic layers were dried over Na_2SO_4 and concentrated under reduced pressure. The crude product was not purified to provide the product (142 mg, 0.91 mmol, 91% yield) as white solid.

^{1}H NMR (400 MHz, chloroform-*d*) δ 3.3 (t, *J* = 6.9 Hz, 2H), 2.4 (t, *J* = 7.4 Hz, 2H, 2), 1.7 (dp, *J* = 18.1, 7.3 Hz, 4H), 1.5 (qd, *J* = 10.0, 9.2, 6.0 Hz, 2H, 4).

^{13}C NMR (101 MHz, chloroform-*d*) δ 180.19 (1), 51.86 (6), 34.49 (2), 29.20 (5), 26.82 (4), 24.83 (3).

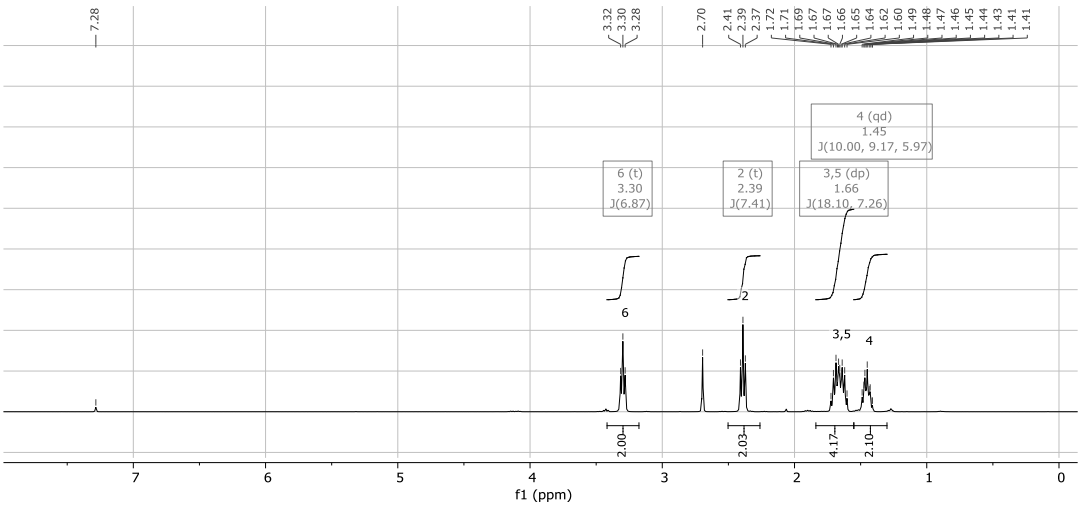

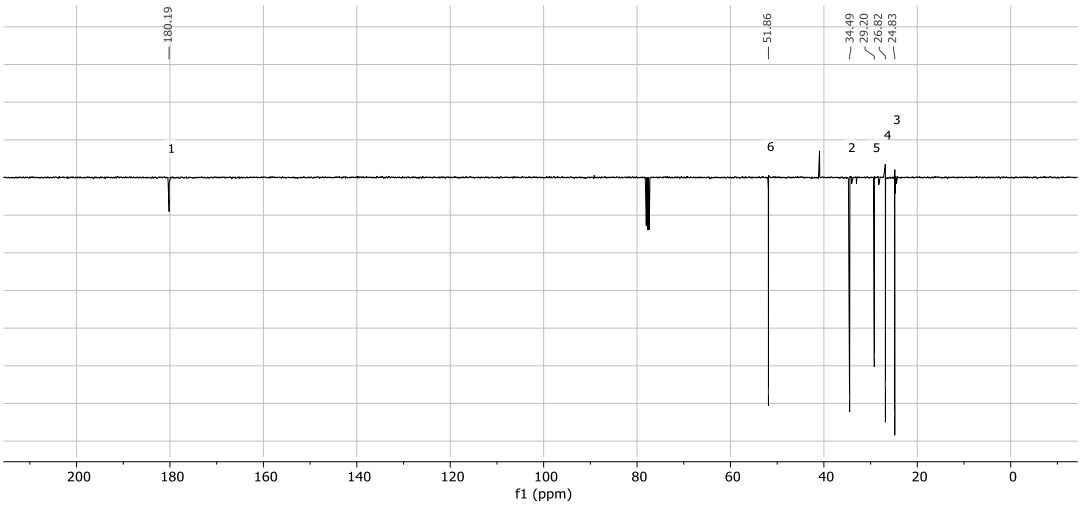

Synthesis of (11)

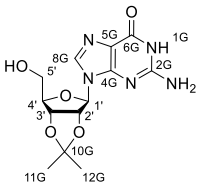

11

To a suspension of guanosine (200 mg, 0.706 mmol) in dry acetone (11.8 ml) was added an aqueous solution of 60% $HClO_4$ 60% (95 µL, 0.946 mmol) and the clear reaction obtained was stirred for 2 h at room temperature. The reaction was quenched by dropping an aqueous solution of 28% NH_4OH (134 µL) at 0°C. The precipitate was recovered by filtration on Buchner washing with cold Et_2O. The solid was dried in *vacuum* to provide 229 mg (>98%) of product as white solid.

^{1}H NMR (400 MHz, DMSO-d_6) δ 7.9 (s, 1H, 8G), 6.4 (s, 2H, NH_2), 5.9 (d, J = 2.8 Hz, 1H, 1'), 5.2 (dd, J = 6.4, 2.8 Hz, 1H, 2'), 5.0 (dd, J = 6.4, 3.1 Hz, 1H, 3'), 4.1 (dt, J = 5.0, 2.5 Hz, 1H, 4'), 3.6 (t, J = 4.7 Hz, 2H, 5'), 2.1 (s, 1H, OH), 1.5 (s, 3H, 11G), 1.3 (s, 3H, 12G).

^{13}C NMR (101 MHz, DMSO) δ 157.18 (6G), 154.17 (2G), 151.22 (4G), 136.30 (8G), 117.36 (5G), 113.56 (10G), 89.07 (1'), 87.14 (4'), 84.11 (2'), 81.71 (3'), 62.15 (5'), 27.55 (11G), 25.76 (12G).

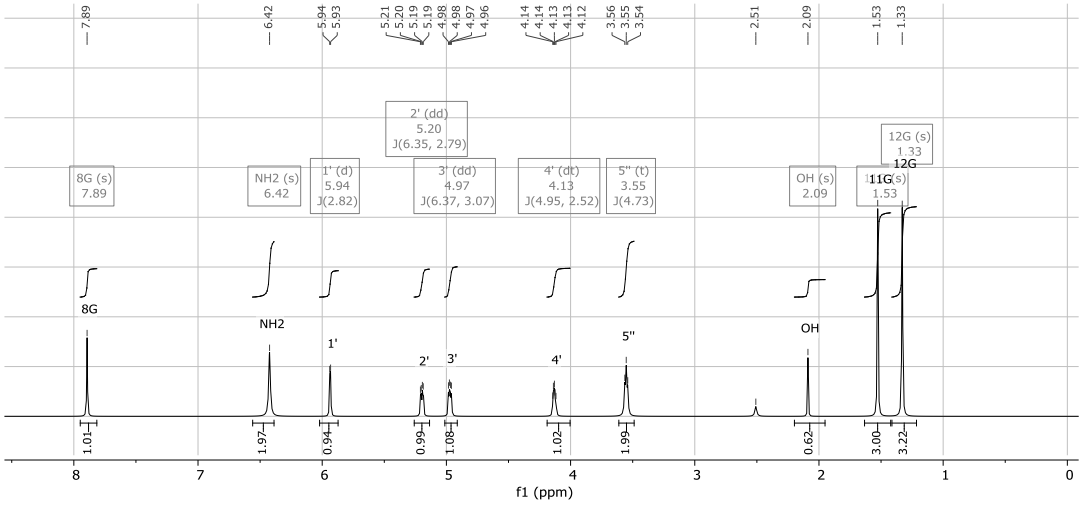

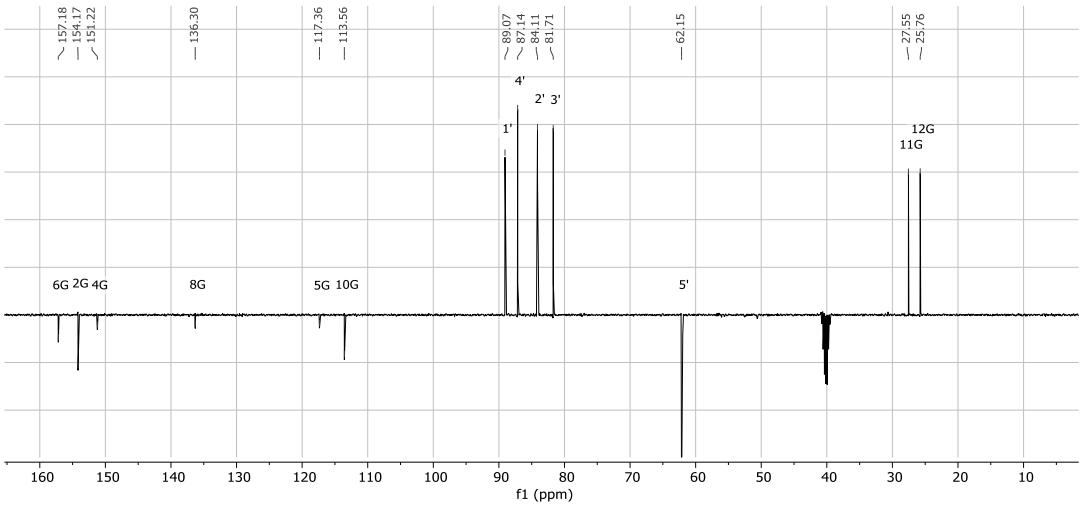

Synthesis of (13)

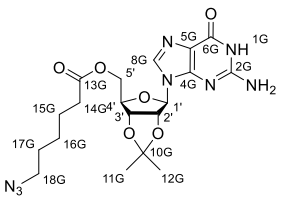

13

To a solution of **11** (100 mg, 0.309 mmol) in dry CH_2Cl_2 (2.5 mL) were added **12** (72 mg, 0.464 mmol), DMAP (22 mg, 0.185 mmol), EDC-HCl (106 mg, 0.557 mmol), and triethylamine dry (95 µL, 0.680 mmol) at room temperature under a nitrogen atmosphere. The reaction was stirred for 18 h before to add H_2O (1 × 2 mL). The organic layer was dried over Na_2SO_4, and concentrated under reduced pressure. Purification with Biotage Isolera™ One System (gradient from 5% to 40% ACN in 22 CV) provided the products (101 mg, 71%) as white powders.

HRMS (ESI) *m/z* $[M+Na]^+$ 485.1881 (calcd for $C_{19}H_{26}N_8O_6Na$, 485.1873)

^{1}H NMR (400 MHz, DMSO-*d*$_6$) δ 10.7 (s, 1H, NH_2), 7.9 (s, 1H, 8G), 6.6 (s, 1H), 6.2 – 5.9 (m, 1H, 1'), 5.5 – 5.2 (m, 1H, 2'), 5.1 (dd, *J* = 5.9, 3.4 Hz, 1H, 3'), 4.2 (dd, *J* = 8.0, 4.0 Hz, 2H, 4', 5'a), 4.1 (dd, *J* = 12.6, 7.9 Hz, 1H, 5'b), 3.3 (t, *J* = 6.9 Hz, 2H, 18G), 2.3 (dt, *J* = 7.0, 3.4 Hz, 2H, 14G), 1.6 – 1.4 (m, 7H, 11G, 15G, 17G), 1.3 (s, 5H, 12G, 16G).

^{13}C NMR (101 MHz, DMSO-*d*$_6$) δ 173.65 (13G), 157.81 (6G), 154.78, 151.61 (4G), 137.25, 118.07 (5G), 114.40 (10G), 89.44 (1'), 85.32 (4'), 84.77 (2'), 82.19 (3'), 65.05 (5'), 51.58 (18G), 34.18 (14G), 29.01 (17G), 28.12 (11G), 26.66 (15G), 26.43 (12G), 24.96 (16G).

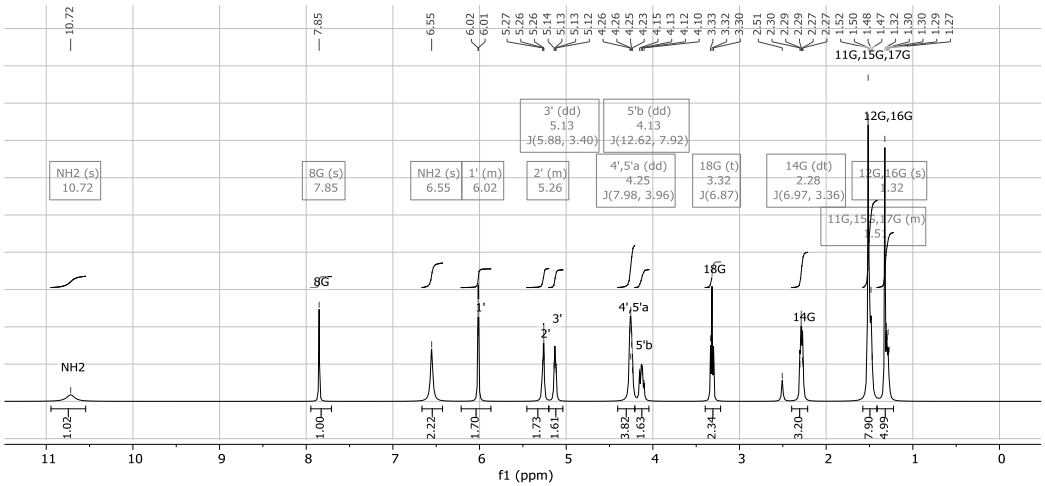

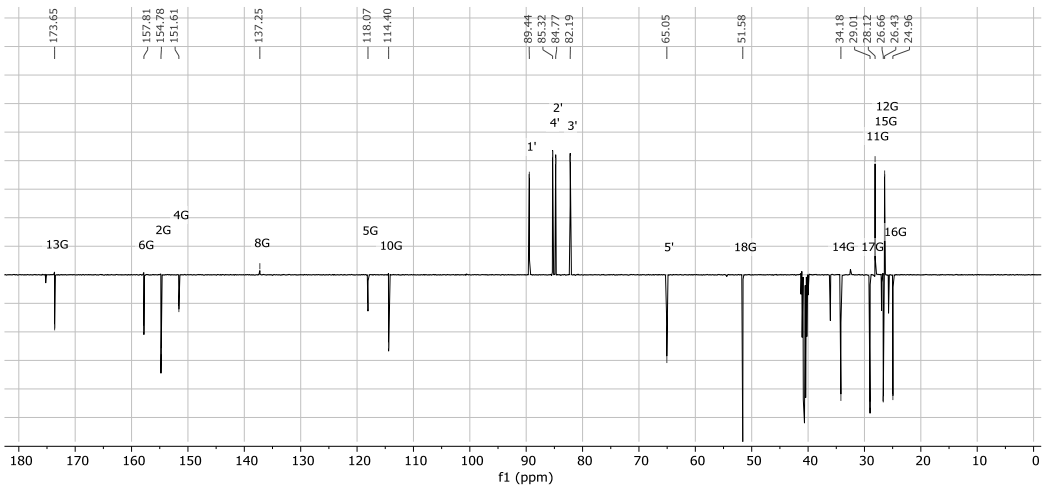

Synthesis of (14)

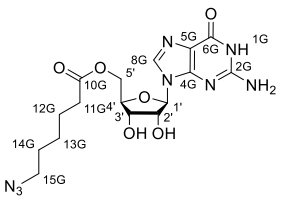

14

To a solution of **13** (49 mg, 0.11 mmol) was added aqueous TFA 80% (1.52 mL). The mixture was stirred at room temperature for 30 min. Then, the solvent was removed in *vacuum*, a solution of EtOH +1% Et_3N (2.5 mL) were added and the solvent was evaporated to remove the TFA salt form. Purification of the crude with Biotage Isolera™ One System (gradient from 5% to 40% ACN in 22 CV) provided the products (46 mg, >98%) as white powders.

HRMS (ESI) *m/z* $[M+Na]^+$ 445.1569 (calcd for $C_{16}H_{22}N_8O_6Na$, 445.1560)

^{1}H NMR (400 MHz, DMSO-*d*$_6$) δ 10.8 (s, 1H, 1G), 7.9 (s, 1H), 6.6 (s, 2H, NH_2), 5.7 (d, *J* = 5.1 Hz, 1H, 1'), 4.4 (t, *J* = 5.2 Hz, 1H), 4.3 (dd, *J* = 12.0, 3.7 Hz, 1H, 5'a), 4.2 (dt, *J* = 9.8, 5.3 Hz, 2H, 3', 5'b), 4.0 (q, *J* = 4.8 Hz, 1H), 3.3 (d, *J* = 7.2 Hz, 2H, 15G), 2.3 (t, *J* = 7.4 Hz, 2H, 11G), 1.5 (h, *J* = 6.8 Hz, 4H, 12G, 14G), 1.3 (p, *J* = 4.8, 4.2 Hz, 2H, 13G).

^{13}C NMR (101 MHz, DMSO-*d*$_6$) δ 173.78 (10G), 157.82 (6G), 154.94 (2G), 152.42 (4G), 136.50 (8G), 117.82 (5G), 87.83 (1'), 82.46 (4'), 74.20 (2'), 71.41 (3'), 64.95 (5'), 51.60 (15G), 34.30 (11G), 29.03 (14G), 26.69 (13G), 25.03 (12G).

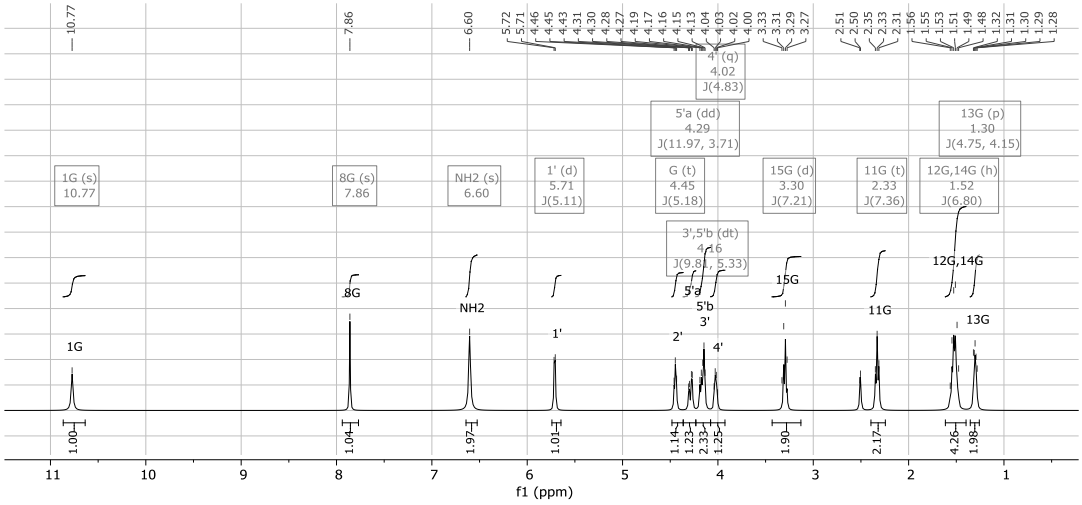

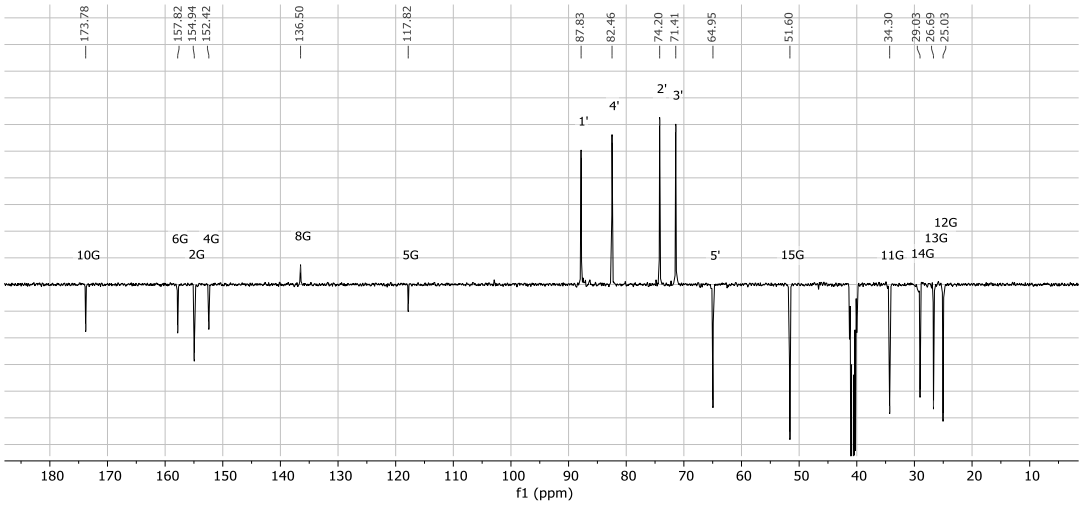

Synthesis of (15)

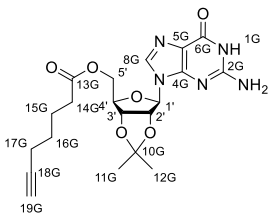

15

To a solution of **11** (150 mg, 0.464 mmol) in dry CH_2Cl_2 (3.8 mL) were added 6-heptinoic acid (88 µL, 0.696 mmol), DMAP (34 mg, 0.278 mmol), EDC-HCl (160 mg, 0.835 mmol), and triethylamine dry (142 µL, 1.021 mmol) at room temperature under a nitrogen atmosphere. The reaction was stirred for 18 h before to add H_2O (1 × 3 mL). The organic layer was dried over Na_2SO_4, and concentrated under reduced pressure. Purification with Biotage Isolera™ One System (gradient from 5% to 40% ACN in 22 CV) provided the products (156 mg, 78%) as white powders.

HRMS (ESI) *m/z* $[M+Na]^+$ 454.1710 (calcd for $C_{20}H_{25}N_5O_6Na$, 454.1703)

^{1}H NMR (400 MHz, DMSO-*d*$_6$) δ 10.7 (s, 1H, 1G), 7.9 (s, 1H, 8G), 6.5 (s, 2H, NH_2), 6.0 (d, *J* = 2.1 Hz, 1H, 1'), 5.3 (dd, *J* = 6.3, 2.0 Hz, 1H, 2'), 5.1 (dd, *J* = 6.3, 3.5 Hz, 1H, 3'), 4.3 (dt, *J* = 6.1, 4.3 Hz, 2H, 4', 5'a), 4.1 (dd, *J* = 12.8, 7.9 Hz, 1H, 5'b), 2.7 (t, *J* = 2.6 Hz, 1H, 19G), 2.3 (td, *J* = 7.4, 3.2 Hz, 2H, 14G), 2.1 (dq, *J* = 7.0, 3.1 Hz, 2H, 17G), 1.6 – 1.5 (m, 2H, 15G), 1.5 (s, 3H, 11G), 1.4 (p, *J* = 7.2 Hz, 2H, 16G), 1.3 (s, 3H, 12G).

^{13}C NMR (101 MHz, DMSO-*d*$_6$) δ 173.61 (13G), 157.81 (6G), 154.80 (2G), 151.63 (4G), 137.26 (8G), 118.09 (5G), 114.44 (10G), 89.43 (1'), 85.31 (18G), 85.28 (4'), 84.76 (2'), 82.21 (3'), 72.40 (19G), 65.08 (5'), 33.78 (14G), 28.36 (16G), 28.13 (11G), 26.44 (12G), 24.59 (15G), 18.50 (17G).

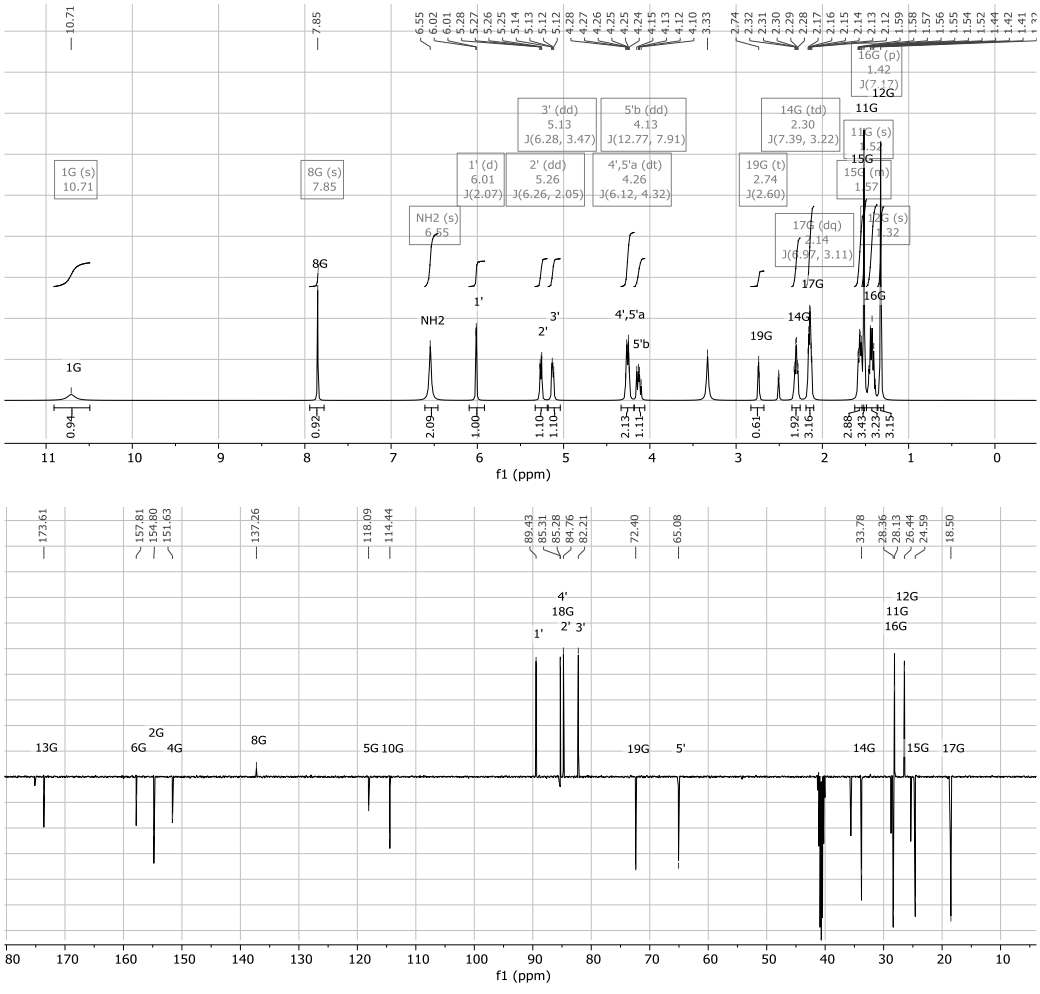

Synthesis of (16)

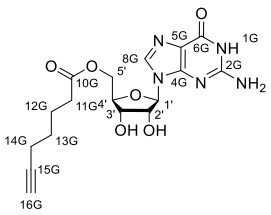

16

To a solution of **15** (52 mg, 0.12 mmol) was added aqueous TFA 80% (1.71 mL). The mixture was stirred at room temperature for 30 min. Then, the solvent was removed in *vacuum*, a solution of EtOH +1% Et_3N (2.5 mL) were added and the solvent was evaporated to remove the TFA salt form. Purification of the crude with Biotage Isolera™ One System (gradient from 5% to 40% ACN in 22 CV) provided the products (46 mg, >98%) as white powders.

HRMS (ESI) *m/z* $[M+Na]^+$ 414.1396 (calcd for $C_{17}H_{21}N_5O_6$, 414.1390)

^{1}H NMR (400 MHz, DMSO-d_6) δ 10.7 (s, 1H, 1G), 7.9 (s, 1H, 8G), 6.5 (s, 2H, NH_2), 5.8 – 5.7 (m, 1H, 1'), 5.5 (d, *J* = 5.4 Hz, 1H, 2'OH), 5.3 (d, *J* = 4.8 Hz, 1H, 3'OH), 4.4 (d, *J* = 5.0 Hz, 1H, 2'), 4.3 (dd, *J* = 11.9, 3.5 Hz, 1H, 5'a), 4.2 – 4.1 (m, 2H, 3', 5'b), 4.0 (q, *J* = 5.9, 4.5 Hz, 1H, 4'), 2.7 (d, *J* = 2.4 Hz, 1H, 16G), 2.3 (t, *J* = 7.2 Hz, 2H, 11G), 2.2 (td, *J* = 6.9, 2.4 Hz, 2H, 14G), 1.6 (q, *J* = 7.4 Hz, 2H, 12G), 1.5 (q, *J* = 7.2 Hz, 2H, 13G).

^{13}C NMR (101 MHz, DMSO-d_6) δ 173.73 (10G), 157.85 (6G), 154.83 (2G), 152.44 (4G), 136.56 (8G), 117.84 (5G), 87.79 (1'), 85.31 (15G), 82.48 (4'), 74.15 (2'), 72.42 (16G), 71.41 (3'), 65.00 (5'), 33.87 (11G), 28.36 (13G), 24.65 (12G), 18.50 (14G).

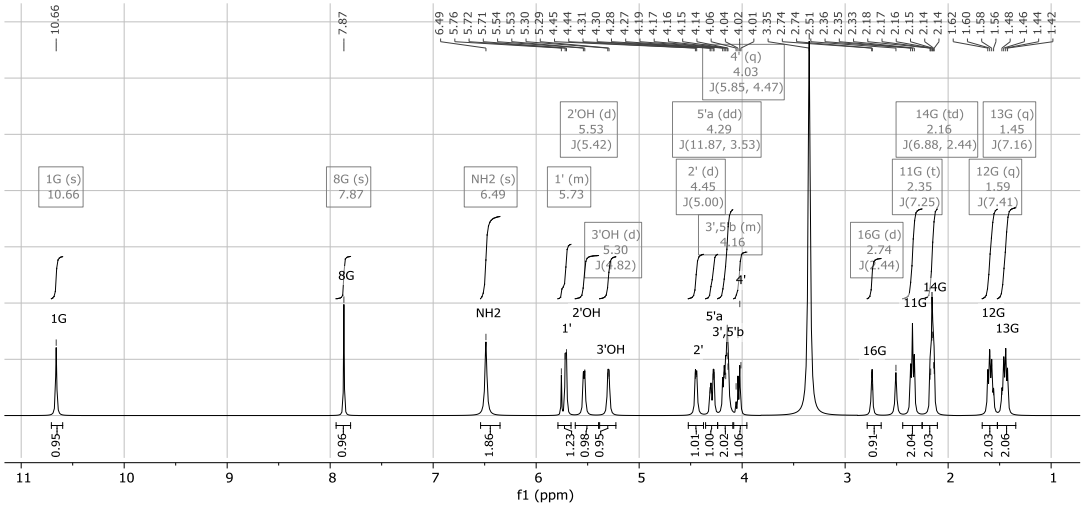

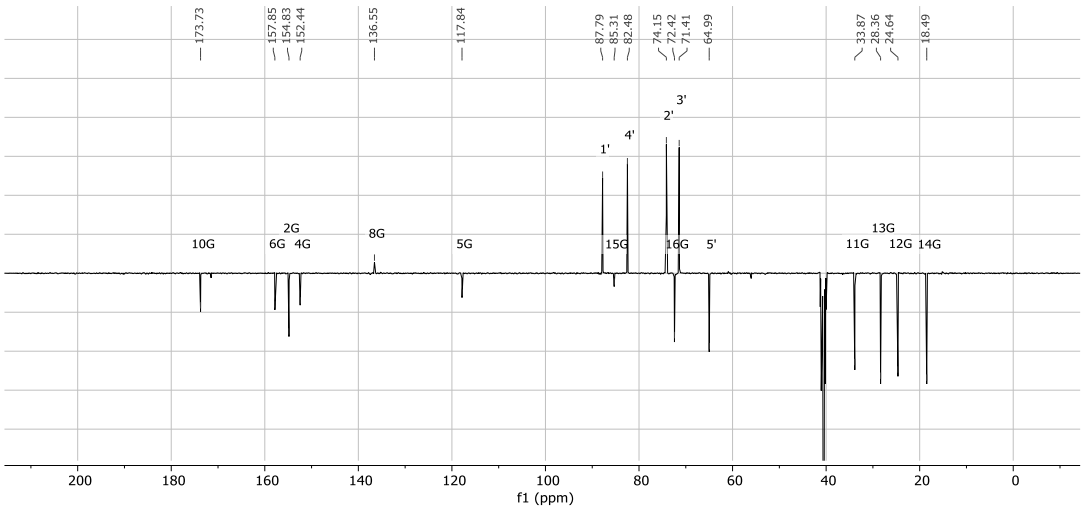

Synthesis of (21)

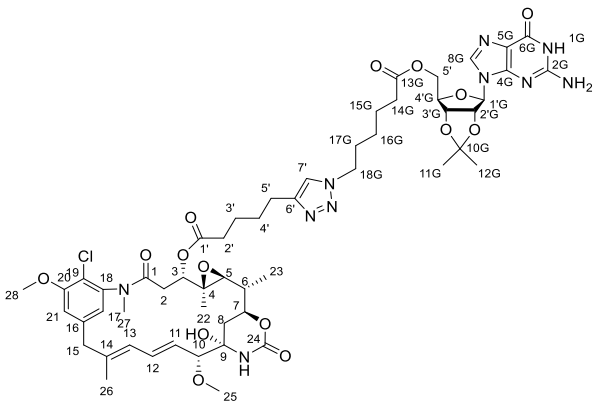

21

To a solution of **1f** (21 mg, 0.031mmol) and **13** (21 mg, 0.047 mmol) in DMSO (690 µL) were added water (225 µL), $CuSO_4$*$5H_2O$ (15 mg, 0.050 mmol), then a solution of Na-ascorbate (39 mg, 0.19 mmol) in H_2O (115 µL) was added dropwise. The mixture was stirred at room temperature for 2 h. Then, water was added (1.4 mL) and the aqueous layer was extracted in DCM. The organic layer was washed with H_2O and brine, dried over Na_2SO_4 and concentrated in *vacuum*. Purification of the crude with Biotage Isolera™ One System (gradient from 5% to 60% ACN in 22 CV) provided the products (31 mg, 89%) as white powders.

HRMS (ESI) m/z $[M+Na]^+$ 1157.4691 (calcd for $C_{54}H_{71}ClN_{10}O_{15}Na$ 1157.4687);

^1H (600 MHz, DMSO-d_6) δ 7.9 (s, 1H, 7'), 7.8 (d, *J* = 2.0 Hz, 1H, 8G), 7.2 (d, *J* = 1.8 Hz, 1H, 21), 7.0 (s, 2H, NH_2), 6.9 (s, 1H, NH), 6.8 (d, *J* = 1.8 Hz, 1H, 17), 6.6 (dd, *J* = 15.4, 11.1 Hz, 1H, 12), 6.2 (d, *J* = 11.1 Hz, 1H, 13), 6.0 (d, *J* = 2.0 Hz, 1H, 1'G), 5.4 (dd, *J* = 15.4, 8.9 Hz, 1H, 11), 5.3 (dd, *J* = 6.3, 2.1 Hz, 1H, 2'G), 5.1 (dd, *J* = 6.3, 3.4 Hz, 1H, 3'G), 4.6 (dd, *J* = 11.9, 2.7 Hz, 1H, 3), 4.3 – 4.2 (m, 4H, 4'G, 5'Ga, 18G), 4.2 – 4.0 (m, 2H, 5'Gb, 7), 3.9 (s, 3H, 28), 3.6 – 3.5 (m, 2H, 10, 15a), 3.3 (s, 1H, 15b), 3.2 (s, 3H, 25), 2.9 (s, 3H, 27), 2.7 (dt, *J* = 13.6, 7.4 Hz, 2H, 5'), 2.6 (d, *J* = 9.8 Hz, 1H, 5), 2.5 – 2.4 (m, 3H, 2', 2a), 2.3 (td, *J* = 7.6, 4.9 Hz, 2H, 14G), 2.0 (dd, *J* = 13.5, 2.3 Hz, 1H, 2b), 1.7 (dt, *J* = 13.3, 6.8 Hz, 4H, 3', 17G), 1.7 – 1.6 (m, 5H, 4', 26), 1.5 (s, 3H, 11G), 1.5 – 1.4 (m, 4H, 6, 8a, 15G), 1.4 – 1.3 (m, 1H, 8b), 1.3 (s, 3H, 12G), 1.2 – 1.1 (m, 2H, 16G), 1.1 (d, *J* = 6.4 Hz, 3H, 23), 0.8 (s, 3H, 22).

^{13}C NMR (151 MHz, DMSO-d_6) δ 172.98 (13G), 172.25 (1'), 168.51 (1), 155.70 (20), 154.88 (6G), 151.77 (24), 151.74 (2G), 151.05 (4G), 146.89 (6'), 141.89 (18), 141.45 (16), 139.51 (14), 136.31 (8G), 132.34 (12), 129.15 (11), 125.00 (13), 122.32 (17), 122.13 (7'), 117.90 (19), 117.37 (5G), 114.38 (21), 113.74 (10G), 88.77 (1'G), 88.54 (10), 84.64 (4'G), 84.10 (2'G), 81.57 (3'G), 80.65 (9), 76.52 (3), 73.85 (7), 66.21 (5), 64.39 (5'G), 61.06 (4), 57.03 (28), 56.65 (25), 49.39 (18G), 46.09 (15), 37.81 (6), 36.54 (8), 35.46 (27), 33.49 (2'), 33.46 (2), 32.74 (14G), 30.23 (4'), 29.88 (17G), 28.84 (5'), 28.77 (11G), 28.66 (12G), 25.37 (3'), 24.56 (15G), 15.72 (26), 14.84 (23), 11.84 (22).

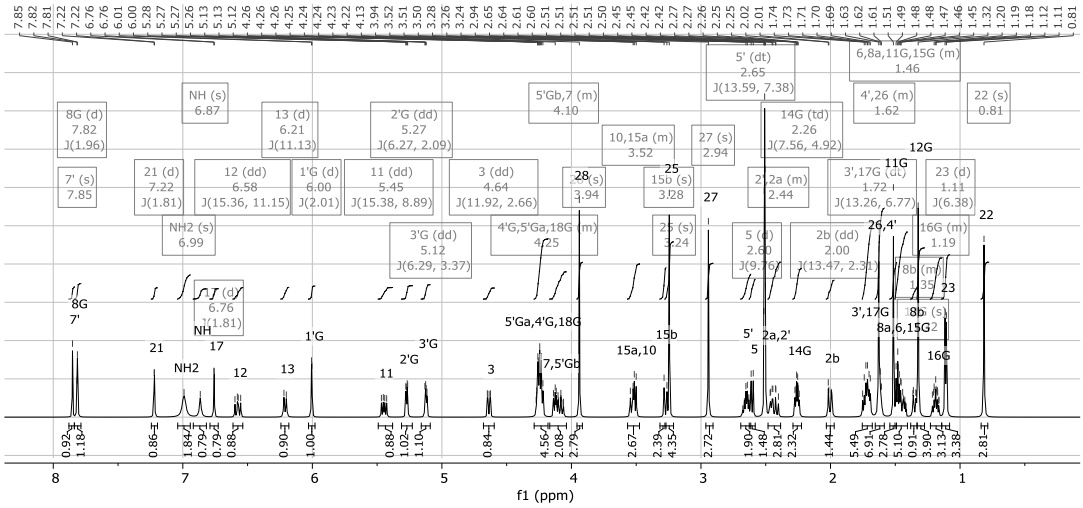
8G (d) 7.82 J(1.96)
7' (s) 7.85
NH (s) 6.87
21 (d) 7.22 J(1.81)
12 (dd) 6.58 J(15.36, 11.15)
13 (d) 6.21 J(11.13)
1'G (d) 6.00 J(2.01)
NH2 (s) 6.99
17 (d) 6.76 J(11.81)
11 (dd) 5.45 J(15.38, 8.89)
2'G (dd) 5.27 J(6.27, 2.09)
3'G (dd) 5.12 J(6.29, 3.37)
3 (dd) 4.64 J(11.92, 2.66)
4'G,5'Ga,18G (m) 4.25
5'Gb,7 (m) 4.10
10,15a (m) 3.52
28 (s) 3.94
15b (s) 3.28
25 (s) 3.24
27 (s) 2.94
5' (dt) 2.65 J(13.59, 7.38)
5 (d) 2.60 J(9.76)
2',2a (m) 2.44
2b (dd) 2.00 J(13:47, 2.31)
14G (td) 2.26 J(7.56, 4.92)
6,8a,11G,15G (m) 1.46
4',26 (m) 1.62
3',17G (dt) 1.72 J(13.26, 6.77)
8b (m) 1.35
16G (m) 1.19
23 (d) 1.11 J(6.38)
22 (s) 0.81
f1 (ppm)

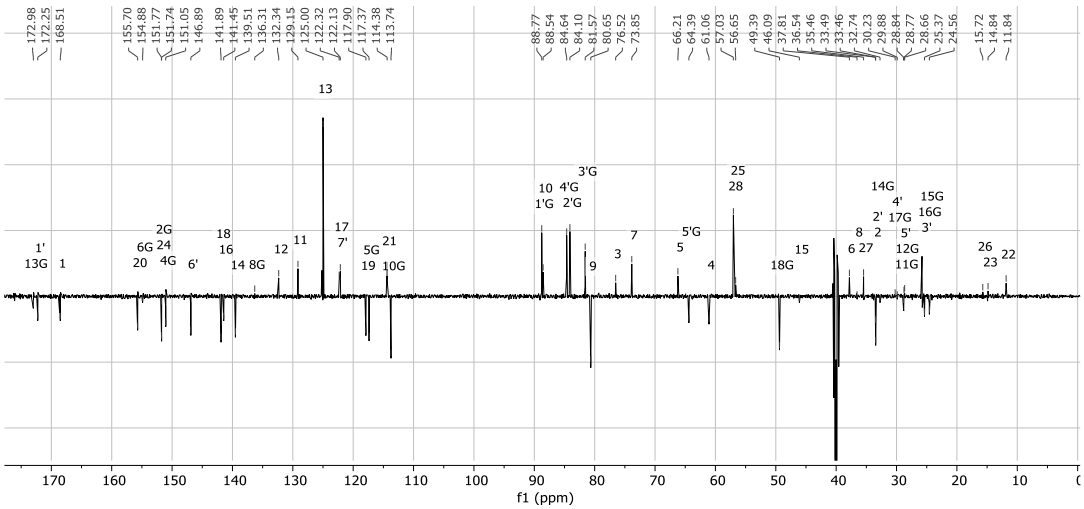
f1 (ppm)

Synthesis of (17)

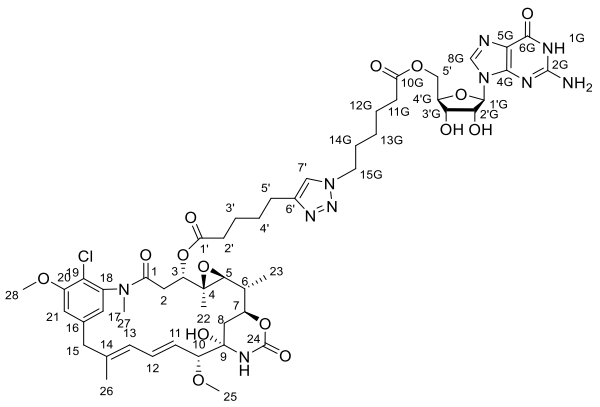

17

To compound **21** (18.3 mg, 0.016 mmol) was added aq. 70% HCOOH (650 µL) and the reaction was stirred for 4 hours at 40°C. Then, the solvent was removed under reduced pressure and the acid was co-evaporated by adding and evaporating three times MeOH. Purification of the crude with Biotage Isolera™ One System (gradient from 5% to 60% ACN in 22 CV) provided the products (11 mg, 62%) as white powders.

HRMS (ESI) m/z $[M+Na]^+$ 1117.4380 (calcd for $C_{51}H_{67}ClN_{10}O_{15}Na$ 1117.4374);

^{1}H (600 MHz, DMSO-d_6) δ 7.9 (s, 2H, 7', 8G), 7.3 – 7.2 (m, 1H, 21), 6.9 (s, 1H, NH), 6.8 – 6.7 (m, 1H, 17), 6.6 (s, 2H, NH_2), 6.6 (dd, *J* = 15.2, 11.2 Hz, 1H, 12), 6.2 (d, *J* = 11.1 Hz, 1H, 13), 5.7 (d, *J* = 5.1 Hz, 1H, 1'G), 5.4 (dd, *J* = 15.3, 8.9 Hz, 1H, 11), 4.6 (dd, *J* = 11.9, 2.3 Hz, 1H, 3), 4.4 (t, *J* = 5.1 Hz, 1H, 2'G), 4.3 (dd, *J* = 11.9, 3.7 Hz, 1H, 5'Ga), 4.2 (t, *J* = 7.1 Hz, 2H, 15G), 4.2 (dt, *J* = 12.8, 5.5 Hz, 2H, 3'G, 5'Gb), 4.1 (t, *J* = 11.9 Hz, 1H, 7), 4.0 (q, *J* = 4.8 Hz, 1H, 4'G), 3.9 (s, 3H, 28), 3.5 (d, *J* = 12.6 Hz, 1H, 15a), 3.5 (d, *J* = 8.8 Hz, 1H, 10), 3.3 (d, *J* = 12.7 Hz, 1H, 15b), 3.2 (s, 3H, 25), 2.9 (s, 3H, 27), 2.6 (q, *J* = 6.8 Hz, 2H, 5'), 2.6 (d, *J* = 9.7 Hz, 1H, 5), 2.5 – 2.4 (m, 3H, 2', 2b), 2.3 (dt, *J* = 7.8, 3.8 Hz, 2H, 11G), 2.0 (d, *J* = 11.9 Hz, 1H, 2a), 1.8 – 1.7 (m, 4H, 3', 14G), 1.6 (s, 5H, 4', 26), 1.6 – 1.4 (m, 4H, 6, 8b, 12G), 1.3 (d, *J* = 12.5 Hz, 1H, 8a), 1.2 (p, *J* = 7.6 Hz, 2H, 13G), 1.1 (d, *J* = 6.3 Hz, 3H, 23), 0.8 (s, 3H, 22).

^{13}C NMR (151 MHz, DMSO-d_6) δ 173.12 (10G), 172.25 (1'), 168.51 (1), 157.39 (6G), 155.70 (20), 154.41 (2G), 151.80 (4G), 151.73 (24), 146.90 (6'), 141.89 (18), 141.45 (16), 139.51 (14), 135.39 (8G), 132.34 (12), 129.14 (11), 125.19 (13), 122.32 (17), 122.14 (7'), 117.89 (19), 117.17 (5G), 114.37 (21), 88.53 (10), 87.14 (1'G), 81.77 (4'G), 80.63 (9), 76.52 (3), 73.85 (7), 73.55 (2'G), 70.74 (3'G), 66.21 (5), 64.29 (5'G), 61.06 (4), 57.03 (28), 56.65 (25), 49.39 (15G), 46.08 (15), 37.81 (6), 36.71 (8), 35.47 (27), 33.56 (2'), 33.49 (11G), 32.73 (2), 29.89 (14G), 28.81 (4'), 25.77 (5'), 25.36 (13G), 24.56 (12G), 24.20 (3'), 15.72 (26), 14.84 (23), 11.87 (22).

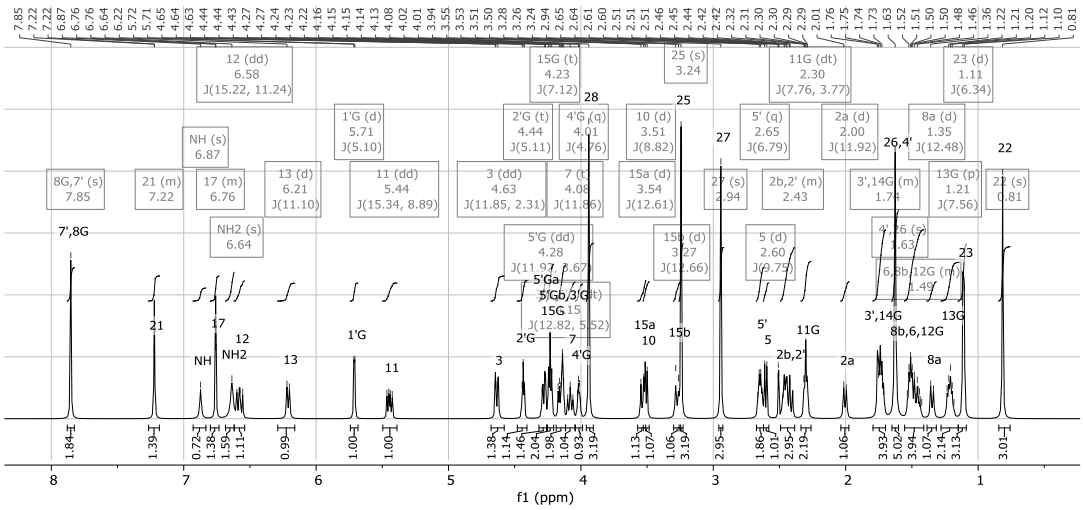
12 (dd) 6.58 J(15.22, 11.24)
NH (s) 6.87
8G,7' (s) 7.85
21 (m) 7.22
17 (m) 6.76
NH2 (s) 6.64
13 (d) 6.21 J(11.10)
1'G (d) 5.71 J(5.10)
11 (dd) 5.44 J(15.34, 8.89)
15G (t) 4.23 J(7.12)
2'G (t) 4.44 J(5.11)
4'G (q) 4.01 J(4.76)
3 (dd) 4.63 J(11.85, 2.31)
7 (t) 4.08 J(11.86)
10 (d) 3.51 J(8.82)
15a (d) 3.54 J(12.61)
25 (s) 3.24
27 (s) 2.94
11G (dt) 2.30 J(7.76, 3.77)
5' (q) 2.65 J(6.79)
2b,2' (m) 2.43
2a (d) 2.00 J(11.92)
8a (d) 1.35 J(12.48)
3',14G (m) 1.74
13G (p) 1.21 J(7.56)
22 (s) 0.81
23 (d) 1.11 J(6.34)
5'G (dd) 4.28 J(11.97, 8.67)
15b (d) 3.27 J(12.66)
5 (d) 2.60 J(9.75)
6,8b,12G (m) 1.49
7',8G
21
17
NH
12
NH2
13
1'G
11
3
2'G
7
4'G
15a
10
15b
27
5'
5
11G
2b,2'
2a
26,4'
3',14G
8b,6,12G
8a
13G
22
23
1.84
1.39
0.72
1.38
1.59
1.11
0.99
1.00
1.00
1.38
1.14
1.46
2.04
1.98
1.04
0.93
3.19
1.13
1.07
3.19
2.95
1.86
1.01
2.95
2.19
1.06
3.93
5.02
3.94
1.07
2.14
3.13
3.01
f1 (ppm)

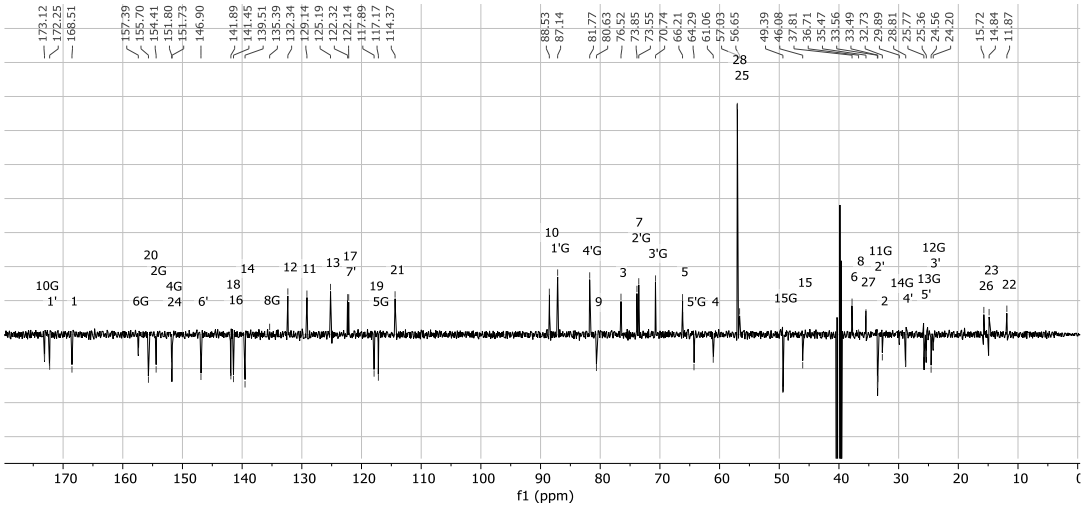
28
25
10G
1'
1
20
2G
6G
4G
24
6'
18
16
14
8G
12
11
13
7'
17
19
5G
21
10
1'G
4'G
9
7
2'G
3'G
3
5
5'G
4
15G
15
8
6
27
2
11G
2'
14G
4'
12G
3'
13G
5'
23
26
22
f1 (ppm)

Synthesis of (22)

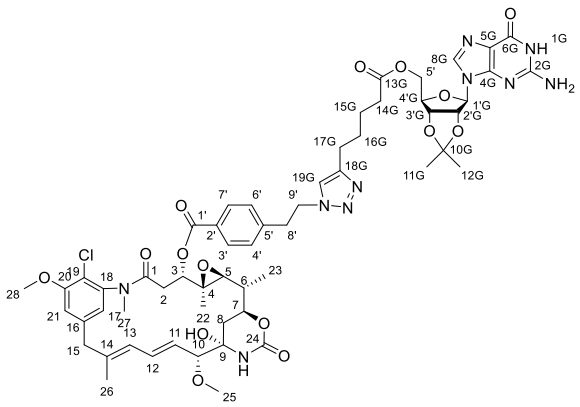

22

To a solution of **1h** (16 mg, 0.022 mmol) and **15** (14 mg, 0.032 mmol) in DMSO (482 µL) were added water (159 µL), $CuSO_4$*$5H_2O$ (10 mg, 0.035 mmol), then a solution of Na-ascorbate (28 mg, 0.139 mmol) in H_2O (82 µL) was added dropwise. The mixture was stirred at room temperature for 2 h. Then, water was added (1.4 mL) and the aqueous layer was extracted in DCM. The organic layer was washed with H_2O and brine, dried over Na_2SO_4 and concentrated in *vacuum*. Purification of the crude with Biotage Isolera™ One System (gradient from 5% to 60% ACN in 22 CV) provided the products (22 mg, 85%) as white powders.

HRMS (ESI) m/z $[M+Na]^+$ 1191.4546 (calcd for $C_{57}H_{69}ClN_{10}O_{15}Na$ 1191.4530).

^1H (600 MHz, DMSO-d_6) δ 7.9 – 7.8 (m, 3H, 3', 7', 8G), 7.8 (s, 1H, 19G), 7.5 (d, *J* = 8.1 Hz, 2H, 4', 6'), 7.2 (s, 1H, 21), 6.9 (s, 1H, 17), 6.8 (s, 1H, NH), 6.7 (s, 2H, NH_2), 6.5 (dd, *J* = 15.2, 11.2 Hz, 1H, 12), 6.0 – 6.0 (m, 1H, 1'G), 5.9 (d, *J* = 11.0 Hz, 1H, 13), 5.3 (dd, *J* = 6.2, 1.6 Hz, 1H, 2'G), 5.1 (dd, *J* = 6.0, 3.4 Hz, 1H, 3'G), 4.9 (dd, *J* = 15.4, 9.1 Hz, 1H, 11), 4.7 (dd, *J* = 12.0, 2.6 Hz, 1H, 3), 4.6 (t, *J* = 7.2 Hz, 2H, 9'), 4.3 – 4.2 (m, 2H, 4'G, 5'Gb), 4.2 – 4.1 (m, 2H, 5'Ga, 7), 4.0 (s, 3H, 28), 3.4 (d, *J* = 12.6 Hz, 1H, 15a), 3.4 (d, *J* = 9.2 Hz, 1H, 10), 3.3 (d, *J* = 7.7 Hz, 3H, 8', 15b), 3.2 (s, 3H, 25), 3.0 (s, 3H, 27), 2.8 (d, *J* = 9.7 Hz, 1H, 5), 2.6 – 2.6 (m, 1H, 2a), 2.5 (d, *J* = 6.7 Hz, 2H, 17G), 2.3 – 2.2 (m, 3H, 2b, 14G), 1.6 (s, 3H, 26), 1.5 (s, 3H, 12G), 1.5 – 1.4 (m, 6H, 6, 8b, 15G, 16G), 1.3 (s, 4H, 8a, 11G), 1.1 (d, *J* = 6.3 Hz, 3H, 23), 0.8 (s, 3H, 22).

^{13}C NMR (151 MHz, DMSO-d_6) δ 173.00 (13G), 168.45 (1), 165.68 (1'), 157.38 (6G), 155.90 (20), 154.38 (2G), 151.67 (24), 150.99 (4G), 146.84 (18G), 144.00 (5'), 141.94 (18), 141.63 (16), 139.47 (14), 136.09 (8G), 132.25 (12), 129.91 (3', 7'), 129.20 (4', 6'), 129.04 (11), 128.44 (2'), 124.97 (13), 122.20 (17), 121.96 (19G), 117.98 (19), 117.39 (5G), 114.24 (21), 113.76 (10G), 88.91 (10), 88.76 (1'G), 84.62 (4'G), 84.10 (2'G), 81.51 (3'G), 80.43 (9), 76.85 (3), 73.73 (7), 65.84 (5), 64.40 (5'G), 61.10 (4), 57.09 (28), 56.54 (25), 50.23 (9'), 46.13 (15), 38.42 (6), 36.72 (8), 36.09 (8'), 35.54 (27), 33.35 (2, 14G), 28.67 (15G), 27.46 (11G, 12G), 25.06 (17G), 24.28 (16G), 15.78 (26), 15.03 (23), 12.53 (22).

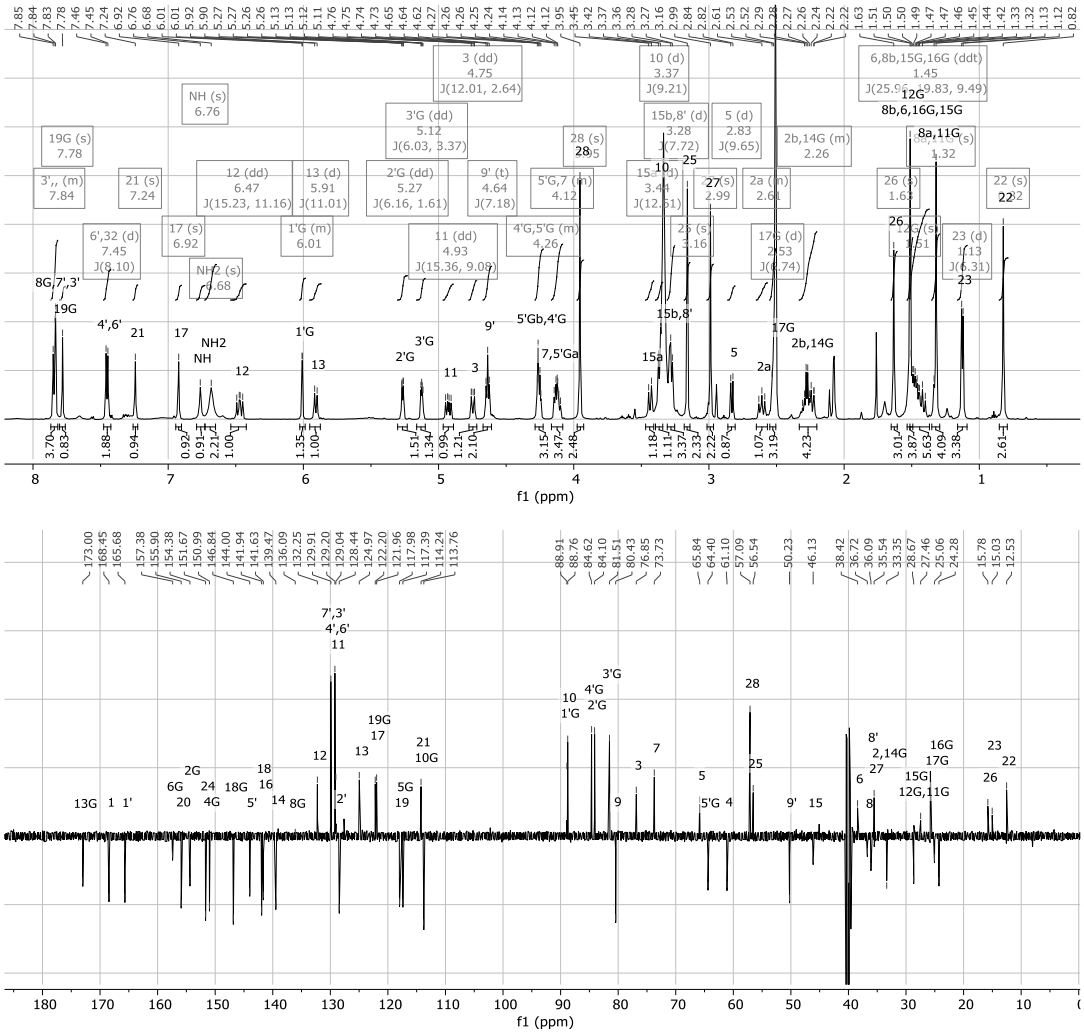
f1 (ppm)
f1 (ppm)

Synthesis of (20)

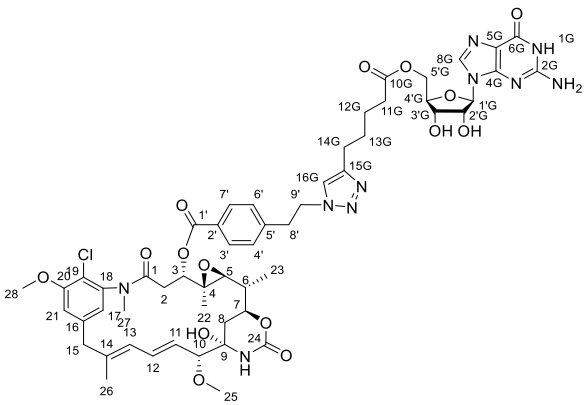

20

To compound **22** (11 mg, 0.009 mmol) was added aq. 70% HCOOH (235 µL) and the reaction was stirred for 4 hours at 40°C. Then, the solvent was removed under reduced pressure and the acid was co-evaporated by adding and evaporating three times MeOH. Purification of the crude with Biotage Isolera™ One System (gradient from 5% to 60% ACN in 22 CV) provided the products (8 mg, 77%) as white powders.

HRMS (ESI) m/z $[M+Na]^+$ 1151.4226 (calcd for $C_{54}H_{65}ClN_{10}O_{15}Na$ 1151.4217);

^{1}H (600 MHz, DMSO-d_6) δ 7.8 (d, J = 7.1 Hz, 3H, 3', 7', 8G), 7.8 (s, 1H, 16G), 7.5 (d, J = 8.1 Hz, 2H, 4', 6'), 7.2 (s, 1H, 21), 6.9 (s, 1H, 17), 6.8 (s, 1H, 1G), 6.7 (s, 2H, NH_2), 6.5 (dd, J = 15.2, 11.3 Hz, 1H, 12), 5.9 (d, J = 11.1 Hz, 1H, 13), 5.7 (d, J = 5.1 Hz, 1H, 1'G), 4.9 (dd, J = 15.5, 9.1 Hz, 1H, 11), 4.7 (dd, J = 12.0, 2.7 Hz, 1H, 3), 4.6 (t, J = 7.1 Hz, 2H, 9'), 4.4 (t, J = 5.0 Hz, 1H, 2'G), 4.3 (dd, J = 11.8, 3.3 Hz, 1H, 5'Ga), 4.2 – 4.1 (m, 3H, 3'G, 5'Gb, 7), 4.0 (q, J = 4.5 Hz, 1H, 4'G), 4.0 (s, 3H, 28), 3.4 (d, J = 12.5 Hz, 1H, 15b), 3.4 (d, J = 9.0 Hz, 1H, 10), 3.3 – 3.2 (m, 3H, 8', 15a), 3.2 (s, 3H, 25), 3.0 (s, 3H, 27), 2.8 (d, J = 9.7 Hz, 1H, 5), 2.6 (t, J = 13.9 Hz, 1H, 2a), 2.6 – 2.5 (m, 2H, 14G), 2.3 (q, J = 7.4 Hz, 2H, 11G), 2.2 (d, J = 12.1 Hz, 1H, 2b), 1.6 (s, 3H, 26), 1.6 – 1.5 (m, 4H, 12G, 13G), 1.5 – 1.4 (m, 2H, 6, 8a), 1.3 (d, J = 12.6 Hz, 1H, 8b), 1.1 (d, J = 6.3 Hz, 3H, 23), 0.8 (s, 3H, 22).

^{13}C NMR (151 MHz, DMSO-d_6) δ 173.13 (10G), 168.47 (1), 165.71 (1'), 157.35 (6G), 155.91 (20), 154.40 (2G), 151.80 (4G), 151.70 (24), 146.87 (15G), 144.02 (5'), 141.94 (18), 141.65 (16), 139.48 (14), 136.22 (8G), 132.27 (12), 129.92 (3', 7'), 129.23 (4', 6'), 129.07 (11), 128.45 (2'), 124.98 (13), 122.21 (17), 121.97 (16G), 117.97 (19), 117.16 (5G), 114.26 (21), 88.91 (10), 87.13 (1'G), 81.81 (4'G), 80.43 (9), 76.86 (3), 73.73 (2'G), 73.59 (7), 70.76 (3'G), 65.86 (5), 64.33 (5'G), 61.10 (4), 57.10 (28), 56.56 (25), 50.23 (9'), 46.12 (15), 39.57, 38.42 (6), 37.78 (8), 36.08 (8'), 35.55 (27), 33.49 (2), 33.46 (11G), 28.70 (12G), 25.09 (14G), 24.37 (13G), 15.78 (26), 15.04 (23), 12.52 (22).

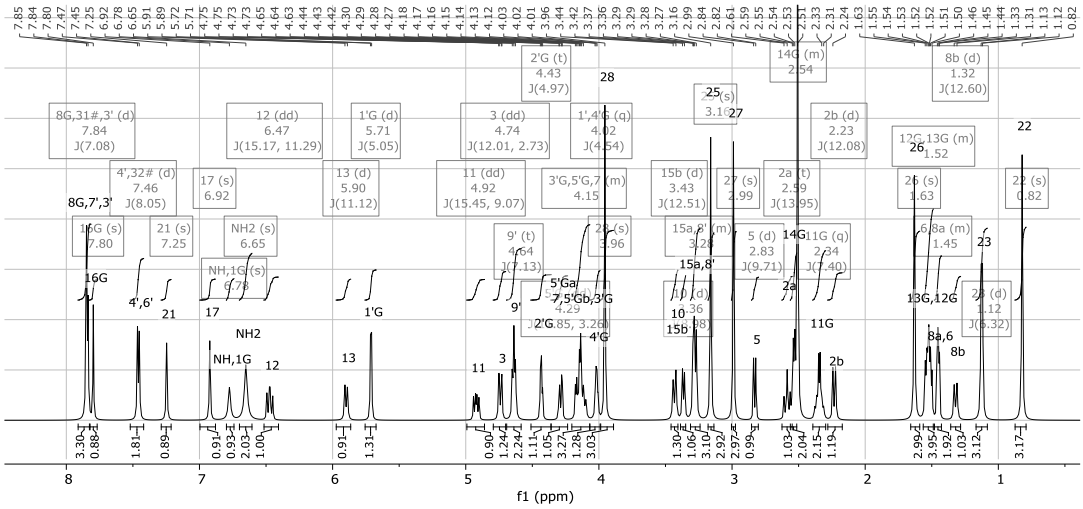
8G,31#,3' (d) 7.84 J(7.08)
4',32# (d) 7.46 J(8.05)
16G (s) 7.80
21 (s) 7.25
17 (s) 6.92
NH2 (s) 6.65
NH,1G (s) 6.78
12 (dd) 6.47 J(15.17, 11.29)
13 (d) 5.90 J(11.12)
1'G (d) 5.71 J(5.05)
11 (dd) 4.92 J(15.45, 9.07)
3 (dd) 4.74 J(12.01, 2.73)
2'G (t) 4.43 J(4.97)
1',4'G (q) 4.02 J(4.54)
3'G,5'G,7' (m) 4.15
15b (d) 3.43 J(12.51)
27 (s) 2.99
2a (t) 2.59 J(13.95)
14G (m) 2.54
2b (d) 2.23 J(12.08)
8b (d) 1.32 J(12.60)
12G,13G (m) 1.52
26 (s) 1.63
22 (s) 0.82
f1 (ppm)

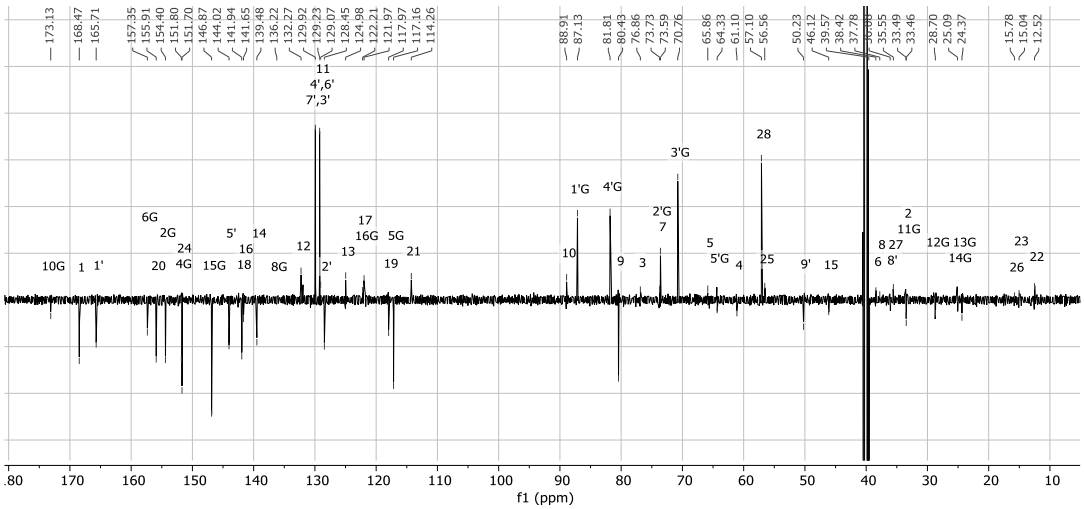
f1 (ppm)

5.2 Cell Biology

Determination of the binding constant (Kb)

A mix of 10nM tubulin in PEDTA buffer (10 mM NaPi, 1 mM EDTA, 0.1 mM GTP and 1.5 mM $MgCl_2$) with 10nM FcMaytansine was incubated at 25ºC with increasing amounts of the different compounds. Up 2.5μM of maytansine was used as a control, while a concentration up to 10μM was employed for maytansinoids. The range was increased to 15μM for **17** and **20**. The competition assay was monitored measuring the anisotropy of the compounds in an Appliskan (Thermo Fisher Scientific) plate reader with excitation and emission wavelengths of 485 nm and 535 nm, respectively.

Determination of the dose-response on tubulin dynamic

25 μM tubulin in GAB buffer (10 mM NaPi, 30% Glycerol, 1 mM EGTA, 6 mM $MgCl_2$ and 1 mM GTP) was polymerized at 37 ºC in the presence of different concentrations of the compounds up to 27.5 μM. DMSO (vehicle) and 27.5 μM of maytansine were used as controls. Polymerisation was monitored by means of the absorbance at 350 nm in a Multiskan (ThermoFisher) plate reader.

Determination of the cell viability (IC50)

Human A549 non-small lung carcinoma cells, human ovarian carcinomas A2780 and A2780AD (MDR overexpressing P-glycoprotein) were cultured at 37 ºC in RPM-1640 supplemented with 10% fetal calf serum, 2 mM L-glutamine, 40 μg/ml gentamycin, 100 IU/ml penicillin and 100 μg/ml streptomycin in a 5% CO_2 air atmosphere. Anti-proliferation assays were performed as described.[88] The statistical significance of differences in IC50 values were evaluated using the t-test option implemented in the Sigma Plot 13 software package (version 14.5, Systat Software, Inc., San Jose, CA, USA).

Indirect immunofluorescence images were obtained using A549 cells plated at a density of 130,000 cells/ml onto 12mm round coverslip, cultured overnight and treated with growing amounts of the ligands or drug vehicle (DMSO) for 24 h. DMSO was always less than 0.5%. Cells were permeated using Triton X-100 and fixed with 3.7 formaldehyde as previously described.[89] Cells were incubated with a DM1A monoclonal antibody reacting with α-tubulin. After that, samples were washed, incubated with FITC goat anti-mouse antibody and 1 mg/ml Hoechst 33342 was added to stain chromatin. The slides were examined and photographed with a Zeiss Axioplan epicfluorescence microscope and images were recorded using an ORCH-FLASH 4.2 cooled CCD camera.

5.3 Docking analysis

The high-resolution crystallographic structure used for the docking studies of the synthesised maytansinoids was obtained from the Protein Data Bank (PDB) entry with ID 4TV81. The molecular structure of each derivative was designed using the Build Structure tool implemented in UCSF Chimera 1.142 by modifying the crystal structure of the maytansine molecule. Docking input files for the β-tubulin protein and ligand structures were prepared with UCSF Chimera 1.142. The original conformation of the macrocycle was derived from the crystalline structure of maytansine. To validate the results of the computational modelling experiments, the best conformer of each maytansinoid was superimposed on its corresponding crystal structure.

5.4 Crystallography

Crystals of the T_2R-TTL complex were prepared as previously described by Prota *et al.*[87b] using the vapor diffusion method. Crystals were grown over two days at room temperature in buffer containing PEG 4K (3%), glycerol (4%), $MgCl_2$ (30 mM), $CaCl_2$ (30 mM), tyrosine (5 mM) and MES/imidazole pH 6.5 (100 mM). The maytansinoid compounds were soaked into the crystals over 6 hours, at 2.5 mM final concentration. Before flash-cooling in liquid nitrogen, crystals were successively transferred into cryo-protectant solutions containing the

88 R. M. Buey, I. Barasoain, et al., *Chem. Biol.* **2005**, *12*, 1269–1279.

89 C. D. I. Biologicas, C. Superior, et al., **1994**, 75–84.

crystallization buffer with increased concentrations of PEG 4K (10%) and glycerol (16% and 22%). X-Ray diffraction data were collected at beamline X06DA of the Swiss Light Source (Paul Scherrer Institute, 5232 Villigen PSI, Switzerland) at 100 K and 1.0 Å wavelength. The obtained datasets were processed using XDS[90] and the structures were determined by the difference Fourier method in PHENIX[91] using the phases of a T_2R-TTL model in the absence of solvent molecules (modified from PDB ID: 5LXT). After one cycle of rigid-body refinement with grouped atomic displacement parameters (ADP), followed by several cycles of restrained individual coordinate and isotropic ADP refinement, ligand-shaped difference density was observed within the maytansine sites of all crystal structures. Waters were added using PHENIX and geometry, Ramachandran and rotamer outliers were corrected in Coot.[92] The geometries of the compounds were energy-minimized in Moloc[93] and restraints for refinement were generated using the eLBOW tool in PHENIX. The ligands were positioned within the difference density and refined in several cycles of restrained refinement. MolProbity[94] was used for model validation. In the final models only small root-mean-square deviations (rmsd) from the ideal bond lengths and angles were accepted. The molecular graphics were generated in PyMOL (the PyMOL Molecular Graphics System Version 2.3.2, Schrödinger, LLC).

90 W. Kabsch, *Acta Crystallogr. Sect. D Biol. Crystallogr.* **2010**, *66*, 125–132.

91 P. D. Adams, P. V. Afonine, et al., *Acta Crystallogr. Sect. D Biol. Crystallogr.* **2010**, *66*, 213–221.

92 P. Emsley, B. Lohkamp, et al., *Acta Crystallogr. Sect. D Biol. Crystallogr.* **2010**, *66*, 486–501.

93 P. R. Gerber, K. Müller, *J. Comput. Aided. Mol. Des.* **1995**, *9*, 251–268.

94 I. W. Davis, L. W. Murray, et al., *Nucleic Acids Res.* **2004**, *32*, W615-619.

Chapter III Enantioselective Total Synthesis of Cannabidiol-C_4

Phytocannabinoids indicate the terpenophenolic molecules naturally contained within the *Cannabis* plant. Cannabis extracts have been used for centuries and in different areas of the world for both recreational and medical purposes. There is evidence of the therapeutic effects of *Cannabis* against some symptoms, but although many cannabinoids demonstrate biological activity, they have not been well studied due to the difficulty of isolation. A synthetic source of them, as well as the creation of derivative analogues, would allow a greater understanding of the effects. Cannabidiol is the main cannabinoid of cannabis extracts, however cannabidiol-C_4 is also present. This molecule has always been extracted in complex mixtures with other natural products present in the plant, consequently making isolation impossible. Hence the need for a synthetic way to obtain the compound.

1 Introduction

Cannabis (**Figure 1.1**) is a genus of angiosperm plants from the *Cannabaceae* family. It originated in the valleys of Asia along the slopes of the Himalayas, and many cultures have traditionally used it for different purposes. Initially, it was grown on a large scale in China for fibre and seed production and later for resin production in India. *Cannabis* species from European and Asian regions were generally low in tetrahydrocannabidiol (THC, <1%) and high in cannabidiol content (CBD, 20-40%). On the other hand, African, Middle Eastern, South and Southeast Asian cultures used it extensively for its psychoactive effects as the available plants were rich in THC (5-10%) with variable CBD content (0-5%). The three species of *Cannabis* identified (*Cannabis Sativa*, *Cannabis Indica* and *Cannabis Ruderalis*)[95] were spread throughout the West and the modern varieties of drugs used as medical *Cannabis* derive from these two original gene pools. The psychotic, dietary and fibre properties have encouraged domestication as a cultivated plant and accelerated the distribution around the world in natural and artificial environments more recently.

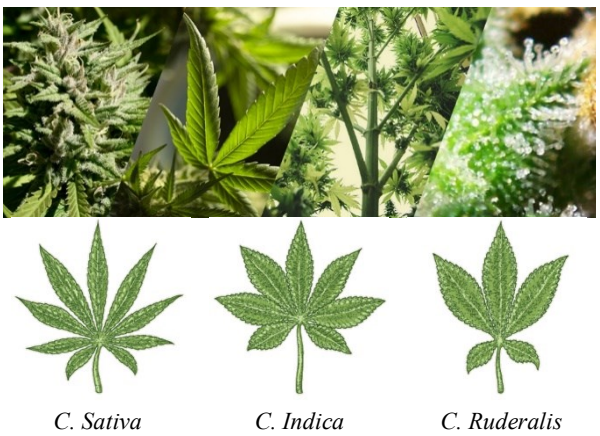

Figure 1.1 *Cannabis* anatomy: female flowers, leafs, stem, trichomes.

Cannabis contains a broad chemical class of compounds, e.g., mono- and sesquiterpenes, sugars, hydrocarbons, steroids, flavonoids, nitrogenous compounds, amino acids, and others that make the composition complex. More than 540 molecules have been identified[96] that are divided into 120 cannabinoids and 420 non-cannabinoids. In recent decades, the name "cannabinoid" has become increasingly vague. The term was originally coined in the phytochemical field to refer to a class of meroterpenoids typical of *Cannabis*; subsequently the word was associated with the main psychotropic constituent of marijuana losing its meaning. The effects caused mainly consist in the inhibition of pain and generation of the sensation of pleasure due to the binding of cannabinoids with the

95 W. A. Emboden, *Econ. Bot.* **1974**, *28*, 304–310.

96 H. Peng, F. Shahidi, *J. Agric. Food Chem.* **2021**, *69*, 1751–1774.

CB1 and CB2 receptors (Cannabinoid Receptor types 1 and 2) located respectively in the central nervous system and in the immune system. The mechanism of action prevents the production of biomolecules involved in pain perception and induces the release of dopamine at levels higher than those observed in response to natural stimuli. Instead, components such as terpenes and flavonoids have different kinds of effects.[97] More than 100 identified terpenes are present as monoterpenes, sesquiterpenes, and triterpenes, and are responsible for the aroma in different *Cannabis* varieties due to their high volatility. Pharmacological activity is described as anti-inflammatory, analgesic, and anticonvulsant; in addition, they modulate the activity of THC and the receptors involved. Twenty are the flavonoids identified in the plant; they have a phenolic structure and activities shared with the terpenes.

The structural characteristic of phytocannabinoids is a resorcinic nucleus decorated with *para*-oriented terpenyl and pentyl groups, or with compounds having different degrees of isoprenylation, or with a shortened alkyl group. Among these compounds, cannabinoids such as cannabidiol (CBD) are non-psychoactive compounds, while Δ9-tetrahydrocannabidiol (Δ^9-THC), cannabinol (CBN), and cannabinodiol (CBND) are known to be psychoactive.[98] Terpenophenols and decarboxylated, oxidised and reduced derivatives obtained from metabolic transformations of primary molecules belong to the C_{21} group of cannabinoids (**Figure 1.2**). The content of secondary

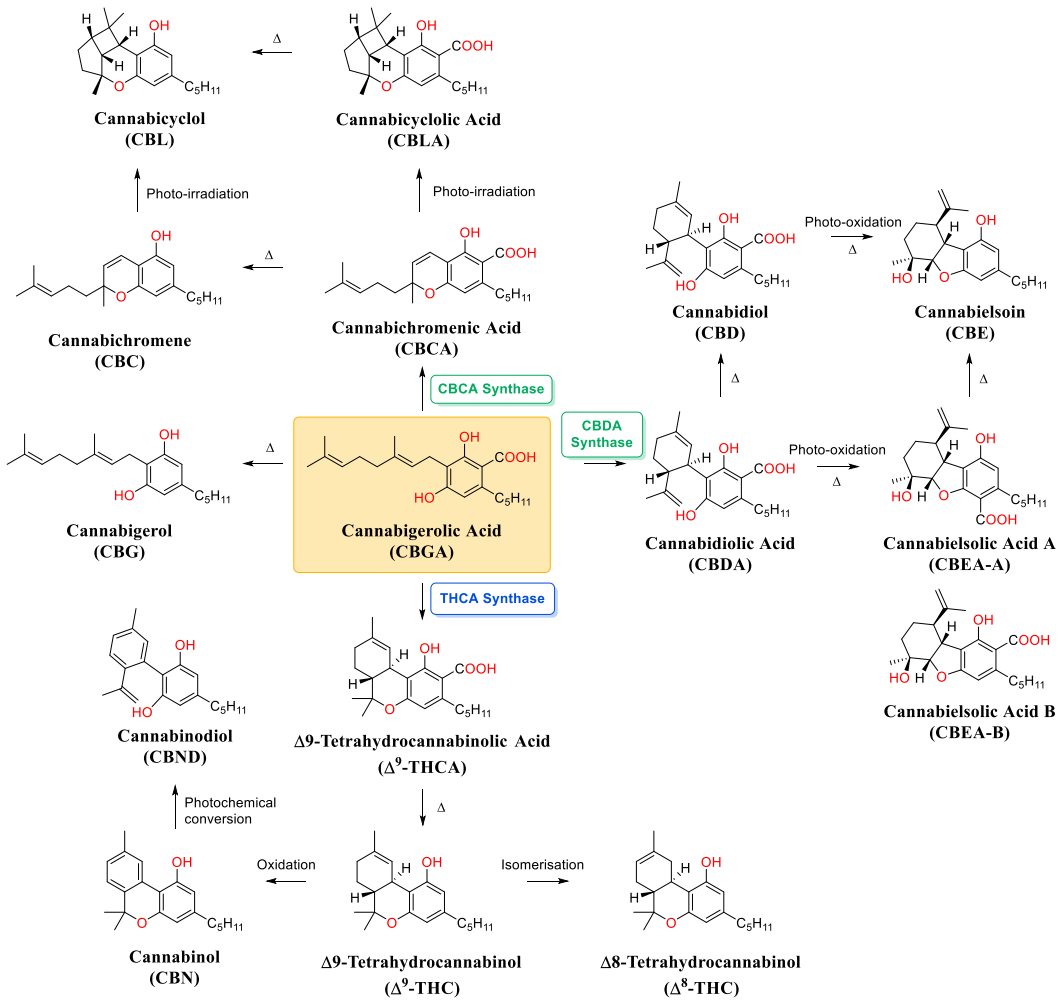

Figure 1.2 Biosynthesis of major phytocannabinoids starting from CBGA.

97 **a]** V. Borgonetti, P. Governa, et al., *Curr. Bioact. Compd.* **2019**, *15*, 147–158; **b]** J. K. Booth, J. Bohlmann, *Plant Sci.* **2019**, *284*, 67–72.

98 R. Pertwee, Ed. , *Handbook of Cannabis*, Oxford University Press, **2014**.

metabolites constrains the classification into two subclasses according to the enzyme responsible for the biosynthesis of cannabinoids:[99]

- CBD chemotype, characterised by the CBDA-synthase enzyme that distinguishes hemp destined for agroindustrial and therapeutic uses;
- THC chemotype, characterised by the THCA-synthase enzyme present in the varieties of *Cannabis* destined to produce inflorescences and medicaments.

During the biosynthesis of various phytocannabinoids, cannabigerolic acid (CBGA) synthesised from geraniol and C_{12} polyketides by CBGA synthase in *Cannabis*[100] is the key branching point for a number of cannabinoids such as Δ^9-THC, CBD, cannabielsoin (CBE), cannadichromene (CBC), cannabicyclol (CBL), and their relative analogs.[96,101] This pathway consists of four types of reactions: enzymatic catalysis, thermal reaction, oxidation, and irradiation. The conversion of CBGA to Δ^9-THCA, cannabidiolic acid (CBDA), and cannabicromenic acid (CBCA) is catalysed by the corresponding synthases.[101bc] CBCA and CBC can be further converted to cannabicyclolic acid (CBLA) and CBL, respectively, when exposed to UV light irradiation.[102] Δ^9-THC is transformed into CBN through oxidative aromatisation,[101b] and CBN can be photochemically rearranged into CBND.

However, chemical composition, pharmacological profiling, and complete physiological effects of *Cannabis* remain to be fully understood.[103] Thus, the huge variety of compounds contained and the possibility of interaction between them make the chemistry of cannabis complex, preventing the approval as a medicine. [104]

1.1 C_{21} cannabinoid analogs in *Cannabis*

As mentioned, more than 100 phytocannabinoids have been identified, but many remain poorly described and characterised. They are divided in 10 subclasses, depending on the structure.

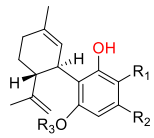

CBD-type

Cannabidiol (CBD) was isolated in 1940[105] and all of the known CBD-type cannabinoids have *trans*-(3*R*,4*R*) absolute configuration. Despite the structural similarity between CBD and Δ^9-THC, CBD is an allosteric negative modulator of CB1 and CB2 receptors.[106] CBD exerts pharmacological effects through specific molecular targets such as adenosine, glycine, opioid, serotonin, nonendocannabinoid G protein-coupled, nicotinic acetylcholine, and proliferator-activated receptors.[107] In addition, CBD shows medical evidence as painkiller, anticonvulsant, antispasmodic, anxiolytic, antinausea, antirheumatoid arthritis, and neuroprotective properties.[106] Recently, it has been demonstrated that CBD is an inverse agonist for G protein-coupled orphan receptors, such as GPR3, GPR6, and GPR12, suggesting new therapeutic uses of CBD for Alzheimer's and Parkinson's.[108]

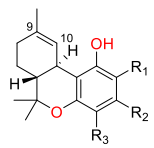

Δ^9-THC-type

The structure of tetrahydrocannabinol (THC) was unknown until 1964, when Gaoni and Mechoulam isolated Δ^9-THC and used NMR to assign the double bond position and the *trans*-(6a*R*, 10a*R*) configuration.[109] Δ^9-THC has the highest psychoactive effects among cannabinoids.[106] This compound is a partial agonist at both CB1 as a modulator of psychoactive effects, and CB2 as a modulator of immunological and anti-inflammatory effects. The psychoactive effects of Δ^9-THC include anxiety, paranoia, perceptual alterations, and cog-

99 M. M. Lewis, Y. Yang, et al., *ACS Omega* **2017**, *2*, 6091–6103.

100 **a]** M. A. ElSohly, Ed. , *Marijuana and the Cannabinoids*, Humana Press, **2007**; **b]** F. Taura, S. Tanaka, et al., *FEBS Lett.* **2009**, *583*, 2061–2066.

101 **a]** B. De Backer, K. Maebe, et al., *J. Forensic Sci.* **2012**, *57*, 918–922; **b]** S. Morimoto, K. Komatsu, et al., *Phytochemistry* **1998**, *49*, 1525–1529.

102 **a]** Y. Shoyama, R. Oku, et al., *Chem. Pharm. Bull.* **1972**, *20*, 1927–1930; **b]** Y. Shoyama, T. Fujita, et al., *Chem. Pharm. Bull.* **1968**, *16*, 1157–1158.

103 **a]** M. M. Radwan, M. A. ElSohly, et al., *J. Nat. Prod.* **2015**, *78*, 1271–1276; **b]** S. A. Ahmed, S. A. Ross, et al., *Phytochemistry* **2015**, *117*, 194–199.

104 M. A. ElSohly, D. Slade, *Life Sci.* **2005**, *78*, 539–548.

105 R. Adams, M. Hunt, J. H. Clark, *J. Am. Chem. Soc.* **1940**, *62*, 196–200.

106 **a]** R. G. Pertwee, *Br. J. Pharmacol.* **2008**, *153*, 199–215; **b]** C. Casajuana Kögel, A. Gual, et al., *Adicciones* **2018**, *30*, 140–151.

107 C. Ibeas Bih, T. Chen, et al., *Neurotherapeutics* **2015**, *12*, 699–730.

108 A. S. Laun, S. H. Shrader, et al., *Acta Pharmacol. Sin.* **2019**, *40*, 300–308.

109 **a]** Y. Gaoni, R. Mechoulam, *J. Am. Chem. Soc.* **1964**, *86*, 1646–1647; **b]** R. Mechoulam, Y. Gaoni, *Tetrahedron Lett.* **1967**, *8*, 1109–1111.

nitive deficits. All of these CB1-mediated effects are caused by disruption of GABA (γ-aminobutyric acid)/glutamatergic neurotransmission and dopamine release. It also causes hypolocomotion, hypothermia, catalepsy, analgesia, and increased food intake. The effects produced are generally acute, transient and self-limiting. In addition to Δ^9 there is the Δ^8 isomer of THC in nature, which has a different double bond position and is about 20% less active than Δ^9-THC.

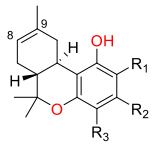

Δ^8-THC-type

In addition to Δ^9-THC there is the Δ^8 isomer of THC in nature, which has a different 8-9 double bond position. The compound is approximately 20% less active than Δ^9-THC and thermodynamically more stable.[100a]

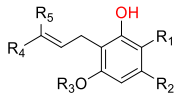

CBG-type

Cannabigerol (CBG) was the first compound isolated from the resin of marijuana as a pure chemical substance.[110] Although CBG-type compounds are inactive compared to Δ^9-THC,[111] they show considerable antibacterial activity against gram-positive bacteria.[112]

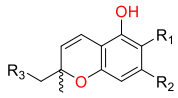

CBC-type

Cannabichromene (CBC) is one of the hundreds of cannabinoids found in the *Cannabis* plant[113] and has a structural similarity to THC and CBN. CBC and its derivatives are abundant in *Cannabis* and it is not scheduled as psychotropic substances. CBC has shown anticancer effects in breast cancer xenoplants in mice[114] and has anticonvulsant activity.[115] Starting from 2017, CBC is under research to identify the possible pharmacological properties. *In vitro*, CBC is not active on CB1 or CB2 receptors, but is a TRPA1 (Transient Receptor Potential cation channel, subfamily A, member 1), TRPV3, and TRPV4 (Transient Receptor Potential cation channel, subfamily V, member 3 and 4) agonist.[113]

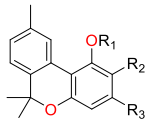

CBN-type

Cannabinol-type cannabinoids (CBN) are the fully aromatised derivatives of THC and were first isolated in the late 1800s. The first structure was determined in the 1930s and it was obtained by chemical synthesis in 1940.[116] The concentration of CBN in cannabis products increases as cannabis ages because of the degradation of THC.[104] CBN acts as a weak agonist of CB1 receptor, but has a higher affinity for CB2 receptor although it is lower than THC. The information on this cannabinoid is still few due to the poor studies, but its percentage in medical cannabis is often considered alongside THC and CBD because it reduces insomnia and increases appetite.

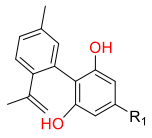

CBND-type

Cannabinodiol-type cannabinoids (CBND) are the fully aromatised derivatives of CBD and produced by the photochemical conversion of CBN.[114] It is a psychoactive cannabinoid[99] present at low concentrations in the plant and therefore slight information is available. CBND being an aromatic type of CBD has no direct interaction with cannabinoid receptors; rather, it stimulates the endocannabinoid system in the human body to produce its own cannabinoids.

110 Y. Gaoni, R. Mechoulam, *Proc. Chem. Soc.* **1964**, 82.

111 **a]** Y. Grunfeld, H. Edery, *Electroencephalogr. Clin. Neurophysiol.* **1969**, *27*, 219–20; **b]** R. Mechoulam, A. Shani, et al., *Science (80-.).* **1970**, *169*, 611–612.

112 R. Mechoulam, Y. Gaoni, *Tetrahedron* **1965**, *21*, 1223–1229.

113 S. E. Turner, C. M. Williams, et al., **2017**, pp. 61–101.

114 A. Ligresti, A. S. Moriello, et al., *J. Pharmacol. Exp. Ther.* **2006**, *318*, 1375–1387.

115 L. L. Anderson, A. Ametovski, et al., *ACS Chem. Neurosci.* **2021**, *12*, 330–339.

116 R. G. Pertwee, *Br. J. Pharmacol.* **2006**, *147*, S163–S171.

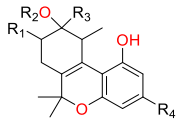

CBT-type

Cannabitriol (CBT) was first isolated in 1966 and the structure determined in 1976.[117] Scientists have since analysed and confirmed the presence of at least nine different types of CBT in the plant, each with a slight difference in the molecular structure. Its pharmacology has been little studied, though it has been found to act as an antiestrogen and aromatase inhibitor.[118]

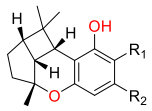

CBL-type

Cannabicyclol (CBL) is a non-psychotropic cannabinoid found in the *Cannabis* plant for the first time in 1967.[119] It is a degradation product of CBC by light activated conversion. It has 16 stereoisomers and, like other cannabinoids, further studies are needed to verify its properties.

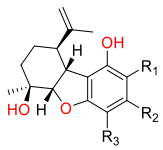

CBE-type

The first mention of cannabielsoin (CBE) in the literature dates back to 1973,[120] although no details on the structure are provided. Subsequently the structure and the absolute configuration were established by synthesising CBE-C_5 and comparing it with the CBE obtained by decarboxylation of the natural cannabielsoin acid.[121]

Several miscellaneous cannabinoid derivatives are considered in addition to these subclasses. They have unusual structures e.g. with a furano ring (dehydrocannabifuran, cannabifuran), carbonyl function (cannabichromanon, 10- oxo-δ-6a-tetrahydrocannabinol), or tetrahydroxy substitution (cannabiripsol).

1.2 *Cannabis* and cannabinoids in medicine

Cannabis Sativa has been classified as an illegal substance, but it has also been classified as medicinal due to the interesting therapeutic properties. While THC has been one of the cannabinoids of greatest interest in recent decades, CBD is now receiving most of the attention. This non-psychoactive compound is the subject of studies that explore and confirm the potential of cannabis as a medicinal substance. CBD is believed to have physiological and psychological modifying effects on the primary psychoactive compound THC. Therefore, it can have modulatory effects on THC useful in a medical context. However, the use of cannabinoids does not involve a cure, but their function is mainly palliative to relieve or counter the side effects that most traditional therapies cause in an attempt to cure diseases or medical conditions.[122]

Medical use concerns analgesia in pathologies involving spasticity associated with pain (e.g. multiple sclerosis and spinal cord injury), analgesia in chronic pain with particular reference to neurogenic pain, the stimulating effect of appetite in diseases such as anorexia or in cancer or AIDS patients, and the reduction of involuntary body and facial movements such as Tourette's syndrome.

Multiple sclerosis is a chronic autoimmune inflammatory disease of the central nervous system where the cells of the immune system stop recognising myelin, an insulating lipid structure that surrounds the extensions of neurons and ensures rapid and efficient transmission of the nerve impulse. The autoimmune reaction attacks myelin in multiple places causing lesions in the central nervous system. Symptoms largely depend on the location of the lesions and can be sensory (tingling, numbness, pain), motor (difficulty in coordination, muscle spasms, exhaustion), and cognitive (memory impairment, speech disorders). Pharmacological approaches are for the most

117 **a]** Y. Obata, Y. Ishikawa, *Agric. Biol. Chem.* **1966**, *30*, 619–620; **b]** W. R. Chan, K. E. Magnus, H. A. Watson, *Experientia* **1976**, *32*, 283–284.

118 **a]** S. Baroi, A. Saha, et al., *Dhaka Univ. J. Pharm. Sci.* **2020**, *19*, 47–58; **b]** B. Kikiowo, A. J. Ogunleye, et al., *Recent Pat. Anticancer. Drug Discov.* **2021**, *16*, 273–284.

119 F. Korte, H. Sieper, *J. Chromatogr. A* **1964**, *13*, 90–98.

120 C. A. L. Bercht, R. J. J. Lousberg, et al., *J. Chromatogr. A* **1973**, *81*, 163–166.

121 **a]** A. Shani, R. Mechoulam, *J. Chem. Soc. D Chem. Commun.* **1970**, 273; **b]** F. J. E. M. Küppers, R. J. J. C. Lousberg, et al., *Tetrahedron* **1973**, *29*, 2797–2802.

122 *The Health Effects of Cannabis and Cannabinoids*, National Academies Press, Washington, D.C., **2017**.

part symptomatic or based on the administration of immunosuppressant, which reduce part of the inflammation affecting the central nervous system by reducing the response capacity of the immune system. However, since there are no definitive treatments, immunosuppressants must be taken for life despite having many side effects, sometimes even serious ones. For several years, it has also been understood that phytotherapy can be a complementary aid to classic drugs for people with multiple sclerosis by reducing some physical or psychological symptoms. A particular interest was addressed to *Cannabis Sativa* that can interact with specific receptors located in the nervous system at the level of the neuromuscular plate with possible therapeutic effects in the reduction of muscle spasms and pain. Some studies conducted on experimental autoimmune encephalitis (EAE), a disease that has some characteristics of multiple sclerosis, have shown that cannabinoids can have neuro-protective effects in addition to their potential in symptomatic therapy. While the effects of THC are primarily neuronal, CBD-mediated neuro-protection is thought to occur due to its interaction with astrocytes, cells in the nervous system that contribute to neuroinflammation.

The treatments can take place orally, as a decoction or oil, or by inhalation, using specific vaporisers. Due to the vastness of compounds contained in *Cannabis*, approval as a drug and production by other establishments is complicated, so it is necessary to isolate every single component and characterise it in order to have a number of information that allows correct attribution. An important aspect to note is the entourage effect. It refers to the synergistic effects of cannabinoids, terpenes and other compounds, since the effectiveness of the pharmacological effect of the *Cannbis* phytocomplex is much higher than using the single component.[97,123] The entourage effect can extend to combinations of cannabinoids with "other established or overlapping mechanisms of analgesia" (pain relief) with the modulation of pain signaling, giving the possibility to reduce the doses of the main drugs.

2 Aim of the project

Although many cannabinoids demonstrate biological activity, they have not been well studied due to their limited quantities and the difficulty of isolation. A synthetic source of them, as well as the creation of derivative analogs, would allow a greater understanding of the effects. CBD is the main cannabinoid of *Cannabis* extracts; however, seven CBD-type cannabinoids with C_1 to C_5 side chains have been identified.

Table 2.1 CBD-type cannabinoids.

CBD-type	Compound	R_1	R_2	R_3
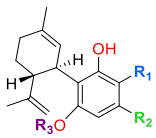	Cannabidiolic acid (CBDA-C_5)	COOH	*n*-C_5H_{11}	H
	(–)-Cannabidiol (CBD-C_5)	H	*n*-C_5H_{11}	H
	Cannabidiol monomethyl ether (CBDM-C_5)	H	*n*-C_5H_{11}	CH_3
	Cannabidiol-C4 (CBD-C_4)	H	*n*-C_4H_9	H
	Cannabidivarinic acid (CBDVA-C_3)	COOH	*n*-C_3H_7	H
	(–)-Cannabidivarin (CBDV-C_3)	H	*n*-C_3H_7	H
	Cannabidiorcol (CBD-C_1)	H	CH_3	H

CBD-C_4 is a molecule with a similar structure, but with one less carbon atom in the side alkyl chain compared do the well-known CBD-C_5. Obtaining a synthetic route of CBD-C_4 is of particular interest to enrich the literature with a complete characterization. In fact, this molecule has always been extracted in complex mixtures with other natural products present in the plant, consequently making isolation impossible.

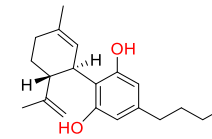

CBD-C_4

2.1 Published CBD synthesis strategies

CBD can be obtained synthetically from the acid-catalysed terpenylation of olivetol **23**, or of the alkyl esters of olivetolic acid followed by saponification and decarboxylation (**Scheme 2.1**, path **a**). In this context, important results have been obtained using isopiperitenol, mentadienol, carene epoxide or their *O*-substituted derivatives as synthetic equivalents of methyl-propenyl-cyclohexene carbocation under acidic conditions (e.g. $ZnCl_2$,

123 R. Brenneisen, in *Marijuana and the Cannabinoids*, Humana Press, Totowa, NJ, Totowa, NJ, **2007**, pp. 17–49.

$BF_3{\cdot}OEt_2$, *p*-TsOH).[112,124] The main drawback of using olivetol as a nucleophilic species for Friedel-Crafts reaction is the low regioselectivity, with the formation of regioisomers of CBD and the double alkylated by-product. Furthermore, this approach is sensitive to operational variables (e.g. temperature, type of acid, and catalyst concentration).

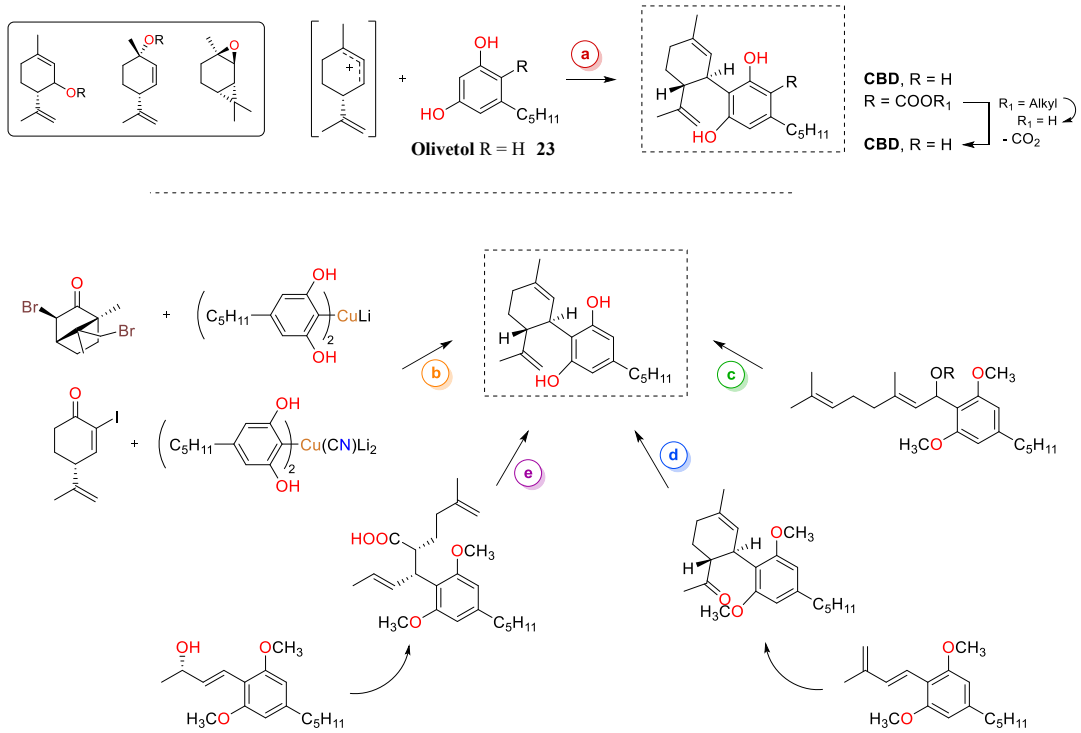

Scheme 2.1 Synthetic approach reported in literature to obtain CBD from olivetol.

Alternative synthetic approaches involve the reaction of lower-order cuprates with (+)-3,9-dibromocamphor or of higher-order cyanocuprates with α-iodocyclohexenone (**Scheme 2.1**, path **b**).[125] The reactions proceed with high regio- and stereoselectivity, but the anionic reductive cleavage of bromide camphor derivatives with Na/naphtalenide is a challenging step. In addition, the main drawbacks concern the synthesis of non-commercial chiral terpene precursors and handling organometallic intermediates, which are sensitive to changes on variables such as temperature, humidity, and addition rate.

Asymmetric strategies have been applied to functionalise olivetol with acyclic structures to obtain CBD in synthetic multi-steps. Instead of combining olivetol with monoterpenic precursors, the construction of the cyclohexene ring was achieved by enantioselective cyclisation. Mechoulam and Gaoni[126] obtained CBD scaffold by addition citral to the lithium derivative of olivetol followed by reaction with *p*-toluenesulfonyl chloride (**Scheme 2.1**, path **c**). Minuti and coworkers[127] combined Diels-Alder reaction and kinetic resolution to obtain the key intermediate (**Scheme 2.1**, path **d**). Leahy and coworkers[128] developed an enantioselective total synthesis of CBD

124 **a]** S.-H. Baek, M. Srebnik, R. Mechoulam, *Tetrahedron Lett.* **1985**, *26*, 1083–1086; **b]** L. O. Hanuš, S. Tchilibon, et al., *Org. Biomol. Chem.* **2005**, *3*, 1116; **c]** W. A. Kinney, M. E. McDonnell, et al., *ACS Med. Chem. Lett.* **2016**, *7*, 424–428; **d]** T. M. Waugh, J. Masters, et al., *ChemMedChem* **2020**, *15*, 114–124; **e]** M. C. Pirrung, *J. Med. Chem.* **2020**, *63*, 12131–12136; **f]** X. Gong, C. Sun, et al., *J. Org. Chem.* **2020**, *85*, 2704–2715.

125 **a]** V. Vaillancourt, K. F. Albizati, *J. Org. Chem.* **1992**, *57*, 3627–3631; **b]** Y. Kobayashi, A. Takeuchi, Y.-G. Wang, *Org. Lett.* **2006**, *8*, 2699–2702.

126 **a]** R. Mechoulam, Y. Gaoni, *J. Am. Chem. Soc.* **1965**, *87*, 3273–3275; **b]** R. Mechoulam, P. Braun, Y. Gaoni, *J. Am. Chem. Soc.* **1972**, *94*, 6159–6165.

127 **a]** E. Ballerini, L. Minuti, O. Piermatti, *J. Org. Chem.* **2010**, *75*, 4251–4260.

128 Z. P. Shultz, G. A. Lawrence, et al., *Org. Lett.* **2018**, *20*, 381–384.

based on the versatility of allylic branched alcohols in a linear strategy (**Scheme 2.1**, path **e**). The Claisen-Ireland rearrangement and the ring-closing metathesis represent the key transformations to obtain the cyclohexene.

The delicate step in all methodologies is to minimise the acid-activated cyclisation of CBD to THC,[129] which can be formed by the attack of the hydroxyl group of olivetol to the tertiary carbocation obtained under acidic conditions on the isoprene moiety. This problem significantly affects the yield of some reported methods.

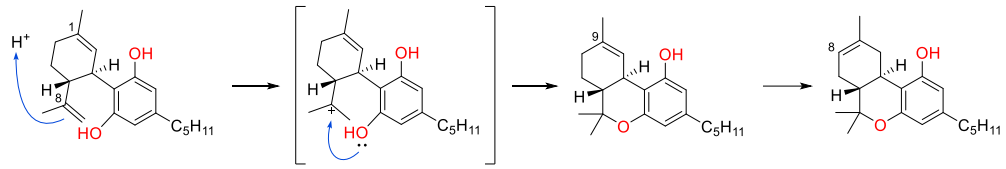

Scheme 2.2 CBD acid promoted cyclization.

3 Results and discussion

3.1 Retrosynthetic approach

Taking into consideration all the weaknesses of the strategies available in the literature, the last type of approach was preferred, which consists in the construction of cyclohexene by functionalisation of the olivetol **23** with acyclic chains in an enantioselective way, although it involves a greater number of steps compared to the other methods.

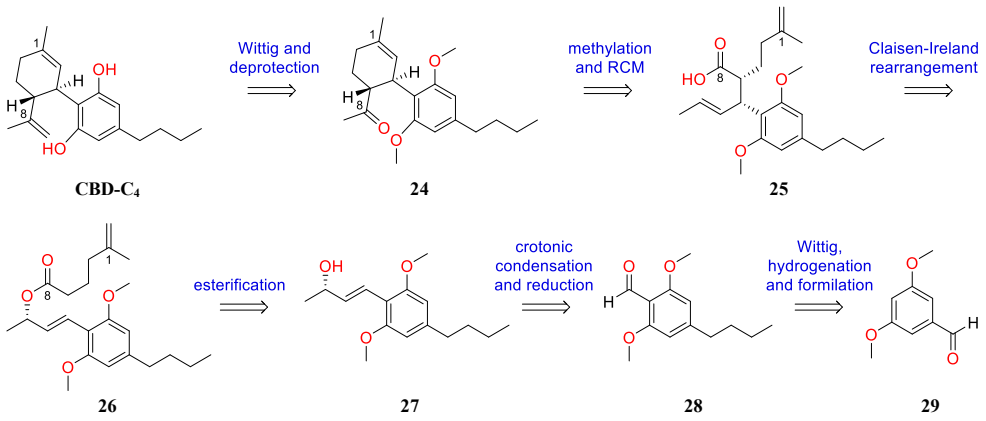

Scheme 3.1 Retrosynthetic approach to obtain CBD-C_4.

Taking inspiration from Leahy's work[128] and trying to improve the yields by applying different reactions in the points identified as critical, the total synthesis of **CBD-C_4** could be accomplished by methylation and deprotection of the corresponding ketone **24**, which would be prepared from **25** through the transformation of acid moiety into ketone and performing ring-closing metathesis (RCM). γ,δ-unsaturated carboxylic acid **25** would be obtained from ester **26** *via* Claisen-Ireland rearrangement with perfect stereogenic control by generating the corresponding silyl ketene acetal under kinetic condition. The carbon framework of **26** could be created from **27** by esterification of the alcohol in coupling condition. **27** would be synthesised with crotonic condensation in basic condition of **28** and acetone followed by enantioselective reduction of the carbonyl. Furthermore, **28** could arise starting from the known aldehyde **29** exploiting the Wittig olefination and the hydrogenation of the resulting double bond.

129 P. Marzullo, F. Foschi, et al., *J. Nat. Prod.* **2020**, *83*, 2894–2901.

3.2 Synthesis of CBD-C_4

Not being commercially available, the resorcinol derivative **32** substituted with a four carbon atoms side chain (analogue of olivetol **23**) was prepared from 3,5-dimethoxybenzaldehyde **29** (**Scheme 3.2**).

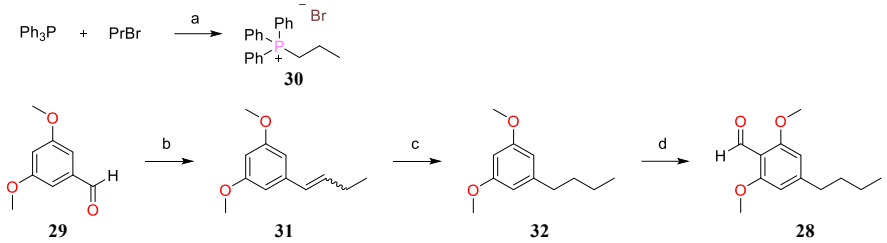

Scheme 3.2 *Reaction conditions*: a) Tol, reflux 95°C, 20 h, 77%; b) *i*) **30** 1 eq, *n*-BuLi 1 eq, THF, 0°C, 2 h, *ii*) **29** 1 eq, -78°C to 65°C, 8 h, 94%; c) H_2, Pd/C 0.5%, MeOH, rt, 3 h, 83%; d) *i*) *n*-BuLi 1.5 eq, TMEDA 1.5 eq, THF, -78 to -20°C, 30 min; *ii*) DMF 1.5 eq, -20°C, 40 min, 94%.

The first step of Wittig olefination required the preparation *in situ* of the active ylide with *n*-BuLi starting from the prepared triphenyl(propyl)phosphonium bromide **30**. Depending on the ylide used, the Wittig reaction can provide both alkenes (*Z*) and alkenes (*E*) in more or less enriched mixtures. Non-stabilized ylides, such as tripheny (propyl)phosphonium bromide **30**, generally give mainly (*Z*)-isomers, while stabilized ylides predominantly form (*E*)-isomers. The outcome was a mixture 2:1 of *Z*/*E* alkene **31** (determinated by NMR) achieved with 94% of yield.

Both isomers were hydrogenated together with catalytic amount of Pd/C in methanol to reduce the double bond. The substrate conversion was monitored by ^{1}H-NMR analysis, because through TLC it was not possible to well discriminate between starting material and product. This allowed adjusting the reaction by reducing the amount of catalyst due to the formation of a large number of by-products in a short time when a greater amount of Pd/C was used as reported in literature.[130] Yields were improved from 12% obtained using 10% w/w of catalyst to 83% with 0.5% w/w of Pd/C.

The following formylation regioselectively exploits *ortho*-lithiation using methoxyls as directing groups. The *ortho*-metalation reaction allows the introduction of an electrophile exclusively in the *ortho* position to a direct metalation group (DMG) present on the aromatic ring generating an aryl-metal compound as intermediate (**Scheme 3.3**).[131] In order to speak about *ortho*-metalation, a group containing a heteroatom capable of donating electrons (such as O and N) must coordinate the attack of the metal. In this case, the aromatic system has two methoxyls as DMG that interact with alkyl-lithium and drive the reactivity in the common *ortho*-position. Then, the alkyl-lithium deprotonates the ring in the *ortho* position forming an aryl-lithium, which can be stabilized through the coordination of the lithium by a tertiary amine added. Now, an electrophile is able to react in the *ortho* position by aromatic electrophilic substitution.

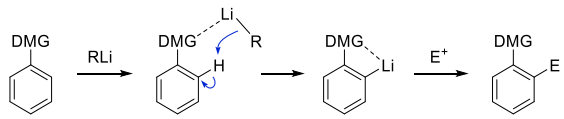

Scheme 3.3 Reaction mechanism of ortho-metalation.

This reaction required a lot of effort to achieve satisfactory yields due to the rapid formation and high reactivity of the lithium intermediate, even using TMEDA as a stabilizing additive. The reaction is very sensitive to the conditions used, in particular to the temperature and the waiting time before adding as electrophile. Any increase

130 **a]** Y. Zhu, D. N. Soroka, S. Sang, *J. Agric. Food Chem.* **2012**, *60*, 8624–8631; **b]** S. C. Dakdouki, D. Villemin, N. Bar, *European J. Org. Chem.* **2010**, *2010*, 333–337; **c]** B. Lesch, J. Toräng, et al., *Synthesis (Stuttg).* **2005**, *2005*, 1888–1900.

131 V. Snieckus, *Chem. Rev.* **1990**, *90*, 879–933.

in the reaction time or temperature in the formation of the intermediate caused a drastic decrease in yield or a failure in functionalisation of the aryl (**Table 3.1**). In fact, aryl-lithium reagents can also react with ethers used as solvents, so the half-life depends on their stability in the reaction environment.[132] Therefore, the conditions reported by Leahy have been deeply changed. Analysing with ^{1}H-NMR techniques aliquots of reaction mixtures quenched with deuterated water determined that the aryl-lithium was completely formed within 30 min of stirring after the addition of *n*-BuLi at -78°C. The subsequent addition of DMF provided **28** with 94% of yield in 40 min at -20°C.

Table 3.1 Reaction conditions applied to optimise ortho-lithiation in THF.

Conditions	Ar-Li formation		After DMF addition		Yield [%]
	Time [h]	T [°C]	Time [h]	T [°C]	
n-BuLi (1.2eq), TMEDA (1.2eq), DMF (1.2eq)	1.5	-78° to 0°C	1.5	0°C to rt	0
n-BuLi (1.2eq), TMEDA (1.2eq), DMF (1.2eq)	1.5	-78° to 0°C	1.5	0°C to rt	36
n-BuLi (1.2eq), TMEDA[a] (1.2eq), DMF (1.2eq)	1.5	-78° to 10°C	1.0	10°C to rt	57
n-BuLi (1.2eq), TMEDA[a] (1.2eq), DMF (1.2eq)	1.7	-70° to 15°C	2.5	15°C to rt	0
n-BuLi (1.2eq), TMEDA[a] (1.2eq), DMF (1.2eq)	1.2	-78° to 5°C	2.5	-78°C to rt	17
n-BuLi (1.5eq), TMEDA[a] (1.5eq), DMF (3.0eq)	2.0	0° to rt	18	rt	0
n-BuLi (1.5eq), TMEDA[a] (1.5eq), DMF (1.5eq)	1.5	-40° to -5°C	1.5	-5°C to rt	0
n-BuLi (1.5eq), TMEDA[a] (1.5eq), DMF (1.5eq)	1.5	0° to 5°C	1.5	5° to rt	0
n-BuLi (1.5eq), TMEDA[a] (1.5eq), DMF (1.5eq)	1.5	-78° to 10°C	1.5	10°C to rt	0
n-BuLi (1.2eq), TMEDA[a] (1.2eq), DMF (1.5eq)	0.4	-78° to -20°C	0.3	-20°C	66
n-BuLi (1.5eq), TMEDA[a] (1.5eq), DMF (1.5eq)	0.5	-78° to -20°C	0.7	-20°C	94

[a] freshly distilled

Next, crotonic condensation of **28** and acetone in aqueous basic condition provided the α,β-unsaturated ketone **33** in 80% of yield, supporting the reaction by heating to favour the elimination of a water molecule (**Scheme 3.4**).

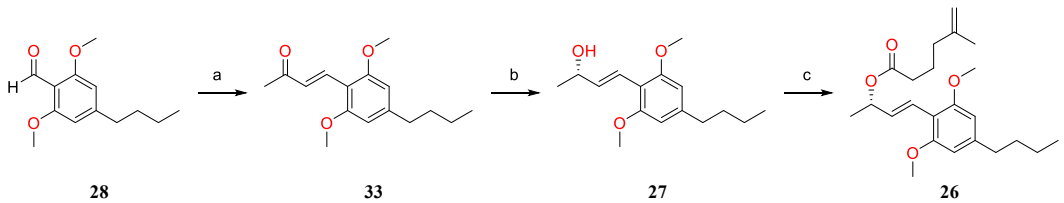

28 **33** **27** **26**

Scheme 3.4 *Reaction conditions*: a) 2.5 M NaOH 3.5 eq, acetone 5 eq, H_2O, 60°C, 15 h, 80%; b) (*R*)-(+)-2-Methyl-CBS-oxazaborolidine 0.2 eq, BH_3 1.4 eq, THF, -78°C, 18 h, 87%, 74 ee; c) 5-methyl-5-hexenoic acid 1.5 eq, EDC-HCl 1.8 eq, TEA 1.8 eq, DMAP 0.5 eq, DCM, 0°C to rt, 15 h, 80%.

The alcohol **27** was obtained from the ketone **33** with 87% of yield through the enantioselective reduction of Corey-Bakshi-Shibata, which involved the use of a catalyst based on oxazaborolidine (CBS) and BH_3 formed *in situ* at -78°C as a reducing agent.[133]

The mechanism of the reduction (**Scheme 3.5**) begins with the coordination of BH_3 to the Lewis basic nitrogen atom of CBS to form the oxazaborolidine-BH_3 complex fused in *cis*. The coordination of the electrophile serves to activate BH_3 as a hydride donor and also to strongly increase the Lewis acidity of the endocyclic boron atom. The strongly acidic Lewis complex binds to the ketone minimising steric interactions and in the *cis* position to the vicinal group BH_3. Therefore, the bulkier substituent (R_L) is directed away from the R' group of the catalyst determining the facial selectivity. Carbonyl and borane are aligned in the TS for the intramolecular transfer of a hydride. The chiral alkoxyborane produced releases the catalyst and the alcohol is obtained by hydrolysis.

132 P. Stanetty, H. Koller, M. Mihovilovic, *J. Org. Chem.* **1992**, *57*, 6833–6837.

133 **a]** A. Hirao, S. Itsuno, et al., *J. Chem. Soc. Chem. Commun.* **1981**, 315; **b]** E. J. Corey, C. J. Helal, *Angew. Chemie Int. Ed.* **1998**, *37*, 1986–2012.

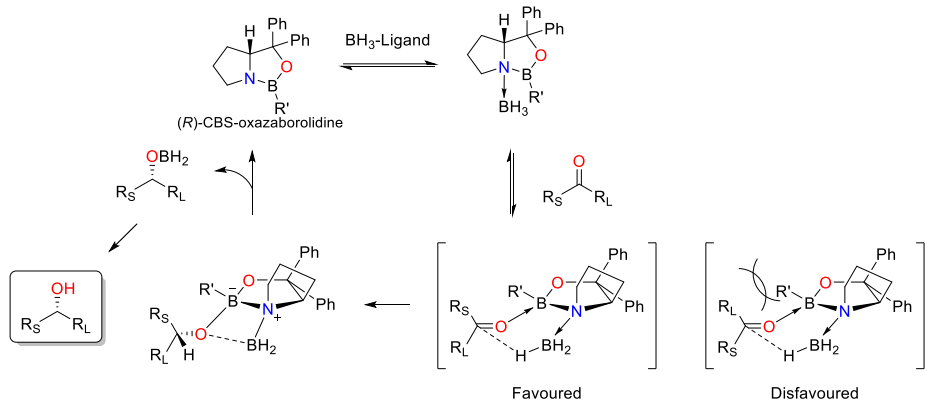

Scheme 3.5 Corey-Bakshi-Shibata reduction mechanism.

To confirm the enantioselectivity of the reaction, an HPLC analysis was performed on chiral lux 3u amylose -2 column which resulted in an ee of 74% (**Figure 3.1**). The synthetic route continued without carrying out the resolution of the two enantiomers, therefore the ee was maintained for all subsequent products obtained. **27** was joined to the commercially available 5-methyl-5-hexenoic acid to obtain the ester **26**. When this reaction is carried out with DCC as condensing agent there are problems in the purification of the product with consequent lowering of the yields (58%). For this reason, EDC was used as a coupling agent obtaining higher yields (80%).

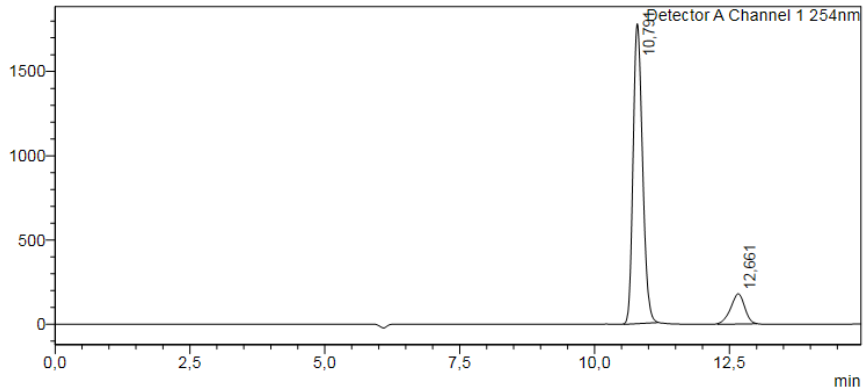

Figure 3.1 HPLC chromatogram of **27** to determine the ee. Lux 3u amylose -2 column (petroleum ether/*i*-propylalcohol 85:15, 0.5 mL/min, 31.5°C), λ = 254 nm; rt (–)**27** = 10.79, (+)**27** = 12.66.

The Claisen-Ireland rearrangement,[134] a [3,3] sigmatropic transposition reaction, was exploited to obtain the key intermediate **25b**. The first reaction was performed applying the same conditions reported by Leahy, which foresee the use of potassium hexamethyldisilazide (KHMDS) and trimethylsilyl chloride (TMS-Cl). Although the type of base used should lead to the undesired diastereoisomer **25a** through the formation *in situ* of the silyl enol ether **26‡a** in (*Z*) configuration, the product obtained was **25b** with a yield of 75%. The relative stereochemistry was confirmed by X-ray crystallographic analyses.

To improve the yield, an allyl silyl ketene acetal was generated *in situ* with kinetic control starting from ester **26**. The use of lithium diisopropylamide (LDA) at -78°C in the presence of TMS-Cl provided the formation of the *E* enolate,[135] which can evolve stereoselectively in the **26‡b** chair TS. Heating induced the concerted shift of the two π bonds and the breaking of the σ bond to form a new one. In this way, the desired product was obtained with 85% yield as a single diasteroisomer because the starting (*E*,*E*) configuration in the chair TS guaranteed the

134 R. E. Ireland, R. H. Mueller, *J. Am. Chem. Soc.* **1972**, *94*, 5897–5898.

135 E. J. Corey, A. W. Gross, *Tetrahedron Lett.* **1984**, *25*, 495–498.

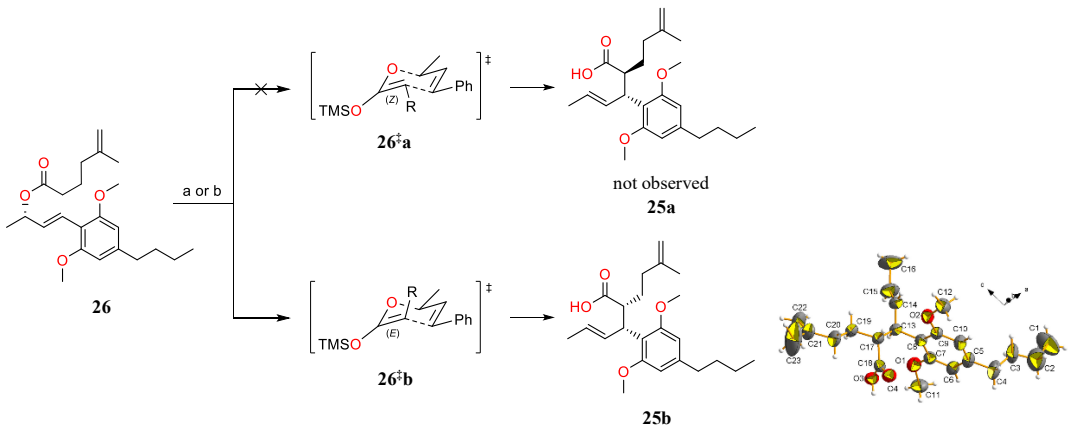

Scheme 3.6 *Reaction conditions*: a) *i*) KHMDS 3 eq, **26** 1 eq Tol, -78°C, 1h, *ii*) [Py 4.5 eq + TMSCl 6 eq, Tol, 0°C], -78°C 10 min then rt 4 h, 73%; b) *i*) TMSCl 4.9 eq, TEA 4.4 eq, THF, -78°C, *ii*) **26** 1 eq, LDA 1.5 eq, THF, -78°C 1.5 h to rt 1 h, then reflux 5 h, 85%.

cis outcome. The non-enantiopurity of the substrate did not determine the formation of the *anti*-diastereomer, but led to the formation of the other *cis* enantiomer.

Ireland first described this reaction in 1972 as a reinterpretation of the Claisen rearrangement,[136] which is a pericyclic reaction of allyl vinyl ethers belonging to the [3+3] sigmatropic transpositions based on the migration of a σ bond by the displacement of one or multiple π bonds to form γ,δ-unsaturated carbonyls (**Scheme 3.7**). The TS for this type of reactions is generally chair-like and has neither charges nor ionic intermediates because it exploits a concerted-type mechanism of the π system.

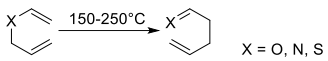

Scheme 3.7 Claisen transposition rearrangement.

Unlike the Claisen rearrangement, the characteristic of Claisen-Ireland version is the formation of an enolate starting from an ester, obtaining a γ,δ-unsaturated carboxylic acid as product. The reaction can be divided into two parts (**Scheme 3.8**):

- the formation of the enolate, characterised by a low temperature and the choice of a suitable base to obtain the desired stereoisomer;
- the transposition to room temperature, unlike the Claisen which requires more extreme conditions (150-300°C). The increase in temperature induces a concerted movement of electrons which results in the displacement of two π bonds and the breaking of a σ bond to form a new one.

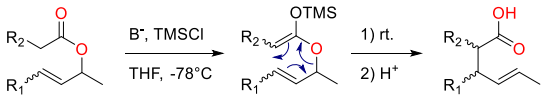

Scheme 3.8 Claisen-Ireland transposition rearrangement mechanism.

The stereochemistry of this reaction is given by the *E* or *Z* configuration of the enolate formed *in situ*, and by the configuration of the double bond at γ,δ position to the carbonyl. The latter depends exclusively on the type of substrate used and cannot be changed during the reaction, but with the appropriate reaction conditions it is possible to choose which enolate to form (**Scheme 3.9**). For the formation of the *E*-enolate kinetic conditions are applied using strong bases that are not hindered and prefer cyclic deprotonation TS, typically LDA is used. While to obtain *Z*-enolate weak and bulky bases are used that prefer open TS, such as HMDS (hexamethyldisilazide).

136 L. Claisen, *Berichte der Dtsch. Chem. Gesellschaft* **1912**, *45*, 3157–3166.

Another method is to use a co-solvent such as HMPA (hexamethylphosphoramide) or DMPU (*N*,*N*′-dimethylpropyleneurea) in the presence of LDA because they are able to solvate the counter ion favoring an open transition state. The addition of silyl in the reaction environment allows to form the corresponding more stable silyl enol ether required for the rearrangement.

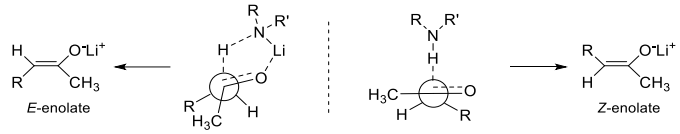

Scheme 3.9 *E-, Z*-enolate formation.

Once the silyl enol ether is obtained, the Claisen-Ireland rearrangement proceeds through a six-member TS that is preferentially organised in a chair (**Scheme 3.10**); the boat-like one is possible, but is very disadvantaged for steric reasons and would lead to the formation of the diastereomer.

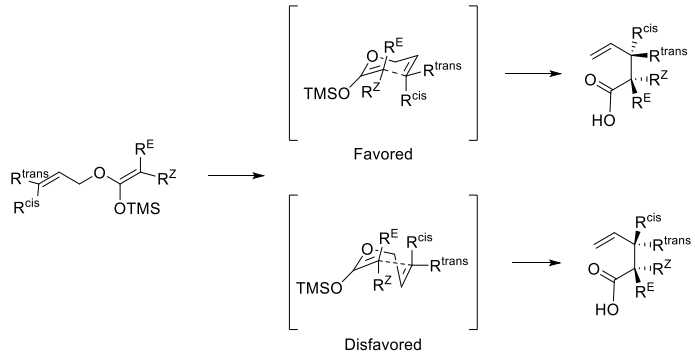

Scheme 3.10 Chair and boat TS.

If the silyl enol ether has double bonds (*Z*,*Z*) or (*E*,*E*), a *cis* product is obtained following the favoured chair TS. While if the double bond are in configuration (*E*,*Z*) or (*Z*,*E*) the outcome will be *anti*. On the contrary, with a boat TS an opposite stereochemical result is obtained, therefore (*Z*,*Z*) and (*E*,*E*) lead to *anti* products, while (*E*,*Z*) or (*Z*,*E*) provides *cis*. If the alkoxide is branched, the stereochemistry of C-O determines which enantiomer is obtained.

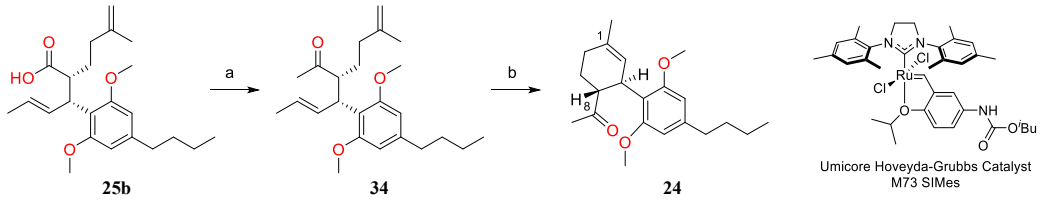

Scheme 3.11 *Reaction conditions*: a) MeLi 2.5 eq, Et_2O, 0°C to rt, 4 h, 78%; b) Umicore M73 SIMes 0.1 eq, DCM, 40°C, 15 h, 90%.

Treating acid **25b** with 2.5 equivalent of methyl lithium yielded the corresponding ketone **34** in 78%, which was subjected to the RCM (**Scheme 3.12**). This reaction was performed with two types of catalysts: Grubb's 2nd generation (yield 79%) and Umicore M73 SIMes (yield 90%). The latter resulted to be more efficient for obtaining and purifying the product **24**, therefore was selected as catalyst.

Methylation by Wittig type reaction required optimisation of the method to achieve satisfactory yields (**Scheme 3.12**). The main issue found in this protocol was being able to obtain the *in situ* formation of a highly unstable ylide. Therefore, the reaction time required for the formation of the active species at 0°C with *n*-BuLi was reduced from 2 h, which gave a 40% yield in product isolation, to 10 min that led to a 56% yield in the isolation of **35**.

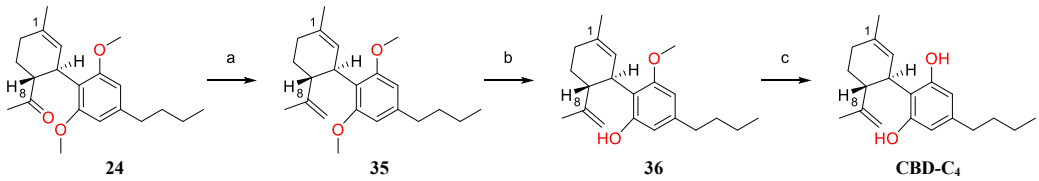

Scheme 3.12 *Reaction conditions*: a) $MePPh_3Br$ 1.2 eq, *n*-BuLi 1.2 eq, THF, 0°C 45 min, to rt 18 h, 56%; b) NaSEt, 20 eq DMF, 140°C, 24 h, 79%; c) NaSEt 30 eq, DMF, 145°C, 20 h, 28%.

Finally, basic conditions were applied to deprotect the phenol moieties because BBr_3 causes degradation of the substrate and other Lewis acids induce the activation of the Δ8 or Δ1 double bond with consequent intramolecular cyclisation with the electron rich OH forming derivatives of the isomer THC.[129] Treatments at various temperatures with MeMgBr were unsuccessful, while some encouraging results were obtained by treating **35** with a large excess of NaSEt in DMF at 140°C. Removal of the first methyl proceeded smoothly, but the second was more difficult. By increasing the eq of NaSEt the conversion did not advance, therefore the reaction was purified and repeated on the intermediate **36**, which was obtained with a yield of 79%. It has been observed that deprotection proceeds much faster if performed in a seal tube and starting immediately with a large excess of NaSEt. For the second deprotection, it was necessary to further increase the reagent equivalents to activate the reaction allowing to obtain the **CBD-C4** with a yield of 28% after 20 h. The reaction was stopped at this time rather than add more NaSEt to avoid the risk of lower yields. Even if the reaction was particularly difficult and with low yields, the product **CBD-C4** was obtained after several attempts. HPLC was requested to better distinguish the possible derivatives obtained, since THC and CBD have very similar Rf in TLC, and above all to more accurately monitor the conversion (**Figure 3.2**).

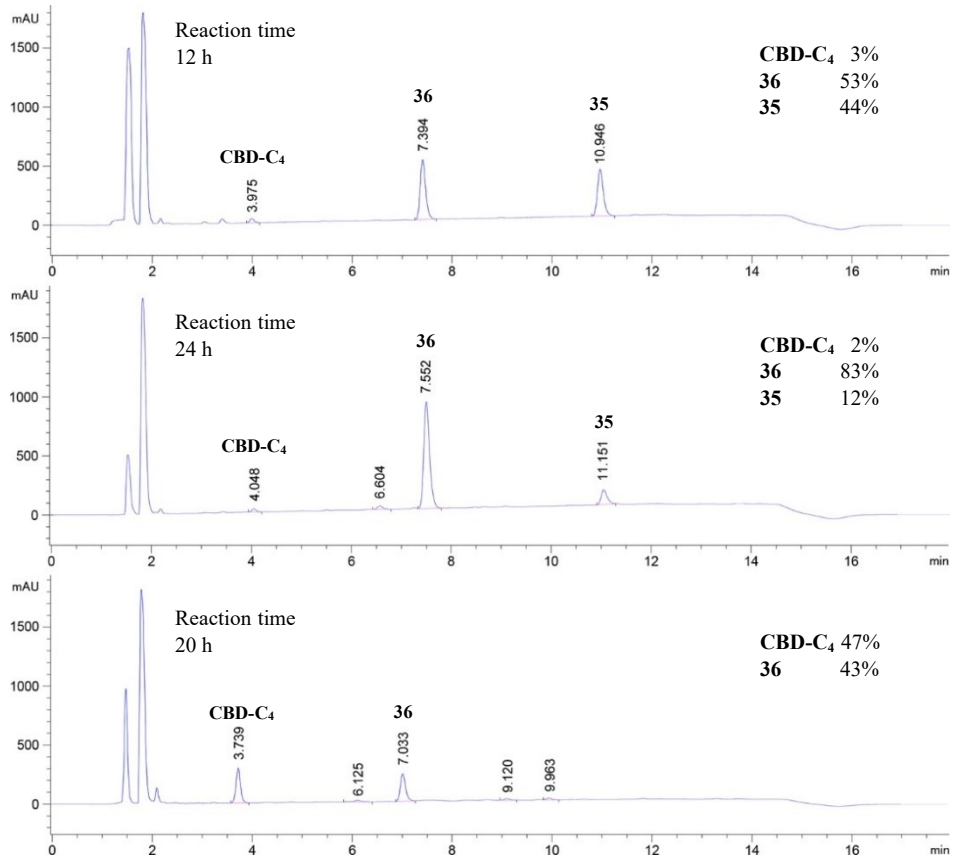

Figure 3.2 HPLC chromatogram of the proceeding of the deprotection reaction performed with NaSEt.

Once **CBD-C$_4$** was obtained, it was used as a reference to identify the presence of the compound within a CBD extract. Therefore, a comparison HPLC analysis was performed by superimposition of the chromatograms to highlight the corresponding peak (**Figure 3.3 a**). The investigation was also carried out using **CBD-C$_4$** as the internal standard of the extract providing a single peak (**Figure 3.3 b**). The positive results of the analysis confirmed the presence in traces of **CBD-C$_4$** within CBD extracts.

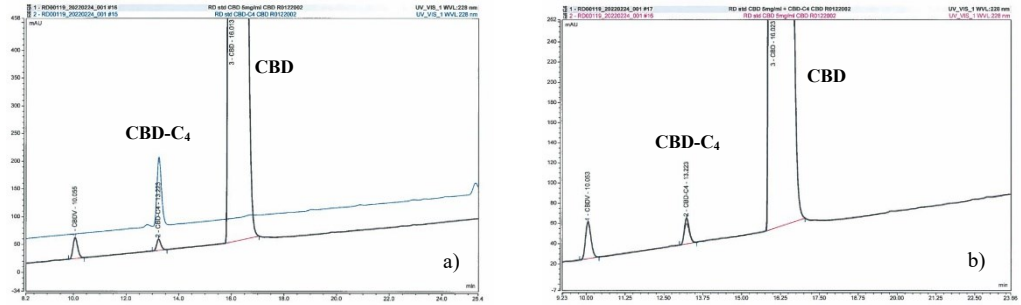

Figure 3.3 HPLC chromatogram of the *a*) CBD extract (black line) compared to CBD-C$_4$ used as reference (line blue) and *b*) CBD extract with synthetised CBD-C$_4$ as internal standard to identify the impurity.

4 Conclusion

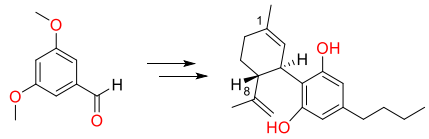

29 **CBD-C$_4$**

In conclusion, the asymmetric total synthesis of **CBD-C$_4$** was achieved in 12 steps by using common 3,5-dimethoxybenzaldehyde **29**. The introduction of a single stereocentre by the enantioselective reduction and the *E* configuration of the double bond represent the bases for the correct stereochemical evolution of the Claisen-Ireland rearrangement. The last deprotection reaction was the main problem, for this reason considering other protecting groups (such as -MOM or -Piv) for the future total synthesis of natural and semi-synthetic cannabinoids would be a right strategy. Finally, the presence of **CBD-C$_4$** within CBD extracts was confirmed by HPLC analysis.

5 Experimental procedures

5.1 Chemistry

General Experimental Procedures

Unless otherwise stated, reagents were purchased from general suppliers (Sigma Aldrich, Fluorochem, and TCI) and used without further purification. All solvents were of reagent grade or HPLC grade. All reactions were carried out in oven-dried glassware and dry solvents, under nitrogen atmosphere and were monitored by glasses or aluminium TLC on silica gel (Merck precoated 60F254 plates), with detection by UV light (254 nm), or by TLC stains as permanganate, or by HPLC. Products were purified by flash column chromatography, using silica gel Merk 60 (230-400 mesh) as stationary phase. Analytical HPLC was performed on Agilent 1100 Series System RP column ZORBAX SB-C8 (3.5µm x 4.6 x 150 mm). The pressure was about 193 bar, with a constant flow rate of 1 mL/min. UV spectra were recorded at 228 nm and 210 nm with DAD detection. The mobile phase consisted of a mixture of H_2O/MeOH and the method was programmed using a gradient flow from 80% to 90% MeOH in 10 min followed by 2.5 min isocratic at 90% MeOH. ^{1}H-NMR spectra were recorded on a Bruker Avance Spectrometer 400 MHz and ^{13}C-NMR spectra were recorded on the same instrument 101 MHz, using commercially available deuterated (chloroform-d) solvent at room temperature. Chemical shifts are reported in parts per million (ppm), compared to TMS as an internal standard. Multiplicities in ^{1}H-NMR are reported as

follow: s – singlet, d – doublet, t – triplet, m – multiplet, br – broad. Data for ^{13}C NMR are reported in chemical shift (δ/ppm). High resolution mass spectra (HR-MS) were recorded on a Water QToF Premier high resolution UPLC ES MS/MS.

Synthesis of propyl-triphenyl-phosphonium bromide (30)

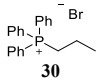

30

1-bromopropane (2.66 g, 21.6 mmol) was added dropwise to a solution of triphenylphosphine (4.10 g, 16.0 mmol) in anhydrous toluene (3.48 mL). The mixture was heated at reflux for 22 hours, then the solid was filtered and washed with toluene. The product was dried in the oven at 100°C for 12 hours to give **30** (4.76 g, 12.3 mmol, 77% yield) as white solid.

^1H NMR (400MHz, DMSO-d_6) δ 7.93-7.89 (m, 3H), 7.84-7.76 (m, 12H), 3.60-3.52 (m, 2H), 1.61-1.53 (m, 2H), 1.08 (m, 3H).

Synthesis of 1-(but-1-en-1-yl)-3,5-dimethoxybenzene (31)

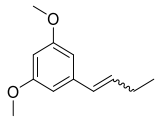

31

n-BuLi (7.5 mL, 12 mmol, 1.6M) was added to a solution of **30** (4.64 g, 12 mmol) in anhydrous THF (120 mL) at 0°C, under nitrogen atmosphere. The reaction mixture was stirred for 2 hours at 0°C, then cooled to -78°C and 3,5-dimethoxybenzaldehyde (2.00 g, 12 mmol) was added. The reaction mixture was heated at reflux for 8 hours. The mixture was quenched with saturated aqueous NH_4Cl solution (100 mL) and extracted with AcOEt (3 × 60 mL). The combined organic layers were washed with water, then dried over Na_2SO_4, filtered, and concentrated under reduced pressure. The crude was purified on silica gel (eluent: *n*-Hex/EtOAct 5:1) to provide 2.16 g (94%) as pale-yellow oil.

HRMS (ESI) *m/z* $[M+Na]^+$ 215.1055 (calcd for $C_{12}H_{16}O_2Na$, 215.1048);

^1H NMR (400 MHz, chloroform-*d*) δ 6.5 (d, *J* = 2.3 Hz, 1H, 2E, 6E), 6.5 (d, *J* = 2.3 Hz, 1H, 2Z, 6Z), 6.4 (t, *J* = 2.3 Hz, 0H, 4Z), 6.4 – 6.2 (m, 1H, 1'E, 2'E, 4E, 1'Z), 5.7 (dt, *J* = 11.7, 7.3 Hz, 0H, 2'Z), 3.8 (s, 6H, 7, 8), 2.4 (pd, *J* = 7.4, 1.8 Hz, 1H, 3'Z), 2.3 (qd, *J* = 7.4, 5.5 Hz, 1H, 3'E), 1.2 – 1.0 (m, 2H, 4');

^{13}C NMR (101 MHz, chloroform-*d*) δ 160.54 (3E, 5E), 160.53 (3Z, 5Z), 139.68 (1Z, 1E), 135.21 (2'Z), 133.22 (2'E), 128.80 (1'E), 128.25 (1'Z), 106.88 (2Z, 6Z), 104.05 (2E, 6E), 99.19 (4E), 98.75 (4Z), 55.29 (7Z, 8Z, 7E, 8E), 25.97 (3'E), 22.11 (3'Z), 14.43 (4'Z), 13.57 (4'E).

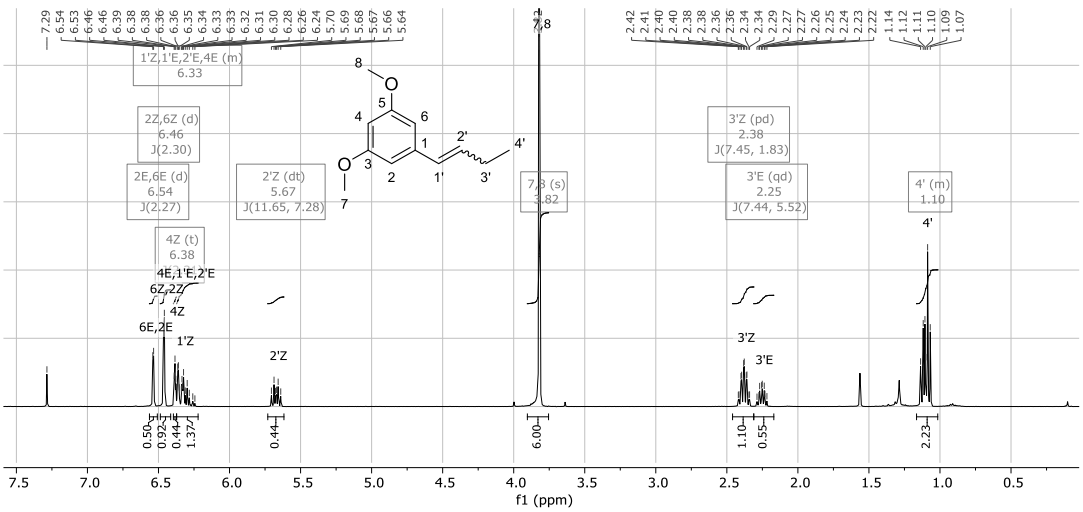

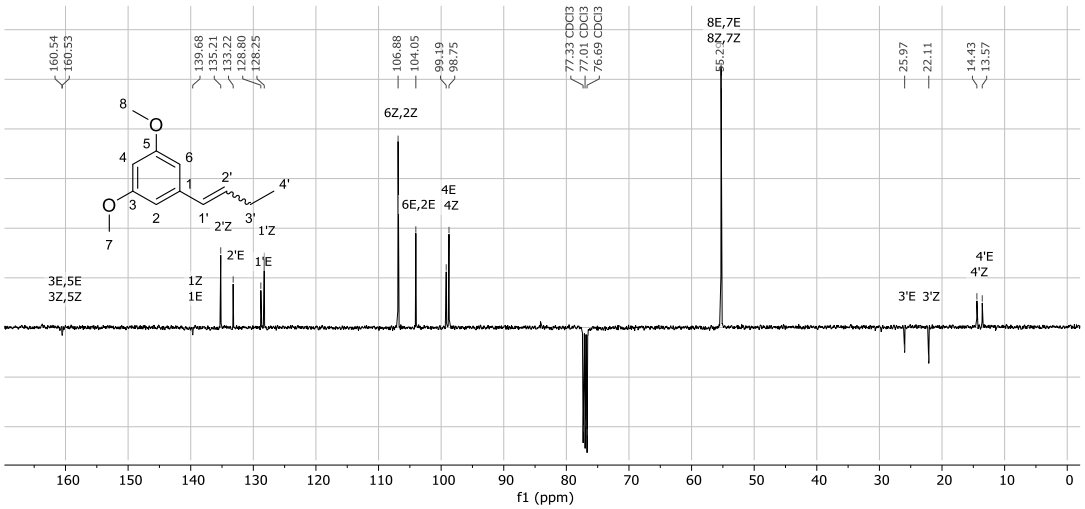

Synthesis of 1-butyl-3,5-dimethoxybenzene (32)

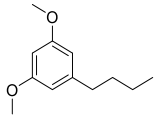

32

Pd/C (0.5% w/w) was added to a solution of **31** (1.92 g, 10.2 mmol) in MeOH (20.4 mL). The reaction mixture was stirred for 3 hours at room temperature under hydrogen. After filtration through a pad of celite, the residue was concentrated and the yellow crude oil was purified on silica gel (eluent: *n*-Hex/EtOAc 96:4) to give 1.62 g (83%) of product as pale-yellow oil.

HRMS (ESI) *m/z* $[M+Na]^+$ 217.1210 (calcd for $C_{12}H_{18}O_2Na$, 217.1205);

^{1}H NMR (400 MHz, chloroform-*d*) δ 6.4 (d, *J* = 2.3 Hz, 2H, 2, 6), 6.3 (d, *J* = 2.3 Hz, 1H, 4), 3.8 (s, 6H, 7, 8), 2.6 (t, *J* = 7.8 Hz, 2H, 1'), 1.7 – 1.5 (m, 2H, 2'), 1.4 (h, *J* = 7.3 Hz, 2H, 3'), 1.0 (t, *J* = 7.3 Hz, 3H, 4');

^{13}C NMR (101 MHz, chloroform-*d*) δ 161.37 (3, 5), 146.02 (1), 107.18 (2, 6), 98.24 (4), 55.87 (7, 8), 36.65 (1'), 34.07 (2'), 23.04 (3'), 14.60 (4').

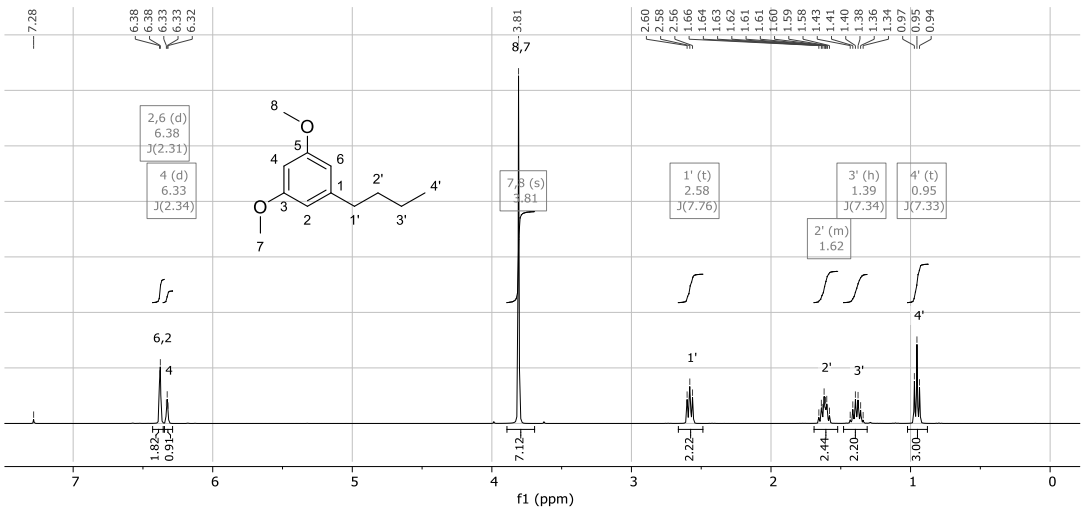

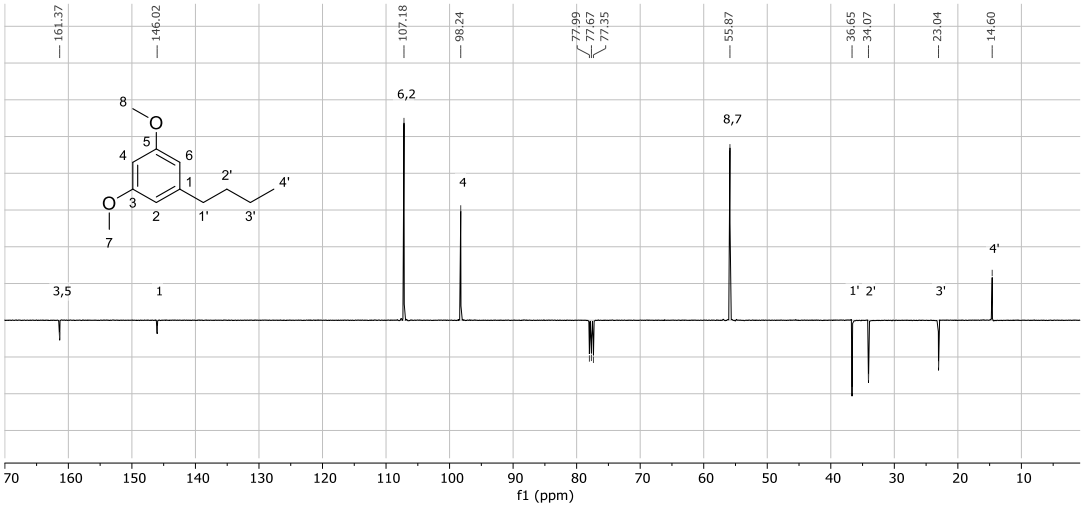

Synthesis of 4-butyl-2,6-dimethoxybenzaldehyde (28)

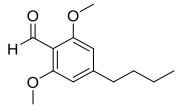

28

A solution of **32** (843 mg, 4.34 mmol) in anhydrous THF (25.5 mL) was cooled at -78°C under nitrogen atmosphere and freshly distilled TMEDA (0.976 mL, 6.51 mmol) was added to give a yellow solution. Then, *n*-BuLi (4.07 mL, 6.51 mmol, 1.6M in hexane) was added dropwise. After 15 min, the reaction was warmed to -20°C, and after additional 15 min anhydrous DMF (0.504 mL, 6.51 mmol) was added dropwise to the mixture. The reaction was stirred at -20°C for 40 minutes before warming to room temperature and quenching with saturated aqueous NH_4Cl and water. The aqueous layer was extracted with EtOAc (3 × 20 mL) and the combined organic layers were washed with brine, dried over Na_2SO_4, filtered, and concentrated under *vacuum*. The crude was purified on silica gel (eluent: *n*-Hex/EtOAc 8:2) to provide 900 mg (93%) of product as pale-yellow oil.

HRMS (ESI) *m/z* $[M+Na]^+$ 245.1161 (calcd for $C_{13}H_{18}O_3Na$, 245.1154);

^{1}H NMR (400 MHz, chloroform-*d*) δ 10.5 (s, 1H, 2'), 6.4 (s, 2H, 3, 5), 3.9 (s, 6H, 7, 8), 2.7 – 2.5 (m, 2H, 1"), 1.7 – 1.6 (m, 2H, 2"), 1.4 (dq, *J* = 14.6, 7.3 Hz, 2H, 3"), 1.0 (t, *J* = 7.3 Hz, 3H, 4");

^{13}C NMR (101 MHz, chloroform-*d*) δ 188.97 (1'), 162.28 (2, 6), 152.55 (4), 112.33 (1), 104.01 (3, 5), 55.96 (7, 8), 36.96 (1"), 33.03 (2"), 22.43 (3"), 13.89 (4").

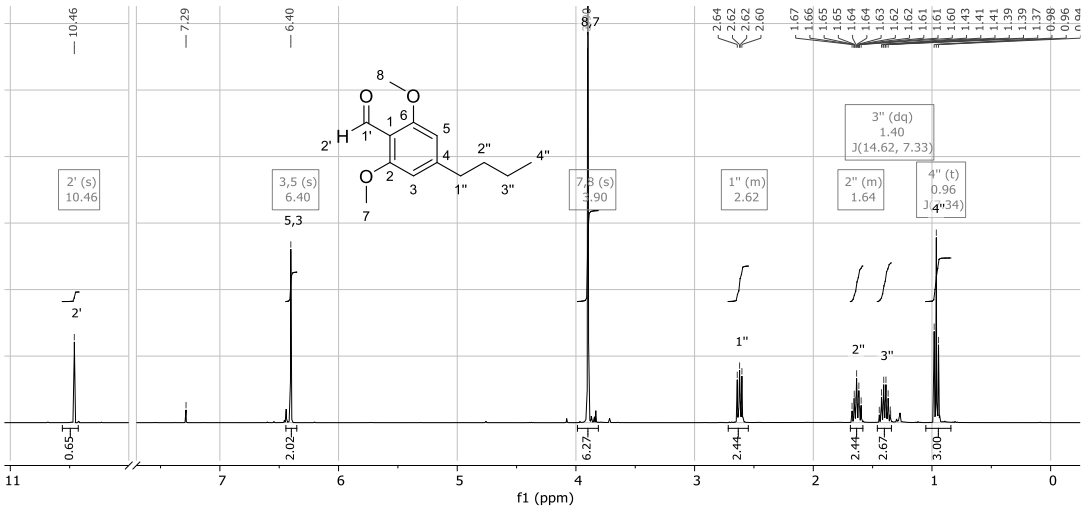

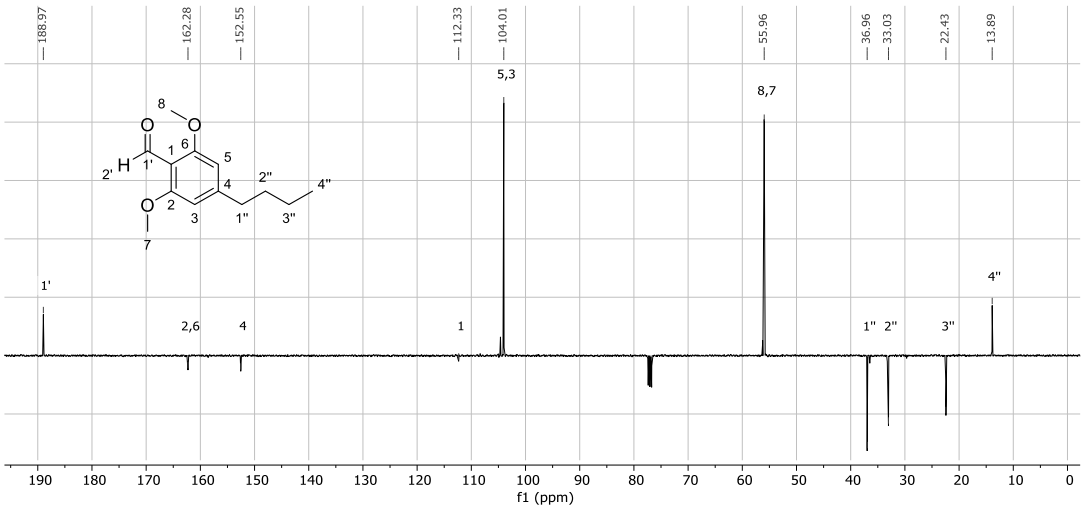

Synthesis of (*E*)-4-(4-butyl-2,6-dimethoxyphenyl)but-3-en-2-one (33)

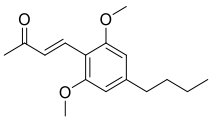

33

A solution of acetone (1.82 mL, 24.6 mmol) and NaOH (6.68 mL, 16.7 mmol, 2.5 M) was quickly added to a solution of **28** (1.09 g, 4.91 mmol) in water (24.6 mL). The reaction was heated at 60°C for 7 hours, then cooled to room temperature, and diluted with Et_2O. The aqueous layer was extracted with Et_2O (3 × 20 mL) and the combined organic layers were washed with HCl (1 M) and brine, dried over Na_2SO_4, filtered, and concentrated under reduced pressure. The crude was purified on silica gel (eluent: *n*-Hex/EtOAc 75:25) to provide 919 mg (80%) of product as light-yellow solid.

HRMS (ESI) *m/z* $[M+Na]^+$ 285.1485 (calcd for $C_{16}H_{22}O_3Na$, 285.1467;

^{1}H NMR (400 MHz, chloroform-*d*) δ 8.0 (d, *J* = 16.6 Hz, 1H, 1'), 7.2 (d, *J* = 16.8 Hz, 1H, 2'), 6.4 (s, 2H, 3, 5), 3.9 (s, 6H, 7, 8), 2.6 (t, *J* = 7.8 Hz, 2H, 1"), 2.4 (s, 3H, 4'), 1.7 – 1.6 (m, 2H, 2"), 1.4 (h, *J* = 7.4 Hz, 2H, 3"), 1.0 (t, *J* = 7.3 Hz, 3H, 4");

^{13}C NMR (101 MHz, chloroform-*d*) δ 169.23 (3'), 160.66 (2, 6), 148.31 (4), 135.74 (2'), 130.04 (1'), 110.48 (1), 104.63 (3, 5), 56.37 (7, 8), 37.32 (1"), 33.97 (2"), 27.57 (4'), 23.12 (3"), 14.60 (4").

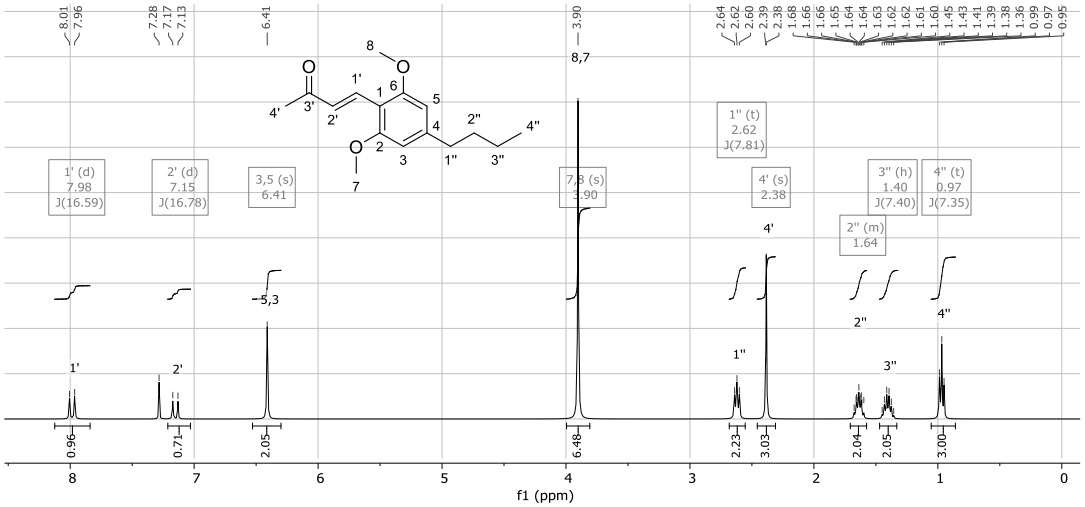

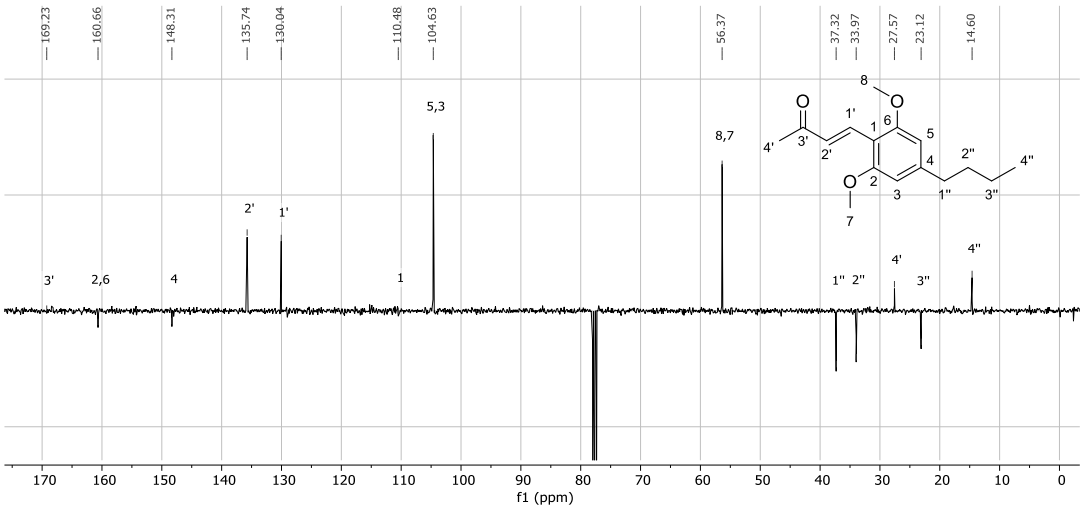

Synthesis of (*S*, *E*)-4-(4-butyl-2,6-dimethoxyphenyl)but-3-en-2-ol (27)

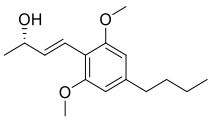

27

A solution of (*R*)-CBS (1.13 mL, 1.13 mmol, 1 M in THF) in anhydrous THF (8.4 mL) was cooled at -78°C under nitrogen atmosphere and $BH_3 \cdot THF$ (7.92 mL, 7.92 mmol) was added. After 30 min, a solution of **33** in THF (1.48 g, 5.66 mmol) was added dropwise and the reaction was stirred at -78°C for 4 hours. The reaction was warmed to room temperature and stirred for 12 hours. Then, the mixture was diluted with EtOAc, NaOH (1 M) was added, and the aqueous layer was extracted with EtOAc (3 × 20 mL). The combined organic layers were washed with $NaHCO_3$ and brine, dried over Na_2SO_4, filtered, and concentrated under *vacuum*. The crude was purified on silica gel (eluent: *n*-Hex/EtOAc 7:3) to provide 1.31 g (87%, ee 74%) of product as pale-yellow oil.

$[\alpha]_D^{22}$ −11.9 (*c* 1.00 in $CHCl_3$);

HRMS (ESI) *m/z* $[M+Na]^+$ 287.1627 (calcd for $C_{16}H_{24}O_3Na$, 287.1623);

^{1}H NMR (400 MHz, chloroform-*d*) δ 6.9 (dd, *J* = 16.1, 1.1 Hz, 1H, 1'), 6.7 (dd, *J* = 16.2, 6.9 Hz, 1H, 2'), 6.4 (s, 2H, 3, 5), 4.5 – 4.4 (m, 1H, 3'), 3.9 (s, 6H, 7, 8), 2.7 – 2.5 (m, 2H, 1"), 1.7 – 1.6 (m, 2H, 2"), 1.4 – 1.3 (m, 5H, 3", 4'), 1.0 (t, *J* = 7.3 Hz, 3H, 4");

^{13}C NMR (101 MHz, chloroform-*d*) δ 159.02 (2, 6), 144.36 (4), 137.20 (2'), 120.86 (1'), 111.88 (1), 104.82 (3, 5), 71.55 (3'), 56.31 (7, 8), 37.03 (1"), 34.19 (2"), 24.10 (4'), 23.12 (3"), 14.65 (4").

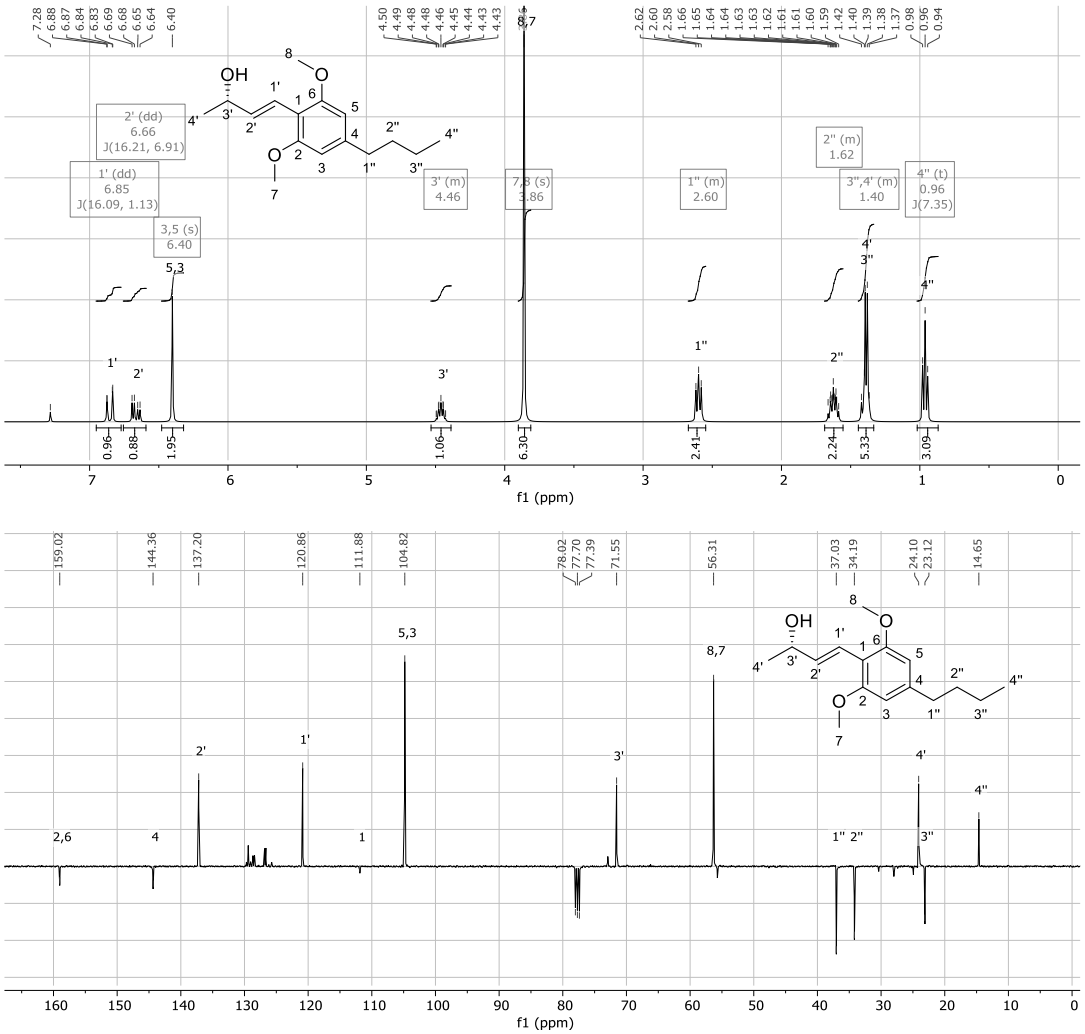

Synthesis of (*S*, *E*)-4-(4-butyl-2,6-dimethoxyphenyl)but-3-en-2-yl 5-methylhex-5-enoate (26)

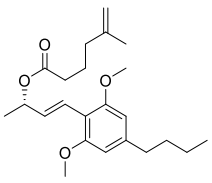

26

To a solution of **27** (1.62 g, 6.13 mmol) in anhydrous DCM (20.4 mL), DMAP (0.37 g, 3.07 mmol), EDC·HCl (2.12 g, 11.0 mmol) and 5-methylhex-5-enoic acid (1.24 mL, 9.20 mmol) were added. Anhydrous triethylamine (1.53 mL, 11.0 mmol) was added dropwise and the solution was stirred for 16 hours. The mixture was washed with HCl (14 mL, 1 M) and brine, dried over Na_2SO_4, filtered, and concentrated under reduced pressure. The crude was purified on silica gel (eluent: *n*-Hex/EtOAc 75:25) to provide 1.83 g (80%) of product as colorless solid.

[α]$_D^{22}$ −28.2 (*c* 1.00 in $CHCl_3$);

HRMS (ESI) *m/z* $[M+Na]^+$ 397.2562 (calcd for $C_{23}H_{34}O_4Na$, 397.2355);

^{1}H NMR (400 MHz, chloroform-*d*) δ 6.9 (dd, *J* = 16.3, 1.2 Hz, 1H, 1'), 6.6 (dd, *J* = 16.2, 7.1 Hz, 1H, 2'), 6.4 (s, 2H, 3, 5), 5.6 – 5.5 (m, 1H, 3'), 4.8 – 4.7 (m, 2H, 10'), 3.9 (s, 6H, 7, 8), 2.6 (t, *J* = 7.8 Hz, 2H, 1"), 2.3 (t, *J* = 7.5 Hz, 2H, 6'), 2.1 (t, *J* = 7.6 Hz, 2H, 8'), 1.8 (p, *J* = 7.6 Hz, 2H, 7'), 1.7 (t, *J* = 1.1 Hz, 3H, 11'), 1.7 – 1.6 (m, 2H, 2"), 1.4 – 1.3 (m, 5H, 3", 4'), 1.0 (t, *J* = 7.3 Hz, 3H, 4");

^{13}C NMR (101 MHz, chloroform-*d*) δ 173.63 (5'), 159.17 (2, 6), 145.63 (9'), 144.57 (4), 132.11 (2'), 122.84 (1'),

111.70 (1), 111.22 (10'), 104.82 (3, 5), 77.99, 77.68, 77.36, 73.56 (3'), 56.31 (7, 8), 37.76 (8'), 37.02 (1''), 34.87 (6'), 34.15 (2''), 23.59 (7'), 23.07 (3''), 22.86 (11'), 21.42 (4'), 14.61 (4'').

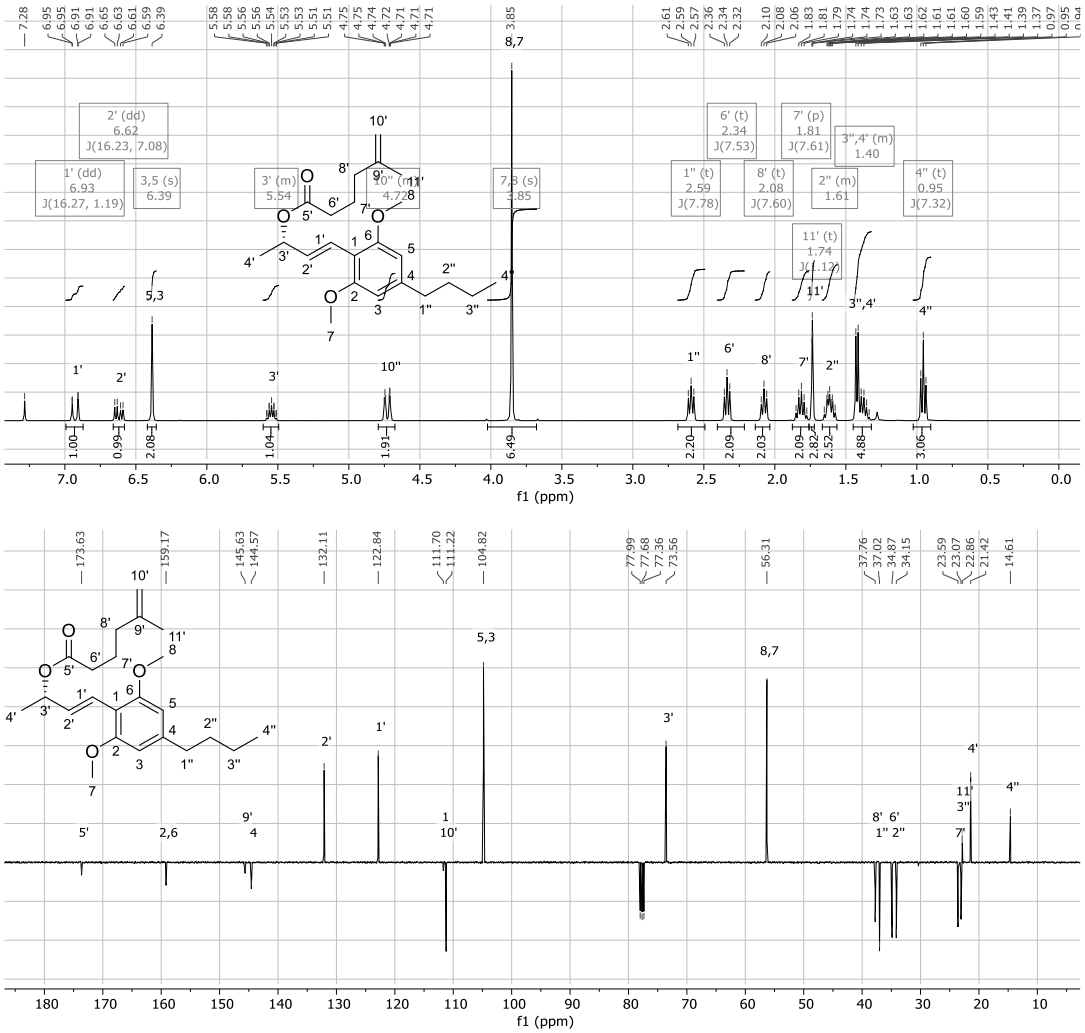

Synthesis of (2*S*,3*R*,*E*)-3-(4-butyl-2,6-dimethoxyphenyl)-2-(3-methylbut-3-en-1-yl)hex-4-enoic acid (25b)

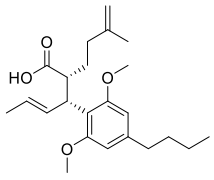

25b

To a solution of KHMDS (1.96 mL, 1.96 mmol, 1M THF) in anhydrous Tol (5.3 mL) at -78°C under nitrogen atmosphere was added a solution of **26** (245 mg, 0.65 mmol) in anhydrous Tol (5.5 mL) and the mixture was stirred at -78°C for 1 h. Then a solution prepared at 0°C of anhydrous pyridine (0.24 mL, 2.93 mmol) and TMS-Cl (0.413 mL, 3.27 mmol) in anhydrous Tol (5 mL) was added to the reaction. After 10 min of stirring, the temperature was warmed at room temperature for 4 h. The reaction was quenched with NH_4Cl and HCl (8 mL, 1 M) and the aqueous layer was extracted with EtOAc (3 × 20 mL) and the combined organic layers were washed with brine, dried over Na_2SO_4, filtered, and concentrated under reduced pressure. The crude was purified on silica gel (eluent: *n*-Hex/EtOAc 8:2) to provide 179 mg (73%) of product as white solid.

[α]$_D^{22}$ +2.4 (*c* 1.00 in $CHCl_3$);

HRMS (ESI) *m/z* $[M+Na]^+$ 397.2364 (calcd for $C_{23}H_{34}O_4Na$, 397.2355);

^{1}H NMR (400 MHz, chloroform-*d*) δ 6.30 (s, 2H, 3, 5), 5.78 (ddd, *J* = 15.21, 9.65, 1.87 Hz, 1H, 4'), 5.53 (dq, *J* = 15.15, 6.36 Hz, 1H, 5'), 4.68 (d, *J* = 10.90 Hz, 2H, 10'), 4.03 (t, *J* = 10.04 Hz, 1H, 3'), 3.73 (s, 6H, 7, 8), 3.17 – 3.06 (m, 1H, 2'), 2.56 – 2.47 (m, 2H, 1''), 1.98 (dd, *J* = 9.54, 6.17 Hz, 2H, 8'), 1.85 – 1.72 (m, 1H, 7'a), 1.70 (s, 3H, 11'), 1.69 – 1.49 (m, 6H, 2'', 6', 7'b), 1.37 (p, *J* = 7.38 Hz, 2H, 3''), 0.93 (t, *J* = 7.33 Hz, 3H, 4'');

^{13}C NMR (101 MHz, chloroform-*d*) δ 180.76 (1'), 158.11 (2, 6), 145.57 (9'), 142.78 (4), 131.07 (4'), 127.18 (5'), 116.20 (1), 110.28 (10'), 105.08 (3, 5), 56.00 (7, 8), 47.70 (2'), 42.16 (3'), 36.33 (1''), 35.82 (8'), 33.58 (2''), 29.67 (7'), 22.71 (3''), 22.54 (11'), 18.07 (6'), 14.12 (4'').

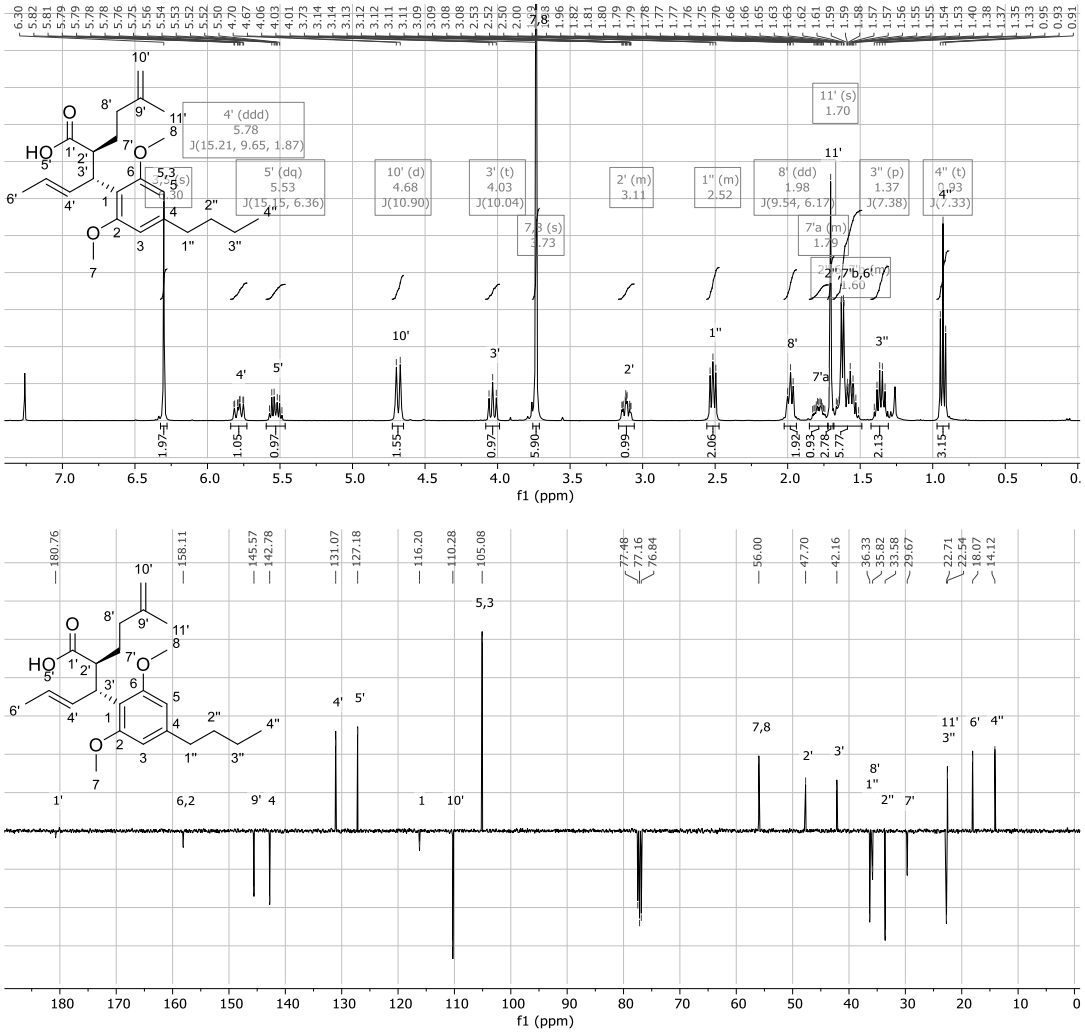

Synthesis of (2*R*,3*R*,*E*)-3-(4-butyl-2,6-dimethoxyphenyl)-2-(3-methylbut-3-en-1-yl)hex-4-enoic acid (25b)

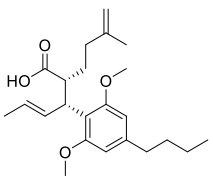

25b

A solution of TMS-Cl (3.95 mL, 31.6 mmol) and triethylamine (3.95 mL, 28.3 mmol) in anhydrous THF (24 mL) was prepared at -78°C under nitrogen atmosphere. A solution of **26** (2.41 g, 6.44 mmol) in anhydrous THF (97 mL) at -78°C was added and then a solution of LDA (9.66 mL, 9.66 mmol, 1 M in THF/hexane) in anhydrous THF (9.66 mL) at -78°C was added dropwise. The mixture was stirred at -78°C for 90 min, then at room temperature for 1 hour and then at reflux for 5 hours. It was quenched with NH_4Cl and HCl (80 mL, 1 M) and the aqueous layer was extracted with EtOAc

(3 × 20 mL) and the combined organic layers were washed with brine, dried over Na_2SO_4, filtered, and concentrated under reduced pressure. The crude was purified on silica gel (eluent: *n*-Hex/EtOAc 9:1) to provide 2.06 g (85%) of product as white solid.

$[\alpha]_D^{22}$ +14.3 (*c* 1.00 in $CHCl_3$);

HRMS (ESI) *m/z* $[M+Na]^+$ 397.2364 (calcd for $C_{23}H_{34}O_4Na$, 397.2355);

^{1}H NMR (400 MHz, chloroform-*d*) δ 6.3 (s, 2H, 3, 5), 5.9 – 5.7 (m, 1H, 4'), 5.6 (dd, *J* = 15.0, 6.5 Hz, 1H, 5'), 4.7 (d, *J* = 10.8 Hz, 2H, 10'), 4.1 (t, *J* = 10.0 Hz, 1H, 3'), 3.8 (s, 6H, 7, 8), 3.1 (td, *J* = 10.6, 3.2 Hz, 1H, 2'), 2.7 – 2.4 (m, 2H, 1''), 2.0 (t, *J* = 7.6 Hz, 2H, 8'), 1.9 – 1.8 (m, 1H, 7'a), 1.7 (s, 3H, 11'), 1.7 – 1.5 (m, 6H, 2'', 6', 7'b), 1.4 (h, *J* = 7.3 Hz, 2H, 3''), 1.0 (t, *J* = 7.3 Hz, 3H, 4'');

^{13}C NMR (101 MHz, chloroform-*d*) δ 181.84 (1'), 158.63 (2, 6), 146.08 (9'), 143.28 (4), 131.61 (4'), 127.67 (5'), 116.72 (1), 110.82 (10'), 105.60 (3, 5), 56.51 (7, 8), 48.30 (2'), 42.69 (3'), 36.85 (1''), 36.35 (8'), 34.11 (2''), 30.16 (7'), 23.24 (3''), 23.05 (11'), 18.59 (6'), 14.64 (4'').

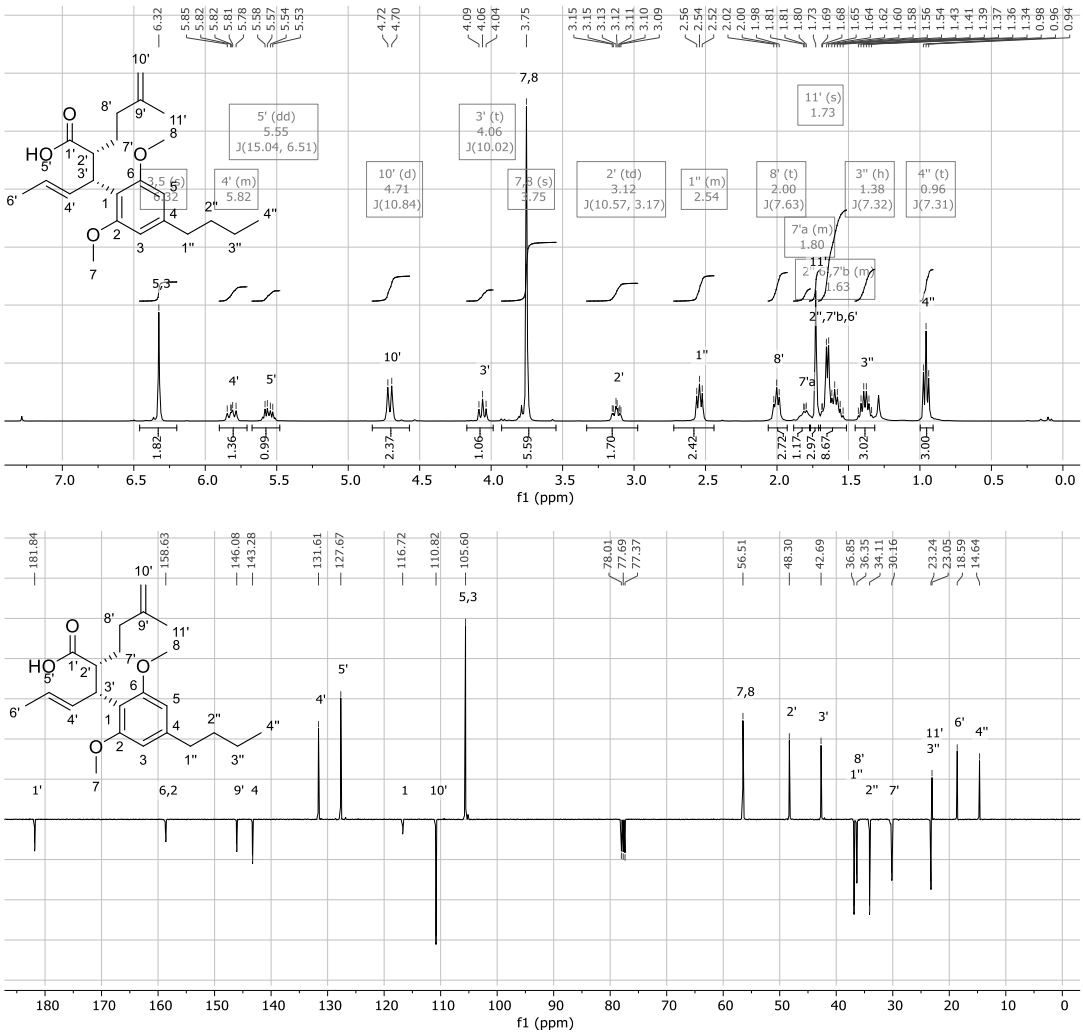

Synthesis of (3*R*,4*R*,*E*)-4-(4-butyl-2,6-dimethoxyphenyl)-3-(3-methylbut-3-en-1-yl)hept-5-en-2-one (34)

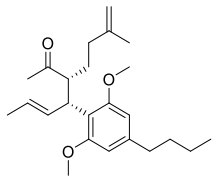

34

A solution of **25** (2.05 g, 5.48 mmol) in anhydrous ether (55 mL) was cooled at 0°C and methyllithium (8.6 mL, 13.7 mmol, 1.6 M in ether) was added dropwise. The mixture was stirred at 0°C for 1 hour and at room temperature for 3 hours. Then, the reaction was quenched with NH_4Cl (10 mL) and the aqueous layer was extracted with DCM (3 × 15 mL). The combined organic layers were dried over Na_2SO_4, filtered, and concentrated under reduced pressure. The crude was purified on silica gel (eluent: *n*-Hex/EtOAc 95:5) to provide 1.59 g (78%) of product as colourless oil.

$[\alpha]_D^{22}$ +17.2 (*c* 1.00 in $CHCl_3$);

HRMS (ESI) *m/z* $[M+Na]^+$ 395.2571 (calcd for $C_{24}H_{36}O_3Na$, 395.2562);

^{1}H NMR (400 MHz, chloroform-*d*) δ 6.3 (s, 2H, 3, 5), 5.8 (ddq, *J* = 15.1, 9.3, 1.5 Hz, 1H, 4'), 5.7 – 5.5 (m, 1H, 5'), 4.8 – 4.7 (m, 2H, 11'), 4.1 – 4.0 (m, 1H, 3'), 3.8 (s, 6H, 7, 8), 3.3 (td, *J* = 10.9, 3.4 Hz, 1H, 2'), 2.6 – 2.5 (m, 2H, 1''), 2.0 – 1.9 (m, 2H, 9'), 1.9 – 1.8 (m, 4H, 7', 8'a), 1.7 (t, *J* = 1.1 Hz, 3H, 12'), 1.7 – 1.6 (m, 4H, 6', 8'b), 1.7 – 1.5 (m, 2H, 2''), 1.5 – 1.3 (m, 2H, 3''), 1.0 (t, *J* = 7.3 Hz, 3H, 4'');

^{13}C NMR (101 MHz, chloroform-*d*) δ 157.65 (2, 6), 145.73 (10'), 142.88 (4), 131.29 (4'), 126.77 (5'), 115.96 (1), 109.99 (11'), 104.84 (3, 5), 55.74 (7, 8), 54.74 (2'), 42.12 (3'), 36.18 (1''), 35.87 (9'), 33.46 (2''), 29.46 (8'), 28.85 (7'), 22.51 (3''), 22.36 (12'), 17.93 (6'), 13.97 (4'').

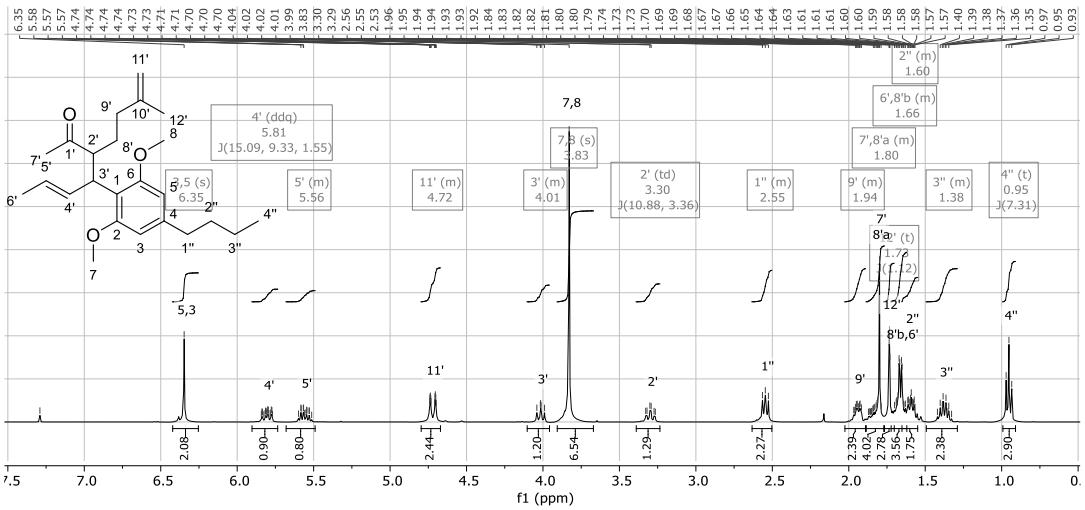

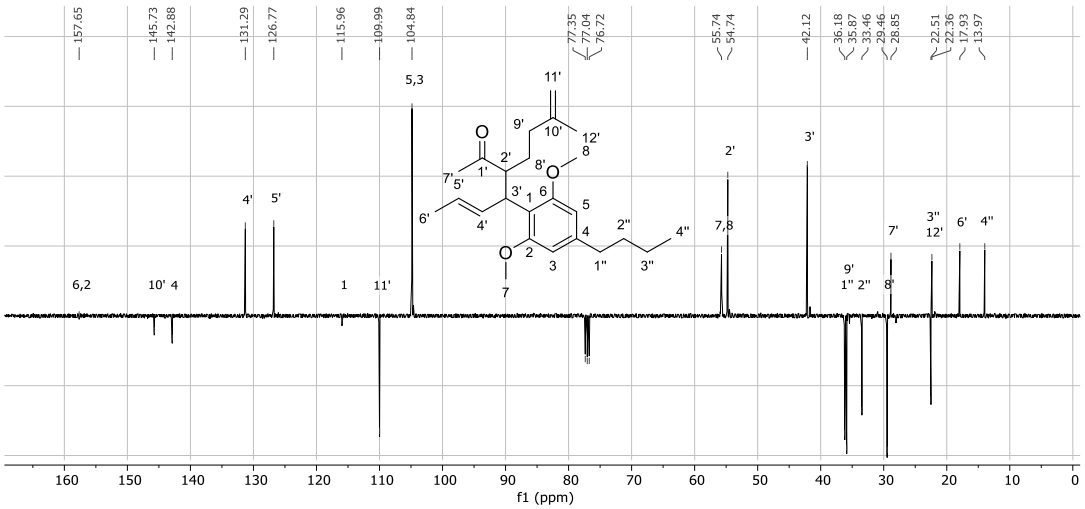

Synthesis of 1-{(1*R*,2*R*)-4'-butyl-2',6'-dimethoxy-5-methyl-1,2,3,4-tetrahydro-[1,1'-biphenyl]-2-yl}ethan-1-one (24)

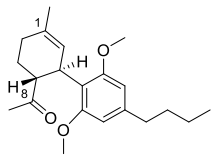

24

Umicore M73 SIMes catalyst (35.5 mg, 6.7 µmol, 14% w/w) was added to a solution of **34** (50 mg, 0.134 mmol) in anhydrous DCM (6.7 mL) under nitrogen atmosphere. The reaction mixture was stirred for 10 hours at 40°C and then another portion of Umicore M73 SIMes catalyst (35.5 mg, 6.7 µmol, 14% w/w) was added. The mixture was stirred for further 5 hours at 40°C. The solvent was removed under *vacuum* and the crude was purified on silica gel (eluent: *n*-Hex/EtOAc 95:5) to provide 40 mg (90%) of product as colourless oil.

[α]$_D^{22}$ −54.5 (*c* 1.00 in $CHCl_3$);

HRMS (ESI) *m/z* $[M+Na]^+$ 353.2099 (calcd for $C_{21}H_{30}O_3Na$, 353.2093);

^{1}H NMR (400 MHz, chloroform-*d*) δ 6.4 (s, 2H, 4', 6'), 5.2 (d, *J* = 2.6 Hz, 1H, 2), 4.2 (ddt, *J* = 13.0, 4.5, 2.3 Hz, 1H, 3), 3.8 (s, 6H, 7', 8'), 3.3 (ddd, *J* = 13.0, 10.4, 3.0 Hz, 1H, 4), 2.6 (t, *J* = 7.8 Hz, 2H, 1"), 2.2 – 2.1 (m, 1H, 6a), 2.1 – 2.0 (m, 1H, 6b), 1.9 (s, 3H, 9), 1.9 – 1.8 (m, 2H, 5), 1.8 – 1.6 (m, 3H, 7), 1.6 (qd, *J* = 8.7, 8.0, 6.5 Hz, 2H, 2"), 1.4 (h, *J* = 7.2 Hz, 2H, 3"), 1.0 (t, *J* = 7.3 Hz, 3H, 4");

^{13}C NMR (101 MHz, chloroform-*d*) δ 158.49 (1', 3'), 142.82 (5'), 131.12 (1), 124.86 (2), 117.19 (2'), 104.93 (4', 6'), 55.93 (7', 8'), 51.13 (4), 36.21 (1"), 34.67 (3), 33.55 (2"), 29.56 (6), 28.64 (9), 26.61 (5), 23.35 (7), 22.54 (3"), 14.03 (4"). 8 not detected because out of ppm range.

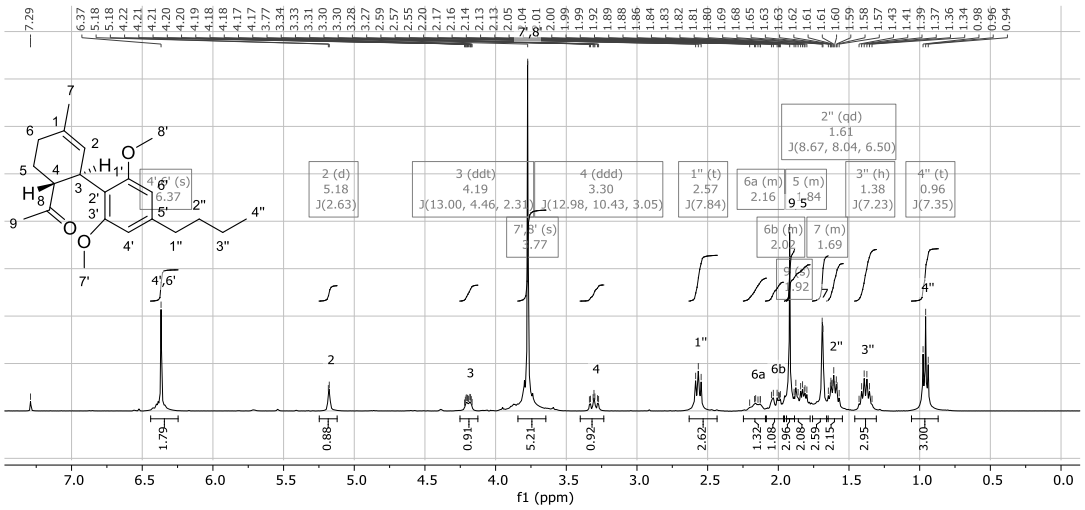
2 (d)
5.18
J(2.63)
3 (ddt)
4.19
J(13.00, 4.46, 2.31)
4 (ddd)
3.30
J(12.98, 10.43, 3.05)
1" (t)
2.57
J(7.84)
2" (qd)
1.61
J(8.67, 8.04, 6.50)
3" (h)
1.38
J(7.23)
4" (t)
0.96
J(7.35)
f1 (ppm)

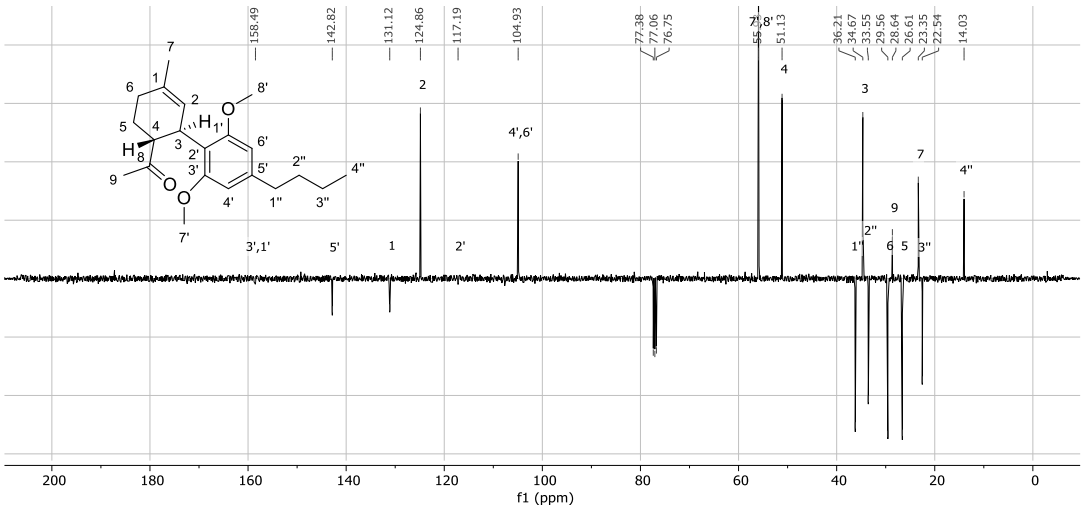
f1 (ppm)

Synthesis of (1*R*,2*R*)-4'-butyl-2',6'-dimethoxy-5-methyl-2-(prop-1-en-2-yl)-1,2,3,4-tetrahydro-1,1'-biphenyl (35)

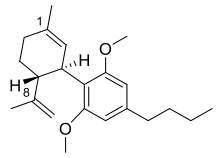

35

n-BuLi (0.145 mL, 0.232 mmol, 1.6 M) was added dropwise to a solution of $MePPh_3Br$ (83 mg, 0.232 mmol) in anhydrous THF (2.43 mL) at 0°C under nitrogen atmosphere. The mixture was stirred at 0°C for 45 min and **24** (60 mg, 0.184 mmol) was added. The reaction was stirred at room temperature for further 18 hours. The reaction was quenched with NH_4Cl and the aqueous layer was extracted with *n*-Hex (3 × 15 mL). The combined organic layers were washed with water, dried over Na_2SO_4, filtered, and concentrated under reduced pressure. The crude was purified on silica gel (eluent: *n*-Hex/EtOAc 97:3) to provide 64 mg (56%) of product as yellow oil.

$[\alpha]_D^{22}$ −56.3 (*c* 1.00 in $CHCl_3$);

HRMS (ESI) *m/z* $[M+Na]^+$ 351.2307 (calcd for $C_{22}H_{32}O_2Na$, 351.2300);

^{1}H NMR (400 MHz, chloroform-*d*) δ 6.4 (s, 2H, 4', 6'), 5.2 (s, 1H, 2), 4.5 – 4.4 (m, 2H, 9), 4.1 – 3.9 (m, 1H, 3), 3.8 (s, 6H, 7', 8'), 2.9 (td, *J* = 10.7, 4.1 Hz, 1H, 4), 2.6 – 2.5 (m, 2H, 1''), 2.3 – 2.1 (m, 1H, 6a), 2.0 (d, *J* = 16.8 Hz, 1H, 6b), 1.9 – 1.7 (m, 2H, 5), 1.7 (s, 3H, 7), 1.7 – 1.5 (m, 6H, 2'', 10), 1.4 (h, *J* = 7.3 Hz, 2H, 3''), 1.0 (t, *J* = 7.3 Hz, 3H, 4'');

^{13}C NMR (101 MHz, chloroform-*d*) δ 159.77 (1', 3'), 150.22 (8), 142.50 (5'), 131.86 (1), 126.60 (2), 119.59 (2'), 110.24 (9), 105.59 (4', 6'), 56.60 (7', 8'), 45.86 (4), 36.83 (1''), 36.76 (3), 34.18 (2''), 31.42 (6), 30.38 (5), 24.13 (7), 23.23 (3''), 19.73 (10), 14.69 (4'').

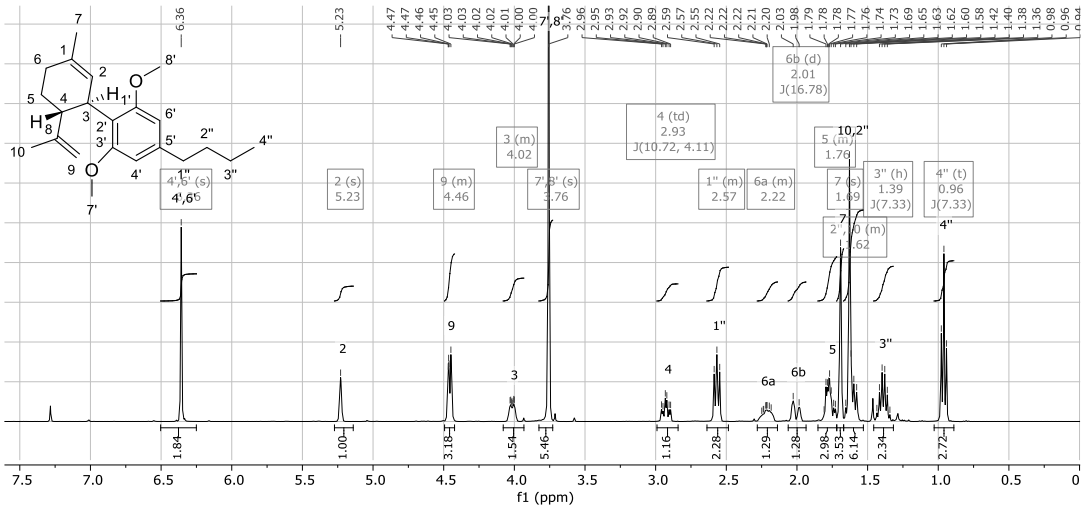

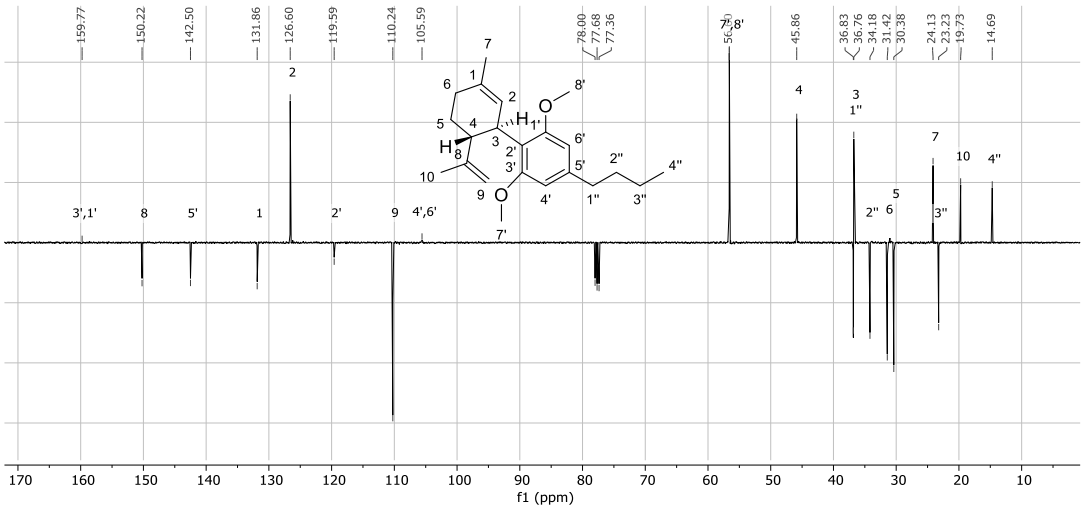

Synthesis of (1'*R*,2'*R*)-4-butyl-5'-methyl-2'-(prop-1-en-2-yl)-1',2',3',4'-tetrahydro-[1,1'-biphenyl]-2,6-diol (CBD-C$_4$)

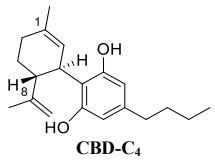

CBD-C$_4$

a) Sodium ethanethiolate (360 mg, 4.26 mmol) was added to a solution of **35** (70.0 mg, 0.213 mmol) in anhydrous DMF (2.13 mL) into sealed tube under nitrogen atmosphere. The reaction mixture was stirred at 140°C for 24 hours. Once cooled, the reaction was quenched with $NaHCO_3$ and the aqueous layer was extracted with EtO_2 (3 × 2 mL). The combined organic layers were washed with water (1 × 2 mL), brine (1 × 2 mL), dried over Na_2SO_4, filtered, and concentrated under reduced pressure. The crude was purified on silica gel (eluent: *n*-Hex/EtOAc 99:1 to 85:15) to provide 53 mg (79%) of **36** as pale-yellow oil.

b) Sodium ethanethiolate (610 mg, 7.25 mmol) was added to a solution of **36** (76.0 mg, 0.242 mmol) in anhydrous DMF (4.00 mL) into sealed tube under nitrogen atmosphere. The reaction mixture was stirred at 145°C for 18 hours. Once cooled to room temperature, the reaction was quenched with $NaHCO_3$ and the aqueous layer was extracted with EtO_2 (3 × 2 mL). The combined organic layers were washed with water (1 × 2 mL), brine (1 × 2 mL), dried over Na_2SO_4, filtered, and concentrated under reduced pressure. The crude was purified on silica gel (eluent: *n*-Hex/EtOAc 99:1 to 85:15) to provide 20.4 mg (28%) of product as pale-yellow oil.

[α]$_D^{22}$ −220.7 (*c* 1.00 in $CHCl_3$);

HRMS (ESI) *m/z* $[M+Na]^+$ 323.1992 (calcd for $C_{20}H_{28}O_2Na$, 323.1987);

^{1}H NMR (400 MHz, chloroform-*d*) δ 6.4 – 5.9 (m, 2H, 4', 6'), 5.6 (s, 1H, 2), 4.8 – 4.5 (m, 2H, 9), 3.9 (ddq, *J* = 10.5, 4.5, 2.2 Hz, 1H, 3), 2.6 – 2.3 (m, 3H, 1", 4), 2.4 – 2.2 (m, 1H, 6a), 2.1 (dp, *J* = 15.3, 2.7 Hz, 1H, 6b), 1.8 (d, *J* = 13.3 Hz, 5H, 5, 7), 1.7 (s, 3H, 10), 1.6 (p, *J* = 7.6 Hz, 2H, 2"), 1.3 (q, *J* = 7.3 Hz, 2H, 3"), 0.9 (t, *J* = 7.3 Hz, 3H, 4");

^{13}C NMR (101 MHz, chloroform-*d*) δ 154.12 (1', 3'), 149.32 (8), 142.98 (5'), 140.01 (1), 124.16 (2), 113.77 (2'), 110.85 (9), 108.48 (4', 6'), 46.17 (4), 37.20 (3), 35.19 (1"), 33.11 (2"), 30.40 (6), 28.41 (5), 23.68 (7), 22.33 (3"), 20.47 (10), 13.96 (4").

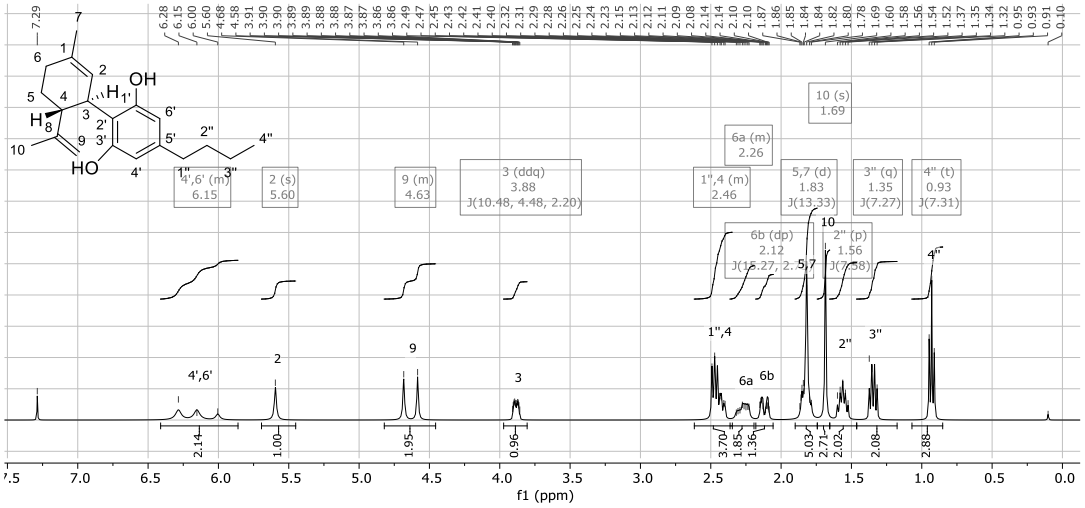
10 (s)
1.69
6a (m)
2.26
4',6' (m)
6.15
2 (s)
5.60
9 (m)
4.63
3 (ddq)
3.88
J(10.48, 4.48, 2.20)
1",4 (m)
2.46
5,7 (d)
1.83
J(13.33)
3''' (q)
1.35
J(7.27)
4''' (t)
0.93
J(7.31)
6b (dp)
2.12
2''' (p)
1.56
f1 (ppm)

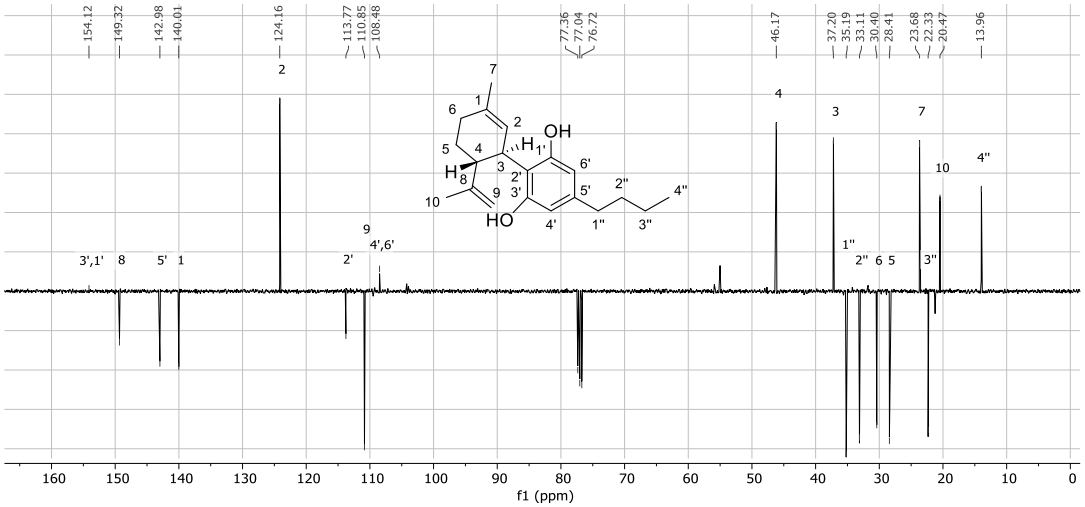
154.12
149.32
142.98
140.01
124.16
113.77
110.85
108.48
77.36
77.04
76.72
46.17
37.20
35.19
33.11
30.40
28.41
23.68
22.33
20.47
13.96
f1 (ppm)

Chapter IV Enantioselective Synthesis of C_{11}-C_{15} and C_{16}-C_{27} Fragments of Callyspongiolide

The enantioselective synthesis of two unsaturated fragments of callyspongiolide was carried out during the 5 months of period abroad as host in laboratory of Organic Chemistry at Faculty of Pharmacy and Food at the University of Barcelona with Professors Núria Llor Brunes and Maria Mercedes Amat Tuson.

1 Introduction

Macrolides constitute a large family of compounds isolated from several natural sources that often have biologically interesting properties.[137] Macrolides have been isolated from various marine microorganisms and are particularly abundant in marine sponges, as exemplified by the discovery of dictyostatin,[138] salicylihalamides A and B,[139] leiodermatolide A, B and C,[140] phormidolides B and C[141] or kabiramides J and K,[142] and many others.

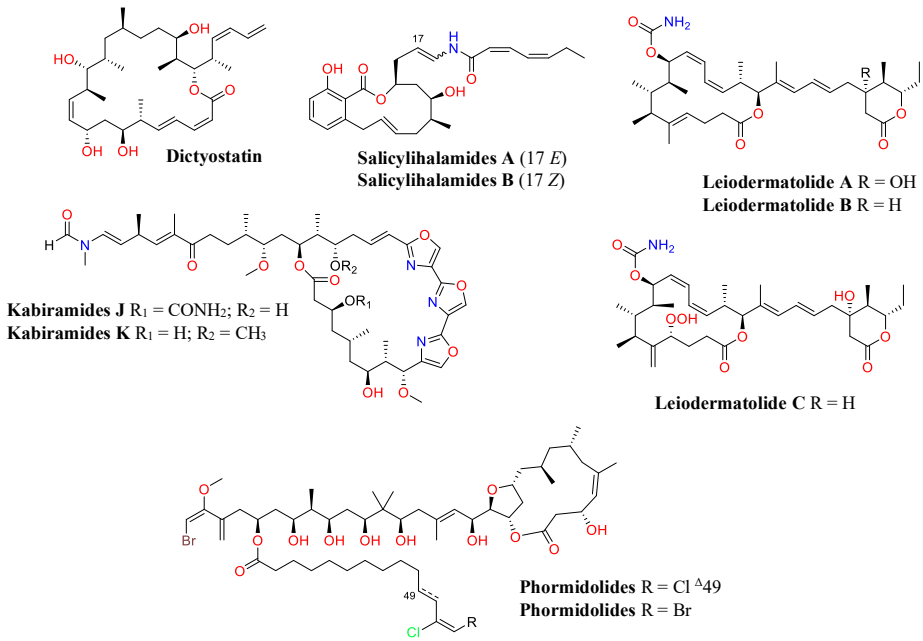

Figure 1.1 Macrolides isolated from various marine microorganisms.

137 H. Ebrahim, K. El Sayed, *Mar. Drugs* **2016**, *14*, 57; R. D. Norcross, I. Paterson, *Chem. Rev.* **1995**, *95*, 2041–2114; J. G. Napolitano, A. H. Daranas, et al., *Anticancer. Agents Med. Chem.* **2012**, *9*, 122–137.

138 G. R. Pettit, Z. A. Cichacz, et al., *J. Chem. Soc. Chem. Commun.* **1994**, 1111–1112.

139 E. KL, B. JA, et al., *J. Org. Chem.* **1997**, *62*, 8188–8192.

140 I. Paterson, S. M. Dalby, et al., *Angew. Chemie Int. Ed.* **2011**, *50*, 3219–3223; W. AE, R. JC, et al., *J. Nat. Prod.* **2017**, *80*, 735–739.

141 A. Lorente, A. Gil, et al., *Chem. – A Eur. J.* **2015**, *21*, 150–156.

142 T. Sirirak, S. Kittiwisut, et al., *J. Nat. Prod.* **2011**, *74*, 1288–1292.

Sponges belonging to the genus *Callyspongia* (order Haplosclerida, family Callyspongiidae) constitute a large taxonomic group that includes more than 100 species. These sponges are rich sources of several types of cytotoxic substances, such as polyketides,[143] polyacetylenes,[144] alkaloids,[145] and cyclic peptides,[146] and only with the isolation of the callyspongiolide,[147] the first macrolide belonging to this species was described.

In 2014, Proksch and co-workers reported the isolation of trace amounts of callyspongiolide from the Indonesian coastal sponge *Callyspongia* sp.[147] The structure was elucidated via a combination of NMR experiments and HRMS. It contains a conjugated diene-ynic side chain terminating on one side with a brominated benzyl ring, while a 14-membered macrocyclic lactone ring is attached to the other end. In addition, six stereogenic centres are present in callyspongiolide, of which five are in the macrocyclic ring and one in the side chain. The relative stereochemistry of the macrocyclic core was assigned based on coupling constants and advanced 1D NOE and 2D NOESY experiments. Nevertheless, the absolute stereochemistry of callyspongiolide remained unknown and it was not possible to determine the relative configuration of the asymmetric C_{21} in the side chain because it is too far from the macrocycle.

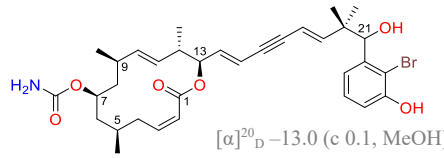

$[\alpha]^{20}_{D}$ –13.0 (c 0.1, MeOH)

Callyspongiolide

The complex structure is an excellent source of inspiration for the development of new anticancer agents because callyspongiolide kills cells in a caspase-independent manner. Compounds that exert their cytotoxicity through non-apoptotic mechanisms are potential tools to be explored as novel therapeutic strategies, as in most cancers apoptotic signalling is suppressed leading to drug resistance in many treatments.[148] Callyspongiolide is strongly cytotoxic toward L5178Y murine lymphoma cells and exhibits significant *in vitro* cytotoxicity against human Jurkat J16 T and Ramos B lymphocytes (IC_{50} 70 and 60 nM, respectively). The low amount of isolated callyspongiolide (4.6 mg) made further biological studies difficult, thus a synthetic route to obtain this molecule is indispensable.

In 2016, Z. Xu, T. Ye *et al.*[149] published the synthesis of the four possible stereoisomers of callyspongiolide with the relative macrocyclic stereochemistry established above. Based on the comparison of specific rotation value and spectroscopic NMR data, compound **37** is identical to the extracted callyspongiolide, thus determining the absolute configuration of the NP.

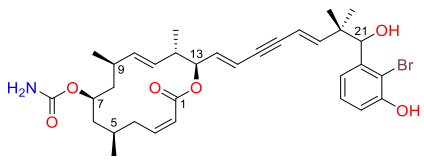

Callyspongiolide **37** (21 *R*) $[\alpha]_D^{20}$ –13.0 (*c* 0.1, MeOH)
ent- **37** (21 *S*) $[\alpha]_D^{20}$ +12.0 (*c* 0.1, MeOH)

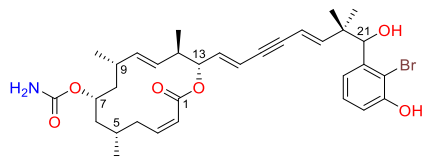

epi- **37** (21 *S*) $[\alpha]_D^{20}$ –68.8 (*c* 0.1, MeOH)
ent-epi- **37** (21 *R*) $[\alpha]_D^{20}$ +66.0 (*c* 0.1, MeOH)

143 M. Kobayashi, K. Higuchi, et al., *Tetrahedron Lett.* **1997**, *38*, 2859–2862.

144 D. T. A. Youssef, R. W. M. van Soest, N. Fusetani, *J. Nat. Prod.* **2003**, *66*, 679–681.

145 M. S. Buchanan, A. R. Carroll, et al., *J. Nat. Prod.* **2007**, *70*, 2040–2041.

146 B. N, R. A, et al., *Org. Lett.* **2004**, *6*, 2543–2545; S. R. M. Ibrahim, C. C. Min, et al., *Bioorg. Med. Chem.* **2010**, *18*, 4947–4956; G. Daletos, R. Kalscheuer, et al., *J. Nat. Prod.* **2015**, *78*, 1910–1925.

147 C.-D. Pham, R. Hartmann, et al., *Org. Lett.* **2013**, *16*, 266–269.

148 T. M. Caserta, A. N. Smith, et al., *Apoptosis 2003 84* **2003**, *8*, 345–352; Y. Pommier, O. Sordet, et al., *Oncogene* **2004**, *23*, 2934–2949.

149 J. Zhou, B. Gao, et al., *J. Am. Chem. Soc.* **2016**, *138*, 6948–6951.

2 Aim of the project

At the beginning, several studies related to total synthesis[150] and constituent fragments[151] have been published, highlighting the interest aroused by callyspongiolide. In all the syntheses described, the assembly of the macrocyclic ring foresees the presence of an unsaturated substituent at C_{13} suitable for subsequent processing for the introduction of the side chain.

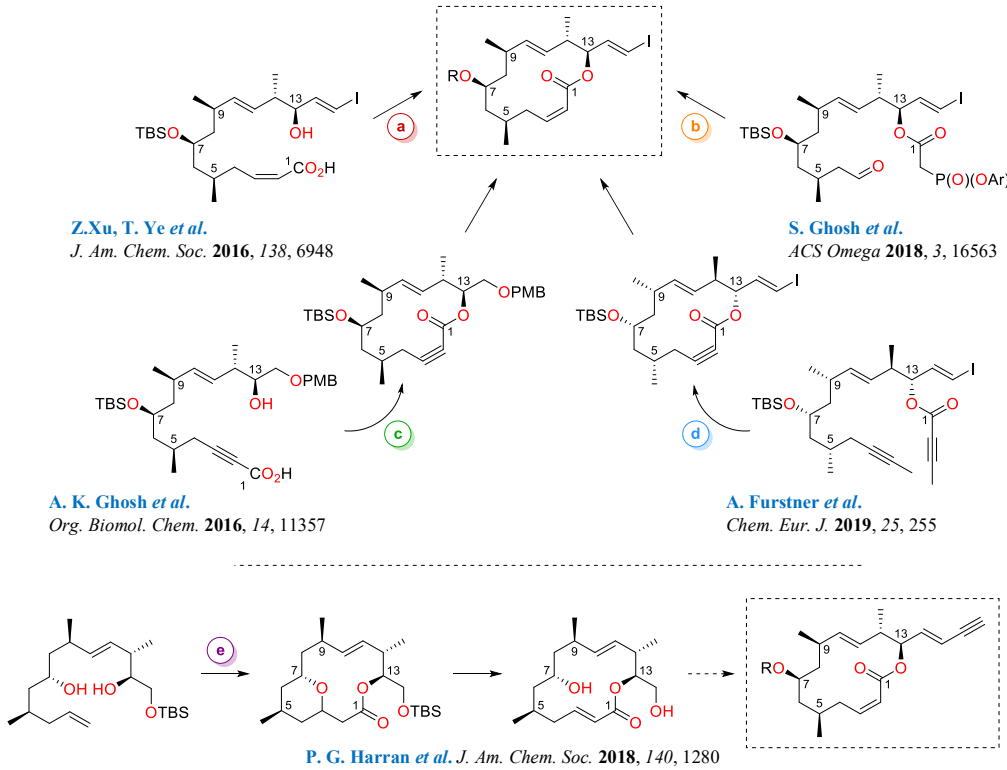

Scheme 2.1 Different synthetic approaches reported in literature for the construction of the macrocycle.

Macrocycle closure was achieved by macrolactonisation[149,150a,152] (C_1-O bond formation, path **a** and path **c**), Horner-Wadsworth-Emmons olefination[150c] or ring-closing alkyne metathesis[150d] (C_2-C_3 bond formation, path **b** and path **d**), and carbonylative macrolactonisation[150b] (C_2-C_1-O bond formation, path **e**). Other synthetic studies included the assembly of C_{11}-C_{21}[151a] and C_3-C_{15}[151b] fragments and the synthesis of 9,12-didemethyl and C_{10}-C_{11} alkyne analogues.[153]

In all plans, the ring-closing metathesis reaction (RCM) at position C_{10}-C_{11} was not considered for macrocycle formation. Therefore, the goal to achieve was to complete the synthesis of callyspongiolide using a different route. The strategy for the synthesis of callyspongiolide was based on the construction of the macrolide (fragment **A**) and side chain (fragment **B**), which would then be joined in the final stages of the synthesis by Sonogashira coupling with bond formation C_{15}-C_{16}. The ring closure of fragment **A** would be obtained by the RCM of the

150 **a]** A. K. Ghosh, L. A. Kassekert, *Org. Lett.* **2016**, *18*, 3274–3277; **b]** F. Manoni, C. Rumo, et al., *J. Am. Chem. Soc.* **2018**, *140*, 1280–1284; **c]** A. Sharma, S. Athe, S. Ghosh, *ACS Omega* **2018**, *3*, 16563–16575; **d]** B. Wölfl, G. Mata, A. Fürstner, *Chem. - A Eur. J.* **2019**, *25*, 255–259.

151 **a]** E. Matoušová, P. Koukal, et al., *Org. Lett.* **2016**, *18*, 5656–5659; **b]** G. Reddy Ramidi, J. S. Yadav, D. K. Mohapatra, *Tetrahedron Lett.* **2018**, *59*, 3579–3582.

152 A. K. Ghosh, L. A. Kassekert, J. D. Bungard, *Org. Biomol. Chem.* **2016**, *14*, 11357–11370.

153 G. Mata, B. Wölfl, A. Fürstner, *Chem. - A Eur. J.* **2019**, *25*, 246–254.

ester formed between the alcohol **C** (fragment C_{11}-C_{15}) and the carboxylic acid **D** (fragment C_1-C_{10}), which would be prepared from aldehyde **E** using a stereoselective homocrotylation reaction and Still-Gennari olefination as key steps. The contribution to the aim was the stereoselective synthesis of fragments **B** and **C**.

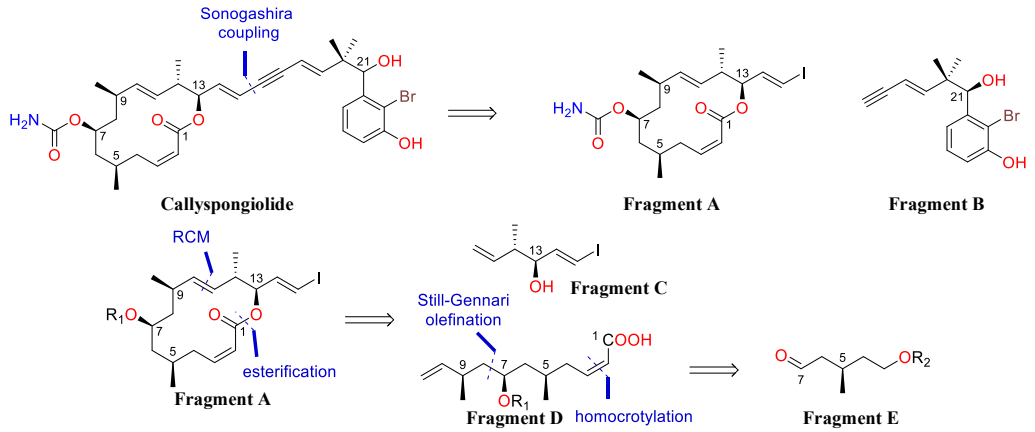

Scheme 2.2 The main fragments into which callyspongiolide can be broken up.

3 Results and discussion

3.1 Fragment C of callyspongiolide

3.1.1 State of art

Initially, a first retrosynthetic analysis planned at University of Barcelona to obtain fragment **A** identified the macrocyclic intermediate from crotyl alcohol **38**. Subsequently, the vinyl iodide C_{15} would be installed by a Takai olefination (**Scheme 3.1**). The alcohol **38** could be constructed by the reductive ozonolysis of the allyl alcohol properly protected and subjected to the Leighton enantioselective crotylation reaction to introduce the two stereocentres of known configuration.

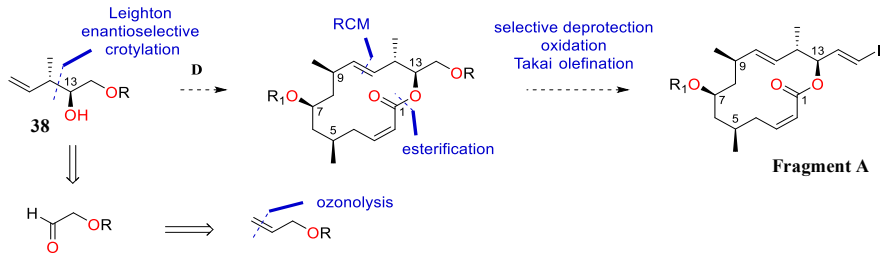

Scheme 3.1 The first synthetic strategy applied.

However, the union between carboxylic acid **D** and alcohol **38** according to the Yamaguchi[154] protocol produced traces of ester, recovering most of the starting products. Moreover, considering the difficult purification of **38** due to an incomplete conversion of the precursors as an additional problem, this first pathway has been abandoned.

The second approach involved a convergent synthetic strategy by esterification of carboxylic acid **D** with alcohol

154 L. C. Dias, E. C. Polo, *J. Org. Chem.* **2017**, *82*, 4072–4112.

C. In fact, the number of steps is reduced since the fragment C_{11}-C_{15} already incorporates the iodo-vinyl group with appropriate configuration of the stereocentres. The stereogenic centres would be generated by the enantioselective Leighton crotylation of aldehyde **39** synthesised from ethyl *cis*-iodoacrylate **40**.

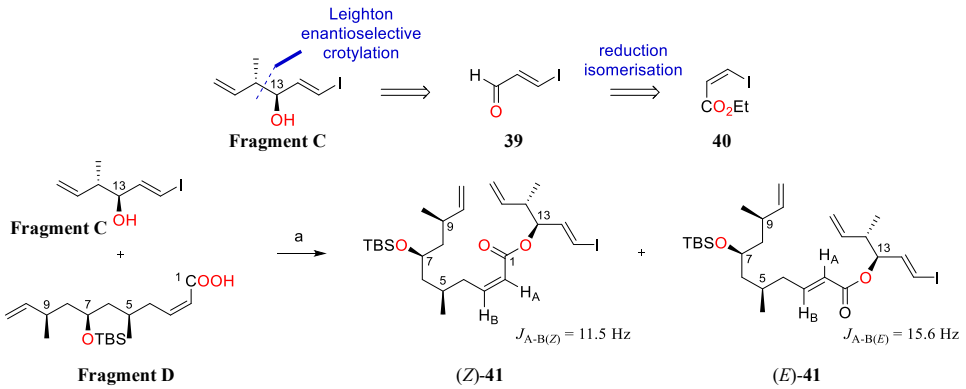

Scheme 3.2 The second synthetic strategy applied. *Reaction condition*: a) TCBC, DMAP, TEA, Tol, 42% (dr *Z*:*E* 1.2:1).

Unexpectedly, the Yamaguchi esterification coupling of alcohol **C** with carboxylic acid **D** resulted in a mixture of (*Z*)-**41** and (*E*)-**41** isomers (**Scheme 3.2**). The isomerization of the α/β-unsaturated ester can be attributed to the 1,4 addition of the DMAP followed by an elimination process that leads to the loss of the stereochemical information of the double bond configuration.[88b, 116] Therefore, it was necessary to carry out an esterification using a procedure that did not use the DMAP.

Therefore, a Mitsunobu[155] was planned to avoid the isomerisation of the unsaturated α/β double bond of the ester. This reaction allows not only the esterification of the alcohols, but also the conversion of the alcohols into other functional groups. Unlike other more commonly used coupling reagents that work by activating the carboxylic acid for the nucleophilic attack of alcohol, in the Mitsunobu reaction it is the alcohol that is activated to be attacked by the carboxylic acid. It is a versatile method and widely used that employs an oxidising azodicarboxylate (DIAD or DEAD mainly) and a reductive phosphine (typically PPh_3) under mild reaction conditions. The reaction proceeds with the inversion of configuration at the alcoholic stereocentre.[156] For this reason, the diastereoisomer of the alcohol **C** (epi-**C**) with the opposite configuration at the stereogenic centre in C_{13} was required.

3.1.2 Retrosynthetic approach

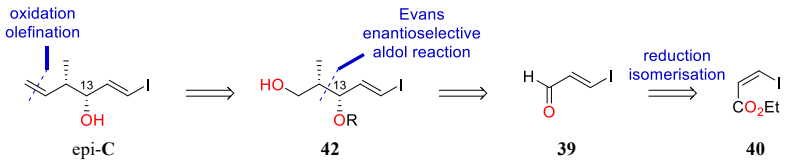

Scheme 3.3 Retrosynthetic analysis to obtain the diastereoisomer of Fragment **C**.

The synthesis of epi-**C** could be achieved by methylation and deprotection of the aldehyde prepared from alcohol **42** through oxidation. The controlled formation of the C_{12} and C_{13} stereocentres of **42** would be obtained *via* the Evans enantioselective aldol reaction starting from the α/β-unsaturated aldehyde **39** followed by alcoholic protection and removal of the chiral auxiliary under reductive conditions. **39** could derive from the known ethyl *cis*-iodoacrylate **40** exploiting the isomerisation of the double bond during the reduction to aldehyde.

155 O. Mitsunobu, M. Yamada, *Bull. Chem. Soc. Jpn.* **1967**, *40*, 2380–2382.

156 **a]** T. Y. S. But, P. H. Toy, *Chem. – An Asian J.* **2007**, *2*, 1340–1355; **b]** K. C. K. Swamy, N. N. B. Kumar, et al., *Chem. Rev.* **2009**, *109*, 2551–2651; **c]** S. Fletcher, *Org. Chem. Front.* **2015**, *2*, 739–752; **d]** For a discussion of the mechanism of the Mitsunobu reaction see: S. Schenk, J. Weston, E. Anders, *J. Am. Chem. Soc.* **2005**, *127*, 12566–12576.

3.1.3 Synthesis of fragment epi-C C_{11}-C_{15} of callyspongiolide

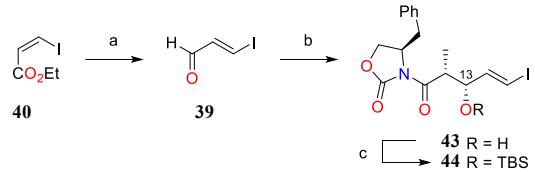

Scheme 3.4 *Reaction conditions*: a) DIBAL-H 1.1 eq, CH_2Cl_2, -78°C, 2 h, then 0°C for 45 min, then -78°C, MeOH 12 eq, Et_2O, Rochelle salt, 1 h, rt; b) Evans base enolate: [(*R*)-(+)-4-Benzyl-3-propionyl-2-oxazolidinone 1.1 eq, nBu_2BOTf 1.2 eq, TEA 1.4 eq, CH_2Cl_2, -78°C, 15 min to 0°C, 15 min], **39** 1 eq, CH_2Cl_2, -78°C, 1 h to 0°C, on, 42% over two steps; c) 2,6-lutidine 2 eq, TBSOTf 1.5 eq, CH_2Cl_2, 0°C, 1 h, 91%.

The synthesis of fragment epi-**C** began with the reduction of the known (*Z*)-β-iodoacrylate to the corresponding (*E*)-aldehyde **39** (**Scheme 3.4**). Reaction of ethyl (*Z*)-β-iodoacrylate with DIBAL-H at low temperature (-78°C, 2 h) leads to the formation of the very sensitive (*Z*)-aldehyde,[157] which can be isolated from the reaction mixture by dropping of an excess of methanol to the reaction mixture immediately followed by alkaline hydrolysis with Rochelle salt. The over reduction is not a problem due to the strength of the Al-O bond that inhibits the expulsion of the alkoxide ion from the intermediate at low temperature. Nevertheless, (*E*)-aldehyde was directly obtained with 96:4 *E*/*Z* ratio through the isomerisation of the double bond by warming the reaction to 0°C and quenching the reaction with methanol at -78°C, according to Meyer's work reported in literature (**Scheme 3.5**). The thermally labile aluminoxyacetal, generated by delivery of one hydride to the ester group, collapse at an intermediate temperature to provide the (*Z*)-β-iodoacrolein by the α elimination of $EtOAl(iBu)_2$. This weak Lewis acid is responsible for the *Z* to *E* isomerisation.

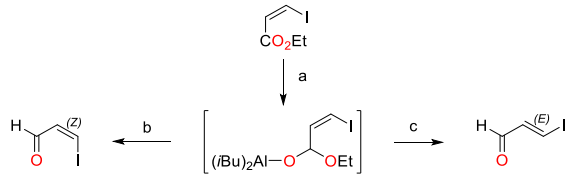

Scheme 3.5 *Reaction conditions*: a) DIBAL-H, CH_2Cl_2, -78°C, 2 h; b) MeOH, Rochelle salt, -78°C; c) 0°C, 45 min then MeOH, Rochelle salt at -78°C.

The (*E*)-β-iodoacroleyn aldehyde was obtained as yellow liquid without purification due to instable and explosive behaviour,[158] but it can be easily handled as ether o dichloromethane solutions stored under inert atmosphere and low temperature. After ^{1}H-NMR confirmed the stereochemistry, **39** was immediately subjected to an enantioselective aldol reaction with the di-*n*-butylboron enolate of (*R*)-4-benzyl-3-propionyl-2-oxazolidinone to obtain the *syn*-product **43**[159] using the Evans chemistry,[160] which involves the use of oxazolidinones as chiral auxiliaries to control the stereochemistry (**Scheme 3.4** b).

A chiral auxiliary is an enantiomerically pure molecule derived from a chiral pool that is placed on an achiral substrate to control the stereoselective transformation of the latter. The chiral auxiliary is then removed and possibly recycled once its task has been accomplished (**Scheme 3.6**).

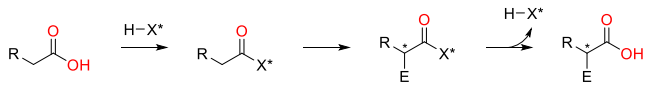

Scheme 3.6 General scheme for employing a chiral auxiliary in asymmetric synthesis

157 **a]** C. Meyer, I. Marek, J.-F. Normant, *Synlett* **1993**, 386–388; **b]** I. Marek, C. Meyer, J.-F. Normant, *Org. Synth.* **1997**, *74*, 194.

158 H. Fuwa, T. Suzuki, et al., *Chem. – A Eur. J.* **2011**, *17*, 2678–2688.

159 C. R. Reddy, N. N. Rao, *RSC Adv.* **2012**, *2*, 7724–7734.

160 D. A. Evans, J. Bartroli, T. L. Shih, *J. Am. Chem. Soc.* **1981**, *103*, 2127–2129.

An ideal chiral auxiliary must *a*) be cheap and easily available in both enantiomeric forms; *b*) be inserted into the substrate and removed from the product without racemisation and in quantitative yield; *c*) provide stereoselection > 90%; *d*) promote the formation of crystalline products to allow the purification of the isomers by crystallization.

In the 1980s, Evans designed and synthesised 2-oxazolidinones as novel chiral auxiliaries, which can be acylated at nitrogen. The obtained *N*-acyloxazolidinones can undergo highly stereoselective transformations by transferring stereochemical information to the desired product. The origin of stereocontrol derives from two factors[161] (**Scheme 3.7**): only the formation of the (*Z*)-enolate is allowed due to the steric factors into TS of the hydrogen deprotonation in α-position at the carbonyl, and the steric hindrances of the intramolecularly chelated enolate that define the attack direction of the electrophile.

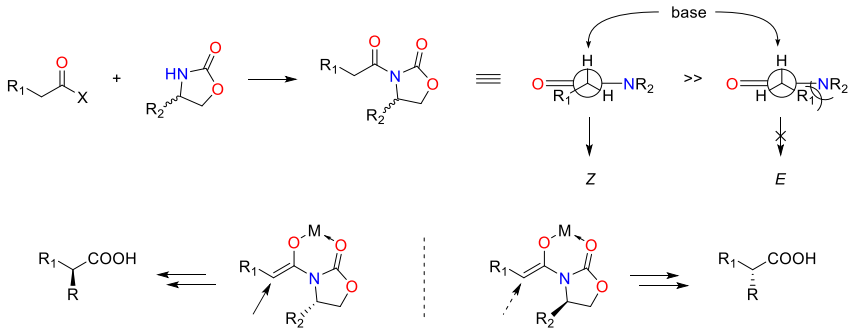

Scheme 3.7 Origin of stereocontrol in *N*-acyloxazolidinones.

An aldol reaction can be stereocontrolled at the level of relative and absolute stereochemistry. Therefore, it is possible the selective formation of one of the two diastereoisomer in a condensation between a stereogenic enolate and a pro[1]-chiral carbonyl compound (*syn vs anti*), or the selective production of one of the two enantiomers of a given diastereoisomer (e.g. *syn*-1 *vs syn*-2).

The correlation between the geometry of the enolate and the aldol configuration determines the *syn*/*anti* selectivity: the (*Z*)-enolate forms *syn* aldol, while the (*E*)-enolate gives *anti* aldol. The validity of this relationship depends on the nature of the R_1, R_2, R_3 groups and the metal counter-ion of the enolate according to Zimmerman-Traxler TS model for steric interactions[162] (**Scheme 3.8**). When R_1 is small and linear and R_2 is sterically demanding, the relationship (*Z*)-enolate/*syn*-aldol and (*E*)-enolate/*anti*-aldol is respected to minimising the 1,3-diaxial and 1,5-*syn*-pentane interactions, however R_3 can induce a strong deviation from the equation depending on its bulkiness.

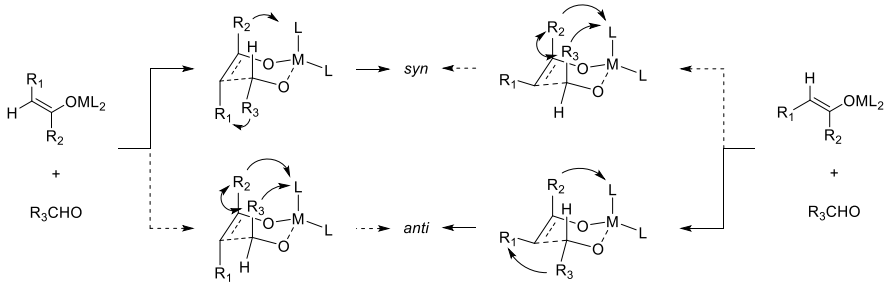

Scheme 3.8 Zimmerman-Traxler TS model for stereoselection.

161 D. A. Evans, J. M. Takacs, et al., *Pure Appl. Chem.* **1981**, *53*, 1109–1127.

162 **a]** H. E. Zimmerman, M. D. Traxler, *J. Am. Chem. Soc.* **1957**, *79*, 1920–1923; **b]** J. E. Dubois, P. Fellmann, *Tetrahedron Lett.* **1975**, *16*, 1225–1228; **c]** C. H. Heathcock, C. T. Buse, et al., *J. Org. Chem.* **2002**, *45*, 1066–1081.

One version of the Evans aldol reaction involves the use of boron enolates: cyclic TS similar to that for metal enolates with the same relationship between enolate configuration and product stereochemistry is conserved (**Scheme 3.9**). The O–B bond distance is very short and this leads to a compact TS structure magnifying the steric interactions that control stereoselectivity. The use of boron triflates and amine favours the (*Z*)-enolate that predominantly lead to the *syn*-aldol stereoisomer.[160,161,163] The substituents direct the approach of the aldehyde that displaces the oxazolidinone oxygen at the tetravalent boron in the reactive TS.[164] The conformation of the addition TS for boron enolates has the oxazolidinone ring oriented with opposed dipole of the ring and the aldehyde carbonyl groups. In this way, aldehyde can approach the enolate showing a preferential face to minimise the steric interaction leading to the formation of one stereoisomer with high stereoselectivity.

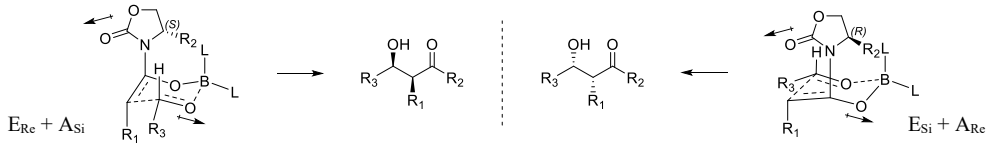

Scheme 3.9 TS model for stereoselection in Evans aldol reaction.

Therefore on this basis, it was possible to control very well the stereochemical evolution of the aldol reaction, selectively leading to the formation of the *syn* diastereoisomer **43** depending on the Evans base chosen. It should be noted that the yield on the first two reaction steps is low. The main problem related to high instability of aldehyde **25** was the removal of the residual water after work-up, which considerably affected the yield of the aldol reaction. First, the strong emulsion that formed during the extraction was solved by increasing the stirring time at rt after the addition of Rochelle salt until a perfect separation of two clear layers was obtained. This in fact allows a correct carrying out of the basic hydrolysis. Subsequently, it was considered to modify the work-up, which involved evaporation in *vacuum* at 0-10°C after extraction with diethyl ether, washing with brine and dehydration. An extraction with dichloromethane was tried with poor results due to the difficult separation. Consequently, a stage after evaporation was added in the work-up foresaw by the literature. The crude was dissolved in dichloromethane to better separate water, unlike the diethyl ether that retains it, to then dehydrate again and evaporate at the same temperatures. These changes allowed increasing yields from 18 to 42% over two steps, but the literature expected 61% of yield.[158]

Exposure of **43** to TBSOTf/2,6-lutidine in CH_2Cl_2 gave the TBS-ether **44** in 91% yield, which was treated with $NaBH_4$ in THF/H_2O 4:1 for the reductive removal of the chiral auxiliary[165] to quantitatively provide alcohol **45**. Treatment of **45** under oxidative conditions using the Dess-Martin periodinane (DMP) produced the corresponding aldehyde **46** in quantitative yields without the need for purification. The subsequent methylation under the Wittig reaction conditions led to the formation of product **47** with 71% yield. Final deprotection of the alcohol group produced the desired epi-**C** fragment with *R* configuration at C_{13}.

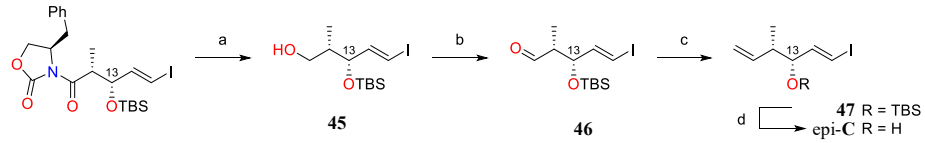

44 **45** **46**

Scheme 3.10 *Reaction conditions*: a) $NaBH_4$ 4.1 eq, THF/H_2O 4:1, rt, 1 d, 85%; b) DMP 1.2 eq, CH_2Cl_2, 0°C, 30 min, >98%; c) ylide: [Ph_3PCH_3Br 4 eq, *n*-BuLi 3.9 eq 1.6 M, THF, 0°C, 15 min], **46** 1 eq, 0°C, 20 min, 71%; d) TBAF 1.5 eq, THF, 0°C to rt, 45 min, >98%.

163 D. A. Evans, R. Gage, *Org. Synth.* **1990**, *68*, 83.

164 K. Hayashi, Y. Hamada, T. Shioiri, *Tetrahedron Lett.* **1991**, *32*, 7287–7290.

165 D. A. Evans, S. L. Bender, J. Morris, *J. Am. Chem. Soc.* **1988**, *110*, 2506–2526.

3.2 Ene-ynic fragment B C_{16}-C_{27} of callyspongiolide

3.2.1 State of art

As mentioned, examples of different total synthesis approaches of callyspongiolide are reported in the literature, and therefore they include synthetic strategies to obtain fragment **B**.

In 2016, Z. Xu, T. Ye *et al.*[149] described the first synthesis of fragment **B** (**Scheme 3.11**) starting from aldehyde **48** with the protection of the phenolic OH as TBS ether. The subsequent aldol reaction[166] with methyl trimethylsilyl dimethylketene acetal (MTDA) in the presence of oxazaborolidinone (derived from N-Tos-D-valine and BH_3·THF)[167] gave the corresponding (*R*)-β-hydroxy ester **49** with a yield of 97% in two steps. The β-hydroxy group was protected with triethylsilyl triflate (TESOTf) to provide the corresponding TES ether which was then reduced with DIBAL-H to primary alcohol **50** in 93% of yield in two steps. The hydroxyl group was oxidised with Dess-Martin periodinane to the corresponding aldehyde, which was homologated using the Takai[168] protocol to give (*E*)-vinyl iodide **51** with 68% of yield. No formation of the (*Z*)-isomer was observed, but the undesired cleavage of a protective group occurred. Sonogashira coupling[169] between vinyl iodide **51** and ethynyltrimethylsilane followed by removal of the TMS group yielded the corresponding enino. **52** was obtained after re-protection of phenolic OH as TBS ether with a yield of 88% over three steps.

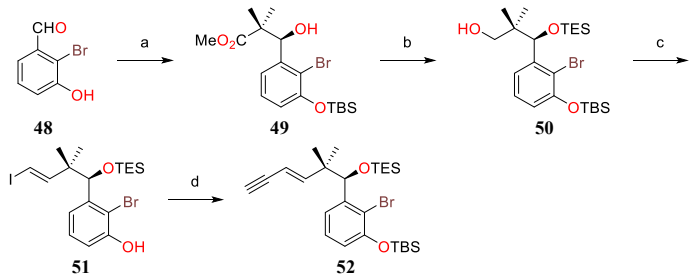

Scheme 3.11 *Reaction conditions*: a) *i*) TBSCl, ImH, CH_2Cl_2, 0°C to rt, *ii*) N-Tos-D-valine, BH_3·THF, MTDA, THF, 0 to -78°C, 97%; b) *i*) TESOTf, TEA, CH_2Cl_2, -50 to -30°C, *ii*) DIBAL-H, CH_2Cl_2, -78 to -40°C, 93%; c) *i*) DMP, $NaHCO_3$, CH_2Cl_2, 0°C to rt, *ii*) $CrCl_2$, CH_3I, THF, K_2CO_3, MeOH, rt, 68%; d) *i*) ethynyltrimethylsilane, $Pd(PPh_3)_4$, CuI, THF, K_2CO_3, MeOH, rt, *ii*) TBSCl, ImH, CH_2Cl_2, 0°C to rt, 88%.

In 2016 simultaneously to Z. Xu's work, A. K. Ghosh *et al.*[152] published another total synthesis of callyspongiolide in which fragment **B** was obtained in a different way (**Scheme 3.12**). The 2-bromo-3-hydroxybenzaldehyde was protected as TBS ether and subjected to nucleophilic addition using 3,3-dimethylallylmagnesium chloride to obtain racemic alcohol **53** with 98% yield on the two steps. The racemic alcohol was oxidised to ketone with PCC and enantioselectively reduced to alcohol **54** by CBS reduction of Corey[170] to introduce the stereogenic centre C_{21} with a yield of 59% and ee of 99%. The secondary alcohol was protected using TESOTf and the Nicolaou[171] conditions for the oxidative cleavage of the olefins provided the corresponding aldehyde **55** with excellent yields. Wittig olefination followed by global deprotection, produced **B** with 39% yield over two steps.

Also in 2016, M. Kotora *et al.*[151a] accomplished the synthesis of fragment **B** exploiting a different pathway (**Scheme 3.13**). Considerable efforts were made to optimise the preparation of the aldol product having a quaternary carbon. The asymmetric aldol reaction between **48** and 2-methylpropanal was studied with the catalytic use of the chiral auxiliary (*S*)-(+)-1-(2-pyrrolidinylmethyl)pyrrolidine. After a screening of solvents and protecting

166 J. Matsuo, M. Murakami, *Angew. Chemie Int. Ed.* **2013**, *52*, 9109–9118.

167 S. Kiyooka, Y. Kaneko, et al., *J. Org. Chem.* **1991**, *56*, 2276–2278.

168 K. Takai, K. Nitta, K. Utimoto, *J. Am. Chem. Soc.* **1986**, *108*, 7408–7410.

169 K. Sonogashira, Y. Tohda, N. Hagihara, *Tetrahedron Lett.* **1975**, *16*, 4467–4470.

170 **a]** E. J. Corey, R. K. Bakshi, S. Shibata, *J. Am. Chem. Soc.* **1987**, *109*, 5551–5553; **b]** E. J. Corey, R. K. Bakshi, et al., *J. Am. Chem. Soc.* **1987**, *109*, 7925–7926.

171 K. C. Nicolaou, V. A. Adsool, C. R. H. Hale, *Org. Lett.* **2010**, *12*, 1552–1555.

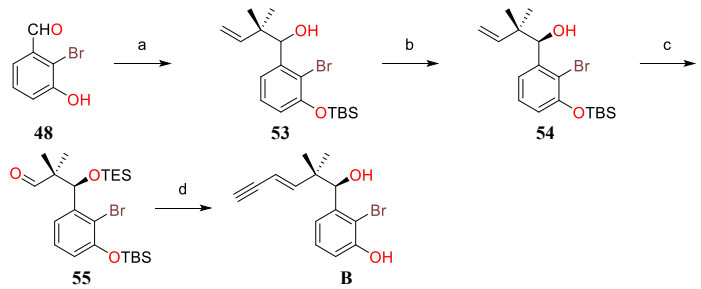

Scheme 3.12 *Reaction conditions*: a) *i*) TBSCl, DIPEA, CH_2Cl_2, rt, 98%, *ii*) 3,3-dimethylallyl-MgCl, THF, 0°C, >98%; b) *i*) PCC, CH_2Cl_2, rt, 93%, *ii*) (*R*)-Me-CBS, $BH_3{\cdot}SMe_2$, Tol, 0°C, 58%; c) *i*) TESOTf, TEA, CH_2Cl_2, 0°C, 96% *ii*) OsO_4, NMO, 2,6-lutidine, then $PhI(OAc)_2$, rt, 93%; d) *i*) 3-(trimethylsilyl)propargyl-triphenylphosphonium bromide, LiHMDS, THF, -78 °C to rt, 96%, *ii*) TBAF, THF, rt, 41%.

groups of phenolic OH, the conditions to obtain **58** with 90% of yield and 93% ee were found. The most suitable solvent was DMSO (*vs* DMF, THF, DCM, ACN) and the most convenient protecting group was pivaloyl (*vs* Ac, Bz and Me). The benzyl alcohol of the aldol product **58** was protected with an acetyl group to prevent racemization and then converted into vinyl iodide by Takai-Utimoto[168] olefination with the exclusive formation of (*E*)-alkene **59** in 52% of yield. Reaction of **59** with trimethylsilyletine under standard Sonogashira conditions followed by selective desilylation produced **57** with 64% of yield over two steps.

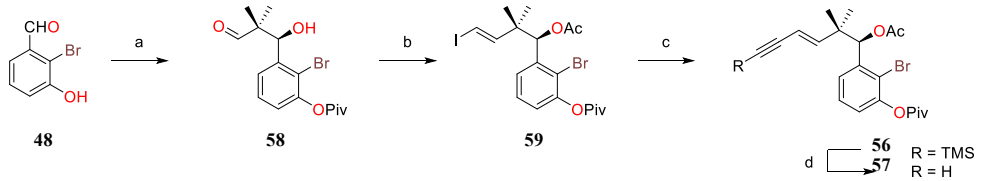

Scheme 3.13 *Reaction conditions*: a) *i*) TBAI, PivCl, CH_2Cl_2, 0°C, K_2CO_3 aq, 30 min, 95%, *ii*) isobutyraldehyde, (*S*)-(+)-1-(2-pyrrolidinylmethyl)pyrrolidine, TFA, DMSO, rt, 26 h, 90%; b) *i*) Ac_2O, TEA, CH_2Cl_2, 0°C to rt, 1h, 81%, *ii*) $CrCl_2$, CH_3I, THF, 0°C, 4 h, 52%; c) $Pd(PPh_3)_4$, CuI, TEA, TMS-acetylene, THF, rt, on, 84%; d) $AgNO_3$, NaI, EtOH/H_2O 4:1, rt, 3.5 h, 76%.

Some years later in 2019, A. Fürstner *et al.*[150d,153] proposed an alternative strategy to Xu and co-workers (**Scheme 3.14**). Fragment **B** was prepared starting from aldehyde **48** that reacted with MTDA through Mukaiyama aldol reaction[166] in the presence of a chiral Lewis acid catalyst formed *in situ* from *N*-Tos-D-valine and $BH_3{\cdot}THF$.[167] The product obtained with an ee of 99% after recrystallization was protected in the alcoholic portions as TBS and **60** was subjected to reduction. In this way, the ester was transformed into aldehyde, which was converted into olefin by the Horner-Wadsworth-Emmons reaction to give **61** with *E*/*Z* 95:5 ratio. The global deprotections with HF·Py provided fragment **B** with an overall yield of 48%.

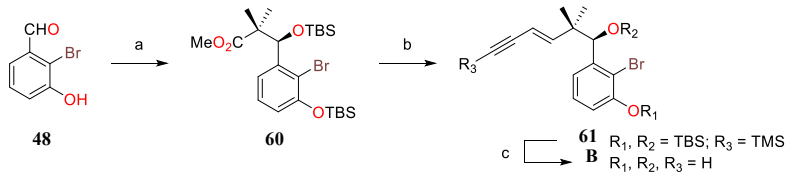

Scheme 3.14 *Reaction conditions*: a) *i*) *N*-Tos-D-valine, $BH_3{\cdot}THF$, MTDA, THF, 0 to -78°C, 72%, *ii*) TBSOTf, 2,6-lutidine, CH_2Cl_2, rt, 97%; b) *i*) DIBAL-H, Tol, -78°C, 96%, *ii*) DMP, CH_2Cl_2, rt, 76%, *iii*) 3-(trimethylsilyl)propargyl-phosphonate, *n*-BuLi, THF, -78°C, 96%, *E*/*Z*=95:5; c) HF·Py, 98%.

3.2.2 Retrosynthetic approach

Fragment **B** can be prepared through various reactions. The synthetic strategy achieved within the laboratories

of the University of Barcelona was planned as a result of the analysis of the above-mentioned syntheses. Therefore, the reactions that gave the best outcomes in terms of yields and ee were considered to reach the goal with the fewest steps possible.

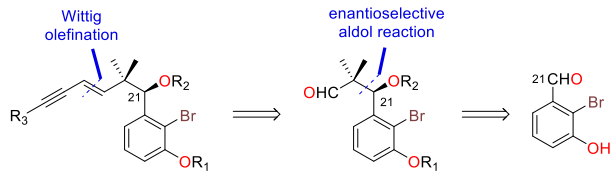

Scheme 3.15 Retrosynthetic analysis to obtain fragment **B**.

The desired compound **B** could be obtained by Wittig olefination with 3-(trimethylsilyl)propargyl-triphenylphosphonium salt starting from protected aldehyde **62** followed by general deprotection, as described by A. K. Ghosh *et al*. The stereochemical control for the formation of stereocenter C_{21} could be achieved with the enantioselective aldol reaction described by M. Kotora *et al*. using the protected phenol as pivaloyl (Piv) of the known starting material **48**.

3.2.3 Synthesis of Fragment B C_{16}-C_{27} of callyspongiolide

The synthesis of fragment **B** started with phenol protection of **48** as OPiv (96% yield) because it was observed as the best protecting group for the subsequent enantioselective aldol reaction step.[151a] The Piv protection gave better yields and ee compared to the free-OH, Ac, Me, and Bz tested by Kotora. The reaction of **48** having a free phenolic hydroxyl group proceeded with a very low efficiency, as in the case of OBz. When the hydroxyl group was protected as OAc the yield was low due to a gradual cleavage of the acetyl group from the starting material during the course of the reaction. The use of OMe produced high yields, however its subsequent cleavage should not be neglected, which could be difficult. On the other hand, OPiv provided high yields and ee in the aldol reaction and it is easily removable; therefore, it has been selected as suitable protecting group.

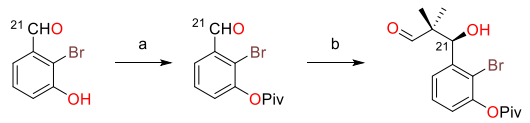

Scheme 3.16 *Reaction conditions*: a) TBAI 0.1 eq, PivCl 1 eq, CH_2Cl_2, 0°C, K_2CO_3 aq 1.9 M 5 mL, 30 min, 96%; b) isobutyraldehyde 2 eq, (*S*)-(+)-1-(2-pyrrolidinylmethyl)pyrrolidine 0.1 eq, TFA 0.1 eq, DMSO, rt, 46 h, 88%.

In the next step, the asymmetric aldol reaction in DMSO with isobutyraldehyde was performed by exploiting the use of a pyrrolidine-derived compound as organocatalyst in the presence of trifluoroacetic acid (TFA).[151a] Pyrrolidine and other chiral amines have been shown to be efficient catalysts in asymmetric intermolecular aldol reactions.[172] The amine-catalysed aldol reaction proceeds *via* an enamine intermediate on the enolisable aldehyde. Enamines are labile fractions that can be produced through an acid-catalysed nucleophilic reaction of secondary amines with ketones or aldehydes containing a hydrogen in α position. If the pKa of the amine is high enough, acid catalysis is not required (such as pyrrolidine that has a pKa of 44). Primary amines are not used for enamine synthesis due to the preferential formation of the thermodynamically more stable imines. On the contrary, the secondary amines form the iminium ions, which go to enamine by loss of the proton in α.

The mechanism represented in **Scheme 3.17** involves the attack of the amino nitrogen to the acid-activated carbonyl carbon in a 1,2 addition and the subsequent transfer of the nitrogen proton to the oxygen. Then nitrogen

172 **a]** B. List, R. A. Lerner, C. F. Barbas, *J. Am. Chem. Soc.* **2000**, *122*, 2395–2396; **b]** K. Sakthivel, W. Notz, et al., *J. Am. Chem. Soc.* **2001**, *123*, 5260–5267; **c]** N. S. Chowdari, D. B. Ramachary, et al., *Tetrahedron Lett.* **2002**, *43*, 9591–9595; **d]** A. Bøgevig, N. Kumaragurubaran, K. Anker Jørgensen, *Chem. Commun.* **2002**, 620–621; **e]** M. Nakadai, S. Saito, H. Yamamoto, *Tetrahedron* **2002**, *58*, 8167–8177; **f]** A. B. Northrup, D. W. C. MacMillan, *J. Am. Chem. Soc.* **2002**, *124*, 6798–6799.

shares the electrons to eject H_2O forming the iminium ion, which loses a proton generally at less-substituted α-carbon restoring the neutral charge on the nitrogen. The hydrogen is captured by pyrrolidinylmethyl, the most basic functional group present.

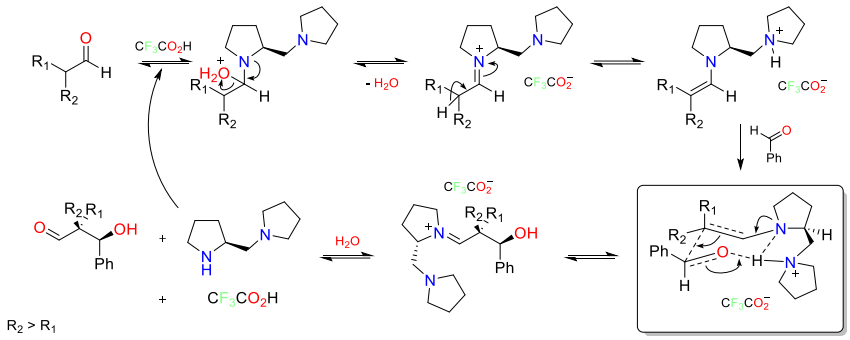

Scheme 3.17 Reaction mechanism in the aldol reaction of organocatalysed pyrrolidine/TFA non-stereogenic enolates.

In case of aldehydes, the regioselectivity of double bond formation is not a problem, but the geometry of the double bond does. First, the double bond is formed *anti* with respect to the bulkier substituent of the amine thus avoiding steric repulsion. The conjugation between the nitrogen atom and the π orbitals of the double bond results in coplanarity, which is the steric effect responsible for the geometric formation preference. Secondly, the nature of the substituents on the amine influences the distribution of the *E*/*Z* isomers, however the (*E*)-configuration of the enamine double bond is preferred as a consequence of steric factors and is also thermodynamically more stable (the double bond in (*Z*)-configuration is known to be the kinetic product).

The enamine has reactivity similar to the enolates, so it is able to attack an electrophile, such as a carbonyl carbon in aldol reaction. The use of amines as organocatalysts to generate optically active enamines allows to control the absolute stereochemistry in an aldol reaction whose reaction partners are non-stereogenic. In fact, they are able to express strong preferences on attack directions due to the formation of coordinated cyclic TSs that minimise steric interactions. In the case of the reaction carried out, the *S*-pyrrolidine with TFA controls the facial selectivity of the aldol addition by catalysing a *Re*-face attack on the aryl aldehyde through the enamine intermediate whose formation geometry is defined. The reason for the high enantioselectivity is to be found in the conformation of the TS (**Scheme 3.17**), which exploits the formation of a cyclic intermediate. The aldehyde oxygen can approach only from the direction in which the proton bound to the nitrogen is exposed to form the coordination, and the aldehyde can approach only with the face that places the phenyl group in equatorial position to access the lower energy TS. After the electron transfer and bonding, the water already formed during the reaction hydrolyses the iminium ion, the aldol is released and the pyrrolidine and TFA are regenerated to start a new organocatalysed aldol cycle.

The α_D of aldol **58** obtained with 88% of yield was perfectly comparable with the value reported in literature, thus it is reasonable to assume that the same configuration and 93% ee were gained. However, some changed in the procedure was done to improve the results. Reaction time was increased up to 46 h in order to have a high degree of conversion, compared to the 26 h reported in the literature. Furthermore, the procedure foresaw a direct purification of the crude on silica without work-up, but addition of EtOAc and washing of the organic phase with water were introduced to remove DMSO because this solvent created some problems during the flash chromatographic purification as it retained the crude in the column.

The alcohol moiety of aldol **58** was protected as acetyl with 86% of yield using acetic anhydride[151a] and the obtained product **64** was subjected to the olefination with Wittig reaction.

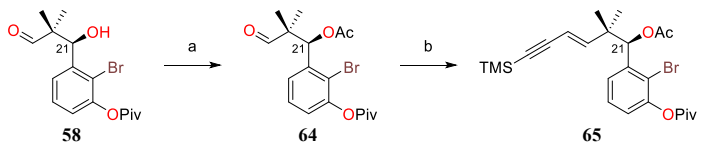

58 **64** **65**

Scheme 3.18 *Reaction conditions*: a) Ac_2O 1.28 eq, TEA 1.3 eq, DMAP 0.1 eq, CH_2Cl_2, 0°C 20 min then rt, on, 86%; b) 3-(trimethylsilyl)propargyl-triphenylphosphonium bromide 2.5 eq, LiHMDS 2.4 eq, THF, -78 °C to rt, on, 36% *E*/*Z* 3:1.

Applying the same conditions used by Ghosh[150a] (entry 1) led to the formation of **65** as a non-separable mixture of 3:1 *E*/*Z* isomers (estimated by ^{1}H-NMR analysis) with a yield of 8% differently from the 96% expected, with no starting material. Decreasing the quantities of reagents necessary for the *in situ* formation of the ylide (phosphonium salt and LiHMDS) with respect to the aldehyde provided the product with a yield of 31% and with an *E*/*Z* ratio of 3:1 (entry 2). Furthermore, 45% of the starting aldehyde was recovered. Decreasing the formation temperature of the ylide to -78°C caused a worsening (entry 3); therefore, it can be assumed that the stability of the species was not a problem and that the low temperature was kinetically and energetically unfavourable. To favour deprotonation, the reaction was carried out at 0°C and increasing the equivalents of reagent (entry 4). The yield obtained in this way was 33% while maintaining the *E*/*Z* ratio of 3:1 unchanged. By evaluating the commercially available phosphonium salt as a hygroscopic species, it was possible that the retained humidity made the reaction difficult. To strip the traces of water present, the salt was suspended in a mixture of THF/Tol and evaporated under *vacuum* several times, taking care not to let the compound come into contact with the air. The olefination was repeated with the first condition tried obtaining 32% of yield (entry 5) and with less equivalent of phosphonium salt and base still obtaining 36% of yield (entry 6) without further improvements even by refluxing for 6 h. The use of a different base (e.g. *n*-BuLi) did not lead to any satisfactory result (entries 7, 8), therefore this path was not followed.

Table 3.1 Conditions used for Wittig olefination on aldehyde **64**.

Entry	Phosph. salt [eq]	Base [eq]		T [°C]	Time [min]	Yield [%]	*E*/*Z*
1	4.0	LiHMDS	4.0	-78 to -40	30	8	3:1
2	1.5	LiHMDS	1.45	-78 to -40	30	31	3:1
3	2.5	LiHMDS	2.4	-78	60	18	4:1
4	2.5	LiHMDS	2.4	0	5	33	3:1
5	4.0*	LiHMDS	3.9	-78 to -40	30	32	3:1
6	2.5*	LiHMDS	2.4	-78 to -40	30	36	3:1
7	1.5	*n*-BuLi	1.45	-78	40	12	3:1
8	2.1	*n*-BuLi	2.0	-78 to -40	30	nr	

This functionalization proved to be very difficult despite the modifications made to the procedure and the different reaction conditions tried to increase the yields. Considering the poor results, the low *E*/*Z* ratio, and the non-separable isomers, Wittig reaction was abandoned to focus on the more selective olefination of Horner-Wadsworth-Emmons.

The first step in the Wittig reaction is the attack of the carbon atom of the ylide to the carbonyl. The product is oxaphosphethane through a cycloaddition reaction (2+2), while the presence of Li counter-ion leads to the formation of betaine, which subsequently evolves to oxaphosphethane (**Scheme 3.19**).

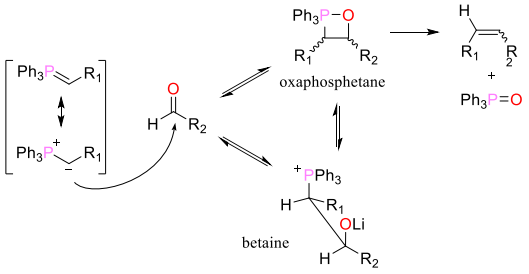

Scheme 3.19 Wittig reaction mechanism.

The Wittig reaction allows the preparation of an alkene by the reaction of an aldehyde (or ketone) with the ylide generated from a phosphonium salt by deprotonation of the methyl adjacent to P with a base (e.g. NaH, NaOMe, Et_3N, NaHMDS, LiHMDS, BuLi). The stereochemical outcome of the resulting alkene depends on the type of the ylide. If R_1 is an alkyl group, then the ylide is non-stabilized and the TS involved leads to (*Z*)-alkene, since it minimises the steric interactions 1,2 between the substituents and 1,3 with phenyls (**Scheme 3.20**). If R_1 is an EWG, then the ylide is stabilized and gives

predominantly (*E*)-alkenes, as the TS minimises dipolar interactions more than steric ones. If the ylide has vinyl, aryl or slightly EWG residues it is semi-stabilized and shows no preference of the two previous models for the stereochemical course. Therefore, the results are *E*/*Z* mixtures of isomers in a ratio of approximately 1:1, as in the case of reaction performed.

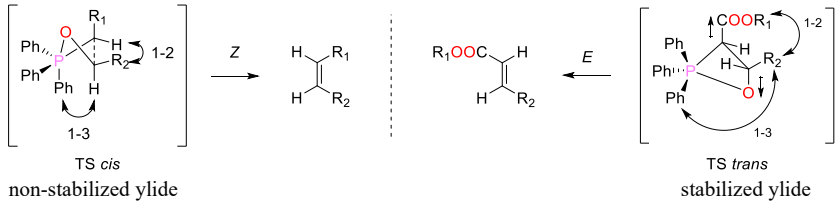

Scheme 3.20 TS of non-stabilized and stabilized ylides justifying the stereochemical outcome in Wittig reaction.

Horner-Wadsworth-Emmons is a variant of Wittig reaction and involves the use of stabilized phosphonates instead of phosphonium salts. Phosphonate carbanions have many advantages: they are more nucleophilic and are easily alkylated, they can be removed easily by aqueous washing (unlike phosphine oxide), and they provide high stereoselectivity. The reaction mechanism is similar to the Wittig reaction; however, the stereochemistry is determined by the control of the steric approach. The attack on the carbonyl carbon is favoured when the small hydrogen aldehyde eclipses the bulky phosphoryl portion disposing R_1 *syn* to the aldehyde group R_2. The alkene can assume the (*E*)-orientation after the rotation required to form the oxaphosphethane.

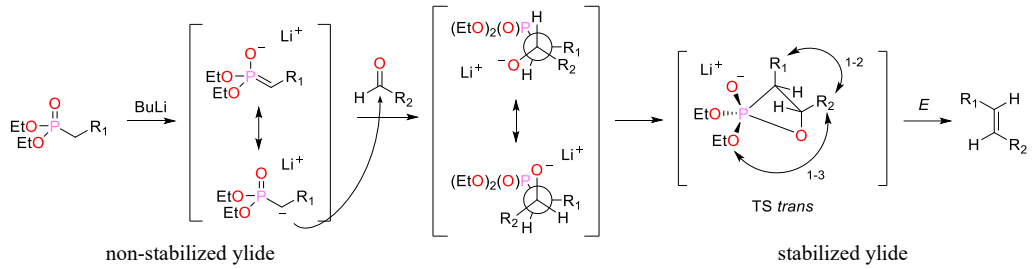

Scheme 3.21 Horner-Wadsworth-Emmons mechanism reaction and the favoured TS stabilized ylides.

To perform this promising reaction,[153,173] the required reagent [3-(trimethylsilyl)propargyl-phosphonate] **66** was freshly prepared with 77% of yield by treating diethyl phosphonate with NaHMDS at -10°C in THF for 15 min, and subsequently adding the 3-(trimethylsilyl)propargyl bromide.[173,174] The active species was generated *in situ* using *n*-BuLi as base at 0°C in THF and the reaction acquired the characteristic red colour typical of the ylide formation by ongoing the stirring at rt for 10 min. Then, the aldehyde was added at -78°C to ensure the maximum *E*/*Z* ratio between the two isomers that can form. The deprotonation step of the phosphonate with *n*-BuLi proved

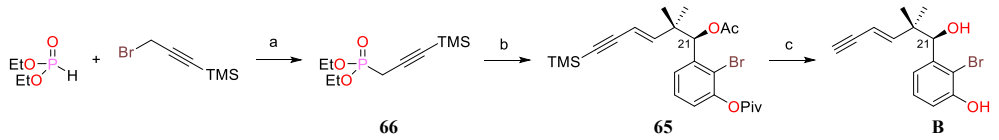

Scheme 3.22 *Reaction conditions*: a) NaHMDS 1 eq, diethyl phosphonate 1 eq, THF, -10°C, 15 min, then 3-(trimethylsilyl)propargyl bromide 1 eq, -10°C, 1 h, 77%; b) **64** 1 eq, **66** 2 eq, *n*-BuLi 2 eq, THF, -78°C, 2 h, 65%, *E*/*Z* 96:4; c) K_2CO_3 7.3 eq, MeOH, 45°C, 2.5 h, 82%.

to be crucial and very sensitive to humidity. In fact, if the solution remained yellow/orange colour, indicating that the ylide was not completely formed, the olefination yields drastically decreased, the recovered aldehyde was little, and a small formation (8%) of a by-product obtained from the deprotection of the Piv was observed. However, it was possible to get the desired product **65** with a moderate yield of 65% and *E*/*Z* ratio of 96:4.

173 R. P. Van Summeren, B. L. Feringa, A. J. Minnaard, *Org. Biomol. Chem.* **2005**, *3*, 2524–2533.

174 A. W. Gibson, G. R. Humphrey, et al., *Synthesis (Stuttg).* **1991**, *1991*, 414–416.

Lastly, the general deprotection in basic condition provided the final product fragment **B** with 82% of yield.[149,151] Heating at 40°C was applied in addition to the procedure reported in the literature to favour the conversion.

4 Conclusion

In conclusion, the enantioselective synthesis of fragment epi-**C** was completed in 7 steps with 23% of overall yield starting from ethyl *cis*-iodoacrylate **40**. Despite the efforts made, the first reactions of the synthetic pathway to obtain **43** remain critical and significantly reduce the overall yield of the synthesis. However, the evolution of stereochemistry appears to be very well controlled on the whole synthetic path by exploiting isomerisation and Evans aldol reactions.

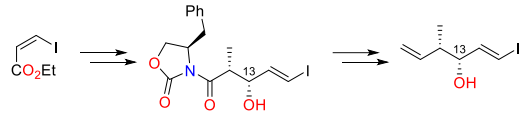

40 **43** epi-**C**

The synthon epi-**C** will be used in the synthesis of fragment **A**, which will be jointed with the fragment **B** by Sonogashira coupling.

Fragment **B** was obtained in 5 steps starting from aldehyde **48** with 39% overall yield and with excellent stereocontrol by exploiting the pyrrolidine derivative as a chiral auxiliary in the aldol reaction. Furthermore, switching from the Wittig to the Horner-Wadsworth-Emmons reaction allowed to increase the yield and to improve the stereocontrol in the formation of the double bond with a high selectivity towards the (*E*)-configuration.

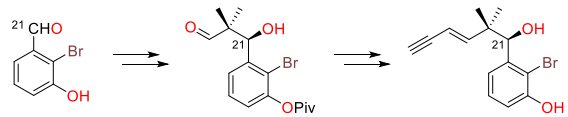

48 **58** **B**

5 Experimental procedures

General Experimental Information

All air sensitive manipulations were carried out under a dry argon or nitrogen atmosphere, with dry solvents. Solvents and reagents were purchased from Sigma- Aldrich, Alfa-Aesar or Carlo Erba, and were used without further purification. Drying of organic extracts during work-up of reactions was performed with anhydrous MgSO4 or Na_2SO_4. Evaporation of solvent was accomplished with a rotatory evaporator. Thin-layer chromatography was done on SiO_2 (silica gel 60 F254), and the spots were located by UV and either a 1% $KMnO_4$ solution. Chromatography refers to flash column chromatography and was carried out on SiO_2 (silica gel 60, 230-400 mesh). ^{1}H-NMR spectra were recorded at 400 MHz and ^{13}C-NMR at 100.6 MHz, and chemical shifts are reported in δ values, in parts per million (ppm) relative to TMS (0 ppm) or relative to residual chloroform-*d* (7.26 ppm, 77.0 ppm) as internal standards, at 25 ºC. Data are reported in the following manner: chemical shift, multiplicity, coupling constant (*J*) in Hertz (Hz), integrated intensity, and assignment (when possible). Assignments and stereochemical determinations are given only when they are derived from definitive two-dimensional NMR experiments (g-HSQC−COSY). Optical rotations were measured in a Perkin-Elmer 241 polarimeter, using a Na lamp. $[\alpha]_D$ values are given in 10-1 deg $cm^2 \cdot g^{-1}$. High-resolution mass spectra (HRMS) was performed by the *Centres Científics i Tecnològics de la Universitat de Barcelona*.

Synthesis of (*E*)-3-iodoacrylaldehyde (39)

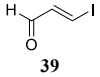

39

DIBAL-H (1.2 mL of a 1.0 M solution in hexanes, 1.2 mmol) was added dropwise to a solution of ethyl (*Z*)-β-iodoacrylate (142 µL, 1.1 mmol) in CH_2Cl_2 (2.2 mL) at -78ºC, and the resulting

mixture was stirred at -78ºC for 2 h and then at 0ºC for 45 min. After being cooled back to -78ºC, the solution was treated with MeOH (500 µL), Et_2O (7 mL), and saturated aqueous potassium sodium tartrate (7 mL). The mixture was allowed to warm up to room temperature and stirred vigorously until the layers became clear. The mixture was extracted with Et_2O (7 mL × 4), and the organic phase were washed with brine, dried three times, filtered, and carefully concentrated under *vacuum* at 10ºC. The crude was suspended in CH_2Cl_2, dried, filtered and carefully evaporated under *vacuum* at 10°C. The crude (*E*)-iodoacrolein **39** was dissolved in CH_2Cl_2, cooled at -78°C, and used immediately in the next reaction without further purification.

^{1}H NMR (400 MHz, chloroform-*d*) δ 9.53 (d, *J* = 7.4 Hz, 1H), 8.03 (d, *J* = 15.0 Hz, 1H), 7.17 (dd, *J* = 15.0, 7.4 Hz, 1H).

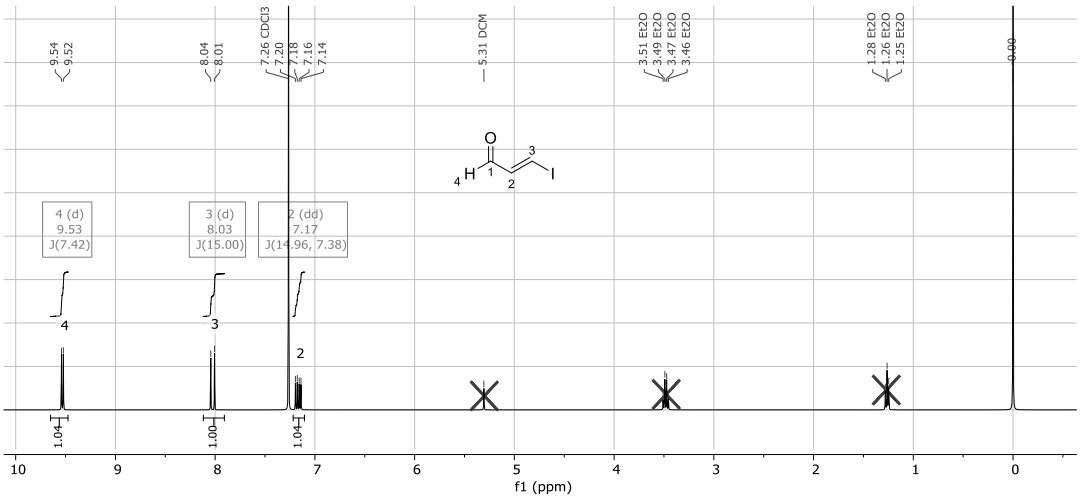

Synthesis of (*R*)-4-benzyl-3-[(2*R*,3*R*,*E*)-3-hydroxy-5-iodo-2-methylpent-4-enoyl]oxazolidin-2-one (43)

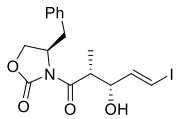

43

n-Bu_2OTf (1.1 mL, 1.15 mmol) was dropped into a solution of (*R*)-(+)-4-benzyl-3-propionyl-2-oxazolidinone (244 mg, 1.05 mmol) in CH_2Cl_2 (6 mL) at -78°C. Subsequently, TEA (160 µL, 1.14 mmol) was slowly added and the resulting reaction mixture was warmed at 0°C after 15 min and stirred for additional 15 min. Then, the reaction was cooled at -78°C and a solution of **39** (173 mg, 0.951 mmol) in CH_2Cl_2 (1 mL) was added dropwise. The reaction was stirred for 1 h before warming to 0°C for 18 h. The reaction was quenched with MeOH/pH 7 buffer 2:1 (1.5 mL), MeOH/H_2O_2 2:1 (1.5 mL), and stirred at 0°C for 1.5 h. The organic solvent was evaporated under *vacuum* and the aqueous phase was extracted with Et_2O (3 mL × 3). Organic layer was washed with $NaHCO_3$ and brine, dried, filtered, and concentrated under *vacuum*. Column chromatography of the residue on silica gel (gradient elution: *n*-Hex/EtOAc 8:2 → 75:25) provided 194 mg (42% over two steps) of the product as yellow oil.

[α]$_D^{22}$ −50.2 (c = 2.27 in $CHCl_3$);

HRMS (ESI) *m/z* $[M+Na]^+$ 438.0184 (calcd for $C_{16}H_{19}INO_4Na$ 438.0173);

^{1}H NMR (400 MHz, chloroform-*d*) δ 7.34 (t, *J* = 7.2 Hz, 2H), 7.30 (d, *J* = 6.9 Hz, 1H), 7.20 (d, *J* = 7.3 Hz, 2H), 6.55 (dd, *J* = 14.4, 4.9 Hz, 1H), 6.47 (d, *J* = 14.6 Hz, 1H), 4.72 (td, *J* = 8.9, 8.0, 3.5 Hz, 1H), 4.49 (t, *J* = 4.2 Hz, 1H), 4.30 – 4.16 (m, 2H), 3.85 (qd, *J* = 7.0, 3.4 Hz, 1H), 3.24 (dd, *J* = 13.4, 3.4 Hz, 1H), 2.80 (dd, *J* = 13.4, 9.3 Hz, 1H), 1.26 (d, *J* = 7.0 Hz, 3H).

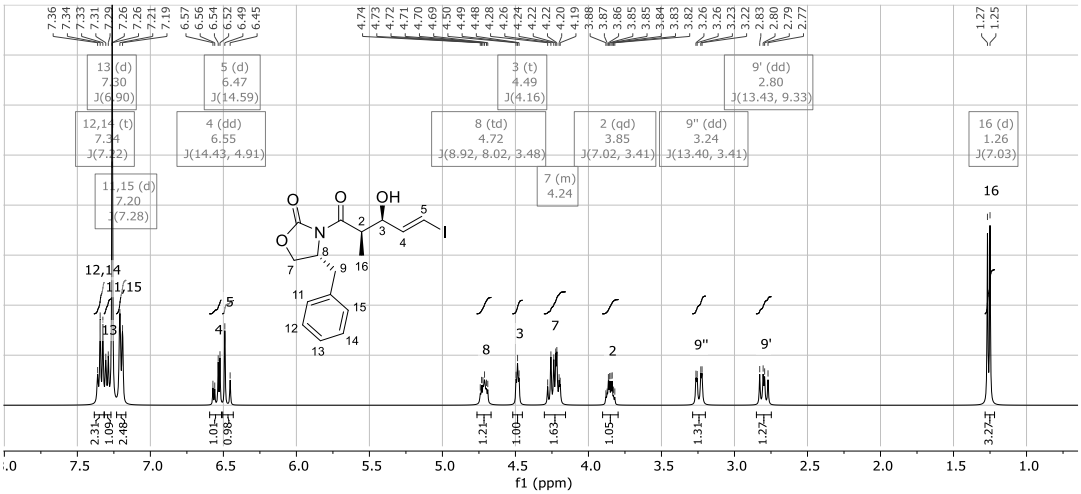

Synthesis of (*R*)-4-benzyl-3-{(2*R*,3*R*,*E*)-3-[(tert-butyldimethylsilyl)oxy]-5-iodo-2-methylpent-4-enoyl}oxazolidin-2-one (44)

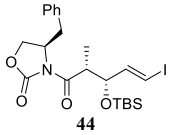

44

To a solution of **43** (1.09 g, 2.62 mmol) in CH_2Cl_2 (24.4 mL) at 0°C were added 2,6-lutidine (0.56 g, 5.24 mmol) and TBSOTf (906 µL, 3.94 mmol). After being stirred at 0°C for 1 h, the reaction was quenched with saturated aqueous $NaHCO_3$ solution. The resultant mixture was extracted with EtOAc (15 mL × 3), and the organic layers were washed with brine, dried, filtered, and concentrated under reduced pressure. Column chromatography of the residue on silica gel (*n*-Hex/EtOAc 95:5) provided 1.27 g (91%) of the product as a colorless oil.

^{1}H NMR (400 MHz, chloroform-*d*) δ 7.38 – 7.26 (m, 3H), 7.21 (d, *J* = 6.7 Hz, 2H), 6.59 (dd, *J* = 14.5, 6.9 Hz, 1H), 6.28 (dd, *J* = 14.6, 1.0 Hz, 1H), 4.60 (ddt, *J* = 9.8, 6.5, 3.4 Hz, 1H), 4.29 (t, *J* = 6.5 Hz, 1H), 4.24 – 4.12 (m, 2H), 3.97 (p, *J* = 6.8 Hz, 1H), 3.26 (dd, *J* = 13.3, 3.4 Hz, 1H), 2.78 (dd, *J* = 13.4, 9.6 Hz, 1H), 1.22 (d, *J* = 6.8 Hz, 3H), 0.88 (s, 9H), 0.02 (d, *J* = 4.3 Hz, 6H).

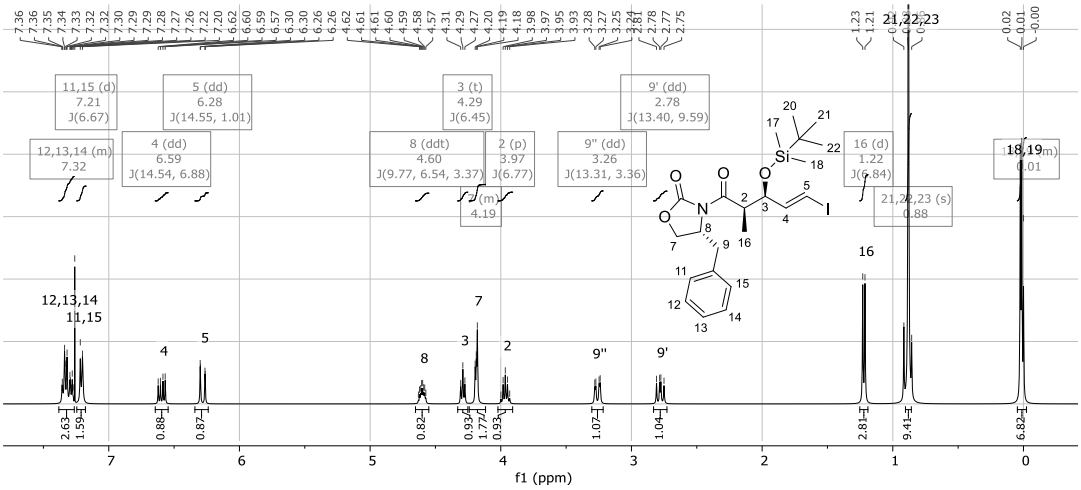

Synthesis of (2*S*,3*R*,*E*)-3-[(tert-butyldimethylsilyl)oxy]-5-iodo-2-methylpent-4-en-1-ol (45)

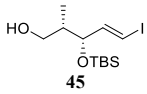

45

To a solution of **44** (1.03 g, 1.94 mmol) in THF/H_2O (4:1, v/v, 20 mL) at 0°C was added $NaBH_4$ (300 mg, 7.9 mmol), and the resultant mixture was stirred at room temperature for 24 h. After being cooled to 0°C, the reaction was quenched with saturated aqueous potassium sodium tartrate solution. The reaction mixture was diluted with EtOAc and stirred at room temperature for 24 h. Then, the aqueous layer was extracted with EtOAc (20 mL × 3) and the combined organic phases were washed with brine, dried, filtered, and concentrated under *vacuum*. Column chromatography of the residue on silica gel (*n*-Hex/EtOAc 95:5) provided 583 mg (85%) of the product as a colorless oil.

^{1}H NMR (400 MHz, chloroform-*d*) δ 6.59 (dd, *J* = 14.5, 6.2 Hz, 1H), 6.28 (dd, *J* = 14.4, 1.3 Hz, 1H), 4.25 (t, *J* = 5.1 Hz, 1H), 3.63 (t, *J* = 9.7 Hz, 1H), 3.50 (dt, *J* = 10.7, 5.2 Hz, 1H), 2.32 (dd, *J* = 5.9, 3.4 Hz, 1H), 1.92 (ddd, *J* = 14.4, 7.5, 3.6 Hz, 1H), 0.90 (s, 9H), 0.83 (d, *J* = 7.1 Hz, 3H), 0.06 (d, *J* = 12.8 Hz, 6H).

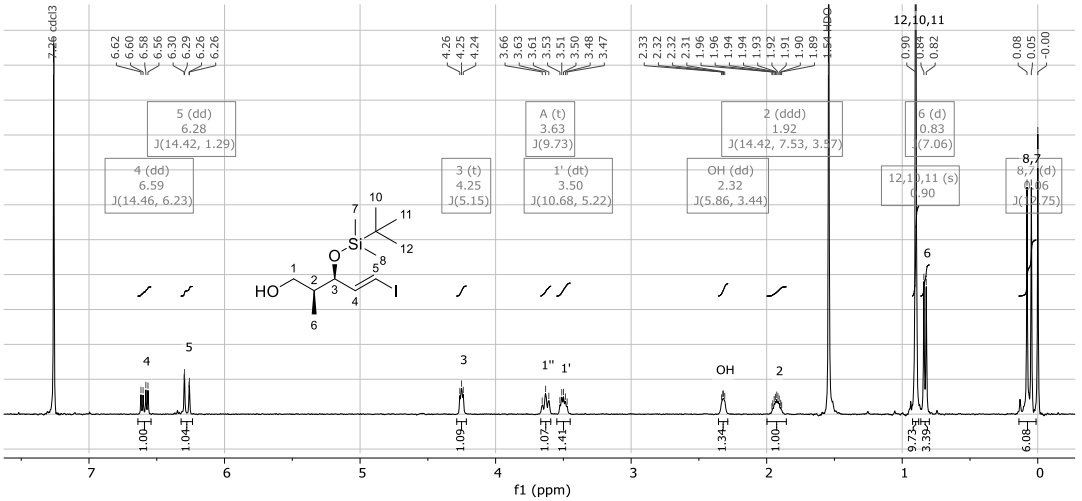

Synthesis of (2*R*,3*R*,*E*)-3-[(tert-butyldimethylsilyl)oxy]-5-iodo-2-methylpent-4-enal (46)

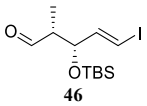

46

To a solution of **45** (504 mg, 1.41 mmol) in CH_2Cl_2 (14 mL) at 0°C was added Dess–Martin periodinane (720 mg, 1.70 mmol), and the resultant mixture was stirred at room temperature for 30 min. The reaction was quenched with a 1:1 mixture of saturated aqueous $NaHCO_3$ solution and saturated aqueous Na_2SO_3 solution at 0°C. The solution was extracted with diethyl ether (20 mL × 3), and the organic layers were washed with brine, dried, filtered, and concentrated under reduced pressure. The crude aldehyde was used in the next reaction without further purification.

^{1}H NMR (400 MHz, chloroform-*d*) δ 9.73 (d, *J* = 1.2 Hz, 1H), 6.55 (dd, *J* = 14.5, 6.1 Hz, 1H), 6.35 (dd, *J* = 14.5, 1.2 Hz, 1H), 4.54 (t, *J* = 5.2 Hz, 1H), 2.50 – 2.39 (m, 1H), 1.10 (d, *J* = 7.1 Hz, 3H), 0.87 (s, 9H), 0.04 (d, *J* = 3.6 Hz, 6H).

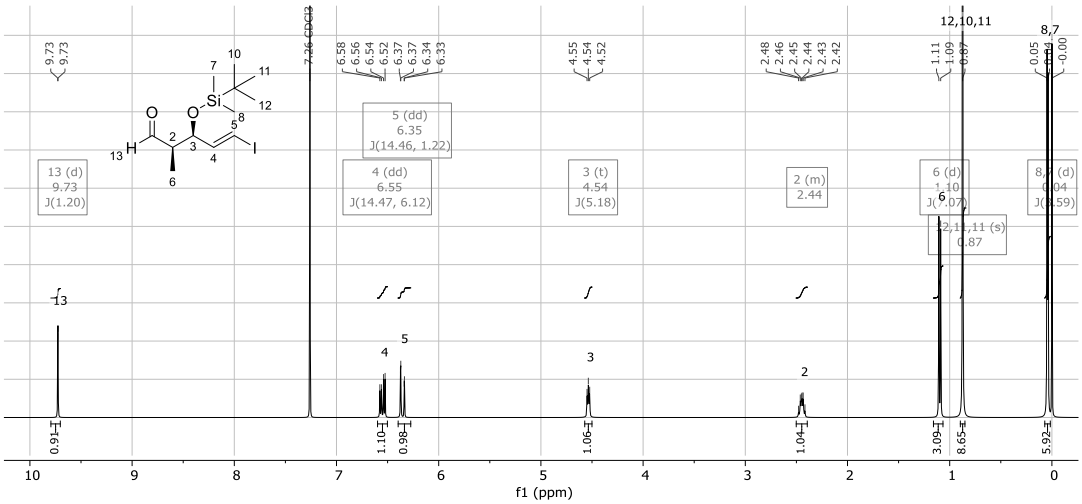

Synthesis of tert-butyl{[(3*R*,4*S*,*E*)-1-iodo-4-methylhexa-1,5-dien-3-yl]oxy}dimethylsilane (47)

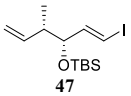

47

To a suspension of methyltriphenylphosphonium bromide (2.02 g, 5.64 mmol) in THF (7 mL) at 0°C was added *n*-BuLi (1.6 M solution in hexanes, 3.4 mL, 5.44 mmol), and the resultant suspension was stirred at 0°C for 15 min. To this suspension was added a solution of **46** in THF (6 mL), and the resultant mixture was stirred at 0°C for 20 min. The reaction was quenched with saturated aqueous NH_4Cl solution. The resultant mixture was extracted with EtOAc (15 mL × 3). The organic layers were washed with H_2O and brine, dried, filtered, and concentrated under reduced pressure. Column chromatography of the residue on silica gel (*n*-Hex/EtOAc 99:1) provided 354 mg (71% over two steps) of the product as a colorless oil.

^{1}H NMR (400 MHz, chloroform-*d*) δ 6.50 (dd, *J* = 14.4, 6.4 Hz, 1H), 6.17 (d, *J* = 14.4 Hz, 1H), 5.77 (ddd, *J* = 17.4, 10.7, 7.1 Hz, 1H), 5.06 – 4.96 (m, 2H), 3.94 (t, *J* = 5.9 Hz, 1H), 2.26 (q, *J* = 6.6 Hz, 1H), 0.99 (d, *J* = 6.8 Hz, 3H), 0.89 (s, 9H), 0.02 (d, *J* = 9.9 Hz, 6H).

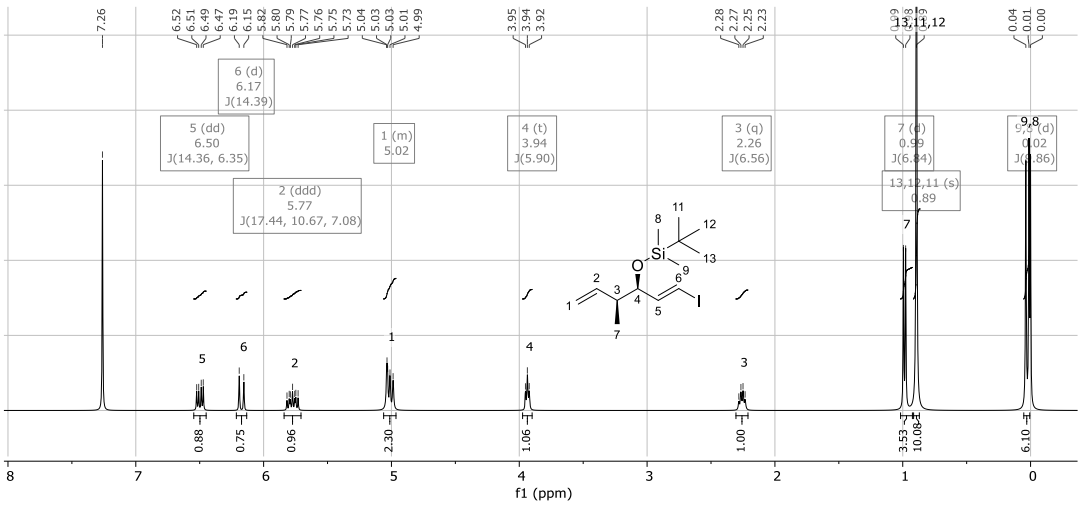

Synthesis of (3*R*,4*S*,*E*)-1-iodo-4-methylhexa-1,5-dien-3-ol (epi-C)

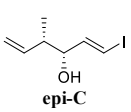

epi-C

To a solution of **47** (354 mg, 1.00 mmol) in THF (9 mL) at 0°C was added TBAF (1.0 M solution in THF, 1.51 mL, 1.51 mmol), and the resultant solution was stirred at room temperature for 45 min. The reaction was quenched with H_2O and extracted with EtOAc (10 mL × 3). The organic layers were washed with brine, dried, filtered, and concentrated under reduced

pressure. Column chromatography of the residue on silica gel (*n*-Hex/EtOAc 9:1) provided 255 mg (99%) of the product as a colorless oil.

$[\alpha]_D^{22}$ +16.3 (*c* 0.39 in $CHCl_3$)

^{1}H NMR (400 MHz, chloroform-*d*) δ 6.57 (dd, *J* = 14.4, 6.0 Hz, 1H), 6.35 (dd, *J* = 14.5, 1.4 Hz, 1H), 5.75 (ddd, *J* = 17.6, 10.6, 7.6 Hz, 1H), 5.19 – 5.09 (m, 2H), 4.03 (t, *J* = 5.6 Hz, 1H), 3.75 (s, 1H), 2.38 (h, *J* = 6.7, 6.1 Hz, 1H), 1.89 – 1.82 (m, 1H), 1.04 (d, *J* = 6.9 Hz, 3H).

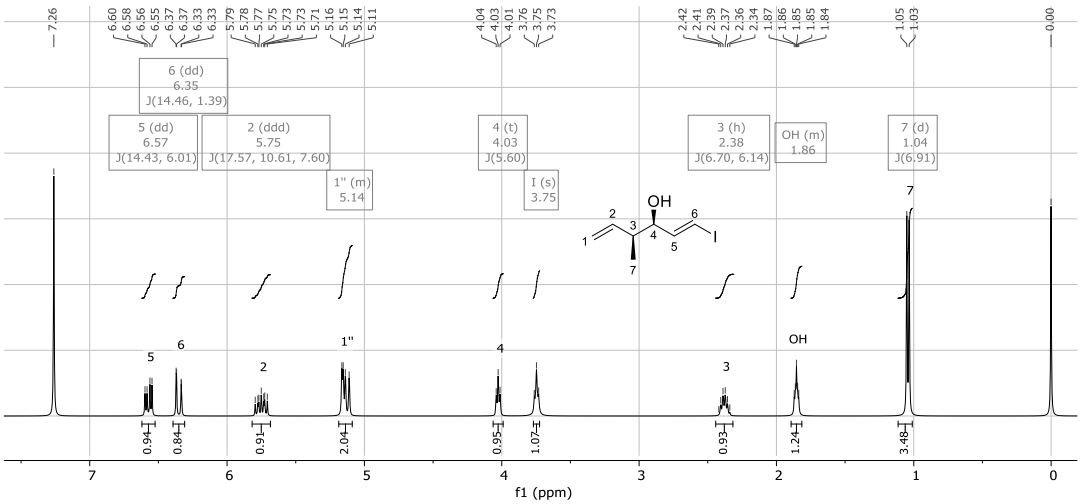

Synthesis of 2-bromo-3-formylphenyl pivalate (48)

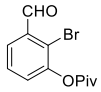

48

To a solution of 2-bromo-3-hydroxybenzaldehyde (1.00 g, 4.97 mmol) in DCM (5 mL) was added tetrabutylammonium iodide (184 mg, 0.50 mmol) and pivaloyl chloride (612 µL, 4.97 mmol). The reaction was cooled to 0 °C, an aqueous solution of K_2CO_3 (1.32 g, 9.55 mmol) in water (5 mL) was added and the mixture was vigorously stirred for 30 minutes at the same temperature. The reaction was extracted with diethyl ether (3 × 25 mL) and the combined organic layers were dried over Na_2SO_4, filtered, and concentrated under reduced pressure. Column chromatography of the residue on silica gel (gradient elution: hexanes/DCM 8:2 → 6:4 → 2:8) provided 1.36 g (96%) of the product as a white crystalline solid.

^{1}H NMR (400 MHz, chloroform-*d*) δ 10.39 (s, 1H), 10.39 (d, *J* = 0.8 Hz, 1H), 7.81 (ddd, *J* = 7.7, 1.6, 0.8 Hz, 1H), 7.45 (td, *J* = 7.8, 0.8 Hz, 1H), 7.33 (ddd, *J* = 8.0, 1.6, 0.8 Hz, 1H), 1.44 (s, 9H).

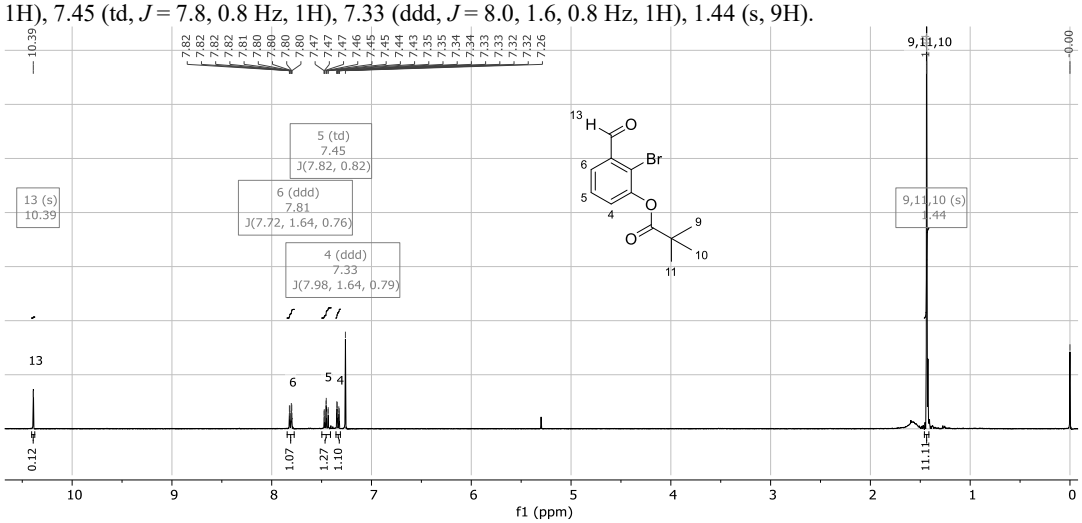

Synthesis of (*R*)-2-bromo-3-(1-hydroxy-2,2-dimethyl-3-oxopropyl)phenyl pivalate (58)

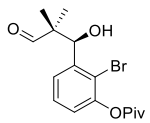

58

Under an atmosphere of argon, a solution of **48** (665 mg, 2.34 mmol) in dry DMSO (2.3 mL) was treated with isobutyraldehyde (424 µL, 4.68 mmol), (S)-(+)-1-(2-pyrrolidinylmethyl)-pyrrolidine (38 µL, 0.23 mmol) and trifluoroacetic acid (18 µL, 0.23 mmol). The reaction mixture was stirred at room temperature for 46 hours. Then, water (5 mL) was added, the aqueous phase was extracted with EtOAc (4 x 5 mL), and the combined organic layers were dried over Na_2SO_4, filtered, and concentrated under reduced pressure. The crude was purified on silica gel (gradient elution: *n*-Hex/EtOAc 9:1 → 85:15) to provide 737 mg (88%) of product as colorless viscous oil.

$[\alpha]_D^{22}$ +21.76 (c 1.0, $CHCl_3$)

^{1}H NMR (400 MHz, chloroform-*d*) δ 9.60 (s, 1H), 7.38 – 7.25 (m, 2H), 6.99 (dd, *J* = 7.7, 1.8 Hz, 1H), 5.45 (s, 1H), 1.37 (s, 9H), 1.06 (s, 3H), 1.00 (s, 3H).

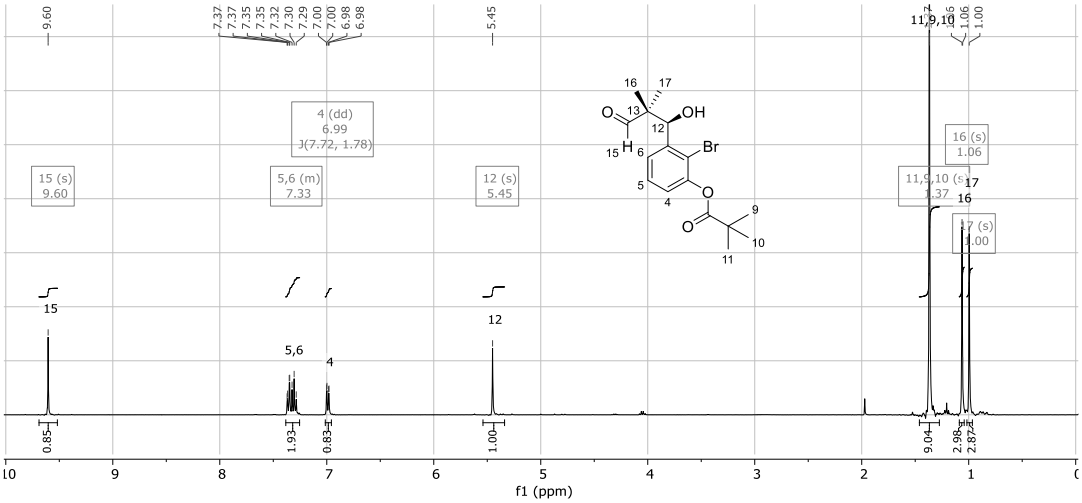

Synthesis of (*R*)-3-(1-acetoxy-2,2-dimethyl-3-oxopropyl)-2-bromophenyl pivalate (64)

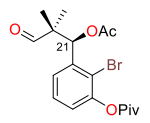

64

Under an atmosphere of argon, a solution of **58** (205 mg, 0.57 mmol) in DCM (1.9 mL) was cooled to 0 °C and then treated with acetic anhydride (69 µL, 0.73 mmol) previously deaerated, triethylamine dry (104 µL, 0.75 mmol) and DMAP (7 mg, 0.06 mmol). The reaction mixture was stirred at 0°C for for 20 minutes, then it was allowed to warm to room temperature and left stirring overnight. The reaction was quenched with a saturated aqueous solution of NH_4Cl (4 mL) and extracted with DCM (3 × 4 mL). The combined organic layers were dried over Na_2SO_4, filtered, and concentrated under reduced pressure. The crude was purified on silica gel (gradient elution: *n*-Hex/EtOAc 9:1 → 85:15) to provide 197 mg (86%).

$[\alpha]_D^{22}$ –59.2 (c 0.52, $CHCl_3$)

^{1}H NMR (400 MHz, chloroform-*d*) δ 9.68 (s, 1H), 7.33 (td, *J* = 7.9, 1.0 Hz, 1H), 7.20 (dt, *J* = 7.9, 1.4 Hz, 1H), 7.07 (dt, *J* = 8.0, 1.4 Hz, 1H), 6.51 (s, 1H), 2.05 (s, 3H), 1.41 (s, 9H), 1.17 (s, 3H), 1.09 (s, 3H).

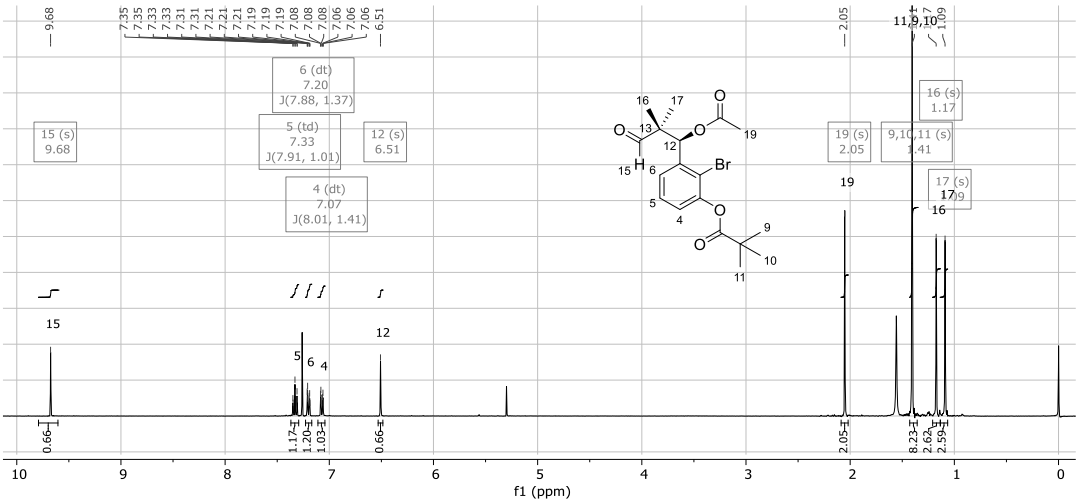

Synthesis of diethyl [3-(trimethylsilyl)propargyl]-phosphonate (66)

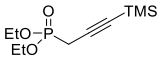

66

Under an atmosphere of argon, to a solution of NaHMDS (1.0 M in THF, 3 mL, 3 mmol) at −10°C was added diethyl phosphonate (387 µL, 3 mmol) in THF (0.9 mL). This solution was stirred for 15 min and then treated with 3-(trimethylsilyl)propargyl bromide (490 µL, 3 mmol) in THF (0.9 mL) maintaining the temperature at −10°C. After stirring for 1 h, the reaction was quenched with water and the aqueous layer was extracted with EtOAc (×2). The combined organic layers were washed with HCl (2 M), then with water, dried over Na_2SO_4, filtered, and concentrated under reduced pressure. The crude was purified on silica gel (eluent: *n*-Hex/EtOAc 1:1) to provide 575 mg (77%) of product as colorless liquid.

^{1}H NMR (400 MHz, chloroform-*d*) δ 4.29 – 4.11 (m, 4H), 2.81 (dd, *J* = 22.3, 0.9 Hz, 2H), 1.36 (ddt, *J* = 7.1, 6.5, 0.6 Hz, 6H), 0.16 (s, 7H).

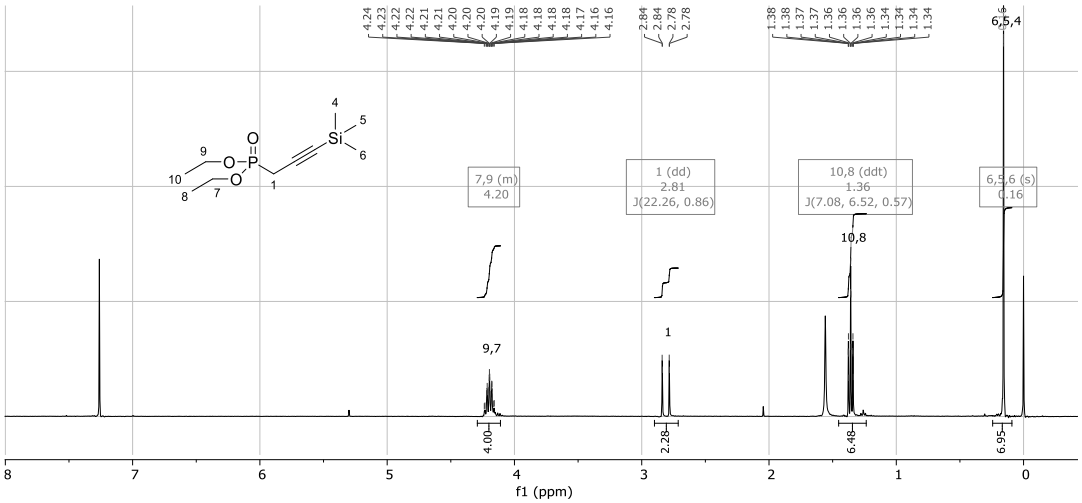

Synthesis of (*R*,*E*)-3-[1-acetoxy-2,2-dimethyl-6-(trimethylsilyl)hex-3-en-5-yn-1-yl)-2-bromophenyl] pivalate (65)

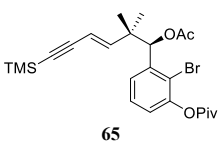

65

Horner-Wadsworth-Emmons: Under an atmosphere of argon, to a solution of **66** (472 mg, 1.90 mmol) in THF (20 mL) at 0°C was added *n*-BuLi (1.42 M in hexane, 1.4 mL, 1.90 mmol). The colorless solution became red and the reaction was stirred for 20 min at 0 °C and for 10 min at rt. After cooling the mixture to -78 °C, a solution

of **64** (380 mg, 0.95 mmol) in THF (5.7 mL) was added dropwise and the stirring was continued for 1 h 30 min. During this time, the color slowly changed to brown. The reaction was quenched with NH_4Cl ss and the aqueous layer was extracted with EtOAc (× 3) and the combined organic layers were dried over Na_2SO_4, filtrated, and concentrated under reduced pressure. The crude was purified on silica gel (eluent: *n*-Hex/EtOAc 97:3) to provide 306 mg (65%, *E*/*Z* 96:4) of product as light yellow viscous oil.

[α]$_D^{22}$ +51.77 (*c* 0.575, $CHCl_3$); **HRMS** (ESI) *m/z* $[M+Na]^+$ 515.1661 (calcd for $C_{24}H_{33}BrO_4SiNa$ 515.1648);

^{1}H NMR (400 MHz, chloroform-*d*) δ 7.30 (t, *J* = 7.9 Hz, 1H), 7.17 (dd, *J* = 7.8, 1.6 Hz, 1H), 7.03 (dd, *J* = 7.9, 1.6 Hz, 1H), 6.37 (d, *J* = 16.3 Hz, 1H), 6.14 (s, 1H), 5.41 (d, *J* = 16.3 Hz, 1H), 2.07 (s, 3H), 1.40 (d, *J* = 1.3 Hz, 9H), 1.13 (s, 3H), 1.05 (s, 3H), 0.20 (s, 9H).

^{13}C NMR (101 MHz, chloroform-*d*) δ 175.90, 169.60, 149.26, 148.17, 139.19, 127.20, 126.33, 122.94, 118.90, 109.28, 103.83, 94.13, 79.08, 42.28, 39.29, 27.18, 24.84, 21.89, 20.92, -0.06.

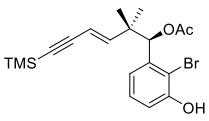

When the ylide has difficult formation, the product deprotected at Piv was obtained as minor by-product (8%, light yellow viscous oil).

[α]$_D^{22}$ +36.34 (*c* 0.96, $CHCl_3$); **HRMS** (ESI) *m/z* $[M+Na]^+$ 431.1812 (calcd for $C_{19}H_{25}BrO_3SiNa$ 431.1802);

^{1}H NMR (400 MHz, chloroform-*d*) δ 7.18 (t, *J* = 7.9 Hz, 1H), 6.94 (dd, *J* = 8.1, 1.5 Hz, 1H), 6.86 (dd, *J* = 7.8, 1.5 Hz, 1H), 6.34 (d, *J* = 16.3 Hz, 1H), 5.97 (s, 1H), 5.90 – 5.74 (m, 1H), 5.42 (d, *J* = 16.3 Hz, 1H), 2.06 (s, 3H), 1.12 (s, 3H), 1.05 (s, 3H), 0.19 (s, 9H).

^{13}C NMR (101 MHz, chloroform-*d*) δ 170.03, 152.13, 149.50, 138.12, 128.02, 121.17, 115.52, 113.32, 109.31, 104.00, 94.34, 79.72, 42.29, 24.65, 22.32, 21.10, 0.11.

Wittig procedure: To a suspension of 3-(trimethylsilyl)propargyl-triphenylphosphonium bromide (164 mg, 0.362 mmol) in THF (2.2 mL) at -78 °C was slowly added LHMDS (1 M THF, 348 µL, 0.348 mmol). After 10 min, the flask was warmed to – 40 °C for an additional 30 min, then recooled to -78 °C. A solution of **64** (58 mg, 0.145 mmol) in THF (870 µL) was then dropped. The flask was then slowly warmed to room temperature and left stirring overnight. After 12 h, the reaction was quenched with a saturated aqueous solution of NH_4Cl, extracted with EtOAc (3 ×), and washed with brine. The combined organic layers were dried over Na_2SO_4, filtered, and concentrated under reduced pressure. The crude was purified on silica gel (gradient elution: *n*-Hex/EtOAc 97:3 → 85:15) to provide 26 mg (36%, *E*/*Z* 3:1) of product as light yellow oil.

[α]$_D^{22}$ +17.6 (*c* 0.49, $CHCl_3$)

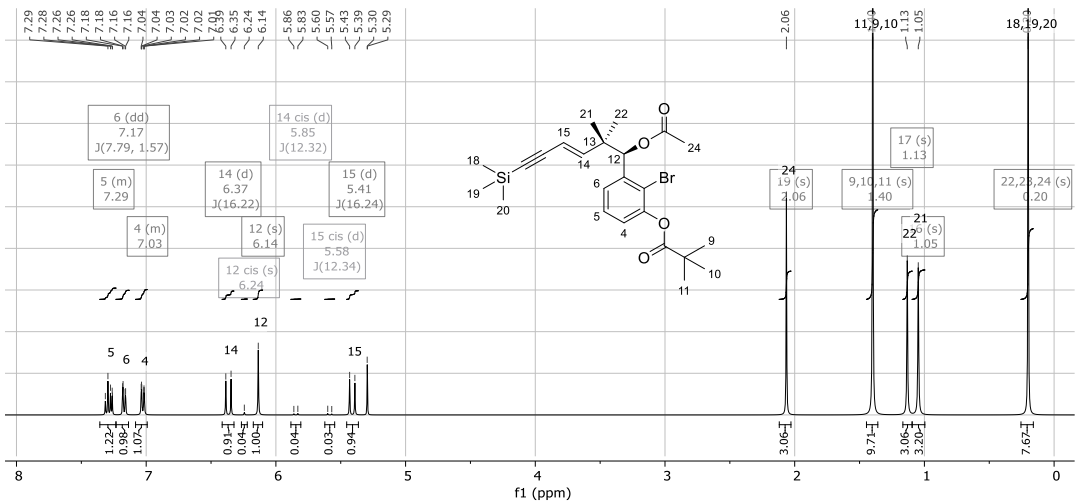

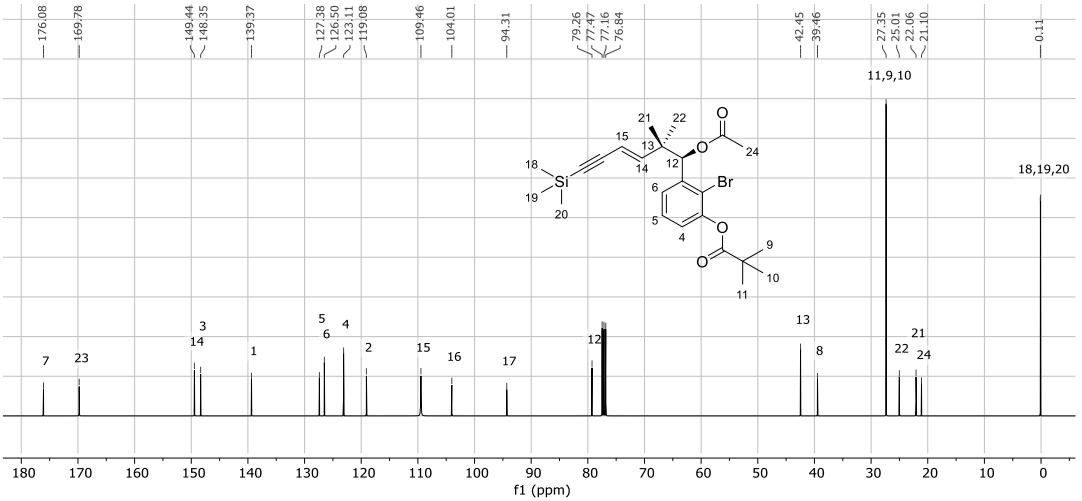
176.08
169.78
149.44
148.35
139.37
127.38
126.50
123.11
119.08
109.46
104.01
94.31
79.26
77.47
77.16
76.84
42.45
39.46
27.35
25.01
22.06
21.10
0.11
11,9,10
18,19,20
f1 (ppm)

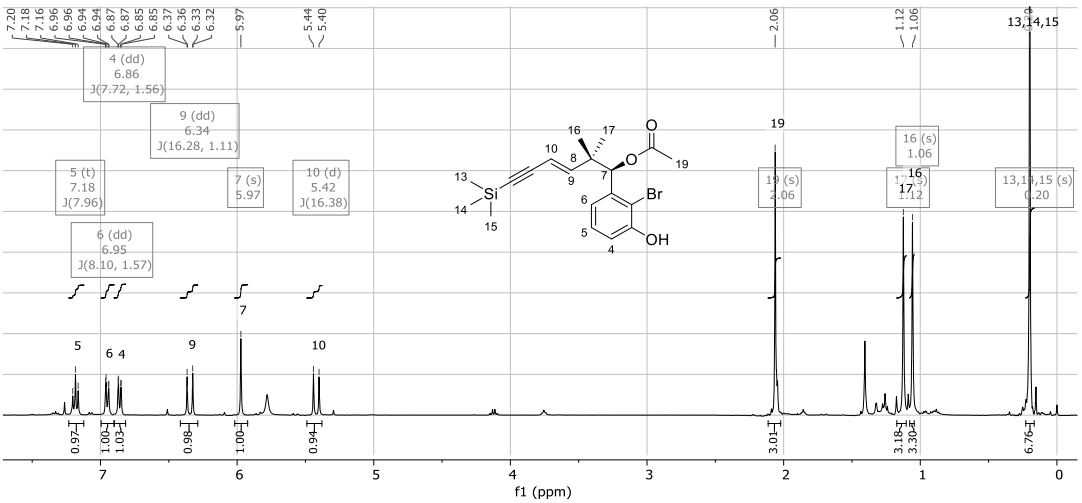
4 (dd)
6.86
J(7.72, 1.56)
9 (dd)
6.34
J(16.28, 1.11)
5 (t)
7.18
J(7.96)
7 (s)
5.97
10 (d)
5.42
J(16.38)
6 (dd)
6.95
J(8.10, 1.57)
16 (s)
1.06
13,14,15 (s)
0.20
f1 (ppm)

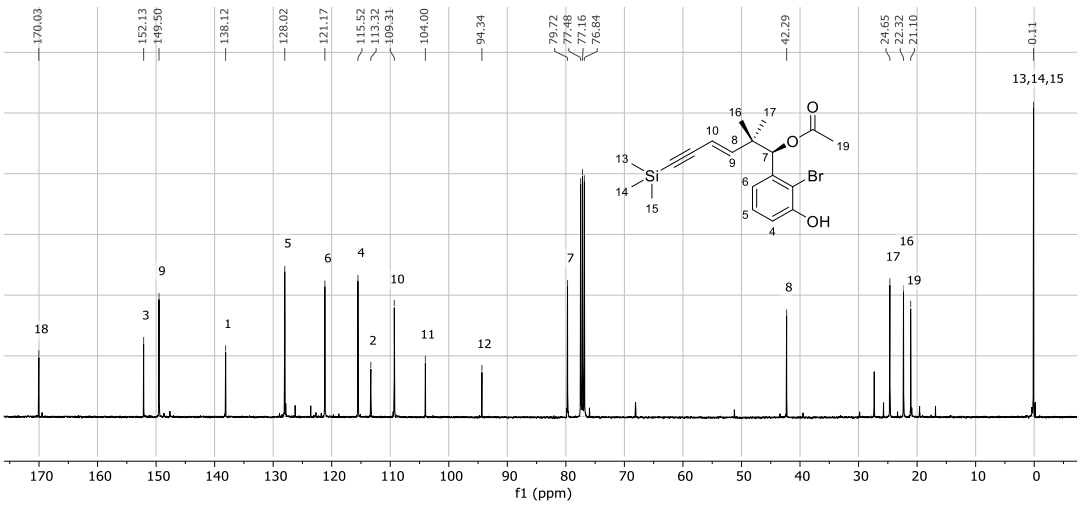
170.03
152.13
149.50
138.12
128.02
121.17
115.52
113.32
109.31
104.00
94.34
79.72
77.48
77.16
76.84
42.29
24.65
22.32
21.10
0.11
13,14,15
f1 (ppm)

Synthesis of (*R*,*E*)-2-bromo-3-(1-hydroxy-2,2-dimethylhex-3-en-5-yn-1-yl)phenol (Fragment B)

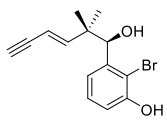

Fragment B

To a solution of **65** (154 mg, 0.32 mmol) in MeOH (16 mL) was added K_2CO_3 (323 mg, 2.34 mmol) and the reaction was stirred at 45°C for 2.5 hour. The mixture was quenched with a saturated aqueous solution of NH_4Cl (10 mL), extracted with EtOAc (3 × 20 mL), and washed with brine (10 mL). The combined organic layers were dried over Na_2SO_4, filtered, and concentrated under reduced pressure. The crude was purified on silica gel (eluent: *n*-Hex/EtOAc 9:1) to provide 86 mg (82%) of product as colorless viscous oil.

$[\alpha]_D^{22}$ +97.9 (*c* 0.845, $CHCl_3$)

^{1}H NMR (400 MHz, chloroform-*d*) δ 7.23 (d, *J* = 7.9 Hz, 1H), 7.03 (dd, *J* = 7.8, 1.4 Hz, 1H), 6.98 (dd, *J* = 8.0, 1.6 Hz, 1H), 6.45 (d, *J* = 16.4 Hz, 1H), 5.68 (s, 1H), 5.42 (dd, *J* = 16.4, 2.2 Hz, 1H), 5.00 (s, 1H), 2.85 (d, *J* = 2.2 Hz, 1H), 2.06 (s, 1H), 1.14 (s, 4H), 1.06 (s, 3H).